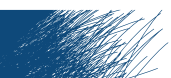


# Experimental and model-based analysis of twin-screw wet granulation in pharmaceutical processes

ir. Ashish Kumar





**Examination Committee:** Prof. dr. ir. Koen Dewettinck  
Chairman  
Department of Food Safety & Food Quality  
Ghent University, Belgium

dr. Mary T. Am Ende  
Pharmaceutical Development  
Pfizer Global Research & Development, USA

Prof. dr. ir. Peter Kleinebudde  
Institute of Pharmaceutics and Biopharmaceutics  
Heinrich-Heine-University, Germany

Prof. dr. ir. Gavin Walker  
Department of Chemical & Environmental Sciences,  
University of Limerick, Ireland

Prof. dr. ir. Frederik Ronsse  
Department of Biosystems Engineering  
Ghent University, Belgium

Prof. dr. Chris Vervaet  
Department of Pharmaceutics  
Ghent University, Belgium

**Promotors:** Prof. dr. ir. Ingmar Nopens  
Department of Mathematical Modelling, Statistics and Bioinformatics  
Ghent University, Belgium

Prof. dr. Thomas De Beer  
Department of Pharmaceutical Analysis  
Ghent University, Belgium

Prof. dr. ir. Krist V. Gernaey  
Department of Chemical and Biochemical Engineering  
Technical University of Denmark, Denmark

**Dean:** Prof. dr. ir. Guido Van Huylenbroeck

**Rector:** Prof. dr. Anne De Paepe

ir. Ashish Kumar

Experimental and model-based  
analysis of twin-screw wet  
granulation in pharmaceutical  
processes

Thesis submitted in fulfillment of the requirements for the degree of

Doctor (Ph.D) in Applied Biological Sciences

Academic year 2014-2015



*Dutch translation of the title:*

Experimentele en modelmatige analyse van farmaceutische dubbele schroef  
natte granulatie

*Please refer to this work as follows:*

Ashish Kumar (2015). Experimental and model-based analysis of twin-screw  
wet granulation in pharmaceutical processes, Ph.D. Thesis, Ghent University,  
Belgium.

प्रज्ञानं ब्रह्मा ॥

prajñānam brahma ॥

*The ultimate reality is wisdom.* [Aitareya Upanishad 3.3 of the Rig Veda]

ISBN: 978-90-5989-836-3

The author and the promoters give the authorisation to consult and to copy parts of this  
work for personal use only. Every other use is subject to the copyright laws. Permission to  
reproduce any material contained in this work should be obtained from the author.



To the memory of my mother,  
Smt. Malti Sharma, my foremost teacher.





---

## Summary

---

A shift from batch to continuous processing is challenging but equally rewarding for the pharmaceutical sector. This opportunity for moving beyond traditional batch processing is possible due to a change of attitude in the regulatory environment by the publication of the process analytical technology (PAT) guidance. However, in order to utilise this opportunity, detailed process understanding about the key processes in pharmaceutical manufacturing is required to turn this transformation to the continuous mode into a success. Continuous wet granulation is a crucial part of future continuous manufacturing of solid dosage forms. Continuous high shear wet granulation is performed using a twin-screw granulator (TSG) which is characterized by a modular screw profile including a sequence of different screw elements with various shapes, orientations and functions. A TSG achieves mixing and granulation by a complex interplay between the screw configuration and process settings (e.g. feed rate, screw speed, etc.) to produce granules with certain specifications in a short time. Therefore a fundamental understanding of these complex phenomena is required to optimise and control this new technology. Analysing the twin-screw wet granulation to a satisfactory degree is only possible when sufficient information on the rheo-kinetic characteristics of the granulation mixture is available. Thus an investigation of residence time distribution (RTD), the solid-liquid mixing, and the resulting granule size distribution (GSD) evolution governed by the field conditions in the TSG contain interesting information about mixing and different granulation rate processes such as aggregation and breakage. For this purpose, a combination of experimental and mathematical techniques/approaches was applied in this work. Additionally, a single placebo formulation based on  $\alpha$ -lactose monohydrate was granulated in the experimental studies performed to verify the hypothesis proposed in this work.

The characterisation of wetted material transport and mixing inside the confined spaces of the rotating screws was performed by the experimental determination of the residence time distribution at different process conditions and screw configurations using near infrared chemical imaging. The experimental data was later compared with a conceptual model based on classical chemical engineering methods to estimate the parameters of the model and to analyse the effects

of changes in number of kneading discs and their stagger angle, screw speed, material throughput and liquid-to-solid ratio (L/S) on RTD. According to this study, increased screw speed resulted in a low mean residence time  $\bar{t}$  and wider RTD, i.e. more axial mixing. Increasing powder feed rate increased  $\bar{t}$  by higher throughput force while increasing L/S increased  $\bar{t}$  by raising the sluggishness or inertia of the material in the barrel. The material transport in the mixing zone(s) of the TSG became more plug-flow like. Thus, an increase in the number of kneading discs reduced the axial mixing in the barrel.

In addition, to understand the GSD dynamics as function of individual screw modules along the TSG barrel, the change in GSD was investigated both experimentally and mathematically. Using a TSG which allows opening of the barrel, samples from several locations inside the TSG barrel were collected after granulation at different process conditions and screw configurations. A detailed experimental investigation was hence performed to understand the granule size and shape dynamics in the granulator. The experimental data from this study together with the residence time measurements was then used for calibrating a population balance model for each kneading disc module in the twin-screw granulator in order to obtain an improved insight into the role of the kneading discs at certain locations inside the TSG. The study established that the kneading block in the screw configuration acts as a plug-flow zone inside the granulator. It was found that a balance between the throughput force and conveying rate is required to obtain a good axial mixing inside the twin-screw granulator. Also, a high throughput can be achieved by increasing the liquid-solid ratio and screw speed. Furthermore, the study indicated that the first kneading block after wetting caused an increased aggregation rate, which was reduced after the material processing by the second kneading block. In contrast, the breakage rate increased successively along the length of the granulator. Such a reversion in physical phenomena indicated potential separation between the granulation regimes, which can be promising for future design and advanced control of the continuous twin-screw granulation process.

In another experimental study the transport and mixing (both axial and bulk mixing of solid-liquid) was linked to the GSD of the produced granules. This study demonstrated that insufficient solid-liquid mixing due to inability of the currently used kneading discs is the reason behind the inferior performance of the TSG in terms of yield. It was shown that other factors which support mixing such as higher axial mixing at a high screw speed and a low fill ratio support an increase in the yield. However, more effort is required to explore non-conventional screw elements with modified geometries to find screws which can effectively mix the solid-liquid material.

Furthermore, in order to generalise the TSG knowledge, a regime map based approach was applied. Herewith, the scale independent parameters,  $L/S$  and specific mechanical energy (SME) were correlated. It was shown that an increasing  $L/S$  strongly drives the GSD towards a larger mean granule size. However, an increasing energy input to the system can effectively be used to lower the mean granule size and also narrow the width of the size distribution. Along with this, particle-scale simulations for the characterisation of liquid distribution in the mixing zone of the granulator were performed. It was found that the agglomeration is rather a delayed process which takes place by redistribution of liquid once the excess liquid on the particle surface is transferred to the liquid bridges. Moreover, the transfer of liquid from particle surface to liquid bridges, i.e. initialisation of agglomeration, is most dominant in the intermeshing region of the kneading discs.

Besides the major outcomes of this work, i.e. building fundamental knowledge on pharmaceutical twin-screw wet granulation by combining experimental and theoretical approaches to diagnose the transport, mixing and constitutive mechanisms, several gaps and potential research needs were identified as well. As the regulators have opened up to increasingly rely on the science- and risk-based holistic development of pharmaceutical processes and products for commercialisation, the opportunity as well as responsibility lies with academic and industrial partners to develop a systematic framework and scientific approach to utilise this opportunity efficiently.



---

## Samenvatting

---

De overstap van batchgewijze naar continue procesvoering is uitdagend, maar zal zeker zijn vruchten afwerpen voor de farmaceutische industrie. Deze opportuniteit om verder te gaan dan de traditionele batchprocessen, is mogelijk dankzij de nieuwe houding van de regulerende instanties, dewelke tot stand kwam door de publicatie van de 'proces analytische technologie'-richtlijn (PAT). Om deze transitie echter succesvol te laten verlopen, is er een diepgaande kennis nodig van de belangrijke processen in farmaceutische productie. Continue natte granulatie is een cruciaal proces binnen de toekomstige continue productie van vaste toedieningsvormen. Continue 'high shear' natte granulatie wordt uitgevoerd met een dubbele-schroef-granulator (TSG), dewelke gekenmerkt wordt door een modulair schroefprofiel, zijnde een aaneenschakeling van verschillende schroefelementen met diverse vormen, oriëntaties en functies. In een TSG worden menging en granulatie verwezenlijkt via een complexe interactie tussen de configuratie van de schroef en de procesinstellingen (bv. feed rate, schroefsnelheid, etc.), met als resultaat de productie van granules met bepaalde eigenschappen, en dit in korte tijd. Er is dus een fundamentele kennis vereist om deze nieuwe technologie te optimaliseren en te controleren. Analyse van de TSG op een voldoende diepgaand niveau is enkel mogelijk wanneer er genoeg informatie beschikbaar is omtrent de reo-kinetische eigenschappen van te granuleren formulatie. Zodoende bevatten de verblijftijdsdistributie (RTD), kennis van de mengingsgraad van de vaste stoffen met de vloeistof, en de resulterende evolutie van de grootte-distributie van de granules (GSD), uiterst nuttige informatie omtrent menging en de verschillende granuleringsprocessen zoals aggregatie en breking. Om deze te onderzoeken, werd in deze thesis een combinatie van experimentele en wiskundige technieken/methoden toegepast. Daarenboven werd een placeboformulatie, gebaseerd op  $\alpha$ -lactose monohydraat, gegraneerd bij de experimentele studies, om de in dit werk voorgestelde hypothese te verifiëren.

De karakterisatie van transport van nat materiaal en menging binnenin de begrenste ruimtes gecreëerd door de roterende schroeven, werd gedaan d.m.v. het experimenteel bepalen van de verblijftijdsdistributie bij verschillende procesinstellingen en schroefconfiguraties met near infrared chemical imaging. De experimentele data werden vervolgens vergeleken met een conceptueel model

volgens klassieke chemische ingenieursmethoden, met als doel de parameters van het model te schatten, alsook de invloed te analyseren van het aantal kneedelementen en hun kantelhoek, de schroefsnelheid, de hoeveelheid doorvoer van materiaal en de vloeistof-over-vaste stof-ratio (L/S) op de RTD. Volgens dit onderzoek resulteerde een verhoogde schroefsnelheid in een kortere gemiddelde verblijftijd ( $\bar{t}$ ) en bredere RTD, i.e. meer axiale menging. Het verhogen van de snelheid waarmee het poeder toegevoegd wordt, verhoogde eveneens  $\bar{t}$  door de hogere kracht van de doorvoer, terwijl het verhogen van L/S hetzelfde teweegbracht door het verhogen van de traagheid of inertie van het materiaal in de granulatorbuis. Het transport van materiaal in de mengingszones ging meer over naar een plug-flow regime. Zodoende werd de axiale menging in de granulatorbuis gereduceerd bij het verhogen van het aantal kneedelementen.

Bovendien, om de dynamiek van de verandering van de GSD in functie van de individuele schroefmodules te begrijpen, werd de evolutie van de GSD doorheen de granulator zowel experimenteel als wiskundig onderzocht. Middels gebruik van een GSD waarbij de granulatorbuis kan opengeklapt worden, werden monsters vanop verschillende locaties binnen de granulatorbuis verzameld na granulatie met verschillende procescondities en schroefconfiguraties. Hierop volgde een gedetailleerd experimenteel onderzoek om de dynamiek in grootte en vorm van de granules, die binnenin de granulator plaatsvindt, te begrijpen. De experimentele data van dit onderzoek werden vervolgens, samen met verblijftijdsmetingen, gebruikt ter calibratie van een populatiebalansmodel voor elke verschillende module van kneedelementen. Dit werd gedaan om meer inzicht te krijgen in de rol van de locatie van de kneedelementen in de schroefconfiguratie. Zodoende werd vastgesteld dat het kneedelement een plug-flow-zone creëert in de granulator. Er werd geconstateerd dat een balans tussen de kracht van de doorvoer en de transportsnelheid gevonden moet worden voor een goede axiale menging. Er werd ook gevonden dat een hoge doorvoer bereikt kan worden door de L/S en de schroefsnelheid te verhogen. Bovendien werd uit het onderzoek vastgesteld dat bij het eerste kneedelement na de plaats waar de vloeistof wordt toegediend, vooral aggregatie plaatsvond. Deze aggregatie werd gereduceerd door de aanwezigheid van een tweede kneedelement stroomafwaarts. De hoeveelheid breking, daarentegen, verhoogde naarmate het materiaal zich verder in de granulator bevond. Zo een reversie van fysische fenomenen wees op een mogelijke scheiding tussen de granulatieregimes, hetgeen nuttig kan zijn voor het toekomstige ontwerp en de geavanceerde controle van het continue dubbele-schroef-granulatieproces.

In een andere experimentele studie werden transport en menging (zowel axiaal als de menging van vaste stof en vloeistof in de bulk) gelinkt aan de GSD van

de geproduceerde granules. Deze studie toonde aan dat onvoldoende menging van vaste stof en vloeistof, als gevolg van de niet-optimale werking van de kneedelementen, de achterliggende oorzaak is van de inferieure performantie van de TSG op vlak van opbrengst van kwalitatieve granules. Er werd bewezen dat andere factoren die bijdragen tot menging, zoals een betere axiale menging bij een hoge schroefsnelheid en lage vulratio, deze opbrengst verhogen. Voor het onderzoeken van de niet-conventionele schroefelementen met aangepaste geometrieën moeten echter nog meer studies verricht worden, met als doel het vinden van schroeven waarmee de vaste stoffen en vloeistof efficiënt gemengd kunnen worden.

Voor het generaliseren van kennis omtrent de TSG werd als methode de regimemap gebruikt, waarmee de schaalonafhankelijke parameters, de L/S en de specifieke mechanische energie (SME), met mekaar gecorreleerd werden. Er werd aangetoond dat het verhogen van de L/S de gemiddelde grootte van de granules ook sterk vergrootte. Anderzijds levert een hogere energie-input in het systeem een daling op in de gemiddelde grootte van de granules, alsook een vernauwing van de GSD. Er werden eveneens simulaties uitgevoerd op schaal van een partikel voor het in kaart brengen van de vloeistofverdeling in de mengingszone van de granulator. Er werd gevonden dat agglomeratie vooral een vertraagd proces is dat plaatsvindt bij het herverdelen van de vloeistof, nadat het vloeistofoverschot op het oppervlak van het partikel getransfereerd is naar de vloeistofbruggen. Bovendien is deze transfer, dewelke de initialisatie van agglomeratie voorstelt, het meest dominant in de ruimte tussen twee naast mekaar roterende kneedelementen.

Naast de voornaamste uitkomsten van dit werk, i.e. het opbouwen van fundamentele kennis omtrent farmaceutische dubbele-schroef natte granulatie d.m.v. een combinatie van experimentele en theoretische methoden ter onderzoek van het transport, de mening en de onderliggende processen daarvan, werden er ook nog enkele kenniskloven en potentiële onderzoeksnoten gevonden. Aangezien de regulerende instanties zich tegenwoordig meer open stellen voor een wetenschappelijk en risico-gebaseerde, holistische ontwikkeling van farmaceutische processen en producten bestemd voor commercialisatie, liggen zowel de opportuniteit als de verantwoordelijkheid bij academische en industriële partners om een systematisch raamwerk op te stellen, alsook een wetenschappelijke methodiek om deze opportuniteit efficiënt te benutten.





---

## Acknowledgement

---

First and foremost, I am greatly thankful to my supervisor Prof. Ingmar Nopens, Prof. Thomas De Beer and Prof. Krist Gernaey for trusting me to be a suitable person for such a challenging, multi-disciplinary and industry related research. Their invaluable guidance, kind behaviour and given flexibility in work encouraged me to accomplish this research. Working on such a multi-disciplinary project also allowed me to interact with many dynamic and talented researchers from Ghent university (Biomath and Pharmaceutical faculty), industrial partner GEA (esp. Kris) and research partner VTT, Finland (esp. Maunu and Pierre-Emmanuel). Without their humble cooperation, delivering the thesis goals must have been very difficult.

I would like to remember my colleagues from Biomath in the way they played their role in my PhD life. Starting with my immediate surrounding, my colleagues with whom I not only shared the office space and fun but also my troubles from administration to science. In this regard, I would like to thank Ivo, Katrijn, Thomas and Yuri over the last years and Chaïm and Han as well. Next to this, very special thanks to my "local stack overflow" colleagues, Stijn, Timothy and Joris sitting in the next door office where I kept on hopping when stuck in simulation or anything around and they always helped me with great enthusiasm. Thanks to my colleagues of Pharma modelling group Séverine, Niels, Michael and newly introduced Daan for their fruitful interaction and support. The home-brew beers from Wouter, cakes from Tinne added a flavour to this journey, thanks a lot! Elena and Giacomo, thanks for all your help. Short chats with Usman refreshed expressions and jokes we Indians share with Pakistanis, thanks. Also thanks a lot to Jan De Neve and Joris Meys for simplifying the complexity of statistical analysis whenever needed. Ruth, Timpe and Jan Roels: thanks for all the administrative and IT support.

A transition from my process engineering background towards the pharmaceutical engineering was required for this work and my colleagues from pharmaceutical faculty made it easy as possible. Here, I would like to especially thank Jurgen for being there right from the start and filling the gaps in knowledge which I had due to difference in my background. Thanks to Valérie and Fien

who later joined with their invaluable contribution which was no lesser. It was a pleasure working with my master thesis students Jens and Maija, who definitely marked an important place through their thesis work. Also thanks to Bernd, Jeroen and Tinne for fruitful collaborations. More academic activities also required more and more administrative formalities. Thanks to Katharine for that support which never let me stop at any moment.

For my research stay at TU Graz, I would like to thank Prof. Khinast, Dr. Rajniak and Prof. Radl for extending their research support. Also thanks to Andreas, Bhagesh and Jakob for including me in the research as well as social activities. I would also like to thank Prof. Jitendra Kumar from IIT Kharagpur for his help during implementation of the PBM solution method.

No research and its valorisation is possible without funding support. Here I would like to gratefully acknowledge the financial support by BOF (Bijzonder Onderzoeksfonds Universiteit Gent, Research Fund Ghent University) for this research, FWO (Research Foundation - Flanders) for the long term research stay and both FWO and FCWO (Facultaire Commissie voor Wetenschappelijk Onderzoek) for attending different congresses.

I would like to thank my family in India for their strong support over these years. I am sure they will be proud seeing me successfully finishing this milestone as well. Finally, special thanks to my wife Kankana for her support, tolerating my never ending busyness and giving me time to complete this journey.

Ashish Kumar  
Ghent, October 2015

---

# Contents

---

<b>I</b>	<b>Introduction &amp; objectives</b>	<b>1</b>
<b>1</b>	<b>Introduction</b>	<b>5</b>
1.1	Background	5
1.2	Thesis outline	7
<b>2</b>	<b>Theory &amp; Literature survey</b>	<b>9</b>
2.1	Introduction	10
2.2	Current modelling and related measurement tools for HSWG	13
2.2.1	Mathematical modelling of HSWG	15
2.2.2	Measurement techniques	29
2.3	Needs & opportunities for continuous HSWG modelling and measurements	31
2.3.1	Needs of modelling TSG	32
2.3.2	Tools for measurement of state variables	36
<b>3</b>	<b>Granulation system description and Objectives</b>	<b>39</b>
3.1	Continuous twin-screw wet-granulation	40
3.2	Thesis objectives	44
<b>II</b>	<b>Experiments-based analysis of twin-screw wet granulation system</b>	<b>47</b>
<b>4</b>	<b>RTD measurement to study mixing</b>	<b>49</b>
4.1	Summary	49
4.2	Introduction	50
4.3	Materials and methods	52
4.3.1	Pharmaceutical model formulation and twin screw granulation	52
4.3.2	Description of NIR chemical imaging system and measurement set-up	52
4.3.3	Residence time analysis: experimental design and data post-processing	53
4.3.4	Quantification of effects and interactions of factors	56
4.4	Results and discussion	56
4.4.1	Effect of screw speed	57
4.4.2	Effect of material throughput	62
4.4.3	Effect of number of kneading discs	64
4.4.4	Effect of stagger angle	66
4.5	Interaction of different process and equipment parameters	67
4.6	Conclusions	69

<b>5 Particle size evolution in TSG</b>	<b>71</b>
5.1 Introduction	72
5.2 Materials and methods	74
5.2.1 Pharmaceutical model formulation and twin screw granulation	74
5.2.2 Experimental design and sample preparation	74
5.2.3 Determination of torque	75
5.2.4 Characterisation of granules	75
5.3 Results and discussion	77
5.3.1 Influence of process variables on the granules at the outlet	77
5.3.2 Influence of process variables on granule properties along the TSG length	78
5.4 Conclusions	90
<b>6 Linking granulation performance with residence time and granulation liquid distributions</b>	<b>91</b>
6.1 Introduction	92
6.2 Materials and methods	94
6.2.1 Pharmaceutical model formulation and twin screw granulation	94
6.2.2 NIR chemical imaging and Extraction of relevant information from spectral data	95
6.2.3 Sieving test for particle size analysis	98
6.2.4 Quantification of effects and interactions of factors	98
6.3 Results and discussion	99
6.3.1 Change in torque at different process conditions	99
6.3.2 Granulation time at different process conditions	103
6.3.3 Mixing at different process conditions	104
6.3.4 GSD at different process conditions	109
6.3.5 Link between granulation time, mixing and yield	111
6.4 Conclusions	113
<b>III Model-based analysis of twin-screw wet granulation system</b>	<b>115</b>
<b>7 Model-based analysis of RTD</b>	<b>117</b>
7.1 Introduction	118
7.2 System analysis and model formulation	119
7.2.1 Continuous wet-granulation using TSG	119
7.2.2 Experimental determination of RTD	119
7.2.3 Estimation of RTD from experimental data	119
7.2.4 Theoretical models for RTD in TSG	120
7.2.5 Parameter estimation	122
7.2.6 Model analysis	122
7.3 Results and Discussion	123
7.3.1 Comparison of models based on the goodness-of-fit	123
7.3.2 Analysis of RTD using TIS model with plug-flow and dead-volume fractions	125
7.4 Conclusions	131

<b>8</b>	<b>Particle size evolution model in TSG</b>	<b>133</b>
8.1	Introduction	134
8.2	Materials and methods	136
8.2.1	Population balance model for TSG	136
8.2.2	Numerical solution of PBM	137
8.2.3	Model parameter estimation	141
8.2.4	GSD experimental data for model calibration	142
8.3	Results and discussion	142
8.3.1	Parameter estimation for predictive modelling	142
8.3.2	Simulated dynamic behaviour in the mixing zones of the TSG	144
8.4	Model application and future development	147
8.5	Conclusions	148

## **IV Scale-independent analysis of twin-screw wet granulation system 151**

<b>9</b>	<b>Scale independent process map for TSG</b>	<b>153</b>
9.1	Introduction	154
9.2	Materials and methods	156
9.2.1	Pharmaceutical model formulation and twin screw granulation	156
9.2.2	Experimental design	156
9.2.3	Determination of torque and specific mechanical energy	157
9.2.4	Particle size analysis	157
9.2.5	Spatial interpolation and verification	158
9.3	Results and discussion	158
9.3.1	Effect on torque	158
9.3.2	Effect on granule size distribution	159
9.3.3	Effect on SME level	162
9.3.4	Regime map based on GSD, L/S and SME	164
9.4	Future development: from process map to regime map	167
9.5	Conclusions	168
<b>10</b>	<b>DEM simulation of wet granulation in TSG</b>	<b>169</b>
10.1	Introduction	170
10.2	Particle scale modelling approach	172
10.2.1	Particle flow model	172
10.2.2	Liquid bridge model	173
10.2.3	Simulation set-up and input parameters	174
10.3	Results and discussion	177
10.3.1	Solid-liquid mixing in a simple shear flow condition	177
10.3.2	Solid-liquid mixing in the mixing zone of TSG	181
10.4	Conclusions	185

## **V General discussion, conclusions and perspectives 187**

<b>11</b>	<b>General discussion</b>	<b>191</b>
11.1	Summary	191
11.2	Introduction	191
11.3	Material transport and mixing	192
11.3.1	Granulation time	192
11.3.2	Mixing	193

11.4 Granule size evolution	195
11.4.1 Granule size and shape dynamics	196
11.4.2 Link between RTD, liquid distribution and GSD	196
11.5 Model-based analysis	197
11.5.1 Modelling RTD	197
11.5.2 Tracking GSD using PBM	198
11.6 Towards a generic twin-screw granulation knowledge	199
11.6.1 Regime map approach	199
11.6.2 Particle-scale simulation using DEM	200
11.7 Strengths and limitations of the current approach	201
<b>12 General conclusions</b>	<b>203</b>
12.1 Granulation time and mixing quality	203
12.2 GSD transformation by TSG	204
12.3 Overall conclusion	205
<b>13 Perspectives &amp; future work</b>	<b>207</b>
<b>Glossary</b>	<b>221</b>
<b>Acronyms</b>	<b>225</b>
<b>A Supplementary tables from literature survey</b>	<b>229</b>
<b>B Raw data from experimental studies</b>	<b>245</b>
<b>C Parameters estimations results for RTD model and PBM</b>	<b>251</b>
<b>D Testing of the liquid transfer and bridge force models</b>	<b>259</b>

# PART I

Introduction, literature review, system  
description and objectives





This part of the PhD dissertation serves as platform for explaining the timeliness and usefulness of the performed research on the pharmaceutical twin-screw wet granulation process. The text starts with a short introduction to wet-granulation research and efforts towards continuous pharmaceutical manufacturing (Chapter 1 section 1.1). This chapter will also provide the outline of this thesis (Chapter 1 section 1.2), which is a quick reference to the flow of information in the thesis. To make readers aware about the state-of-the-art in modelling techniques applied to high shear wet granulation processes and the measurement techniques used for the experimental studies, a literature overview is provided (Chapter 2). The last chapter of this part of the thesis (Chapter 3) provides a detailed description of the system, i.e. the ConsiGma<sup>TM</sup>, which contains the twin-screw granulation system. At the end of this third chapter, the objectives of this thesis are outlined (Section 3.2).



## Introduction

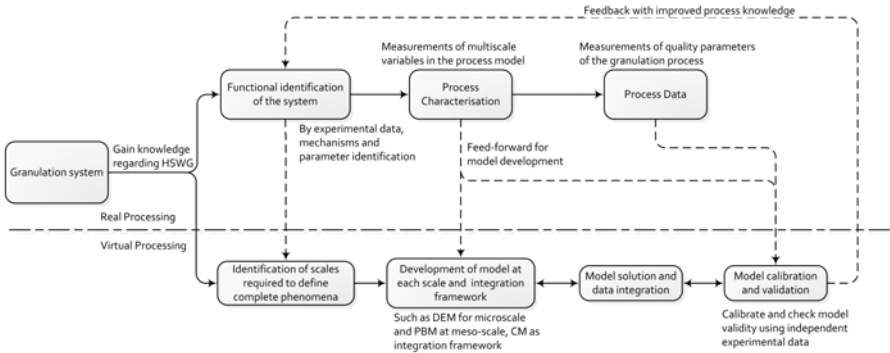
---

### 1.1 Background

Efforts towards making the transition from batch to continuous processing with 24/7 production capacity is one of the major considerations within the pharmaceutical industry for improving the operational efficiency while enhancing quality assurance. The publication of the process analytical technology (PAT) guidance by the Food and Drug Administration (FDA) in 2004 has facilitated the adoption of new and modern manufacturing approaches, and therefore, the possibility exists to take the step towards continuous production processes in the pharmaceutical industries as well. However, a transition to continuous processing requires all the unit operations to be operated in continuous mode with inter-compatibility. In this context, the twin-screw granulation has emerged as a promising technology for continuous wet granulation. A manufacturing line with continuous twin-screw granulator (TSG) is followed by a dryer, product control hopper and tableting machine. A TSG achieves mixing and granulation by a complex interplay between the screw configuration, the process settings (e.g. feed rate, screw speed, etc.) and the formulation properties to produce products with pre-defined end-product specifications in a very short time, i.e. in the order of seconds. However, prior to industrial implementation, an understanding of this complex process is required not only to optimise and control this new technology, but also to understand the influence of process, equipment and raw material parameters on the critical quality attribute (CQA).

Irrespective of the engineering application, process knowledge is developed through a combined experimental and theoretical (i.e. model-based) approach. While experiments are necessary to gather new knowledge about the system, theory is needed to put forth hypotheses to build further on this knowledge

and guide the further development. In the field of pharmaceutical twin-screw wet granulation, a wide range of different experiments has been performed in previous years. However, in lack of a satisfactory link between the experimental result and mechanistic principles or theory, the results from these studies find only limited practical application. Moreover, being an opaque multiphase system working in a high shear environment, several crucial process parameters in TSG, such as mixing, filling degree of the barrel, granule size and shape distribution (GSSD) evolution cannot be easily measured. Thus, such parameters are currently heuristically correlated with other easily obtained responses such as mechanical power consumption leading to a very limited process knowledge, i.e. a "black box". Similarly, theoretical studies based on default or best-guessed model parameters have also been performed as proof-of-concepts. These non-calibrated and non-validated models when tested for real applications, often result in unrealistic estimates. Thus, the development towards a mechanistic description of the twin-screw wet granulation process requires a combination of the experimental and theoretical (i.e. model-based) approaches. The theoretical model can on the one hand provide the fundamental basis to the experimental results by linking them to the constitutive mechanisms of the granulation, whereas on the other hand tuning-in of the model parameters through calibration can improve the ability of granulation models to properly reflect the impact of any change in the process.



**Figure 1.1:** Experimental and model-based knowledge combined for the development of process understanding regarding the granulation system.

This complementarity was well identified in this research and therefore, a combination of experimental and mathematical methodologies is proposed and applied to develop process knowledge regarding the twin-screw wet granulation system (Fig. 1.1). Integration of process engineering (modelling) and pharmaceutical sciences (measurements) disciplines allowed developing knowledge regarding

rate processes, their interaction and quantification by advanced measurement tools, and development of models to improve the prediction of the process state in the continuous system. Filling the knowledge gaps will be helpful in achieving process design and control for efficiency and accuracy and can also be used for scale-up predictions, which is crucial for transition towards continuous processing in industrial solid dosage manufacturing.

## 1.2 Thesis outline

The PhD dissertation is structured in five distinctive parts.

Part I of the thesis contains the introductory material which forms the background for the other parts of the thesis. Chapter 2 gives an overview of the relevant literature in the field of high shear wet granulation (HSWG) modelling and measurements. This chapter discusses the different modelling approaches such as population balance model (PBM) and the discrete element method (DEM) applied for granulation modelling. This chapter also identifies the need for model-based analysis of TSG and the measurement tools available and required for the calibration and validation of the granulation models. Chapter 3 provides a detailed description of the continuous manufacturing line ConsiGma<sup>TM</sup>, which contains the TSG for which experimental and model-based studies were performed. The general aspect of TSG screw design and operational parameters are also covered in this chapter. This follows the thesis objectives which were set to improve the understanding regarding the TSG.

Part II presents experimental studies performed to understand the effect of various process and equipment related parameters of TSG on material flow, mixing and granulation. The first study starts with measurement of residence time distribution using the near infrared chemical imaging (NIR-CI) (Chapter 4). Subsequently, the TSG from the ConsiGma-1 system which provides a possibility to open the barrel was used to quantify the particle size evolution along the length of the barrel (Chapter 5). Granule samples are collected from different locations inside the barrel and are characterised for size and shape using dynamic image analysis (DIA). Thereafter, an experimental study is performed to link the residence time, axial and solid-liquid mixing to the granulation performance (Chapter 6).

In part III, the model-based analysis of the twin-screw granulation process is presented. The experimental data collected in part I is utilised to develop and calibrate the proposed models. In chapter 7, the conceptual modelling

of residence time distribution (RTD) in twin-screw granulation is performed with the aim to propose the most suitable model for residence time analysis in twin-screw granulation among a list of model candidates. Furthermore, the granule size distributions (GSDs) obtained from experiments presented in Chapter 5, are used to develop and calibrate a PBM framework (Chapter 8). This model includes the aggregation and breakage terms for tracking the GSD evolution inside the mixing zones of the TSG.

In part IV, the study utilising scale independent and dimensionless parameters to improve the fundamental level of understanding of the twin-screw granulation process is presented. In chapter 9, granulation regime maps for TSG are developed based on change in the scale independent parameters, liquid-to-solid ratio (L/S) and specific mechanical energy (SME). Thereafter, in chapter 10 some preliminary results of particle scale modelling of the solid-liquid mixing in the HSWG using DEM are presented. The mechanistic cohesion model along with the liquid tracking model is used to simulate the dispersion of liquid in a dense powder bed.

Finally, Part V provides a global discussion on the results obtained in this dissertation coupling back the achievements to the objectives and highlighting the remaining gaps (chapter 11). The major conclusions (chapter 12) of this PhD dissertation as well as the perspectives (chapter 13) for further research and developments in the field of twin-screw wet granulation are presented.

Most of the contents of this thesis are already accepted/published in research Journals. When available, each chapter also reports the respective publication details.

## Theory & Literature survey

---

**Redesignated from:** Ashish Kumar, Krist V. Gernaey, Thomas De Beer, Ingmar Nopens, Model-based analysis of high shear wet granulation from batch to continuous processes in pharmaceutical production - A critical review, European Journal of Pharmaceutics and Biopharmaceutics, Volume 85, Issue 3, Part B, 2013, Pages 814-832.

Research on the granulation process to date has largely focused on developing fundamental understanding of the mechanisms involved and the role of process conditions on the granulation performance. This comprises a large number of both theoretical and experimental studies contributing to the development of knowledge regarding the wet granulation processes in the past. Therefore, in this literature survey, both modelling of high shear wet granulation (HSWG) processes as well as measurements required for a model calibration/validation (not quality measurements in general) are presented. In the introduction (section 2.1), the basis of the existing intention of the pharmaceutical sector to move from batch to continuous production (granulation) is briefly discussed. Furthermore, the benefits, challenges and alternatives of continuous wet granulation are shown. Thereafter, section 2.2 summarises the current state of the art of high-shear batch granulation specific modelling approaches and process measurement techniques. Next to the literature survey, a critical discussion is provided in section 2.3 highlighting current knowledge gaps and potentially interesting new research directions of modelling and measurement tools for the efficient adoption of continuous twin-screw granulator (TSG) systems.



## 2.1 Introduction

Granulation is a size enlargement process to form granules with controlled properties, starting from a particulate feed as raw materials. It is a key process adopted in a range of industries for production of pharmaceuticals, detergents, agricultural and food products, agro-chemicals, enzymes etc. Granulation is mainly performed to improve the flowability of powders, to reduce dustiness and co-mixing of materials which will otherwise segregate or form a cake (Litster and Ennis, 2004; Ennis, 2010). The major granule properties such as granule size distribution (GSD) and porosity, are driven by the rate of various macroscopic mechanisms during the granulation process, e.g. nucleation, aggregation, layering, breakage, consolidation (Litster and Ennis, 2004; Ennis, 2010; Dhenge et al., 2012b).

Despite the challenges involved, continuous processing has become preferable for all major industries in the past decades due to the fact that continuous operation usually comes with several benefits for the process (Table 2.1). However, the pharmaceutical industry is a clear exception, and has for many years mainly relied on conventional batch manufacturing, largely due to a rigid regulatory framework and due to uncertainty in industry about the attitude of the regulators towards more continuous production processes. Moreover, the conventional pharmaceutical quality control systems are based on off-line analysis in analytical laboratories, which is in sharp contrast to the real-time in-process analysis methods which are needed for continuous processing. Continuous real-time quality monitoring and control is indeed indispensable for efficient continuous production.

The introduction of the process analytical technology (PAT) guidance (FDA, 2004) was an important milestone for the pharmaceutical industry, since it is one of the first documents published by regulatory authorities promoting a new pharmaceutical production model based on the Quality by Design (QbD) concept. The QbD concept relies on a science- and risk- based holistic development of processes and products such that, *quality cannot be tested into products; it should be built-in or should be by design*. In addition to the new concepts considered by the Food and Drug Administration (FDA), the use of quality risk management principles and the application of an appropriate pharmaceutical quality system, as defined within the International Conference on Harmonization (ICH) documents Q8, Q9 and Q10 (ICH Harmonised Tripartite Guideline, 2009; Guideline, ICH Harmonised Tripartite, 2005; Guideline, 2006) provided the platform for establishing a new release decision-making strategy for marketed products, i.e. the real time release testing (RTRT) strategy (CHMP, 2012). Fur-

**Table 2.1:** Benefits and challenges of continuous processing

Benefits	Challenges
Improved and more consistent quality.	More precise measurement and control required.
Increased throughput.	Continuous flow and level measurement.
Reduced inventory and associated storage.	Modulating flow and level control.
Reduced raw material usage.	Real-time in-process quality measurement.
Reduced waste products.	Real-time quality control.
Improved process safety.	Integration of several unit operations, also w.r.t. control.
Reduced air, water and power utility usage.	Extensive personnel training, particularly for operators.
Reduced process footprint.	Redundant controls and instrumentation.
Reduced clean-up time.	Rapid corrections to all process variations.
Reduced operator involvement.	Advanced process control.

thermore, ICH published a more recent and extensive guidance for harmonising the scientific and technical principles related to the description and justification of the drug development and complete manufacturing process (Guideline, ICH Harmonised Tripartite, 2012). All these developments and publications have reduced the regulatory uncertainty, and opened new and exciting possibilities for innovation in pharmaceutical manufacturing, resulting in significant efforts for designing new and more efficient production strategies.

Continuous manufacturing of solid dosage pharmaceutical products is in line with the efforts aiming at improving product quality, reducing manufacturing cost, and essentially providing safer products to the patients. The *one-in-one-out* principle for the raw materials in this production scheme leads to reduced cycle times and improved process throughput. Schaber et al. (2011) showed that continuous processing has a clear economic advantage over batch processing. Cervera-Padrell et al. (2012) demonstrated that the switch from batch to continuous processing for organic synthesis of small molecules resulted in a reduction of the process mass intensity by about 50%, thus resulting in a considerably greener continuous production process. The desired paradigm shift from batch to continuous mode at production scale in the pharmaceutical sector

requires a reliable continuous granulation process.

Some of the process steps in the pharmaceutical production process are in fact continuous as such (e.g. milling, tableting), but the production of granules is typically performed using inherent batch unit operations. Various granulation techniques which are widely used in the pharmaceutical industry are summarised in Table 2.2.

**Table 2.2:** Various granulation processes used in the pharmaceutical industries

Method		Process
Dry granulation		Direct compression Slugging (double compression) Roller compaction
Wet granulation	Low shear techniques	Low shear mixer Fluid-bed granulator dryer Continuous fluid-bed granulator/dryer
	High shear techniques	High shear mixer Continuous mixer granulator Twin-screw granulator

Wet granulation is a commonly used unit operation for solid dosage form manufacturing which is attributed to the more uniform distribution of formulation ingredients that is obtained. Various wet granulation techniques including fluidised-bed aggregation and extrusion have been developed and used (Figure 2.1). However, compared to other granulation methods, the HSWG methods offer several advantages as listed in Table 2.3. As the wetting, agglomeration, consolidation and discharge are quickly performed in the same equipment HSWG is also promising with respect to switching towards continuous processing. Despite these advantages, there are some challenges compared with low-shear granulation processes: e.g. HSWG can produce less compressible granules due to over-wetting and requires a narrow range of operating conditions, which demands for strong control over the process. Vervaet and Remon (2005) reviewed the continuous granulation techniques extensively, and due to other inherent benefits in terms of ease in continuous operation, operations-integration and scale-up possibility, the high-shear twin-screw granulation system has received most attention in the last decades. Recently, Seem et al. (2015) and Thompson (2015) reviewed TSG as a potential granulation tool for the implementation into continuous processing lines. Both reviews suggested that a considerable

work remains ahead to properly understand and ensure predictable and consistent granule quality using this technology. To date these systems are even commercially available as continuous TSG, e.g. the ConsiGma™ systems by GEA Pharma Systems nv., Wommelgem, Belgium (Fonteyne et al., 2012) and Pharma 16 TSG by Thermo Fisher Scientific, Karlsruhe, Germany (El Hagrasy et al., 2013b).

Nevertheless, there is a clear need to acquire more fundamental understanding

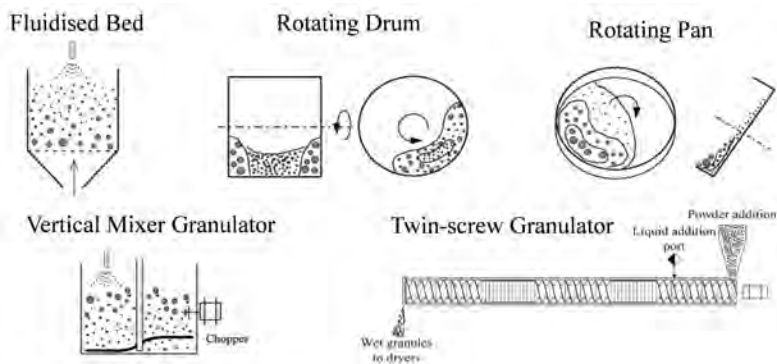
**Table 2.3:** Comparison of high-shear wet granulation to other granulation techniques

Granulation Parameter	High-shear wet granulation	Other granulation methods
Processing time	Short	Long
Operating conditions	Narrow range	Wide range
Use of granulation liquid	Less	More
For highly cohesive materials containing hydrophilic powder	Achievable	Not achievable
Densification of granules	Greater	Lower
Friability of granules	Less	More
Process reproducibility w.r.t. uniform GSD	More	Less
Reduction of process dust	More	Less
Granulation end point determination	Predictable	Poor predictability
Granule compressibility	Less	More
Hardness	More	Less

of the continuous granulation processes. Improved process understanding can then result in improvements in equipment design, process control and processing efficiency. Application of computational process modelling tools is becoming more common and now playing a crucial role in efforts to gain knowledge about these processes. Some recent reviews have underlined their diverse application in the pharmaceutical industry (Gernaey et al., 2012; am Ende et al., 2010), while validation of these models also requires reliable measurement tools to compare model predictions with the measured behaviour of the system.

## 2.2 Current modelling and related measurement tools for HSWG

It is generally accepted that the availability of mathematical process model(s) and suitable measurement device(s) for a pharmaceutical process when success-



**Figure 2.1:** Overview of types of equipment used in wet granulation

fully interlinked (i.e. performing proper model calibration and validation), can lead to functional and robust knowledge based control of process and product quality (Gernaey et al., 2012). Unfortunately, many of the parameters used in HSWG models are difficult to measure in the field, yet they have a substantial impact on the performance of the granulation models. Most of the granulation modelling based analyses are often understood to be carried out under default parameter values or best-guessed values. This is mainly due to either difficulties in experimental data collection or lack of a suitable measurement tool for the simulation model calibration and validation. It is therefore very relevant to discuss potential options among available mathematical modelling practices and related measurement technologies. Not properly calibrated and validated models later when tested result in unrealistic estimates of the impact of any change in process condition. Thus, calibration and validation of simulation models are crucial steps in assessing their value in granulation process modelling. Adjustments or tuning of model parameters through calibration are necessary to improve the ability of granulation models to replicate process measured conditions and properly reflect the impact of any change in it. This section of the review comprises the currently reported developments in modelling practices and related measurement tools of the batch HSWG in order to illustrate the degree to which this potential has been exploited thus far. This overview then allows identifying potential gaps and developing a list of unexplored possibilities for facing the challenges (Table 2.1) inherent to the continuous form of HSWG.

### 2.2.1 Mathematical modelling of HSWG

The first step in development of first-principles models for the granulation processes is to understand the mechanisms of the granulation process at micro or particle-scale. If the particle-scale mechanisms are not understood to a certain extent, an appropriate modelling of the complete system at meso- or macro-scale does not have a fair chance of success. The particle-level mechanisms for some of the key processes that may take place during HSWG have been reviewed by Iveson et al. (2001a) and respective models are summarised in appendix A, Table A.1. As not all particle-level mechanisms are well understood (e.g. wetting and nucleation), some empirical expressions are included in the model (leading to so-called semi-empirical or "grey box" models) in order to allow simulation of the granulation system.

Although the underlying mechanisms of the granulation process are still being investigated, especially in case of TSG where such detailed knowledge is not yet established (Dhenge et al., 2012b), it is well motivated to model the system at meso- or macro-scale such as to exploit the benefits of process system engineering (PSE) methods and tools (Gernaey et al., 2012). PSE tools rely on domain knowledge and mathematical and experimental techniques to build computer models which relate the change at a molecular level to macro-scale system performance in order to develop and optimise the system. The necessity of a multi-scale approach towards granulation process optimisation, monitoring and control has been documented in detail by Cameron and Wang (2007).

Several approaches are adopted for modelling of granulation processes as overviewed in Appendix appendix A Table A.2. Two main modelling approaches mostly used for HSWG processes are (1) population balance model (PBM); and (2) the discrete element method (DEM). The aim of both approaches is to model the mechanisms (discussed in Table A.1) and predict the resulting steady-state distribution characteristics such as GSD, moisture content etc. Some hybrid approaches are discussed as well to demonstrate the benefit of linking one modelling approach to another one.

#### Population balance modelling

A PBM provides a statistical description of a system of particles that are undergoing size change mechanisms leading to size increase and/or reduction. They have numerous applications in the engineering sciences apart from granulation, for example in the field of crystallisation, coagulation of aerosols, polymerisation, and cell growth to name but a few. The balance is solved to obtain statistical

properties, such as the GSD. In a HSWG process, assuming that the aggregation depends only on particle size, where size is a continuous variable, the general form of a population balance equation (PBE) for a well-mixed system is given as (Ramkrishna, 2000):

$$\frac{\partial n}{\partial t}(x, t) + \frac{\partial}{\partial x} \left[ n \frac{dx}{dt} \right] (x, t) = \mathfrak{R}_{birth}(x, t) - \mathfrak{R}_{death}(x, t) \quad (2.1)$$

where,  $x$  is scalar-state variable that represents particle size,  $n(x, t)$  represents the number distribution of particles,  $\frac{\partial}{\partial x} \left[ n \frac{dx}{dt} \right] (x, t)$  represents the continuous growth or attrition loss along the internal coordinate of the particle diameter,  $\mathfrak{R}_{birth}$  and  $\mathfrak{R}_{death}$  represent the net formation and depletion rates of particles resulting from all discrete granulation mechanisms such as aggregation and breakage. Including the effects of aggregation and breakage explicitly, the PBM becomes (Pinto et al., 2007):

$$\begin{aligned} \frac{\partial n}{\partial t}(x, t) + \frac{\partial}{\partial x} \left[ n \frac{dx}{dt} \right] (x, t) = & \frac{1}{2} \int_0^x \beta(x-y, y) n(x-y, t) n(y, t) dy \\ & - n(x, t) \int_0^\infty \beta(x, y) n(y, t) dy \\ & + \int_0^\infty S(y) b(x, y) (y, x-y) n(y, t) dy \\ & - S(x) n(x, t) \end{aligned} \quad (2.2)$$

where,  $\beta$  is the aggregation kernel,  $b(x, y)$  is breakage kernel and  $S$  is the selection function. Equation 2.2 is an integro-partial differential equation, and an analytical solution can only be found for simple  $\beta(x, y)$  and  $b(x, y)$  functions. However, these generally correspond to non-physical cases. Thus, numerical approaches are required for more complex functions describing real-life systems.

## Population balance model development for a continuous system

Granulation operations in the pharmaceutical industry are mostly performed as batch processes and therefore, most modelling studies with respect to pharmaceutical granulation have focused on batch processes. In equation 2.2, there is no spatial coordinate included in the model because a well-mixed system is assumed (i.e. no spatial variation). However, the modelling of a continuous system involves both internal and external (spatial) coordinates, which are specified in the PBEs to capture this spatial variation (Cameron et al., 2005),

as given in equation 2.3:

$$\frac{\partial}{\partial t}n(x, z, t) + \frac{\partial}{\partial x} \left[ n \frac{dx}{dt} \right] (x, z, t) = \mathfrak{R}_{birth}(x, t) - \mathfrak{R}_{death}(x, t) - \frac{\partial}{\partial z} [\dot{Z}n(x, z, t)] \quad (2.3)$$

where,  $\dot{Z}$  is spatial velocity in the external coordinate defined as  $\dot{Z} = dz/dt$ . Thus, a 1-D continuous PBE provides a description of the evolution of one evolving property of particles and the conservation of their internal attributes. Heinrich et al. (2002) discussed the modelling of continuous fluidized-bed spray granulation with recycle, which predicts the occurrence of both oscillatory steady-states as well as unique steady states in these processes. The spatio-temporal variation has also been identified in batch-scale granulators as the intensity of different granulation mechanisms varies between specific zones of the equipment based on the conditions prevailing in a granulator (Drumm et al., 2009; Garth et al., 2011; Freireich et al., 2011; Li et al., 2012). Chaudhury et al. (2015) recently presented compartment based population balance modelling of HSWG to account for the inhomogeneities within the granulator. This study showed that a multi-compartment based approach provides a better physical representation over the single compartment based model for a high-shear granulator. The particle flow pattern and their visit frequency through the specific granulator zone during the operation has been defined numerically with the use of computational fluid dynamics (CFD) and DEM. For instance, a CFD-PBM approach was used in the case of diluted particles/droplets dispersed in a fluid (Drumm et al., 2009; Garth et al., 2011). The DEM can also be combined with the PBM when a dense flow of particles is considered (Li et al., 2012; Freireich et al., 2011). Freireich et al. (2011) used this technique for large particles blended in a dual-axis mixer in the context of coating applications. The domain was separated into two compartments to represent the spray zone and the rest of the particle bed. Only layering granulation and particle coating were investigated. Particle aggregation and breakage mechanisms were not considered in the study. In case of HSWG, the PBM-DEM approach is most suitable. However, no such study was presented for HSWG until recently when Bouffard et al. (2012) demonstrated a PBM-DEM hybrid model where the particle flow was accounted for in simulation by a compartmental model, which was implemented in the PBM considering particle aggregation or breakage mechanisms. Each compartment was considered perfectly mixed and associated with one or more specific granulation mechanisms. Recently, Barrasso et al. (2015b) implemented bi-directional coupling between PBM and DEM to evaluate collision frequencies and liquid distribution as a proof-of-concept, and Sen et al. (2014) combined this work with a CFD model to simulate fluidized bed granulation. Furthermore, Barrasso et al. (2015a) applied bi-directional



coupling between granule scale DEM and PBM in case of a twin-screw wet granulation process. The model showed sensitivities to the screw configuration, process parameters such as screw speed, liquid-to-solid ratio as well as material properties such as binder viscosity and the pore saturation. Although less work has been done on continuous granulation for pharmaceuticals, a clear gain of knowledge has been obtained in other chemical industries by adopting such continuous PBE models (Wang and Cameron, 2002). In specific processes such as crystallization and flocculation where the continuous operation is more well-known, PBEs are used extensively (Kumar et al., 2008a; Hounslow, 1990; Kumar and Ramkrishna, 1996a,b, 1997).

### Multi-dimensional Population Balance Models

The accurate modelling of pharmaceutical granulation processes involving a multi-component system requires the consideration of multi-dimensional PBEs. Along with granule size, granulation liquid content has a major effect on granule growth. Several studies demonstrate that the amount of liquid directly correlates with the rate of granule growth, due to a larger availability of surface-wet granules with increased liquid dosage (Li et al., 2011; Marshall et al., 2013). Similarly, granule porosity is an essential parameter having significant effect on granule growth and breakage behaviour, deformability and strength (Marshall et al., 2013). Consequently, multi-dimensional PBEs incorporating the effect of such parameters are now frequently being developed (Pinto et al., 2007; Vale and McKenna, 2005; Qamar and Warnecke, 2007; Braumann and Kraft, 2010; Darelius et al., 2006; Immanuel and Doyle, 2005). A multi-dimensional PBE can be formulated as:

$$\begin{aligned} \frac{\partial}{\partial t} n(m, \varepsilon, w, x, t) + \frac{\partial}{\partial m} \left[ n \frac{dm}{dt} \right] (m, \varepsilon, w, x, t) + \frac{\partial}{\partial \varepsilon} \left[ n \frac{d\varepsilon}{dt} \right] (m, \varepsilon, w, x, t) \\ + \frac{\partial}{\partial w} \left[ n \frac{dw}{dt} \right] (m, \varepsilon, w, x, t) + \frac{\partial}{\partial x} \left[ n \frac{dx}{dt} \right] (m, \varepsilon, w, x, t) \\ = \mathfrak{R}_{birth} - \mathfrak{R}_{death} \end{aligned} \quad (2.4)$$

where  $m$  is total mass of the granule particle,  $\varepsilon$  is porosity and  $w$  is fractional granulation liquid content. In recent years, the number and types of multi-dimensional PBEs applied to granulation systems has considerably increased. However, care must be taken to model only the primary mechanisms in multi-dimensional PBEs, as the model may become excessively complex and numerical errors can increase prohibitively leading to inaccurate predictions. A hybrid PBE can be formulated to tackle this challenge. For example, in an aggregation only model, a two-dimensional population balance can be presented where

collision is dependent only on particle size but aggregation is dependent on both particle size and surface wetness (or stickiness). Similarly, Biggs et al. (2003) used a pseudo two-dimensional (2-D) PBM that allowed composition on a size-averaged basis to be modelled and coupled to the GSD. Verkoijen et al. (2002) proposed a formulation of the multi-dimensional PBE, where the particle attributes are re-cast in terms of their individual volumes of solid ( $s$ ), liquid ( $l$ ) and gas ( $g$ ). This modelling in terms of its individual volumes enables decoupling of the individual mesoscopic processes (i.e., aggregation, consolidation, etc. in Table A.1) and one can model a single rate process at a time. The resulting multi-dimensional PBE is thus given as (Ramachandran and Barton, 2010):

$$\begin{aligned} \frac{\partial F}{\partial t}(s, l, g, t) + \frac{\partial}{\partial s} \left( F(s, l, g, t) \frac{ds}{dt} \right) + \frac{\partial}{\partial l} \left( F(s, l, g, t) \frac{dl}{dt} \right) \\ + \frac{\partial}{\partial g} \left( F(s, l, g, t) \frac{dg}{dt} \right) = \mathfrak{R}_{birth}(s, l, g, t) - \mathfrak{R}_{death}(s, l, g, t) \end{aligned} \quad (2.5)$$

where,  $F(s, l, g, t)$  is population density of a granule at time,  $t$ ,  $(s, l, g)$  is vector representing solid, liquid, and gas volumes of a granule. This formulation has been used extensively due to the mutually exclusive character of the internal coordinates which substantially improves the numerical solution of the model as the rate processes with distinct time constants are segregated (Darelius et al., 2005, 2006; Ramachandran et al., 2009; Barrasso and Ramachandran, 2012; Chaudhury et al., 2015). Beyond this, it potentially prevents lumping in any of the dimensions due to the heterogeneity of the population distribution with respect to its attributes, which could cause model errors (Ingram and Cameron, 2010).

The increase in the number of dimensions of PBEs causes complexities which have been listed by Pinto et al. (2007). Formulation of multi-dimensional so-called rate kernels to include the constitutive relations for the particle-level rate processes is challenging. Similarly, the numerical solution of such model equations is complicated and computationally expensive. Lastly, to ensure wider validity and predictive capability of these models, the development of instrumentation for detailed measurements is required not only at the macroscopic level, but also at the particle level, i.e. at microscopic levels.

## Formulation of Kernels

Kernels contain the most important physics of the involved mechanism, and the development of multi-dimensional kernels that account for the dependence of the rates on particle properties (i.e., size, liquid content and porosity) requires

a thorough understanding of the underlying physics. Some of the important properties of theoretical, experimental and mechanistic kernels which are widely found in literature and used in granulation studies involving aggregation and breakage mechanisms are discussed here to provide an overview.

### *Aggregation kernels*

The aggregation kernel is essentially a measure of how frequent and successful a binary collision of two particles is. It is affected by two major factors: (1) collision probability of the specified pair of particles (related to transport); (2) successful aggregation or rebounding after collision (related to short range effects) (Kapur and Fuerstenau, 1969). The discrete variant of the aggregation kernel  $\beta_{i,j}(t)$  among the classes  $i$  and  $j$  is defined as the product of the collision frequency  $\beta_{i,j}$  of the particles and the aggregation efficiency,  $\beta_0(t)$  i.e.,

$$\beta_{i,j}(t) = \beta_0(t) \cdot \beta_{i,j} \quad (2.6)$$

The first factor,  $\beta_0(t)$ , depends on various process parameters such as kinetic energies of particles, their path and collision orientation, particle characteristics (e.g. mechanical properties and surface structure), viscous dissipation between approaching particles and inter-particle forces, and granulation liquid properties, aggregation mechanism, etc. Generally,  $\beta_0(t)$  is assumed to remain constant throughout the experiment and is size independent (Rao, 2009). The collision frequency  $\beta_{i,j}$  is a function of particle size, gas velocity, system temperature, etc. Determination of the collision frequency function is a complex task in most of the models and it is very difficult to determine it from experimental data. However, an alternative way of retrieving the kernels based on experimental data is to solve the inverse problem (Wright and Ramkrishna, 1992; Sathyagal et al., 1995). Braumann et al. (2010b) and Braumann and Kraft (2010) studied the inverse problem occurring in a multidimensional population balance model describing granulation employing linear response surfaces and second order response surfaces. There are different collision frequency functions for kernels available in the literature based on theoretical, empirical and experimental calculations and observations (Table A.3). These kernels have evolved from empirical to mechanistic and further to multi-dimensionality. Recently, Pohlman and Litster (2015) modified and evaluated a physically based aggregation kernel earlier proposed by Liu and Litster (2002) that can predict rate processes as a function of experimentally-verified mechanical properties and can be used in a 3D PBM. Incorporation of mechanical properties and the granule composition in the aggregation kernel was used to predict the micro-scale aggregation mechanism, which matches well with experimentally-observed induction growth during HSWG.

### ***Breakage kernel***

Evidently, the breakage functions of a PBM (eq. 2.2) are the breakage kernel,  $b(x, y)$ , and the probability distribution function,  $S$ . Compared to the aggregation kernel, research on the breakage kernels is still in its infancy. The kernels proposed in literature belong to two major categories: the algorithmic breakage kernels and the mechanistic breakage kernels (Kostoglou, 2007). To avoid the breakage kernel in high-shear granulation models, Sanders et al. (2003) and Biggs et al. (2003) tried to model breakage as a negative aggregation rate process, by reporting a reduced aggregation rate constant. However, this approach had serious flaws, as aggregation is a second order rate process and breakage is a first order rate process and will not succeed without considering any physical basis (Reynolds et al., 2005). Many attempts to model the breakage kernel have been made over the years (Table A.4).

The mechanistic breakage functions which are based on physicochemical models of the breakage process are usually very complicated and even hard to be approximated as simpler homogeneous functions (Ramachandran et al., 2009; Reynolds et al., 2005). However, almost all the algorithmic breakage functions are homogeneous and thus have been used extensively in the study of the general properties of the fragmentation equation in physics literature (Kostoglou, 2007). Dhanarajan and Bandyopadhyay (2007) presented an energy-based model for HSWG processes, whereby the extent of granule breakage was considered to be directly proportional to the impact-energy and inversely proportional to granule strength. While their model simulation showed a close association with the experimental results for the granulation recipe, it missed a rigorous physical basis by assuming that kinetic energy was solely a function of mass, and not velocity and that all collisions were elastic (neglecting loss of kinetic energy due to inelasticity). Furthermore, the granule strength was primarily considered as a function of granulation liquid content, without taking the effect of liquid properties such as viscosity, surface tension and contact-angle into account. Recently, a mechanistic breakage kernel for a high-shear mixer granulator was presented by Ramachandran et al. (2009). The derived kernel is a function of several important material properties (i.e., powder and granulation liquid properties) and process/design parameters, which influence the intermittent and end-point properties of the granule.

### **Solution of one- and multi-dimensional PBEs**

The derivation of a numerical scheme for efficient and accurate solution of population balance problems is quite difficult due to the association of integral terms

with the hyperbolic equation. However, during the past few decades, many researchers have solved PBEs and as a result different numerical schemes have been developed. Several reviews of these schemes are available and have been also compared in terms of accuracy of calculation and required computational time (Ramkrishna, 2000; Cameron et al., 2005; Abberger, 2007; Kumar et al., 2009; Marshall et al., 2011). The solution of a multi-dimensional problem is both difficult and computationally very expensive and therefore there are two different approaches to deal with an n-dimensional PBEs: (1) computation on a complete model with computationally efficient techniques and (2) computation on a reduced model.

### **Solving the complete PBE**

During the past few decades, a number of methods have been developed for numerical solution of PBEs. Among these methods, some are used to simulate the evolution of moments, while others are used to solve for the GSD explicitly. Methods available to solve for moments include various quadrature methods of moments (Marchisio et al., 2003; Marchisio and Fox, 2005; Gimbut et al., 2009; Kariwala et al., 2012). On the other hand, to solve for GSD explicitly available methods include, methods of characteristics (Kumar and Ramkrishna, 1997; Lee et al., 2002), Monte Carlo techniques, (Marshall et al., 2013; Smith and Matsoukas, 1998; Spielman and Levenspiel, 1965) and discretised methods like, the fixed-pivot (FP) method (Kumar and Ramkrishna, 1996a, 1997), the moving pivot method (Kumar and Ramkrishna, 1996b), the cell average technique (CAT) (Kumar et al., 2008b, 2006), the hierarchical two-tier method (Immanuel and Doyle, 2003, 2005), the two-level discretisation algorithm (Pinto et al., 2007), the finite volume method (FVM), the finite element method, finite-volume high-resolution method (Koren, 1993; Kurganov and Tadmor, 2000) and most recently the Lattice-Boltzmann method (Majumder et al., 2012).

Although most of the conventional numerical techniques have been applied to multi-dimensional PBEs in various studies, (Vale and McKenna, 2005; Qamar and Warnecke, 2007; Braumann and Kraft, 2010; Darelus et al., 2006; Immanuel and Doyle, 2005) the increase in computational load with increase in dimensions of the PBEs presents the challenge of obtaining the solution in process relevant time frames. Consequently, solution methods such as Monte Carlo techniques which are computationally more efficient have received most attention (Marshall et al., 2013; Braumann et al., 2010b; Marshall et al., 2011). Recently, Yu et al. (2015) presented an optimal sampling strategy based on squared Hellinger distance for the Monte Carlo simulations for an aggregation-only PBE. Their study showed a substantial saving in computational cost for higher dimensional PBEs. In a comparison study of three numerical methodologies, i.e., direct

solution by discretisation, constant-number Monte Carlo (cNMC) and direct quadrature method of moments (DQMOM), to a two-component aggregation PBE with a kernel that depends both on size and composition, (Marshall et al., 2011) showed that the cNMC method is in close agreement with the direct discrete solution in all cases which assumed to provide exact solutions however being computationally very expensive. The DQMOM method has been found to be highly accurate when the kernel is independent of composition. When the kernel is composition dependent, accuracy of this method was found to be variable and very sensitive to the details of the initial distribution.

Due to the inherent nature of discretised methods to preserve the properties of the distribution, extensive work has been done particularly on the F method and the CAT, which have been extended later to improve the applicability with increase in number of dimensions (Kumar et al., 2008a; Vale and McKenna, 2005; Chakraborty and Kumar, 2007; Nandanwar and Kumar, 2008). To compare these developments by solving two-dimensional aggregation PBEs, Kumar et al. (2011) found that the CAT is quite a stable scheme as compared to the F method and improves the results both for the number density and for the higher moments. Thus, the formulation of the CAT can technically be extended to more than two-dimensional problems but it can be computationally very expensive which is also evident by the results shown by Barrasso and Ramachandran (2012).

The overall outcome of such comparison studies are always a compromise between prediction accuracy and speed. To account for more physical parameters in PBM and apply mechanistic kernels based on a Lagrangian model (such as from DEM) the direct solution methods based on Eulerian coordinates are known to be computationally more efficient. As such technique is not developed, discrete stochastic methods based on Monte Carlo techniques still have an advantage on efficiency along with other benefits addressed earlier.

## **Reduced order multi-dimensional PBE**

For each additional component used in the pharmaceutical formulation, a new dimension shall in principle be added to the PBM. While this approach may work in theory, its increased computation time and complexity limits its applicability. A practically more feasible strategy is that a high-dimensional PBM can be reduced to several simpler models of lower dimension (Biggs et al., 2003; Hounslow et al., 2001; Gantt et al., 2006). In a reduced order model, one or more granule characteristics are lumped into the remaining distributions. For

example, a two-dimensional model given by

$$\begin{aligned} \frac{\partial}{\partial t} f(v, v_L, t) = & \frac{1}{2} \int_0^v \int_0^{\min(v_L, v-\varepsilon)} \beta(v-\varepsilon, v_L-\gamma, \varepsilon, \gamma) f(v-\varepsilon, v_L-\gamma, t) f(\varepsilon, \gamma, t) d\varepsilon d\gamma \\ & - f(v, v_L, t) \int_0^\infty \int_0^\varepsilon \beta(v, v_L, \varepsilon, \gamma) f(\varepsilon, \gamma, t) d\varepsilon d\gamma \end{aligned} \quad (2.7)$$

where, the granule is represented by total volume,  $v = v_s + v_L$ , and  $v_L$ , volume of the liquid. In this 2-D model, the coordinate space  $x = (v, v_L)$  can be reduced to two 1-D equations, by assuming that all of the granules of a given size have the same liquid content, as follows (Biggs et al., 2003):

$$\frac{\partial}{\partial t} n(v, t) = \frac{1}{2} \int_0^v \beta(v-v', v) n(v-v', t) n(v', t) dv' - n(v, t) \int_0^\infty \beta(v, v') n(v', t) dv \quad (2.8)$$

$$\frac{\partial}{\partial t} M(v, t) = \frac{1}{2} \int_0^v \beta(v-v', v) M(v-v', t) n(v', t) dv' - M(v, t) \int_0^\infty \beta(v, v') n(v', t) dv \quad (2.9)$$

where,  $M(v, t)$  is mass of granulation liquid in the size range. Reduced order models simplify the solution of the model, but they are not exactly equivalent to the full model. Hounslow et al. (2001) warned against model order reduction for parameters that influence the rates, as it is expected that these rates are a function of composition such as the liquid content within individual granules. Recently, Barrasso and Ramachandran (2012) compared a full 4-D model with a combination of lower-dimensional models resulting from a model reduction using the lumped parameter technique, and showed that although the 3-D model with a lumped solid volume yielded results similar to the full model, it showed differences in the distribution of composition with diameter. This drawback is probably most relevant since the composition is important in multi-component granulation processes with respect to pharmaceutical production.

Rigorous calibration and validation of the PBM is key for scientific and commercial acceptance, but is equally challenging due to high variation in the process output. In the modelling of granulation processes discussed so far, the inverse problem is often unavoidable. Therefore, experiments have to be carried out in order to identify and measure the unknown model parameters, e.g. aggregation rate constants (Wright and Ramkrishna, 1992; Sathyagal et al., 1995; Braumann et al., 2010a; Braumann and Kraft, 2010). Such parameter estimation is normally done through fitting the model to the experimental data

obtained from measurement of macroscopic quantities and will be discussed in section 2.2.2. Once these model parameters are validated, the model can be employed for predicting the granulation process using the system under consideration.

## Discrete Element Method

Whilst the majority of granulation research at the meso- and macro-scales has been performed using PBM, the DEM approach bridges the gap between micro- and meso-scales (Gantt and Gatzke, 2005; Gantt et al., 2006; Lian et al., 1998; Nakamura et al., 2013; Ketterhagen et al., 2009). There are two main classes of DEMs which have been used in granulation modelling: hard-sphere methods and soft-sphere methods, each with their state of development, relative advantages and drawbacks (Table 2.4). These approaches have been applied and reviewed by several researchers (Gantt and Gatzke, 2005; Zhu et al., 2008; Ketterhagen et al., 2009; Herrmann and Luding, 1998; Liu et al., 2013), and a wide variety of different granulation systems have been modelled. The hard-sphere method assumes that particles are rigid so that collisions are instantaneous and binary, which is not valid in highly dense HSWG systems where particle contacts are long-lasting, have low coefficients of restitution and involve multiple particles. In the soft-sphere model, on the contrary, contacts are not assumed to be instantaneous and more than one contact at a time is possible.

Developed by Cundall and Strack (1979), soft-sphere DEM has been preferably used in granulation modelling where positions, velocities, accelerations and the trajectories of every particle are tracked by solving Newton's second law of motion in a particulate assembly individually. This method allows deformation of particles which is modelled as an overlap of the particles in a collision event. The forces are expressed with the use of a spring, dash-pot and slider which separate forces into normal and tangential forces as shown in Figure 2.2. The linear and angular momentum equations for each granule in the granulator are given by

$$m_{ii} \frac{d\mathbf{v}_{ij}}{dt} = m_i g + \vec{F}_p + \vec{F}_w \quad (2.10)$$

$$I_i \frac{d\omega_i}{dt} = \vec{M}_p + \vec{M}_w \quad (2.11)$$

The sum of applied forces includes contributions from contact forces resulting from particle-particle and particle-wall collisions and the gravitational force  $m\vec{g}$ . The viscous drag force is often assumed negligible in high-shear dense granular systems. The associated moment is the sum of the moments of particle-particle

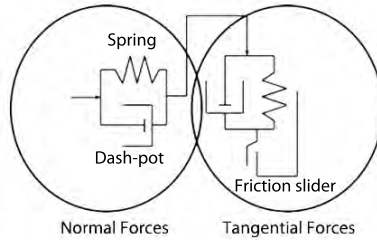


**Table 2.4:** Advantages and drawbacks of various DEM schemes

Hard-sphere models	Soft-sphere models
<p><i>Advantages:</i></p> <ol style="list-style-type: none"> <li>1. High accuracy in the particle dynamics as the Newtonian equations of motion for each individual particle are solved with inclusion of the effects of contact forces acting on the particles and gravitation.</li> <li>2. Larger number of particles can be included into the hard-sphere models compared to soft-sphere models.</li> </ol>	<ol style="list-style-type: none"> <li>1. Promising tool for studying the effect at particle level of changes in some of the physical parameters involved in the granulation process.</li> <li>2. Theoretical particle level models may be validated using the soft-sphere approach as numerous variations in the physical/chemical parameters may be simulated relatively fast once the simulation program is set up.</li> <li>3. Well suited for studying the modelling of impact breakage of pre-existing agglomerates which is important in high shear granulation systems.</li> </ol>
<p><i>Drawbacks:</i></p> <ol style="list-style-type: none"> <li>1. Generally not suitable for realistic representation of the granule microstructure (i.e. the internal distribution of primary solids, granulation liquid and porosity of the granule).</li> <li>2. Present models are only capable of accounting for 1 million particles at a time, thereby making simulations comparable only to experimental data from laboratory scale equipment.</li> </ol>	<ol style="list-style-type: none"> <li>1. Struggle with high computational processing demands.</li> <li>2. Detailed information of binary collisions is far from being representative of the situation inside a dense particle high shear system and requires more research.</li> </ol>

$(\vec{M}_p)$  and particle-wall  $(\vec{M}_w)$  collisions.

DEM models have some advantages over PBM in terms of ability to define complex particle-particle interaction laws and to allow distribution of properties, for instance, distribution of sizes or varying material properties to model a mixture of various components. Since powder characteristics and essential hydrodynamic parameters regarding liquid-solid interaction, particle mixing and segregation are lumped into the kinetic rate constants, PBM cannot be



**Figure 2.2:** Representation of normal and tangential contact forces using a spring, dash-pot and slider approach (Cundall and Strack, 1979).

applied for a-priori process design, unlike DEM. Moreover, DEM can be used to calculate many particle-scale quantities of interest such as local concentrations and particle phase stresses, as well as to examine particle-level phenomena such as segregation or aggregation, as the location of the particles along with the velocity field is known throughout the simulation (Gantt and Gatzke, 2005; Nakamura et al., 2013). However, this all comes at a high computational cost, which is due to the small integration time-step used in DEM, so that particles only have contact with their nearest neighbours. Overlap between particles is assumed to be small in comparison to their size. Since this approach demands significant computational power, DEM cannot handle a very large number of particles which are present in high shear granulation. However, due to the steadily increasing speed of computer hardware and codes with parallel processing capabilities, the size of systems that can be modelled with DEM is continuously increasing. Some recent DEM models simulate systems in the order of a couple of hundred thousand till more than a million particles (Gantt et al., 2006; Cleary and Sinnott, 2008) and, recently the DEM method has been used in scale-up studies (Nakamura et al., 2013). Also, in a study for continuous HSWG using TSG, the DEM can be very valuable to predict the velocity profile of the powder materials which can then be used to calculate the residence time distribution (RTD) in TSG, which is otherwise very hard to measure (Lee et al., 2012). Barrasso et al. (2015c) presented the application of DEM in training of an artificial neural network (ANN), which was subsequently used in iterative simulations using a PBM, for the enhanced computational efficiency. The simulation based on this hybrid model was found to be much faster than PBM-DEM coupled simulation and the GSDs from both PBM-DEM and PBM-ANN simulations showed good agreement.

Talu et al. (2000) modelled aggregation and breakage in 2D shear flow of a mixture of "wet" and "dry" particles showing the effect of the amount of granulation

liquid, the Stokes number, and the capillary number on the GSD. Muguruma et al. (2000) modelled a centrifugal tumbling granulator where the liquid was uniformly distributed. The resulting velocity profiles were in agreement with experimental data using glass beads of the same size. Mishra et al. (2002) examined the aggregation of particulates in a rotary drum with a model that included a spray zone and also considered the drying of particles. The first significant effort for DEM modelling for HSWG systems was undertaken by Gantt and Gatzke (2005), which incorporated three key mechanisms of granulation, i.e. aggregation, consolidation, and breakage. The rates of each mechanism were directly simulated and integrated to model a dynamic GSD. The results from this DEM model were in good agreement with other approaches such as PBM along with additional capability to model dynamic operating conditions. Later Gantt et al. (2006) also used the hybrid approach where a DEM model with periodic boundary conditions was used to represent flow in a high-shear granulator. The particle collision statistics compiled by the DEM simulation were used to develop an aggregation kernel, which was used with a Monte Carlo method to solve multidimensional PBEs. Good agreement with experiments was observed in terms of velocity flow fields. Recently, Liu et al. (2013) investigated the transverse mixing of wet particles in a rotating drum to investigate the effects of liquid surface tension, drum rotation speed and the filling level on particle mixing. DEM was proposed to estimate the circulation periods at different streamlines which were comparable with the simulation results, thus providing a general method to predict mixing performance in the transverse plane. Granulation in fluidized beds has also been modelled using DEM by several researchers (Goldschmidt, 2001; Goldschmidt et al., 2003; Fries et al., 2013).

While these studies indicate a trend of increasingly applying DEM as tool to simulate dense particle systems, there has been no satisfactory effort to calibrate the DEM in order to be able to reproduce the complicated granulation process and deploy the versatility of DEM. The calibration process in DEM is a typical inverse problem similar to PBM and is usually carried out based on data from laboratory test results, which are compared with simulation results for the identified parameters in terms of change in shape, size, strength etc. However, compared to PBM, the calibration and validation of DEM models do not appear to be as rigorous and the procedures certainly are not as well defined. There are several micro-scale related parameters involved in determining the macro-scale behaviour for granules. For calibration of granulation processes incorporation of micro-scale material properties such as wet granule yield strength, Young's modulus, and asperity size are required along with material flow characteristics such as velocity and shear fields. Efforts to develop a calibration and validation procedure for DEM based on experimental data have already been taken in

other processes (e.g. for discharge flow in silos (González-Montellano et al., 2011) and mixing in the turbula mixer (Marigo et al., 2013)). However, despite the fact that a number of measurement tools are already in place for HSWG (section 2.2.2), development of a detailed calibration and validation procedure for DEM applied to HSWG will require several other measurement tools to be developed as well (section 2.2.2) to achieve sufficient process understanding.

## 2.2.2 Measurement techniques

The literature reveals that a wide variety of measurement techniques have been applied to measure and understand the critical process parameters (CPPs), critical quality attributes (CQAs) and their relationships in HSWG. The most frequently reported measurement techniques for HSWG are overviewed in Table A.5. This table furthermore highlights for which type of model the measured value could be useful as calibration and validation input. Although there is sparse work on the model calibration and validation, some of the available studies are cited for reference. Finally, the capability of each measurement technique for real-time monitoring and, hence its applicability to continuous granulation processes is indicated. Discussions on validation studies have appeared considerably more frequently in the literature than those regarding calibration. Most validation studies for granulation models have been qualitative and rely on data from visualisation of experimental flows where the observations are used to validate granulation models for high-shear granulators (Sanders et al., 2003; Braumann et al., 2007; Van Melkebeke et al., 2008; Ramachandran et al., 2009). The qualitative studies have primarily focused on model fitting of endpoint determination parameters such as granule size and their physical properties. As the in-line measurements during HSWG are very complex and challenging due to the high shear conditions these studies applied mostly offline measurement tools. However, several in-line measurement techniques for determination of the GSD have been recently developed as well. Focused beam reflectance measurement (FBRM) and Parsum (spatial filter velocimetry) are designed to directly track real-time changes in particle size and distribution in the process (Fonteyne et al., 2012). El Hagrasy et al. (2013a) performed a feasibility study towards the implementation of Eyecon™, a 3D high-speed imaging camera, for the in-line monitoring of continuous wet granulation using TSG to analyse its capability for real-time process control. This study demonstrated the sensitivity of the Eyecon™ to variation in process parameters, but also suggested a strong leverage towards larger particles during monitoring. Betz et al. (2003) have described a technique for measuring tensile strength of granules, in addition to power consumption measurement, to facilitate optimal endpoint determination. Also, near infrared (NIR) and Raman spectroscopy have shown to be promising due to their ability to provide both chemical as well as physical information such as

moisture content and particle size of the samples while monitoring in-line (De Beer et al., 2011). Other data handling techniques reported in the literature include the use of neural networks to describe and predict the behaviour of the wet granulation (Watano et al., 1997) or control of the endpoint in HSWG on the basis of the data acquired with a high-speed imaging system (Watano, 2001) and audible acoustic emission (AE) piezoelectric sensors. However, extraction of useful information often requires chemometric model development and validation (Roggo et al., 2007). All these techniques have shown to be promising for application in HSWG, and eventually they can be used to validate various conceptual models of the process. However, each process analyser has its own limitations hampering its application as an accurate in-line monitoring and endpoint determination tool (see table A.5). Therefore, adaptations to the various analysers are now being made to solve some of these issues. For example, in new equipment set-ups for the HSWG, the air exhaust has been used to suspend the AE sensor, which eliminates the challenge of maintaining consistent contact between the sensor and the vessel. This allows measurement of a variety of particle interactions instead of localized contacts between the particles in the granulator (Hansuld et al., 2012). Similarly, the fouling issues of the FBRM probe have been solved by providing a pressurized air activated mechanical scraper on the sapphire measurement window to prevent powder from sticking. The effectiveness of the scraper has already been proven in the harsh conditions of a high shear granulator (Huang et al., 2010).

The visualization of experimental flows during validation studies is very challenging due to the opacity of bulk solids which limits the applicability of visualization techniques. Tomographic techniques have also been developed towards validation of 3D granular systems. These techniques are non-intrusive and are not hindered by the opacity of solids. Therefore, they are used to probe the internal microstructure and particle velocities within 3D systems. Nuclear magnetic resonance (NMR) has been used for validation of a long rotating cylinder (Fukushima, 1999) and the packing of particulates has been examined using X-ray micro-tomography (Sakellariou et al., 2004). Nilpawar et al. (2006) applied an optical technique which is known as particle image velocimetry (PIV), where the powder surface provides the texture for determination of surface velocities. The shortcoming of PIV in terms of its capability to interrogate only the powder surface, has been solved by application of the positron emission particle tracking (PEPT) technique which provides an excellent means to interrogate the powder flow patterns in wet granulation (Laurent, 2005). There are still some challenges as it is difficult to obtain spatial high-resolution data through PEPT and also the temporal averaging required makes tracking of the changes in bulk motion during a granulation process very difficult (Reynolds et al., 2007).

However, such developments are very important as they will aid in obtaining better process visualisation and gaining deeper process knowledge and thus they are potentially useful to support the development of strategies for achieving process consistency and improved control in the context of PAT applications.

## **2.3 Needs and opportunities for continuous HSWG modelling and measurements**

Despite the large amount of research that has been done on modelling and measuring the granulation process, much of the work done in this area is still far from application in the pharmaceutical industry. This is partly due to the fact that the granulation studies have been usually approached from either a process engineering (modelling) or a pharmaceutical sciences (measurements) point of view (see chapter I, Fig. 1.1). To have more insight in an optimal granulation process both disciplines have to be integrated. An increased knowledge about rate processes, their interaction and quantification by advanced measurement tools, along with model refinement are required in order to improve the prediction of the process state in a continuous system. This will also help in establishing significant process understanding required in order to successfully shift towards continuous processing in solid dosage manufacturing. Continuous HSWG is performed using TSG, characterized by a modular screw profile including a sequence of different screw elements with various shapes, orientation and functions. Because the residence time is very short in TSG, in general, it is possible to achieve a quasi steady state operation in a few minutes from the start. This state is measured in terms of parameters such as steady torque, stable temperatures, and an acceptable granule quality. Although a stabilization period is needed to reach steady-state conditions the granules and tablets produced during quasi-steady state operation were reported to be within specifications (Vercruyse et al., 2013a). Key independent process variables of the HSWG process using TSG include screw configuration, screw speed, temperature and locations for liquid feed. The key dependent process variables are feed rates of the formulation powder, granulation liquid feed rate and motor torque. The screw design influences the granulation characteristics and the overall processability for a given formulation, i.e. the achievable dry powder blend throughput. For a given screw design and screw speed, the maximum powder feed rate is defined by the rate at which the torque is 80% of the manufacturer-recommended limiting torque (Ghebre-Selassie and Martin, 2003). The maximum liquid feed rate is defined depending on the moisture-carrying capacity of the formulation powder blend.

From a process technology perspective, a TSG is often divided into different zones, e.g., feed (twin screw granulators are generally fed from external feeders), wetting, mixing, and others (Figure 2.3). The processing zones of the TSG are arranged in series, linking each granulation step to the next. Analysing each granulation step in the TSG to a satisfactory degree is only possible when sufficient information on the rheo-kinetic characteristics (such as apparent viscosity) of the granulation mixture is available. However, providing these data is very difficult, particularly in the zone with considerable change in phases (e.g. intrinsic moisture in granules gets squeezed out in the kneading zone). The modular structure complicates the process design as the processing zones are not just governed by the screw profile only but also by factors such as the critical moisture content (solid to liquid ratio) of the particle required for aggregation to occur. This reinforces the need to resort to process modelling and real-time measurements for development of improved process understanding. To understand mixing and granulation using different screw configurations, simulation tools could be useful to reduce the amount of experiments needed in industrial practice. By using in-process measurements, combined with a mechanistic modelling framework, one can have a good mechanistic insight into the important parameters of continuous TSG. Also worth mentioning is that extrusion based devices have been applied successfully in plastics and food industries for several decades, and thus a wealth of relevant knowledge on modelling and measurements developed in these industries during the past years can be obtained (Kohlgrüber and Bierdel, 2008). However, it is also necessary to identify fundamental differences between a twin-screw extruder and TSG design in terms of other structures such as the die (where pressure is built up for shaping) which is not present in TSG.

### 2.3.1 Needs of modelling TSG

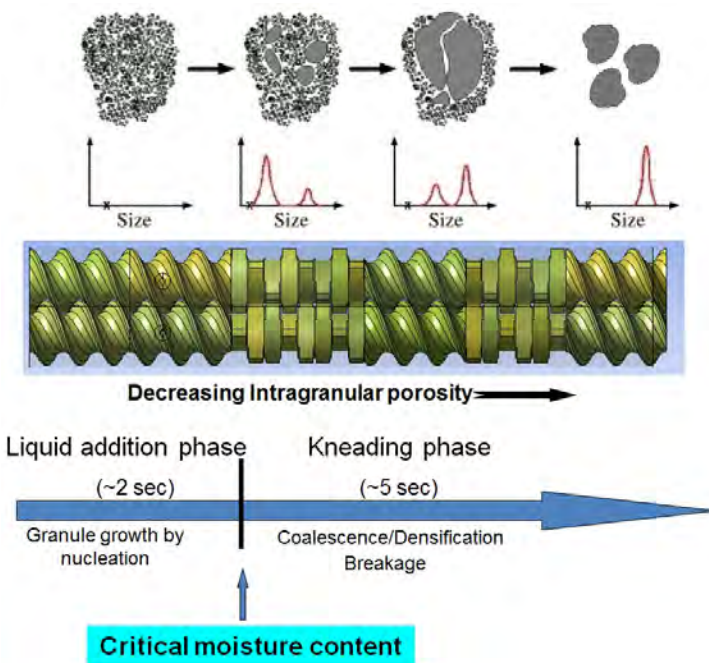
There are different goals for modelling TSG including improved process knowledge, screw design optimisation, simulation of individual effects, qualitative studies, or developing on-line monitoring and control solutions. Several experimental studies have been performed to investigate the effects of key process variables (Fonteyne et al., 2013; Dhenge et al., 2011, 2012a; Vercruysse et al., 2012, 2013a), screw configurations (Lee et al., 2012; Van Melkebeke et al., 2008; Djuric, 2008; Thompson and Sun, 2010; Vercruysse et al., 2015; El Hagrasy and Litster, 2013), formulation variables (El Hagrasy et al., 2013b; Dhenge et al., 2012b) and also to make the regime map (Tu et al., 2013) of the TSG. Similarly, efforts have been made to theoretically simulate the wet-granulation in TSG (Paavola et al., 2013; Barrasso et al., 2013, 2015a,b). However, an integrated effort is required for linking new experimental and theoretical find-

ings regarding granulation mechanisms and kinetics into a coherent modelling framework.

Results obtained from experimental studies on TSG have indicated that the mechanisms occurring in HSWG using continuous TSG are different from those in batch high shear mixers (HSM), since some of the rate processes given in Table A.1 appear to be absent in case of HSWG using continuous TSG (Lee et al., 2012; Dhenge et al., 2012b; Lee et al., 2012). Attributed to the interlinked modular structure of the screws in TSG, this prompts for substantial process understanding both at particle and containing barrel (system) levels, and thus requires a multi-scale approach. Applications of PBM (system level) and DEM (particle level) approaches in granulation have already shown their relevance in modelling batch granulators and mixers. Hence, the opportunity exists to adapt these modelling approaches for appropriate numerical analysis of TSG. However, this adaptation requires consideration of material and equipment properties along with a comprehensive list of process variables and status (Figure 2.4). These basic models at different levels should be linked using multi-scale integration frameworks in such a way that the granule scale model needs to supply the agglomeration kernel to the system scale model (Ingram et al., 2004). To do so, the granule scale model requires the current GSD and the volumetric hold-up of the granules from the barrel scale. This approach has provided good results in other studies with continuous drum (Ingram and Cameron, 2005) and fluidized bed granulators (Rao, 2009).

Various studies have shown that changes in screw configuration (number and location of transport and kneading elements) (Van Melkebeke et al., 2008; Thompson and Sun, 2010) and the screw geometry (such as distributive mixing elements) (Sayin et al., 2015) lead to different GSDs and granule properties. This indicates that although operational regimes are not completely decoupled along the length of the granulator, specific individual rate processes will preferably take place in certain screw regions. Any change to the screw configuration also changes the dominance of one granulation mechanism over the other. Thus the spatio-temporal variation in the macro-environment of the particle dictates the change in the granulation regime in the TSG unlike well-mixed systems. In the current PBM for batch granulation processes, the hydrodynamic parameters are lumped in the rate kernels such that one global equation is applied. However, such assumptions are not valid for TSG with modular structure, and therefore a multi-scale modelling approach is required in which DEM and PBM are combined via a compartmental model (CM) to include the system heterogeneity in the continuous TSG. This approach has already been applied to mixing and coating equipment which involved particle flow patterns having a strong influ-





**Figure 2.3:** Interlinked granulation zones in a twin-screw granulator.

ence on coating distributions (Li et al., 2012). Very recently, a similar approach was applied by Bouffard et al. (2012) to rotor based equipment where a CM was used to model particle flow in different zones of the equipment. The PBM based on time-continuous Markov chain received kernels from DEM to simulate particle motion in each compartment. The results from the study proved that such an approach improves the accuracy of the population balance model while the flow pattern of the particles is also successfully modelled. In short, TSG modelling requires the inclusion of spatio-temporal variations occurring within the system.

The process in the granulator is perceived as a spatially one-dimensional process for simple representation, i.e. the individual processes happen along its length axis in different zones. On the other hand, individual effects over the screw cross-section, such as some "fields" are impossible or extremely difficult to measure due to the number of factors (operational parameters and material properties) involved. However, such parameters are required for the reliable prediction of a number of factors such as mixing degree and moisture content of the formulation mixture in the granulation critical region of the barrel. To

this purpose, process models with at least a two or ideally a three-dimensional spatial consideration are needed. The accuracy of the model, however, depends on the material data used and the peripheral conditions. The spatial borders of the model (between the two screws and between the screw and barrel) require boundary conditions to be defined and stated.

The co-rotating screws are generally operated continuously, so the focus of modelling is on steady processes for process study. However, in addition to the spatial model dimensions, time may be a key factor in TSG. Therefore, key granulation parameters such as granule size, moisture content, and segregation patterns which exist in the form of a distribution can be a characteristic function of the local residence time and RTD of the granulation powder along with the spatial variation in the process model. A pharmaceutical granulation mixture with two or more main flow components travelling differently can cause segregation leading to quality problems identified in later processing steps. Numerous attempts have been made to model and predict RTD in engineering research using TSE in similar isothermal operation. Gao et al. (2012) recently reviewed RTD modelling methods including the investigations focused on the co-rotating twin-screw extrusion devices. The application of DEM or CFD simulation provides particle tracking information which can be used to derive the RTD. However, computational data should be validated with experiments before the simulated RTD profile can be applied in practice with confidence (Gao et al., 2011; Sarkar and Wassgren, 2009).

Thus, the possibilities of the modelling approaches are numerous and can be summarized as: (1) Modelling tools are capable of providing information on process values (pressure, power, stress, etc.) with little effort; (2) Application of 1-D spatial models are limited to the granulation kinetics and can provide information about the changes in the process values along the screw geometry; (3) For detailed knowledge on the granulation process in a continuous system, "field" variables such as rheological effects have to be linked with kinetic parameters in the process model; (4) The detailed modelling approach can enable a rapid process window definition and will help in determination of the effects of changing screw configuration (or geometry), process values and materials; (5) A CM based approach is required to include the system heterogeneity in the continuous TSG (6) RTD determination requires both computational and experimental efforts so that the simulated RTD profile can be validated.

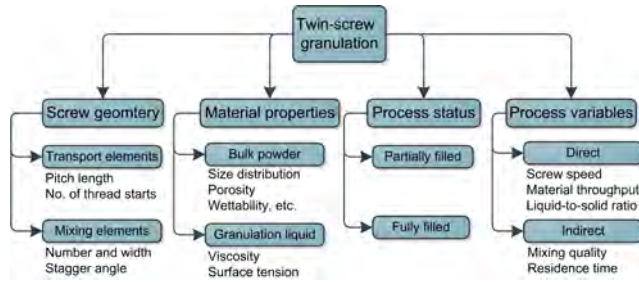
When making a choice between all the possibilities for constructing a process model, limitations are caused by the fact that modelling and simulation are confined to systems with very specific material properties. Moreover, limited

computational power is a major limitation as well. The theory often contains parameters that are not experimentally accessible (such as capillary (surface tension) forces for the aggregation) and this limits its application. Therefore the potential for a successful process modelling study for HSWG in TSG lies either in simpler models with limited applications or in proper planning of modelling studies by (a) defining modelling goals and objectives, (b) determine suitable modelling tool, (c) determining required experimental data, (d) choosing measurement tools to acquire that data and finally (e) apply measured data for model calibration and validation.

### 2.3.2 Tools for measurement of state variables

There has been a significant development in the measurement techniques for end-point determination parameters as discussed previously (section 2.2.2). While, many of these currently measured variables are applicable to various modelling approaches as given in Table A.5, more analytical methods are needed to measure other internal process characteristics (e.g., degree of mixing, moisture content, shear). The developments in measurement tools thus far primarily focused on measuring variables, which are either quality parameters themselves or indirectly used to determine the quality of granules as discharged product (such as torque, NIR). Fonteyne et al. (2013) and Vercruyse et al. (2012) have evaluated the CPPs and CQAs influencing the granule characteristics in a continuous granulation using TSG. For mechanistic understanding of the granulation process in TSG and validation of rheo-kinetic models, local information about numerous parameters such as "field" variables, granulation liquid content, filling degree of the barrel and many more mentioned in Figure 2.4 are required to be measured in-line throughout the granulator barrel. However, it is important to note that these measurements are only required in the stage of knowledge development and later on these measurements are not really required as with mechanistic understanding maybe correlations between them and more easily measurable variables can be obtained.

In the current measurement practices there are two general methods applied, those in which material is withdrawn for analysis, and the other in which material remains in the process and the observation is taken from a free surface or from material next to a wall which is transparent (Bridgwater, 2012). Free surface sampling are only easy in processes containing air and operating close to atmospheric conditions which is not the case in granulation using TSG. Being an opaque multiphase system, several crucial process parameters in TSG such as mixing and filling degree of the barrel which cannot be easily measured and monitored during the granulation are correlated with the mechanical power consumption and in-line dynamic torque of the TSG (Watano, 2007). However,



**Figure 2.4:** Key parameters for measurement and modelling of a twin-screw granulator.

the real world is 3-dimensional and 0-dimensional measurements such as a torque measurement generally relate to the entire screw, making such measurements not suitable to provide local information. In the plastic and food industries where TSE has been used extensively, such studies have been performed by having small windows in the side of a metal barrel or by using a transparent barrel in combination with probes such as Laser Doppler Anemometers (Chiruvella et al., 1996; Bigio and Stry, 1990). The other approach consists of flow visualization in a barrel using radioactive particle tracking methods such as PEPT, or imaging techniques such as PIV (Barigou, 2004). The obtained velocity profile in TSG has further been utilized to construct RTD profiles (Lee et al., 2012) and study the effect of a change in viscosity of the granulation liquid (Dhenge et al., 2012a). Several techniques, which are being used in other areas of research, also facing the challenge of opaque multiphase systems need to be investigated. For instance, magnetic resonance imaging (MRI) is capable of examining various systems and processes non-invasively and non-destructively to provide temporal and spatial information through concentration mapping in a TSG (Choi et al., 2004).

In recent years, considerable attention has been paid to the development of several rapid and non-destructive so called on-line soft sensing methods to estimate hard-to-measure on-line quantities through chemometric models. In essence, the core of a soft sensor is the soft sensing model, which on the basis of other measured variables generates a virtual measurement to replace a real sensor measurement (Kadlec et al., 2009), for example for a variable that is difficult to measure otherwise. The introduction of PAT has led to a tremendous increase of the number of spectroscopic applications in the pharmaceutical industry (Fonteyne et al., 2015). The capability and applications of NIR and Raman spectroscopy to provide both chemical as well as physical information such as moisture content and particle size on a real-time basis using chemometric methods have been discussed in a previous section on measurement techniques.

Soft sensors based partial least squares (PLS) regression or principal component analysis (PCA) are often preferred, since these methods are well-known in the pharmaceutical industry which facilitates validation (Gernaey and Gani, 2010). Nevertheless, it has been shown that a number of chemometric methods can effectively be used to extract relevant information; their application needs more investigation before introduction for field application. With the development of models of the underlying processes in TSG, preferably a model involving in-depth knowledge of the underlying physical phenomena of the process, prospects for application of soft sensors will improve.

The possibilities of the measurement approaches can be summarized as: (1) 0-dimensional measurements such as torque are easy to implement, but do not provide local information required for a detailed process understanding. (2) Higher dimensional measurements are hard-to-measure on-line but mandatory. (3) Obtaining detailed information about the "field" variables in the screw cross-section using flow visualization in a barrel is possible now. Techniques such as PEPT which can provide detailed quantitative information on internal flow-patterns have a great role to play. (4) Developments in other research areas, also facing the challenge of opaque multiphase systems, should be explored. (5) Application of soft sensing methods has shown potential, but their application needs more investigation before introduction of soft-sensors for field application.

As a general conclusion, the modular structure of the TSG is a central issue to be captured in the modelling with the measurement techniques. To understand the changes in the process values along the screw geometry, in-process measurements providing local information and a higher dimensional modelling is required. One single simple model cannot predict the complex granulation behaviour with shifting granulation regimes. Therefore, different parts of the granulation process should be described by different mechanistically based structural models. Once a complex model unravelling the granulation regimes is available, further efforts towards model reduction are required to describe the entire system with a lower computational load, allowing their usage in flow sheet simulations and process control. Additionally, although particle scale simulations can substantially increase the understanding of the processes, not all process steps of TSG can be modelled using this modelling approach due to the high computational burden.

---

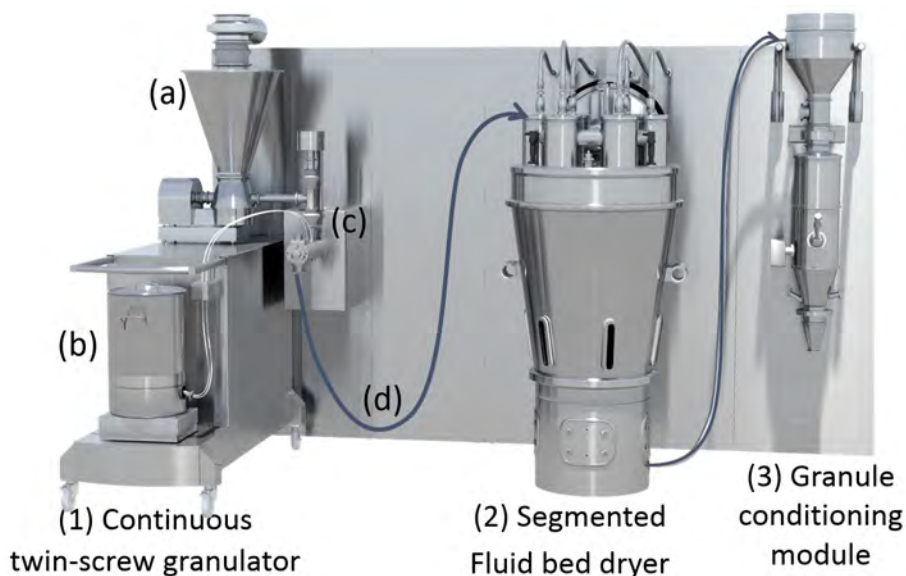
## Continuous twin-screw granulator in ConsiGma<sup>TM</sup> manufacturing line and Thesis objectives

---

The opportunity to change the manufacturing paradigm in the pharmaceutical industry from predominantly batch processing to a fully integrated continuous processing has become accomplishable in the last decade. Beside the recently perceived increased regulatory freedom, a major credit also goes to the equipment manufacturers for their support towards development of a continuous from-powder-to-tablet manufacturing lines. However, extensive research is still needed to support this transition both in terms of developing the detailed understanding of the unit operations, as well as propagating this to process design and control.

The first fully continuous manufacturing line, ConsiGma<sup>TM</sup>-25 introduced by GEA Pharma Systems (Collette<sup>TM</sup>, Wommelgem, Belgium) is installed in the Faculty of Pharmaceutical Sciences at Ghent University (Fig. 3.1). The continuous line consists of three major units: a continuous high shear twin-screw granulator (1 in Fig. 3.1), followed by a six-segmented fluidized bed dryer system (2 in Fig. 3.1) and a granule conditioning module (3 in Fig. 3.1). After discharging, a lubricant can be added and blended into the dried granules, after which this mixture can be compressed using an in-line tablet compression machine.

To develop knowledge regarding different aspects and units of the continuous manufacturing system, several earlier projects (Van Melkebeke, 2009; Fonteyne, 2014; Verduyck, 2014; Mortier, 2014) as well as ongoing projects have been undertaken. The focus of this PhD dissertation is in line with these efforts, having the scope limited to developing knowledge regarding the continuous



**Figure 3.1:** Three main units of the continuous manufacturing line, ConsiGma™ by GEA Pharma Systems (Collette™, Wommelgem, Belgium). The continuous twin-screw granulation system contains (a) powder feeder, (b) liquid addition system and (c) twin-screw granulator (d) wet granules transfer line (Courtesy of GEA Pharma Systems).

twin-screw wet granulation system.

### 3.1 Continuous twin-screw wet-granulation

The twin-screw granulation module consists of a powder feeder, a granulation liquid addition system and a twin-screw granulator (TSG). The powder feeder to the TSG (a in Fig. 3.1) operates based on the loss-in-weight-controlled principle, and feeds the powder continuously into the granulator (c in Fig. 3.1). The weight loss during the feeder calibration is used to calculate the feed factor which is used by the powder dosing motor to determine the necessary speed to obtain a preset powder feed rate. A pre-blended mixture consisting of excipients and active pharmaceutical ingredients (APIs) is fed and passed through a rotational bridge breaker, into the feed segment of the granulator. A bridge breaker prevents bridging and ensures the mixing of feed before entering the granulation unit. Beside the regular feeder, there is a port to add a second feeder to the granulator, which can be used to dose any dry ingredient to a continuously blended inflow from the main pre-installed feeding unit.

To achieve the wet granulation, liquid is pumped into the granulator through two injection nozzles, mounted in the work segment of the granulator (b in Fig. 3.1). The preset liquid addition rate is controlled based on the loss-in-weight principle which is used to determine the rotation speed of the peristaltic pump. As these peristaltic pumps consist of a head with three rollers producing three liquid pulses per revolution, the two pumps related to the liquid injection nozzles are kept out-of-phase.

The granulation unit (c in Fig. 3.1) consists of a barrel enclosing two co-rotating self-wiping screws (Fig. 3.2). Based on the function of specific segment, the granulator can be divided into three segments, i.e. a feed segment, a work segment and a discharge segment (a, b and c in Fig. 3.3). In the feed segment, the dry powder is fed into the barrel containing screws with transport elements. The powder in this segment is dry blended while being transported to the work segment. In the work segment, the powder is mixed, wetted and granulated. The granulation liquid is added via two nozzles, one for each screw, after which the material reaches the mixing zone which consists of kneading discs (Fig. 3.2). Further down, since the granulation occurs by a combination of capillary and viscous forces binding particles in the wet state, the wetted material is distributed, compacted and elongated by the kneading discs of the mixing zones, changing the particle morphology from small (microstructure) to large (macrostructure). The modular structure of the screws allows changing the number of kneading discs, hence the length of the mixing zone. The material is mixed, compacted and chopped to form irregular and porous granules by the succeeding transport elements and kneading blocks. The rotation of the screws conveys the material in axial direction through the different zones of the TSG by the drag and flow-induced displacement forces and thus causing mixing and granulation. The wet granules, produced by the granulator, leave the unit through the discharge zone of the barrel (d in Fig. 3.1) by the wet granules transfer line and are pneumatically transported to the six-segmented fluidized bed dryer (2 in Fig. 3.1).

The granulator screws have a length-to-diameter ratio of 20:1 (Fig. 3.2). The

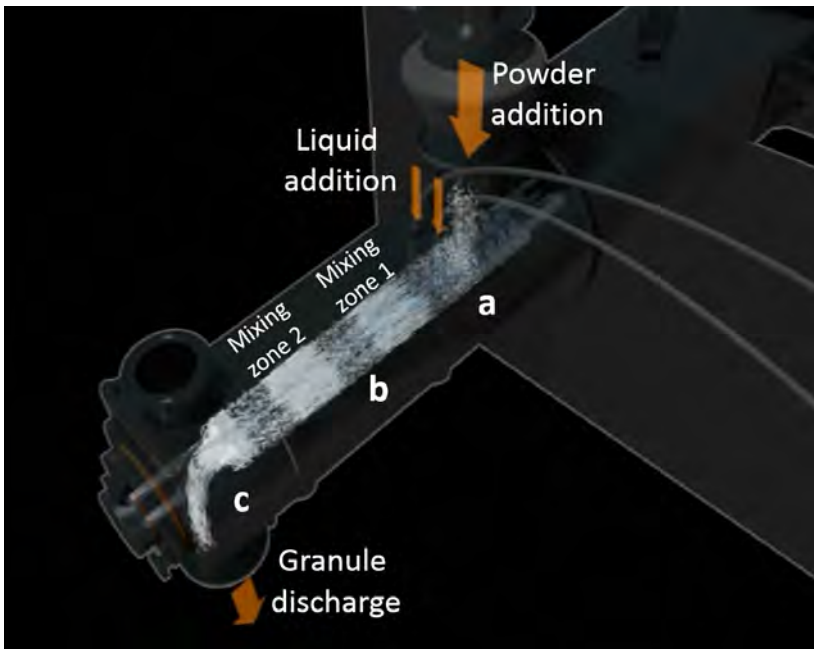


**Figure 3.2:** Screw configuration with 12 kneading discs (2 blocks containing 6 kneading discs each) indicating the geometry of screws used in a TSG.

screw configurations up to 6 kneading discs (Length = Diameter/4 for each kneading disc) are composed of one kneading block. For the screw configuration



with 12 kneading discs, two kneading blocks, each consisting of 6 kneading discs, are used. Both kneading zones are separated by a conveying screw block (Length = 1.5 Diameter). The successive kneading discs in the kneading block are rotated at a certain angle, known as stagger angle, to distribute and mix the material. The stagger angle of the kneading elements is varied between 30°, 60°, 90° and 120°. An extra conveying element (Length = 1.5 Diameter) is implemented after the second kneading block together with 2 narrow kneading discs ( $L = D/6$  for each kneading disc) in order to reduce the amount of oversized agglomerates, as reported by Van Melkebeke et al. (2008).



**Figure 3.3:** The (a) feed segment, (b) work segment and (c) discharge segment of the TSG during operation.

Beside TSG from a full-scale continuous manufacturing line, a lab-scale continuous processing equipment ConsiGma<sup>TM</sup>-1 provides TSG with a possibility to open the granulator barrel. Hence, by opening the barrel after stopping the process running at steady state, the status of granulation at different locations inside the barrel can be investigated by analysing collected samples for different properties such as granule size distribution (GSD) (Fig. 3.4).

Many critical process parameter of twin-screw granulation such as material throughput, screw speed, liquid addition rate, operational torque are logged



**Figure 3.4:** Twin-screw granulator from lab-scale continuous processing equipment ConsiGma<sup>TM</sup>-1 with the granulator barrel that can be opened.

continuously. The steady state criteria for TSG are being decided based on the equilibration of the measured torque by an inbuilt torque gauge within the TSG. The torque values obtained after equilibration of the process are averaged to determine the overall torque during each run. The granulation temperature is controlled by the barrel jacket which is preheated to 25°C or another preset temperature.

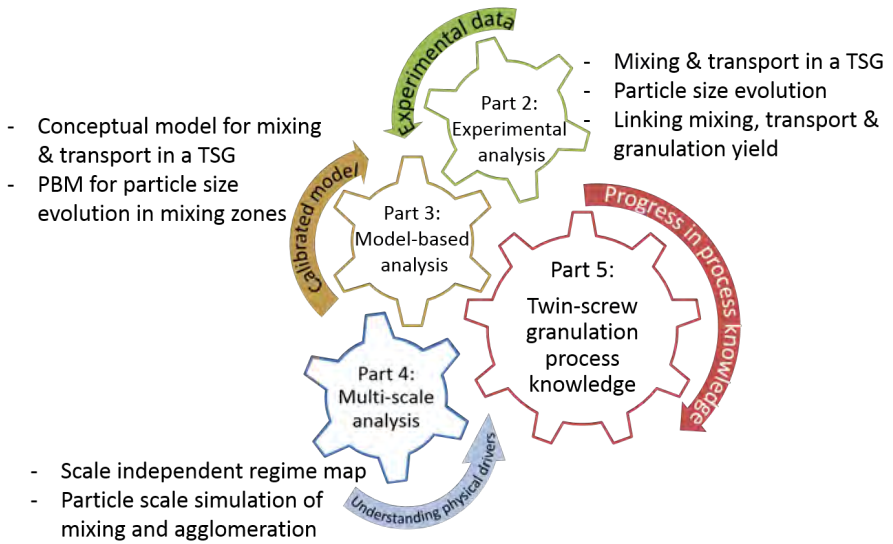
## 3.2 Thesis objectives

The overall objective of this thesis is to improve the understanding of the twin-screw wet granulation process by using strengths of both theoretical and experimental approaches (Fig. 3.5). This leads to several sub-objectives related to different aspects of the continuous twin-screw wet granulation unit operation.

The TSG operates at steady-state, hence the first objective is to **characterise the material flow and mixing**. This can be done based on the characteristic residence time distribution (RTD) of material inside the granulator. The second objective is to **examine the particle size and shape evolution along the length of the granulator barrel** to understand the role of the screw geometry and process conditions in shaping the GSD. Next to this, **it is aimed at investigating the potential link between the residence time, axial and solid-liquid mixing and the resulting GSD inside the twin-screw granulator barrel**. Accounting for the inherent flexibility of the TSG, all the above is performed at varying process and equipment settings based on the design specifications by the manufacturer of ConsiGma<sup>TM</sup>-25 (i.e., GEA pharma systems), and the preliminary experiments with the selected formulation. The preliminary experiments are used to select the range of liquid addition rate. This work focused on one model formulation based on lactose monohydrate to avoid variations in the results by change in formulation properties which is another key sensitive parameter in pharmaceutical twin-screw granulation.

As discussed in the introduction (Chapter 1), the knowledge is derived from the combined effort of experimental and modelling studies. Thus, the hypothesis based on the results from experimental studies is tested through mathematical models which describe the overall granulation process as it progresses along the length of the granulator, to build the knowledge. The experimental data from the RTD study is applied to **identify the most suitable conceptual model for the description of RTD, and transport and mixing in a TSG**. Similarly, to **identify a theoretical framework for tracking the particle size evolution in the individual screw blocks of a continuous TSG**, a population balance model (PBM) framework based on the principal constitutive mechanisms of a granulation system such as aggregation and breakage, is calibrated using the experimental data from the RTD and GSD evolution studies. Although the same formulation has been used and hence the material transport, mixing and granulation behaviour throughout the entire work can be different for other formulations, the experimental data collection and modelling methods applied in this study are generic and can be applied in the same way to other formulations potentially leading to different granulation behaviour.

Finally, in order to consolidate the results for multi-scale applications, a scale-independent approach is desired. **The regime maps theory and particle scale modelling based on fundamental principles of physics is applied to describe the granulation process.**



**Figure 3.5:** An overview of the coherence between the different chapters of the thesis.



## PART II

Continuous granulation system:  
Experimental analysis of residence time,  
mixing and particle size evolution in a  
twin-screw granulator



---

## Mixing and transport during pharmaceutical twin-screw wet granulation: experimental analysis via chemical imaging

---

**Redrafted from:** Ashish Kumar, Jurgen Vercruyse, Maunu Toiviainen, Pierre-Emmanuel Panouillot, Mikko Juuti, Valérie Vanhoorne, Chris Vervaet, Jean Paul Remon, Krist V. Gernaey, Thomas De Beer, Ingmar Nopens, Mixing and transport during pharmaceutical twin-screw wet granulation: Experimental analysis via chemical imaging, *European Journal of Pharmaceutics and Biopharmaceutics*, Volume 87, Issue 2, 2014, Pages 279-289.

### 4.1 Summary

The extent of high shear wet granulation (HSWG) in a twin-screw granulator (TSG) is greatly governed by the residence time and degree of mixing of the granulation materials in the TSG. In order to determine the residence time distribution (RTD) and mixing in TSG, mostly visual observation and particle tracking methods have been used thus far. These are either inaccurate and difficult for short RTD, or provide an RTD only for a finite number of preferential tracer paths. The study presented in this chapter applied near infrared chemical imaging (NIR-CI), which is more accurate and provides a complete RTD. The impact of changes in material throughput (10-17 kg/h), screw speed (500-900 rpm), number of kneading discs (2-12) and stagger angle (30-90°) on the RTD and axial mixing of the material was characterised. The experimental RTD curves were used to calculate the mean residence time, mean centred variance and the Péclet number to determine the axial mixing and predominance of convective over dispersive transport. The results showed that screw speed



is the most influential parameter in terms of RTD and axial mixing in the TSG and established a significant interaction between screw design parameters (number and stagger angle of kneading discs) and process parameters (material throughput and number of kneading discs). The results of the study allow the development and validation of a theoretical model capable of predicting the RTD and macro-mixing in the TSG (Chapter 7). These can later be coupled with a population balance model in order to predict granulation yields in a TSG more accurately (Chapter 8).

## 4.2 Introduction

Twin-screw granulation, which is seen as a promising continuous alternative for traditional batch HSWG, allows a relatively high material throughput with a short residence time (typically few seconds) (Vervaeet and Remon, 2005). In a TSG, besides homogeneous distribution of granulation material, the aim is also to achieve mixing within the shortest screw lengths and at minimum required power input. This is important to govern the extent of different rate processes such as wetting, growth and breakage, which ultimately determine the characteristics of the produced granules. It is evident from several studies that the  $\bar{t}$  in a TSG (which is few seconds) is much shorter compared to the granulation time in a typical batch granulator, which is in the order of minutes. Although from a productivity point of view, this time gain is preferred, its implications on the granulation rate processes needs to be examined (El Hagrasy et al., 2013b). The mixing inside the granulator is related to the functional role of the screw configuration as well as process parameters. Feeding rates of the granulation material, the screw speed and the screw configuration can be independently chosen to yield desired mixing levels of the material. The RTD exhibited by a given system yields distinctive clues both on the average time spent by the material and on the type of axial mixing occurring within the system. RTD is thus one of the most informative characterisation methods of the system (Levenspiel, 1999).

In the high-shear environment of TSG, a good axial mixing in addition to the radial mixing during granulation in TSG is required to avoid the effect of any inhomogeneities at the inlet on the produced granules. A mixing region in a TSG screw contains blocks of several kneading discs with grooved flights, which cause a broadening of the RTD. A broad RTD indicates good axial mixing in a TSG, and hence has a favourable effect on product quality by avoiding inhomogeneities in the final product. The RTD of the material is determined by the bulk flow profiles in the screw channels, generation of partial flows in flow-restrictive zones (e.g., in kneading blocks), and reverse flow in the gaps

at the flight tips and in the inter-meshing zone as well as in mixing zones (See Chapter 3, Fig. 3.2). However, this leads to another optimization challenge regarding the most-suitable screw configuration.

Dhenge et al. (2010) measured the RTD using the impulse-response technique under different processing conditions and showed the variation in the RTD depending on formulation and process parameters. El Hagrasy et al. (2013b) applied the same RTD measurement approach to estimate the response to changes in formulation properties such as raw material attributes as well as granulating liquid properties on granule properties. However, due to the difficulty to visualize the material flow in the barrel, little efforts have been made towards understanding the mixing of the material inside the TSG barrel, which is essential for the optimisation of the obtained granule properties. In a recent attempt, Lee et al. (2012) obtained the RTD using positron emission particle tracking (PEPT) to study the axial mixing. Although this is a very powerful technique, this approach requires several manipulations in the equipment and the process (e.g. thinner TSG barrel wall to make sure that the gamma rays can penetrate the construction material, but it limits the shear handling capability of the barrel). Therefore, it would be beneficial to have a measurement method allowing RTD measurements without the need of manipulation of the equipment. Also, the PEPT involves single particle tracking, which is limited by the number of tracer passes to study the complete RTD adding operational variability to the RTD study. The circulated tracers in the PEPT study may not provide information on the total flow behaviour as some material paths are so rare that they will not be followed by the finite number of tracer paths through the equipment. Therefore, only distributions of passage time rather than true RTD can be measured using the PEPT (Bakalis et al., 2004). Vercruyssen et al. (2013b) applied near infrared (NIR) chemical imaging to evaluate the influence of the liquid addition method, screw configuration, moisture content and barrel filling degree on the moisture homogeneity during TSG.

In this study, a novel sample preparation and an image data collection method based on NIR chemical imaging has been used as an analytical technique to characterise the flow and axial mixing of material in the TSG qualitatively and quantitatively. The study presented here examines the axial mixing inside a continuous TSG based on the characteristic RTD of the tracer component. NIR chemical imaging was used to investigate the residence time of tracer inside the barrel and its distribution as a function of process (screw speed and material throughput) and equipment parameters (number and stagger angle of kneading discs in screw configuration).

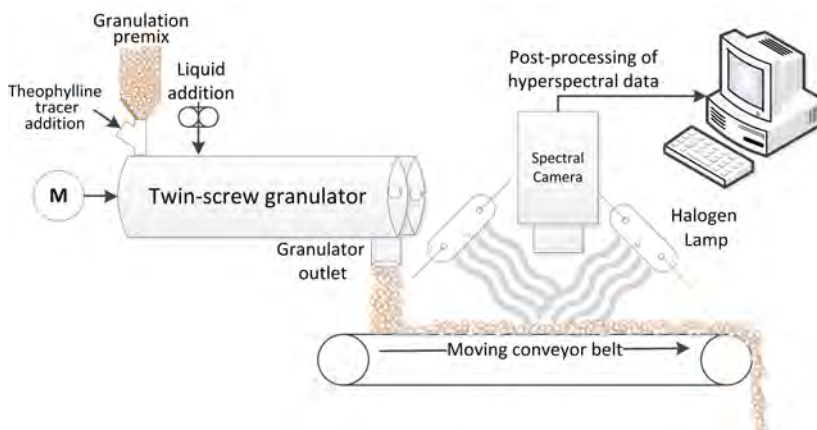
## 4.3 Materials and methods

### 4.3.1 Pharmaceutical model formulation and twin screw granulation

$\alpha$ -Lactose monohydrate (Pharmatose 200M, Caldic, Hemiksem, Belgium) was used as a model excipient ( $D_{90} < 100 \mu\text{m}$ ). Distilled water was added as granulation liquid. To evaluate the residence time of material inside the barrel, theophylline anhydrate (Farma-Química Sur, Malaga, Spain) was used as tracer component. Granulation experiments were performed using a 25 mm diameter co-rotating twin screw granulator, the granulation module of the ConsiGma-25 unit (GEA Pharma Systems, Collette<sup>TM</sup>, Wommelgem, Belgium) (See Chapter 3, section 3.1 for granulator details).

### 4.3.2 Description of NIR chemical imaging system and measurement set-up

Spectral images of wet granules were collected using a line-scanning (pushbroom) hyperspectral camera (SWIR, Specim Ltd., Oulu, Finland). The camera sees a row of 320 spatial pixels at a time, and it disperses the incoming light from each pixel in the spectral range 970-2500 nm onto one column on the 320×256-pixel mercury-cadmium-telluride (MCT) detector (14-bit readout, cooled to  $-70^{\circ}\text{C}$  with a 4-stage Peltier system). Wet granules from the granulator output fell on a conveyor belt (Mini, ENP, Hjärteby, Sweden) which was moving at a speed of 3.12 cm/s. The camera-to-belt distance was set such that the imaged line had the length of 10 cm on the conveyor belt, and the speed of the conveyor belt was adjusted such that the geometry was preserved, i.e., spatial pixels were squares of the size  $312 \times 312 \mu\text{m}^2$  at the maximum frame rate permitted by the camera (100 frames per second). The conveyor belt and the sample material on it were illuminated with two rows of three 75-W halogen lamps (Specim Ltd., Oulu, Finland) at the distance of 35 cm, and the measurement was conducted in diffuse reflectance mode in the  $45^{\circ}$ - $0^{\circ}$ - $45^{\circ}$  geometry (see Fig. 4.1). Each collected spectral image consisted of 2500 frames (25 seconds measurement,  $2500 \times 320$  spatial pixels, 256-element spectrum at each spatial pixel) which corresponds to an area of  $10 \times 64 \text{ cm}^2$  on the conveyor belt. At the material throughput of 10-25 kg/h the dry mass of material in one spectral image was approximately 69-173 g.



**Figure 4.1:** Schematic diagram of the measurement setup at the outlet of the granulator. Granules at conveyor belt moving at constant speed were illuminated using the halogen lamps and scanned by the spectral camera.

### Extraction of relevant information from chemical images

The processing of the hyperspectral images consisted of two steps. First, spatial pixels corresponding to the plastic conveyor belt were eliminated from the analysis via partial least squares discriminant analysis (PLS-DA) classification. Second, the NIR spectra in the remaining pixels corresponding to the wet granules were subjected to semi-quantitative analysis of theophylline content. The spectral range was narrowed to 1100-2200 nm and the spectra were subjected to the standard normal variate (SNV) pretreatment in all analyses. The use of SNV preprocessing eliminates the additive baseline offset variations and multiplicative scaling effects in the spectra which may be caused by shadowed regions near large granules and possible differences in granule density. Both steps have been described in detail by Vercruyssen et al. (2013b).

### 4.3.3 Residence time analysis: experimental design and data post-processing

#### Experimental procedure to collect raw data

Experiments were performed to study the influence of screw speed (500, 700, 900 rpm), material throughput (10, 17.5, 25 kg/h), number (2, 6, 12) and stagger angle (30, 60, 90°) of the kneading discs in the screw configuration on the RTD and axial mixing of the material. For the different experiments, pure  $\alpha$ -lactose monohydrate was fed to the granulator. The screw configuration was composed

of kneading zones consisting of maximum 6 kneading discs in each zone ( $L = D/4$  for each kneading element) at an angle of  $30^\circ$ ,  $60^\circ$  and  $90^\circ$ . Both kneading zones were separated by a conveying element ( $L = 1.5 D$ ). An extra conveying element ( $L = 1.5 D$ ) was implemented after the second kneading block together with 2 narrow kneading discs ( $L = D/6$  for each kneading element) in order to reduce the amount of oversized agglomerates, as reported by Van Melkebeke et al. (2008). The granulation liquid (liquid to solid ratio 10% (w/w) of the material throughput) was added just before the first kneading element.

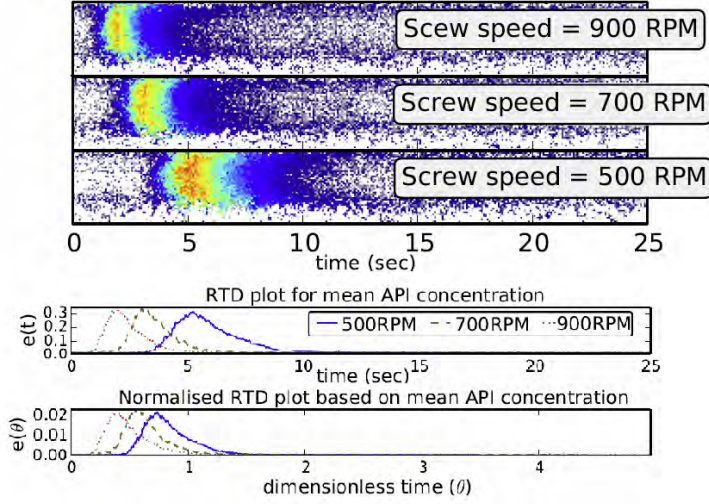
During each experiment, a shot of anhydrous theophylline (2% (w/w) of the material throughput per minute, which corresponds to 3.33, 5.83 and 8.33 g for throughput of 10, 17.5 and 25 kg/h respectively) was manually inserted into the powder inlet port of the granulator. At the outlet of the granulator, the NIR chemical imaging system was used to measure the theophylline dynamics. The chemical imaging measurements were started 5 s after the addition of the theophylline shot. Since it took 5 s for the conveyor belt to move from below the granulator output to the location of the spectral image collection (Fig. 4.1), the first frame of the spectral image corresponded to the instant of theophylline addition. The spatial distribution of theophylline during the 25 seconds measurement was calculated with the spectral matched filter as explained in section 4.3.3. The intensity of the obtained chemical map was thus proportional to the true theophylline level, and the residence time distribution could be determined via inspecting the temporally scanned direction of the spectral image. For each residence time analysis experiment, a semi-quantitative measure of the theophylline level was obtained using the previously described method by Vercruyssen et al. (2013b).

### Estimation of RTD and axial mixing efficiency

Conventionally, a residence time distribution is obtained by injecting a pulse of tracer into the system at the inlet, and the residence time function,  $e(t)$ , is calculated as

$$e(t) = \frac{c(t)}{\int_0^\infty c(t)dt} \quad (4.1)$$

where  $c(t)dt$  is the concentration of the tracer at the outlet between  $t$  and  $t + dt$ . In this study, the residence time of the tracer molecule (theophylline) was applied as the function of the tracer concentration (as estimated with the SMF model) between  $t$  and  $t + \delta t$  in the temporal profile of the discrete tracer map (top of Fig 4.2).



**Figure 4.2:** Representation of active pharmaceutical ingredient (API)-map, corresponding temporal profile and residence time distribution for twin screw granulator at fixed material throughput (25 kg/h), number of kneading discs (6), stagger angle (60°) and different screw speeds

This tracer map was transformed into the exit age distribution curve, i.e. RTD based on the mean tracer concentration,  $e(t)$  between  $t$  and  $t + dt$  (middle plot of Fig 4.2), which was then used to calculate the  $\bar{t}$  as the ratio of the first and the zeroth moment using equation

$$\bar{t} = \frac{\int_0^{\infty} t \cdot e(t) dt}{\int_0^{\infty} e(t) dt} \quad (4.2)$$

The RTD shape, thus obtained was normalised (bottom plot of Fig 4.2) as  $e(\theta) = \bar{t} \cdot e(t)$ , where dimensionless time,  $\theta = t/\bar{t}$ , and used to characterise the axial mixing levels. The degree of axial mixing in the granulator can be quantified by calculating a dimensionless Péclet number  $Pe$  which is a ratio of rate of axial transport by convection and axial transport by diffusion or dispersion. By treating the boundary condition of the granulator as a closed system with no dispersion or radial variation in concentration either upstream or downstream, the following equation can be derived (Fogler, 2006)

$$\frac{\sigma_{\bar{t}}^2}{\bar{t}^2} \approx \frac{2Pe - 2 + 2 \cdot e^{-Pe}}{Pe^2} \quad (4.3)$$

where, the  $\sigma_{\bar{t}}^2$ , which measures the width of the RTD, is calculated by

$$\sigma_{\bar{t}}^2 = \frac{\int_0^{\infty} (t - \bar{t})^2 \cdot e(t) dt}{\int_0^{\infty} e(t) dt} \quad (4.4)$$

and the  $\sigma_{\bar{t}}^2/\bar{t}^2$  in eq. 4.3 stands for the normalised variance  $\sigma_{\theta}^2$ , which is the normalised second central moment of the RTD curve. As  $\sigma_{\bar{t}}^2$  approaches zero, Pe approaches infinity indicating that the extent of axial mixing is low. When the Pe turns out to be large, the granulator characteristics approach those of a plug-flow reactor (PFR). This regime is not favourable in continuous processing as the existence of plug flow indicates poor axial mixing in the granulator which is not desirable.

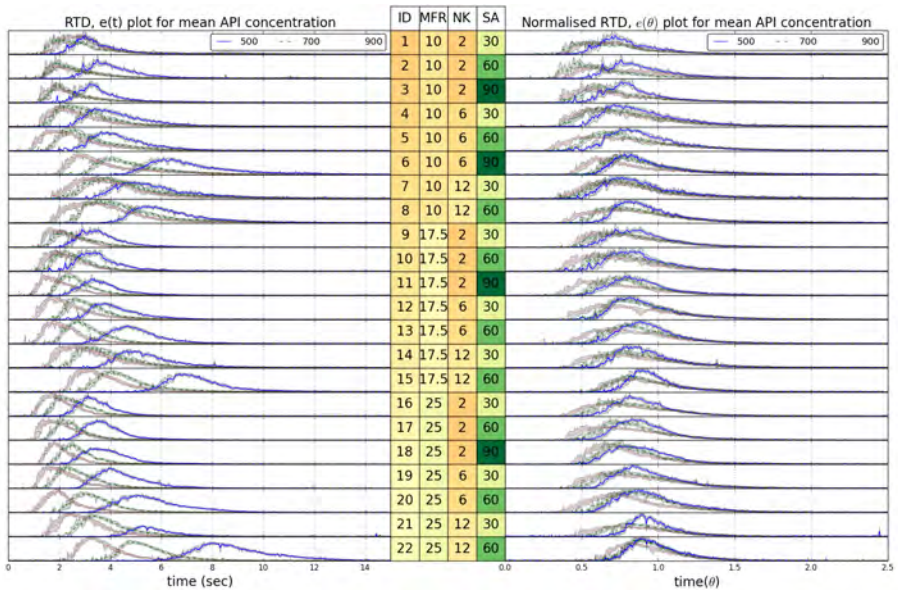
#### 4.3.4 Quantification of effects and interactions of factors

The data collected by the experimental design were used to estimate the effects of the factors on the responses. Since, multiple responses ( $\bar{t}$ ,  $\sigma_{\theta}^2$ , Pe) were quantified from the RTD profile, it was helpful to fit a model simultaneously representing the variation of all responses to the variation and interaction of the factors. Therefore, using Modde 9.0 software (Umetrics, Umeå, Sweden), the partial least squares (PLS) method which is able to deal with many responses simultaneously, taking into account their covariances, was employed. The effect plot was used to show the change in the response when a factor and its combinations vary from low level to high keeping other factors at their averages (Fig. 4.4). The respective 95 % confidence interval is shown for each plot. Insignificant effects are those where the confidence interval includes zero. The interaction plot has been used to display the predicted change in the response when one factor varies, and the second factor is set at both its low and high level, all other factors being set on their center. In this plot, when the two lines are parallel there is no interaction between the two factors, whereas when they cross each other there is a strong interaction.

## 4.4 Results and discussion

Residence time analysis of the tracer molecule (theophylline) was performed as a function of material throughput, screw speed, and screw configuration in terms of number and stagger angle of kneading discs (see overview of performed experiments in Fig. 4.3). The curves based on the exit tracer concentrations display a long tail for all the runs (Fig. 4.3), which indicates that the flow behaviour inside the granulator is not plug flow under the conditions used

in this study and that a significant degree of axial mixing occurs. This was also demonstrated by El Hagrasy et al. (2013b) in a study for RTD in a TSG. Besides changes in RTD profile, the effect of these process and screw design parameters clearly reflected in other responses such as measured torque in the granulator drive (Fig. 4.5), the  $\bar{t}$  (Fig. 4.6), width of the normalised RTD i.e.  $\sigma_{\theta}^2$  (Fig. 4.7) and relative magnitude of convective and dispersive transport capacities (Fig. 4.8) in the TSG. This now allows discussion of each factor and their interactions based on their effect on RTDs ( $R^2=0.85$ ) and the axial mixing of the material in terms of normalised variance  $\sigma_{\theta}^2$  ( $R^2=0.88$ ) and Péclet number  $Pe$  ( $R^2=0.88$ ) (Fig. 4.4). In what follows the observed effects are discussed in more detail.



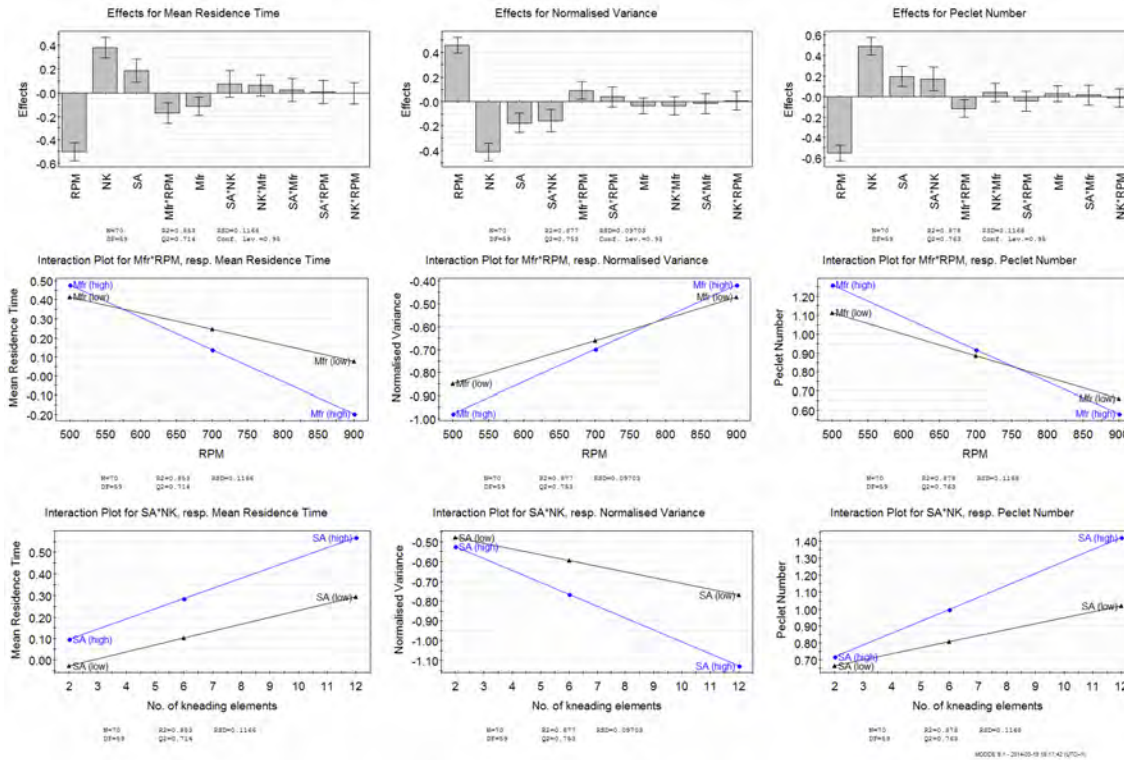
**Figure 4.3:** The age distribution (left) and normalised RTD (right) profiles with a shaded region denoting the standard deviation at different screw speed (— 500, --- 700, ... 900 RPM) during various experiments (ID) using twin screw granulation [SA: stagger angle ( $^{\circ}$ ), NK: number of kneading discs (-), MFR: material throughput (kg/h)]. Several RTD profiles for experimental runs at  $SA = 90^{\circ}$  are not shown as the TSG barrel jammed for those conditions.

#### 4.4.1 Effect of screw speed

Screw speed had the largest effect on the RTD indicating that a highly frictional flow exists and thus the TSG behaves dominantly like a drag flow pump (Fig. 4.4).

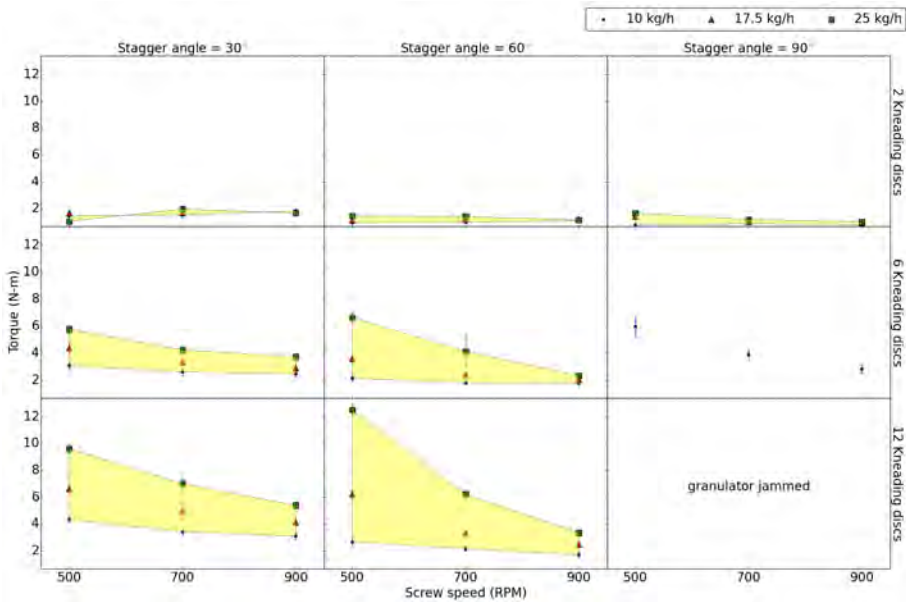


With the increase in screw speed the RTD profiles consistently shifted to the left in Fig. 4.3, suggesting a decrease in the  $\bar{t}$  of the material in the TSG barrel. This is expected as the conveying rate increases with the increased screw speed, which reduces the residence time of the material in the granulator. At lower filling conditions (i.e. low material throughput and low number of kneading discs) the difference between the RTD profiles at higher screw speed (900 and 700 rpm) was less compared to that at low screw speed (500 rpm). With the increase in material throughput, the fill ratio was high enough to induce a difference between RTDs at all screw speeds (right side plots with ID 9-22 in Fig. 4.3). This difference became larger with an increase in the number of kneading discs (such as ID 12 and 14 compared to ID 9 in Fig. 4.3) and their stagger angle (ID 16, 17 and 18 in Fig. 4.3). At low screw speed (500 rpm) significant variation in the RTD was observed between different screw configurations and the mean exit tracer concentration in the active pharmaceutical ingredient (API) maps were detected between 4.1 and 8.6 seconds after injection of the API shot. In contrast, at high screw speed this difference reduced and the mean values of the tracer concentration in the API maps were detected between 2.8 and 4.6 seconds after injection of the API shot. This reduction indicates that the increase in the screw speed leads to a reduction in the influence of other factors under study.



**Figure 4.4:** Effects and related interaction plots of the PLS models showing change in the responses in term of  $\bar{t}$ ,  $\sigma_{\theta}^2$ , Pe and the measured torque when factors number of kneading discs (NK) [2, 6, 12], screw speed (RPM) [500-900 rpm], throughput (Mfr) [10-25 kg/h] and stagger angle (SA) [30-90°] and their interaction varies from average to the high level.

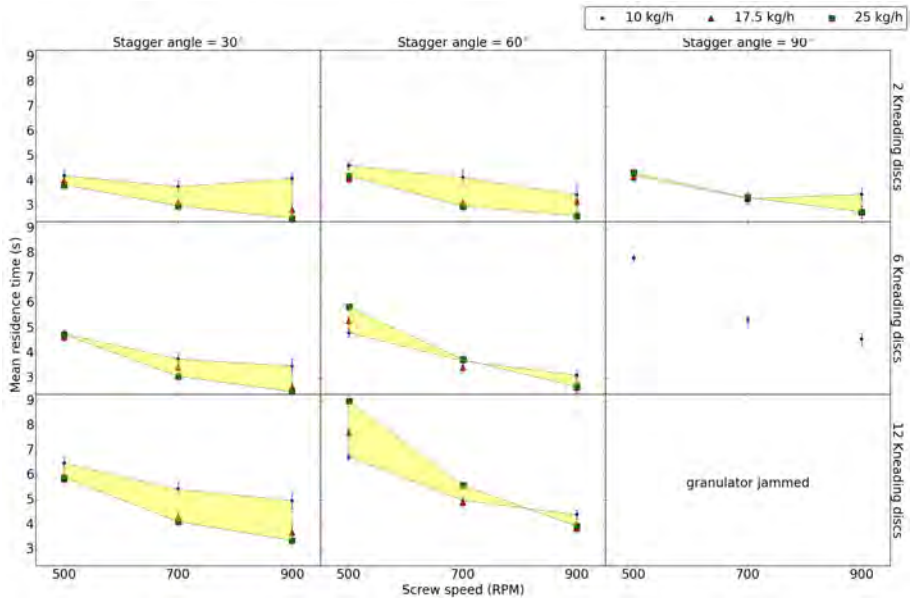
These changes in RTD profile due to changes in screw speed also affected other responses. At a high number of kneading discs, the torque decreased significantly with an increase in screw speed in contrast to the low number of kneading discs (Fig. 4.5). This is due to the increased conveying rate at high screw speed, which reduced fill level of the powder accumulated by a high number of kneading discs (Dhenge et al., 2010). The reduced fill level resulted in reduction in the torque level. The  $\bar{t}$  as well decreased with an increase in the screw speed (Fig. 4.6). However, the difference between  $\bar{t}$  was smaller when the screw speed was increased from 700 to 900 rpm compared to an increase from 500 to 700 rpm. The change in screw speed also affected the  $\sigma_{\theta}^2$  (eq. 4.4), which generally increased with an increase in the screw speed (Fig. 4.7). However, at the high filling condition (material throughput 25 kg/h, 12 kneading discs), the effect of screw speed on the  $\sigma_{\theta}^2$  was the least. This was due to material built up at the two kneading blocks in the TSG, which ensured near-plug flow conditions inside the TSG. An additional conveying cleared the kneading blocks, but could only lead to a minor increase in axial mixing.



**Figure 4.5:** Average torque measured and the standard deviation at various material throughputs (10-25 kg/h), number of kneading discs (2, 6, 12), stagger angle (30-90°) and different screw speeds (500-900 rpm)

An increase in the screw speed resulted a reduction in  $Pe$  reflecting that dispersive transport was high compared to the convective transport in the TSG

(Fig. 4.8). At lower screw speed, Pe increased significantly with an increase in throughput, number of kneading discs and stagger angle, indicating low axial mixing and more plug flow like material transport through the barrel. The high Pe was possibly due to the bulk movement of material in lack of critical strain and homogenisation force. These results contradict the findings by Lee et al. (2012) who suggested more effective axial mixing at lower screw speed as the particles got stuck in the restrictive zones (kneading blocks) more frequently at lower screw speed than at higher screw speed. However, the study by Lee et al. (2012) was performed using screws of lower diameter (16 mm) and at lower screw speed (200-500 rpm). This contradiction can be understood by the results of (Gautam and Choudhury, 1999) who reported that the extent of the axial mixing in the twin screw extruder is significantly affected by the screw types and screw geometries. We believe that possibly due to the small clearance between the two screws and the wall in the TSG used here, the reverse-flow was significantly prevented at lower screw speed in this study, which led to a completely different outcome. The material layering on the barrel wall leading to a reduction in the clearance gaps may also be responsible for this lack of reverse-flow at low screw speed.



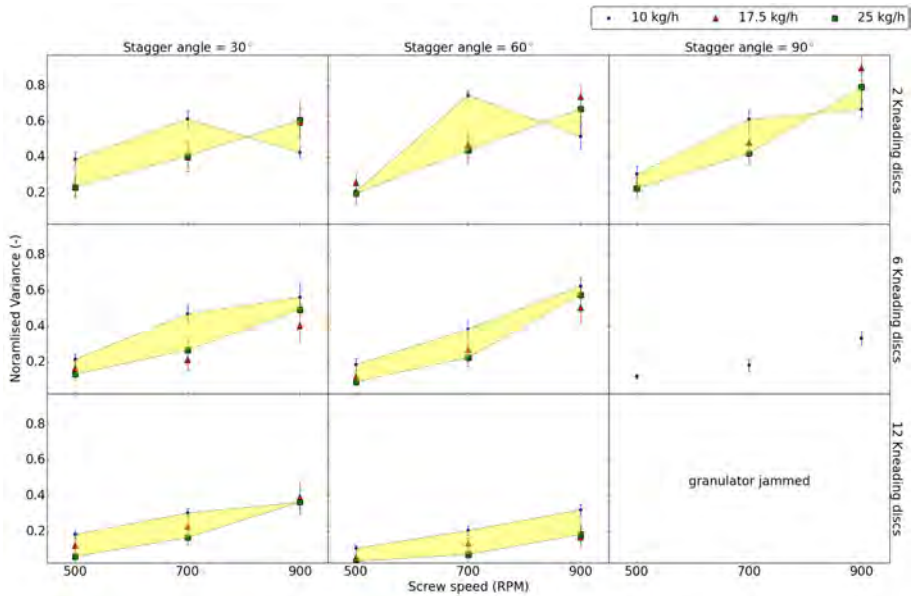
**Figure 4.6:** Mean residence time  $\bar{t}$  and the standard deviation based on the experimental RTD profile at various material throughputs (10-25 kg/h), number of kneading discs (2, 6, 12), stagger angle (30-90°) and different screw speeds (500-900 rpm)

#### 4.4.2 Effect of material throughput

The fill degree which dictates the level of axial mixing in TSG is also controlled by the material throughput. However, the effect of throughput was less significant without interaction with other factors (Fig. 4.4). When the flow in the TSG barrel was less of a constraint (stagger angle of 30 and 2 kneading discs, screw speed 900 rpm), increasing material throughput had no significant effect on the RTD. When the restrictive forces increased (through changes in screw configuration), despite low fill ratio at low throughput, the RTD profile shifted to the right (left side plots with ID 4-8 in Fig. 4.3), indicating an increase in the residence time of the material in the TSG barrel. As the fill ratio was increased by the increase in the material throughput, the RTD shifted also at lower restrictive forces (left side plots with ID 9-11 and 16-18 in Fig. 4.3). The high material throughput caused a higher degree of channel filling of the screws, creating a high throughput force. The shortest time for detecting the mean values of the tracer concentration in the API maps was 2.8 s (left side plot ID 16 in Fig. 4.3) at a material throughput of 25 kg/h at 900 rpm. This might be due to very high throughput force which conveyed the material quickly. However, this shift in RTD did not always translate into an increase in the axial mixing. At the low material throughput the degree of channel filling is low, hence there is a low throughput force of the material, which can lead to more axial mixing (Dhenge et al., 2011). This is also visible in the trends in the study (right side plots with ID 1-8 in Fig. 4.3). But, when the material throughput increases beyond the conveying capacity of the screw, it may have resulted in plug flow of the material leading to poor axial mixing as indicated by reduction in width of the distribution (comparing right side plots with ID 8, 15 and 22 in Fig. 4.3).

The torque profile was less affected by the change in the material throughput when restrictive forces were less i.e. at the low number of kneading discs, low stagger angle and high screw speed (Fig. 4.5). However, with an amplification of restrictive force, the torque changed significantly for changes in the material throughput. At the screw speed of 500 rpm, 12 kneading discs and stagger angle of 60°, the maximum change in the measured torque, from 2.7 Nm to 12.5 Nm for increase in material throughput from 10 kg/h to 25 kg/h, was observed (Fig. 4.5). When the screw speed was increased, the measured torque decreased significantly due to higher thrust of the material by the rapidly moving screws.

An increase in the conveying rate with increasing material throughput also caused reduction in the  $\bar{t}$  (Fig. 4.6). However, at low screw speed (500 rpm), the  $\bar{t}$  increased with increasing material throughput for the screw configuration with 6 kneading discs at stagger angle of 60°. This indicates lack of possibility

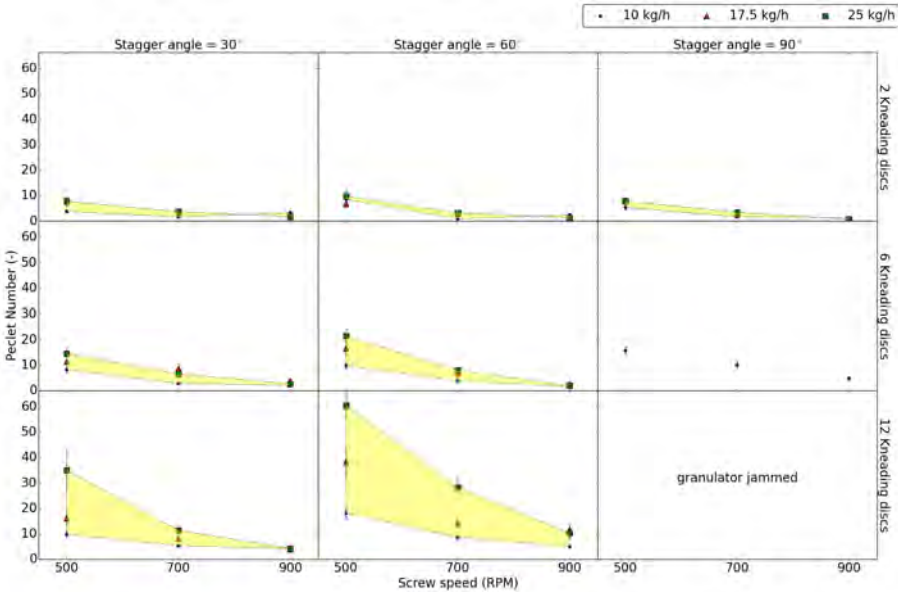


**Figure 4.7:** Normalised variance  $\sigma_{\theta}^2$  and the standard deviation based on the experimental RTD profile at various material throughputs (10-25 kg/h), number of kneading discs (2, 6, 12), stagger angle (30-90°) and different screw speeds (500-900 rpm)

to push forward more material to create extra conveying capacity for this screw configuration, thus causing higher restriction to flow and increase in the  $\bar{t}$ . For the screw configuration with 30° stagger angle, at high screw speed (900 rpm), the difference in  $\bar{t}$  was relatively higher for an increase of the material throughput from 10 to 17.5 kg/h compared to the difference observed when increasing from 17.5 to 25 kg/h. This suggests that extra conveying capacity cannot be achieved constantly by an increase in the material throughput. In contrast, at 60° screw configuration, the material throughput had a larger impact on the  $\bar{t}$  at lower screw speed (500 rpm), which decreased with increase in screw speed. This can be regarded as a requirement of critical fill ratio to be achieved for each screw configuration to extend the  $\bar{t}$  and change the overall RTD profile.

Although, the effect of change in the material throughput on  $\sigma_{\theta}^2$  and Pe was observed to be insignificant by the PLS model when considered alone (Fig. 4.4), the general trend shows a reduction in  $\sigma_{\theta}^2$  with an increase in the material throughput (Fig. 4.7). This was due to the increased throughput force, which led to an increase in compaction and reduction in the wall slippage, and hence the reduced axial mixing in the TSG. Similarly, an increase in Pe was observed

when the material throughput was increased (Fig. 4.8). This suggests that the convective transport dominates over dispersive transport with an increase in the throughput. At the highly restrictive flow condition (12 kneading discs at 60°), the increase in the material throughput led to convective transport outcompeting dispersive transport leading to very high Pe. Therefore, the material flow in the barrel approaches a plug flow regime. The materials in the TSG with a low degree of filling could be less compacted than those in the TSG with a high degree of filling. This led to greater axial transport in the TSG. However, the number of kneading discs and their stagger angle dominated the control of the residence time, which resulted in complete jamming of the granulator at high material throughput, more kneading discs (12) and stagger angle (90°). Hence, a balance between conveying and dispersive forces is required to obtain the desired axial mixing and residence time while changing the material throughput.



**Figure 4.8:** Peclet number (Pe) and the standard deviation based on the experimental RTD profile at various material throughputs (10-25 kg/h), number of kneading discs (2, 6, 12), stagger angle (30-90°) and different screw speeds (500-900 rpm)

#### 4.4.3 Effect of number of kneading discs

Next to the screw speed, the number of kneading discs was a significant factor having effect on the RTD characteristics without interaction with other factors

(Fig. 4.4). In a TSG, the feed material is only rolled forward by the conveying section. A significant mixing occurs in the mixing section since the material in this section flows more slowly than in the previous conveying section and is, hence, forced-mixed with the incoming materials. Thus, it is an important factor in RTD studies for TSG. The influence of kneading discs is primarily reflected by the increase in the driving torque of the TSG with an increase in the number of kneading discs (Fig. 4.5). At a low number (2 kneading discs) for all different screw speeds, material throughputs and stagger angle of the discs the torque was below 2 Nm. However, by increasing the number of discs, the torque value increased to a level as high as 10 Nm. For low screw speed (500 rpm) and high stagger angle (60°), the restrictive forces started to dominate over drag force in the mixing zone, which caused an excessive increase in the torque of the granulator. For a higher number (6 and 12) of kneading discs and stagger angle (90°) the flow of material was so seriously hampered that the TSG barrel jammed and the run could not be performed. Next to the measured torque, this increase in restrictive flow was clearly reflected in the RTD (Fig. 4.2). With an increase in number of kneading discs the RTD shifted towards the right in the experiments with ID 17, 20 and 22 of Fig. 4.3, indicating an increased restriction to the flow of material in the TSG barrel. However, the difference between the RTD profiles for experiments with screw configuration consisting of 2 and 6 kneading discs was smaller compared to the difference observed when shifting between 6 and 12 kneading discs. This may be explained by the fact that up to 6 kneading discs there was only one kneading block in the screw while in the case of 12 kneading discs an additional kneading block containing 6 kneading discs was present. In a TSG with more than six kneading discs, the material has to travel consecutively through a conveying section, a mixing section, again a conveying section and finally a mixing section before being conveyed out.

The increase in number of kneading discs caused an increase in  $\bar{t}$  of the tracer, which was well expected due to increase in flow restriction (Fig. 4.4). Consequently, the local fill level was increased, leading to a material consolidation, until it was expelled to the next section i.e. kneading section (Tu et al., 2013). While the number of kneading discs had little impact on the  $\bar{t}$  at high screw speed (900 rpm), this becomes significant at lower screw speeds (500, 700 rpm) leading to a high  $\bar{t}$  (Fig. 4.6). At a low number of kneading discs, the  $\bar{t}$  was found to be in a lower range (3 - 5 sec) compared to the result obtained for 12 kneading discs (4 - 9 sec). Contrary to  $\bar{t}$ , the  $\sigma_{\theta}^2$  is most influenced at the low number of kneading discs (Fig. 4.7). Due to low hindrance to the axial flow by the shortest fully filled zones around two kneading discs, dispersive transport was most efficient. Also, since flow restrictive influence by kneading discs was the least, the impact of other factors on the axial mixing was more



expressed. On the other hand, at the high number of kneading discs excessive hindrance causes a quick shift towards plug flow, which was supportive of other flow restrictive factors such as, low screw speed (500 rpm) and high stagger angle ( $90^\circ$ ). Therefore, less variation in the  $\sigma_{\theta}^2$  was observed at the high number of kneading discs despite changes in other factors under study. The relative magnitude of the convective to dispersive transport capacities showed that the convective transport dominates over dispersive transport with increase in number of kneading discs (Fig. 4.8). At a low number of kneading discs the Pe was between 2 - 12, while for a screw configuration involving 12 kneading discs, screw speed 500 rpm and material throughput of 25 kg/h the Pe increased up to 45. Increasing the screw speed up to 900 rpm for the same condition reduced the Pe rapidly down to 10.8. Such a behaviour shows that, at a higher number of kneading discs, although the  $\bar{t}$  is increased in the TSG barrel, an increase in screw speed is required to achieve proper axial mixing.

#### 4.4.4 Effect of stagger angle

Change in stagger angle had significant effect on the RTD characteristics of the TSG (Fig. 4.4). However, since the restricted area in the flow channel of the TSG is small per kneading disc, the impact of the stagger angle on the RTD profile is only observed with an increased number of kneading discs. This is due to an additive restriction of the flow at a higher number of kneading discs. Thus, a cumulative effect by increasing number and stagger angle of kneading discs caused an increase in the driving torque of the TSG (Fig. 4.5). At low number of kneading discs, despite changes in stagger angle of the kneading discs, the measured torque of the TSG drive was always below 2 Nm. However, with an increase in the number of discs, the torque value showed variation at different stagger angles and later on became such a dominant factor that several runs at  $90^\circ$  stagger angle could not be performed due to jamming of the TSG barrel. This can be attributed to the excessive restriction to the material flow at the high number of kneading discs and a lack of thrust to flow at a stagger angle of  $90^\circ$ . This increased constrained flow shifted the RTD profile to the right with increasing stagger angle (left side plots with ID 4-8, 12-15 and 19-22 in Fig. 4.3). However, this shift did not always contribute to an increase in width of the distribution, an indicator of axial mixing. For the runs with 6 kneading discs and throughput of 10 kg/h, an increase in stagger angle from  $30^\circ$  to  $60^\circ$  led to widening of the distribution, but further increase to  $90^\circ$  caused narrowing of the distribution (right side plots with ID 4-6 in Fig. 4.3). This can be explained by transition from a less-mixed to a well-mixed and later towards a plug flow profile in the TSG. Similar trends were observed for 12 kneading discs (right side plots with ID 7-8 in Fig. 4.3) as well as increased material throughput (25

kg/h) (right side plots with ID 21-22 in Fig. 4.3). Furthermore, at 2 kneading discs, only when the barrel was highly filled due to high material throughput (25 kg/h), the normalised RTD profile became wider when the stagger angle changed from 30° to 60° and no narrowing of the profile occurred even for an increase up to 90° (right side plots with ID 16-18 in Fig. 4.3). This indicates that stagger angle does play a significant role in axial mixing.

A change in stagger angle affected the  $\bar{t}$  more clearly at 6 and 12 kneading discs and low screw speed (500 rpm) (Fig. 4.6). The  $\bar{t}$  became higher and the material spent an extra 2 to 3 seconds in the TSG barrel. The increase in  $\bar{t}$  was presumably due to the increased restriction and reduced conveying capacity of the 60° kneading discs, compared to that of the 30° configuration. The  $\bar{t}$  using the 90° kneading block configuration was higher than for the 30° and 60° configurations. The material was observed flowing through the granulator at the low number of kneading discs (2 and few runs with 6 kneading discs) and blocked completely for 12 kneading discs at 90°. A mixing zone with 90° kneading discs arrangement in principle gives no conveying capacity (Lee et al., 2012). Hence, it can be suggested that the material transport through the mixing zone occurs largely due to the throughput force and the gradient of filling degree along the granulator, and is strongly coupled with the material throughput and the screw speed. The stagger angle had a significant effect on the axial mixing, which is reflected by a reduction in  $\sigma_{\theta}^2$  with an increase in stagger angle (Fig. 4.4). This reduction in  $\sigma_{\theta}^2$  suggests that the stagger angle increase not only stimulates the reduction of the downstream conveying action of the screw but also impedes the axial dispersion in the granulator (Fig. 4.7). The less variation in Pe upon change in stagger angle at high screw speed (900 rpm) (Fig. 4.8) suggests that stagger angle has less effect when the dispersive transport dominates (low Pe) in TSG. However, at low screw speed along with an increase in feed rate, convective transport dominated over dispersive transport (high Pe). An extremely significant effect of the change in stagger angle on the Pe was observed for 6 and 12 kneading discs where the Pe almost doubled with the increase in the stagger angle from 30° to 60°. Most of the runs for the screw configuration involving 90° stagger angle could not be performed as the flow regime moved to almost pure plug flow due to which the granulator jammed.

## 4.5 Interaction of different process and equipment parameters

The mixing and transport of the material in the TSG shows interactions between screw design, materials throughput and process parameters (Fig. 4.3). Thus,

a combination of these parameters can be used to achieve a further increase in the  $\bar{t}$  and the axial mixing reflected by the increase in  $\sigma_{\theta}^2$  and set a balance between convective and dispersive transport in the TSG barrel. The strongest interaction occurred between the screw speed and the material throughput. Although increasing either screw speed or the throughput caused a reduction in  $\bar{t}$ , their combined effect was less than expected due to their interaction (Fig. 4.4). Physically, the high level of throughput leads to a higher fill degree in the barrel and hence increase in restriction to the material flow. In such condition increasing screw speed can cause a lower reduction in  $\bar{t}$  than low fill condition. The screw speed and the material throughput interaction was also strong in case of  $\sigma_{\theta}^2$  and Pe, where the material throughput with insignificant effect became significant upon interaction with the screw speed (Fig. 4.4). This was mainly due to the interaction between the decreasing screw speed and increasing material throughput, which caused material accumulation in the TSG barrel and the material flow became a dense phase plug flow system, hence leading to reduced  $\sigma_{\theta}^2$ . Increasing screw speed and resulting higher shear in the barrel results in increased  $\sigma_{\theta}^2$  due to the change in the shear-slip velocity relation. As there is a clearance between the wall and the screw, a thin layer of material is expected to be formed on the barrel wall. This thin layer of material is not stationary, but slips slowly in the positive direction due to the high shear at higher screw speed (Lee et al., 2012). Particles from this slow moving layer of granulation material will escape to the bulk flow of the material under the high shear force induced by the rotating screws. At the same time, particles in the normal flow stream may also be trapped in the slow moving thin layer. This phenomenon is anticipated to happen more when the screw speed was increased, subsequently increasing the axial mixing as observed in this study. This change in flow system was also responsible for the inversion of the relation between the convective and dispersive transport with changing screw speed and throughput as reflected by the interaction plot for the Pe in Fig. 4.4.

The second important interaction occurred between the number and stagger angle of kneading discs. Although for  $\bar{t}$  this interaction was insignificant, a mild interaction was observed for the  $\sigma_{\theta}^2$  and the Pe (Interaction plot for  $\sigma_{\theta}^2$  and Pe in Fig. 4.4). This happens mostly due to the strong dependence of the stagger angle on the number of kneading discs. Since the kneading discs in the mixing zones do not avail conveying capacity, material bypassing occurs more regularly in the transport screw zone and mixed flow regime. Thus, when the number of kneading discs and stagger angle are increased simultaneously it leads to reduction in material bypassing and less axial mixing in the TSG barrel.

Therefore, it can be stated that along with the process parameters, the configuration and geometry of the screw and the circumferential clearance between the screws and between screw and wall have a key role to play in this process. However, more work is needed to validate this hypothesis and to obtain more data for the investigation of the RTD tail. Furthermore, the results obtained from this study require to be linked to the granules characterisation study. Together with such a study it can be confirmed which mixing regime is most desirable for the granulation purpose.

## 4.6 Conclusions

NIR chemical imaging was shown to be an adequate tool for residence time analysis as representative and fast measurements could be obtained. Increased screw speed led to a lower  $\bar{t}$  and broader residence time distribution. According to the study, the variations of screw rotation speed, material throughput, number of kneading discs and stagger angle not only have a direct influence on the residence time of the material feed but also on the axial mixing during granulation using TSG. It seems that the screw geometry was one of the important factors affecting the axial mixing. This study has shown that changes in experimental conditions can lead to very different flow regimes, and it is an oversimplification to say that twin-screw granulator shows a plug flow mixing characteristic. The results obtained in this study will be used in future work for linking mixing and transport characteristics in TSG to the particle characterisation study and develop a mathematical model for the continuous granulation considering both mixing and granule characteristics.



---

## Experimental investigation of granule size and shape dynamics in twin-screw granulation

---

**Redrafted from:** Ashish Kumar, Jurgen Vercruyssen, Giacomo Bellandi, Krist V. Gernaey, Chris Vervaet, Jean Paul Remon, Thomas De Beer, Ingmar Nopens, Experimental investigation of granule size and shape dynamics in twin-screw granulation, *International Journal of Pharmaceutics*, Volume 475, Issues 1–2, Pages 485–495.

### Summary

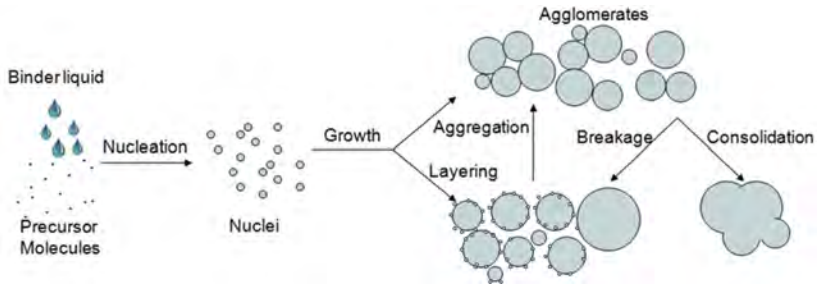
A twin-screw granulator (TSG), a promising tool for continuous high shear wet granulation (HSWG), achieves the desired level of mixing by a combination of the appropriate screw configuration and suitable process settings (e.g. feed rate, screw speed, etc.), thus producing a certain granule size and shape distribution (GSSD). However, the primary sizing and shaping mechanism behind the resulting distribution is not well understood due to the opacity of the multiphase system in the granulator. This study experimentally characterised the GSSD dynamics along the TSG barrel length in order to understand the function of individual screw modules and process settings, as well as their interaction. Particle size analysis of granules collected at the outlet of the TSG suggested significant interaction between the process and screw configuration parameters influencing the heterogeneity in the GSSD. By characterising the samples collected along the screw length, a variable influence of the screw modules at different process conditions was observed. At low liquid-to-solid ratio (L/S), the first kneading module seemed to play a significant role in mixing, whereas

the second kneading module was found to be more involved in reshaping the granules. At high L/S and high throughput, aggregation mainly took place in the second kneading module changing the GSSD. The results obtained from this study will be further used for the calibration and validation of a mechanistic model and, hence, support future development of a more detailed understanding of the HSWG process in a TSG.

## 5.1 Introduction

Twin-screw granulation is a process aiming at enlarging powder particles by HSWG when transported and mixed in a TSG. The size enlargement results in gravity forces exceeding the van der Waals forces, thereby contributing to better flow properties required for improved processability and accurate dosing in further downstream processing. Especially in the pharmaceutical industry, where often highly potent drugs are processed, the amount of dust generated by powder handling is reduced by granulation, resulting in improved safety. Also, segregation (demixing) can be minimized along with the improved downstream processing characteristics of the granules. Therefore, wet granulation is an important process for the particle enlargement during the formulation of solid dosage forms in the pharmaceutical industry (Ennis, 2010). Vervaet and Remon (2005) extensively reviewed continuous granulation techniques. The high shear twin-screw granulation system has received most attention in the last decades due to its inherent benefits, including ease of use in continuous operation and the potential to integrate the TSG with other operations (Seem et al., 2015). The HSWG process in the TSG can be divided into several stages (Fig. 5.1). A number of different mechanisms, including nucleation, growth, aggregation, and breakage, which ultimately determine the characteristics of the produced granules, typically drive the dynamics of wet granulation. Although details about the precise sequence of growth and breakage mechanisms during TSG are not available from the literature, growth and breakage of granules are expected to occur simultaneously due to the inhomogeneous shear force distribution inside the TSG barrel (Dhenge et al., 2012b).

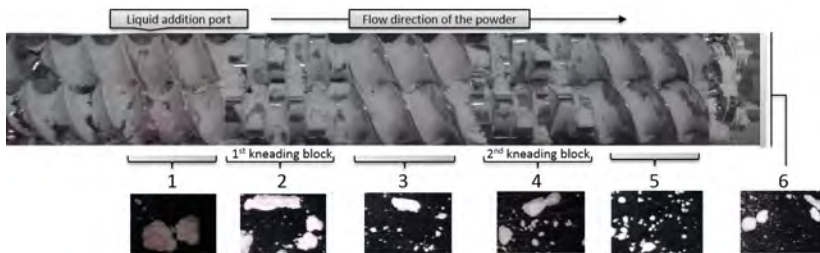
Normally in batch HSWG the granulation time is in the order of minutes, while, in a TSG, it is limited to a few seconds (Chapter 4, section 4.4). The short granulation time is, although desirable from the productivity point of view, challenging for micro to meso scale rate processes in HSWG (Fig. 5.1). The rate processes of wet granulation are required to occur during the short granulation time before the material leaves the TSG. Thus, besides a homogeneous distribution of granulation liquid and powder, the wet mixing in a TSG is also required to be achieved within the shortest possible screw length and



**Figure 5.1:** Schematic presentation of the wet granulation process.

with minimum power input. To facilitate wet granulation, the TSG screw is composed of mainly two blocks (Fig. 5.2). The first and the larger component contains the inter-meshing conveying elements involved in transport of the dry and then wetted powder. The second component is the mixing section, which contains kneading discs staggered at a certain angle to cause restriction to the flow and hence provide the required mixing for wet granulation. These modules change the shear environment of the material being conveyed, which determines the final granule characteristic distribution, such as GSSD, granule strength, etc. (Djuric et al., 2009). Besides the functional role of the screw configuration, performance of a TSG is also related to the applied process parameters. Along with the screw speed and the screw configuration, the feeding rate of the powder and the granulation liquid which together determine the L/S, and the fill ratio inside the barrel are the main process parameters. Therefore, they can be independently chosen to achieve the desired mixing levels of the powder and the granulation liquid, and influence the granulation yield at the outlet (Vercruyssen et al., 2012, 2013b).

However, there is very little understanding regarding the primary shaping



**Figure 5.2:** Screw configuration with 12 kneading discs (2 blocks) used in the twin screw granulator during the study. Sampling locations along the screw length: [1] before first kneading block, [2] on the first kneading block [3] between first and second kneading block, [4] on the second kneading block [5] after second kneading block, [6] outlet of the granulator.



mechanisms behind the particle size and shape distribution in the TSG during wet granulation, due to the opacity of the multiphase system (Dhenge et al., 2012b; El Hagrasy and Litster, 2013). Most of the studies rely on the characterisation of the granules from the outlet of the TSG. Furthermore, the measured torque of the granulator drive is used as the steady state criterion in most studies using TSG. However, torque being a 0-dimensional measurement does not provide information linking the role of change in process parameters to the role of individual screw elements in the TSG.

This study extends the spatial dimension of knowledge regarding HSWG using TSG in order to understand the dynamic change in characteristics of the material while progressing in the TSG barrel. The purpose of this study was to experimentally characterise the change in GSSD along the TSG barrel in order to understand the function of individual screw modules and their interaction with other process parameters such as L/S, screw speed and filling degree in the TSG.

## 5.2 Materials and methods

### 5.2.1 Pharmaceutical model formulation and twin screw granulation

In this study, a premix of  $\alpha$ -Lactose monohydrate (Pharmatose 200M, Caldic, Hemiksem, Belgium) and Polyvinylpyrrolidone (PVP) (Kollidon<sup>®</sup> 30, BASF, Ludwigshafen, Germany) (ratio: 97.5/2.5, w/w) was granulated with distilled water. Granulation experiments were performed using a 25 mm diameter co-rotating twin screw granulator, the granulation module of the ConsiGma-1 unit (GEA Pharma Systems, Collette<sup>™</sup>, Wommelgem, Belgium) (See Chapter 3, section 3.1 for granulator details).

### 5.2.2 Experimental design and sample preparation

A full factorial experimental design was performed to evaluate the influence of number of kneading discs (2, 4, 6, 12), screw speed (500-900 rpm), throughput (10-25 kg/h) and L/S (4.58-6.72% (w/w) based on wet mass) (Table B.1). Three center point experiments were performed as well, resulting in  $32 + 3 = 35$  experiments. For each run, samples were collected from different locations inside the barrel by opening the barrel after stopping the process running at steady state (Fig. 5.2). Sample location 1 was just prior to the first kneading block, sample location 2 on the first kneading block, sample location 3 was between the first and second kneading block, sample locations 4 and 5 were

on and right after the second kneading block. Irrespective of the number of kneading blocks, sample locations on the screw were kept constant during sampling. Sample location 6 was the regular outlet of the granulator and, hence, a large amount of granules was available at that location. The wet granules from all the experiments were dried at room temperature for 24 h and their GSSD was classified in granules size fractions  $<150$ , between 150-1000 and  $>1000$   $\mu\text{m}$  (Appendix B, Table B.1). The particle size distribution of  $\alpha$ -Lactose monohydrate used for this study was 90% not more than 100  $\mu\text{m}$  and 100% not more than 200  $\mu\text{m}$ . Therefore  $<150$ micron was defined as fine to prevent under-prediction of fines. Since several responses were measured, it was helpful to fit a model simultaneously representing the variation of all responses to the variation of the factors. Therefore, the partial least squares (PLS) method was used (employing Modde 9.0 software by Umetrics, Umeå, Sweden), which is able to deal with many responses simultaneously, accounting for their covariances. The effect plot was used to show the change in the response when a factor varies from low to high level, keeping other factors at their averages. The respective 95% confidence interval is shown for each plot. Insignificant effects are those where the confidence interval includes zero. The effects in this plot are ranked from the largest to the smallest.

### 5.2.3 Determination of torque

The TSG has an inbuilt torque gauge and the achievement of steady-state was decided based on the equilibration of the measured torque of the granulator. The torque values obtained after equilibration of the process were averaged to give the overall torque at steady-state during each run. The drive motor torque values are an indication of the shear and consolidation forces experienced by materials inside the barrel.

### 5.2.4 Characterisation of granules

#### Sieve test for particle size analysis

The granule size distribution (GSD) of the granule samples, collected at the outlet of the TSG (sample location 6 in Fig. 5.2) during each design experiment, was determined using the sieve analysis method (Retsch VE 1000 sieve shaker (Haan, Germany)). Granule samples (100 g) were placed on a shaker for 5 min at an amplitude of 2 mm using a series of sieves (150, 250, 500, 710, 1000, 1400 and 2000  $\mu\text{m}$ ). The amount of granules retained on each sieve was determined. All granule batches were measured in triplicate. The fractions  $<150$ , 150-1000 and  $>1000$   $\mu\text{m}$  were defined as the amount of fines, fraction of interest for tableting and oversized fraction, respectively.

## Dynamic image analysis for size and shape analysis of granules

The GSSD of the samples from sampling locations which were inside the TSG barrel (Fig. 5.2), were determined via dynamic image analysis (DIA) used in the EyeTech instrument (Ankersmid B.V., Oosterhout, The Netherlands). A high speed camera (Fig. 5.3a) records pictures (up to 30 pictures /sec) and visualises the particle distribution in real time during the measurement. The camera was synchronized with a pulsing light emitting diode (LED) and takes backlighted images. The captured images of flowing powders were used to calculate GSSD. To ensure good data quality, a measurement confidence level of 95% was imposed for number and volume size distribution. Hence, the instrument continued scanning the sample until the measured mean size of the granules was obtained within  $\pm 2.5\%$  of the true mean.

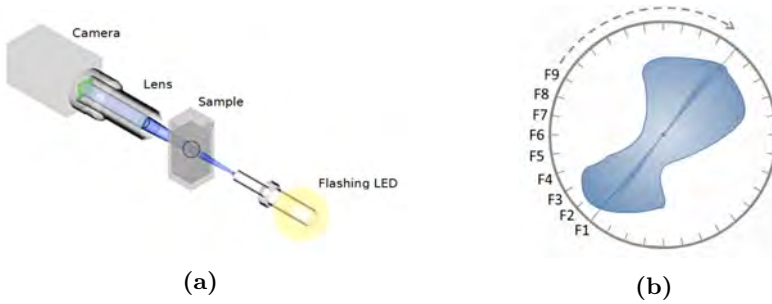
The average Feret diameter was used as the size parameter that provides information on a diameter that is measured every 5 degrees, resulting in an average of a total of 36 diameters for each granule (Fig. 5.3b, eq. 5.1). This size information also serves as a basis for the calculation of shape related parameters such as the aspect ratio, which measures the elongation of the granule and has been used in this study. It is a ratio of the smallest over the largest diameter of the granule (eq. 5.2). The aspect ratio gives information about how far the particles deviate from being spherical. Rod shaped particles have an aspect ratio less than 0.5 while an aspect ratio close to 1 indicates higher sphericity of the granules.

$$\text{Feret Diameter} = \frac{d_1 + d_2 + d_3 + d_4 \dots d_{36}}{36} \quad (5.1)$$

$$\text{Aspect ratio} = \frac{\text{Minimum Feret Diameter}}{\text{Maximum Feret Diameter}} \quad (5.2)$$

The link between mean Feret diameter and aspect ratio of the granules was determined simultaneously by the WINDOX software using Sympatec Image Analysis (QICPIC) (with the same measurement system as the Eyetech) by dispersing the granules under gravity through the focus plane of a high speed camera.

The screw arrangement at sample locations 2 and 4 was changed based on the experimental design, which lead to a deviation in granule characteristics at these locations purely due to the local and experimental run specific conditions. Therefore, they have not been used in the remainder of this study and the samples from location 1, 3 and 5 in Fig. 5.2 were analysed for further study.



**Figure 5.3:** (a) Principle of the dynamic image analysis technique. The shape and size of the granule are determined based on the imaged formed by the LED flashing light passing directly through the sample and captured by the camera. (b) The Ferret diameters provide information on the size (average Ferret diameter), give deep insight into the granules morphology (minimum Ferret and maximum Ferret) and serve as a basis for the calculation of the aspect ratio.

## 5.3 Results and discussion

This study examined the impact of four main factors of HSWG using TSG, which include the screw speed, number of kneading discs, throughput and L/S during granulation on the GSSD.

### 5.3.1 Influence of process variables on the granules at the outlet

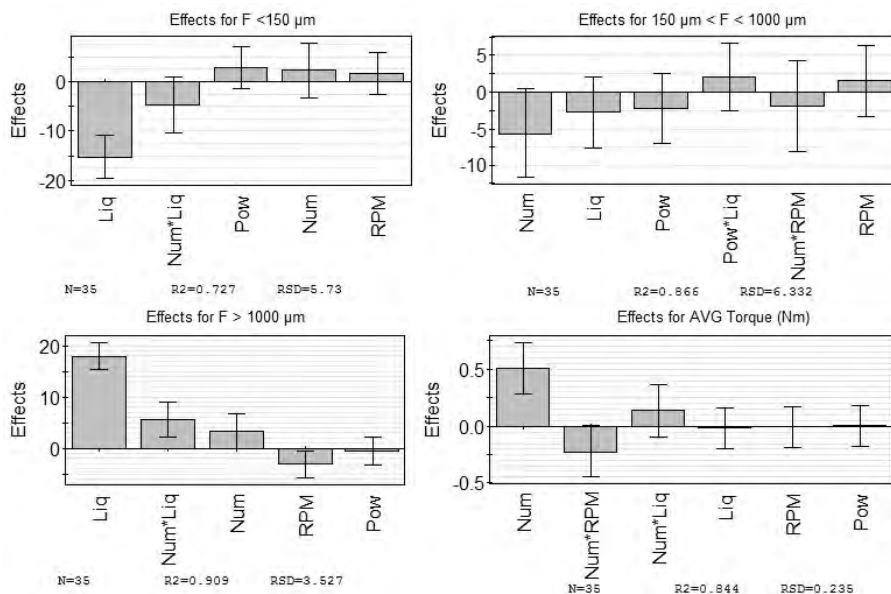
The samples collected at the outlet of the TSG (sample location 6 in Fig. 5.2) were analysed using a sieve test for each experiment. This was useful to understand the effect of the various factors on the granule size fractions (F) defined as fines ( $F < 150 \mu\text{m}$ ) ( $R^2 = 0.72$ ), fraction of interest for tableting ( $150 \mu\text{m} < F < 1000 \mu\text{m}$ ) being the granulation yield ( $R^2 = 0.87$ ), oversized granules ( $F > 1000 \mu\text{m}$ ) ( $R^2 = 0.91$ ) as well as the measured torque (Nm) ( $R^2 = 0.84$ ) determined via the PLS method (Table B.1). The effect of individual factors and their combinations on size fractions, suggested that the L/S had a significant effect on both the fines (16.10–45.87%  $< 150 \mu\text{m}$ ) and oversized fraction (15.21–49.43%  $> 1000 \mu\text{m}$ ) of the granules (Fig. 5.4, Table B.1). From this analysis, it was observed that granules contained a higher fraction of fines when the powder was less wetted at low L/S and vice versa produced more oversized granules. Since the parameters having a positive effect on the oversized fraction had a negative effect on the fines and vice versa, these parameters did not affect the yield of the fraction of interest significantly (yield between 31.01 - 55.90%). Furthermore, low screw speeds resulted in an increase of the oversized fraction,

due to material accumulation at a reduced conveying rate and the lack of proper sheared mixing and less breakage inside the barrel. For the oversized fraction, the interaction between L/S and number of kneading discs was significant as the effect of the change in L/S was observed to be different at a low or high number of kneading discs. At a higher number of kneading discs, L/S variations caused more drastic changes in the oversized fraction compared to similar L/S variations for a low number of kneading elements.

The measured torque of the granulator drive, which is related to the fill level and the shear mixing of material in the TSG, was found to be most affected by the number of kneading discs. The increase in the number of kneading discs caused an enhanced hindrance to the flow of material and hence a high torque of the granulator drive. However, this hindrance to the flow in the screw channel resulted in a greater residence time and more distributive mixing of the powder which is essentially required for a better granulation yield (El Hagrasy and Litster, 2013). Also, the interaction between the number of kneading elements and screw speed was significant with respect to the torque. The torque increase from 2 to 12 kneading elements was higher at a low screw speed compared to that at a high screw speed. This could be explained by the higher filling degree of the barrel at low screw speed.

### **5.3.2 Influence of process variables on granule properties along the TSG length**

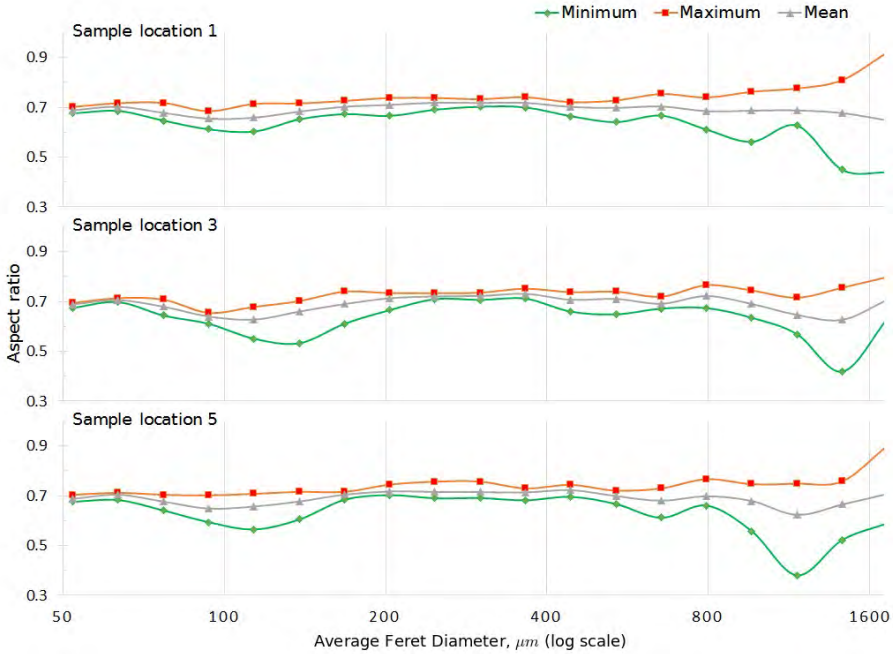
The samples from location 1 (before the first kneading block), location 3 (after the first kneading block) and location 5 (after the second kneading block in the screw configuration with 2 kneading blocks) were used to characterise the change in the GSSD along the TSG length (Fig. 5.2). Firstly, it is important to point out that the granulation using only 2 kneading discs did not yield a sufficient degree of control over the process, and therefore the results were inconsistent (data not shown). We believe that 2 kneading discs in the screw configuration pose too low of a hindrance to flow in the screw channel. Due to this, the primary response by the kneading block in terms of restriction to the flow was significantly asynchronous, thus generating random results. Therefore, for further comparison only results from runs with 4, 6 and 12 kneading discs are presented. The pattern of evolution in granule size and shape indicates that the formation of primary granules (50-200  $\mu\text{m}$ ) led to a loss in the particle shape uniformity via reduction in the aspect ratio (Fig. 5.5). The further growth of granule size (between 200-400  $\mu\text{m}$ ) resulted in a more uniform and higher mean aspect ratio. However, an increase in granule size beyond 400  $\mu\text{m}$  led to a more heterogeneous and relatively lower aspect ratio. For the three sample locations (1, 3 and 5) in Fig. 5.2 it was observed that granules at location 1



**Figure 5.4:** Effect plots of the partial least squares (PLS) models showing the mean responses of number of kneading discs (Num), screw speed (Scr) [500-900 rpm], throughput (Pow) [10-25 kg/h] and liquid-solid ratio (Liq) [4.58-6.72%] on the size fractions (F) defined as fines ( $F < 150 \mu\text{m}$ ), fraction of interest for tableting ( $150 \mu\text{m} < F < 1000 \mu\text{m}$ ) and oversized granules ( $F > 1000 \mu\text{m}$ ) and the measured torque.

(top subplot in Fig. 5.5) had a reasonably homogeneous aspect ratio except for the oversized granules. As the granules moved to sample location 3 (middle subplot in Fig. 5.5) both primary ( $50\text{-}200 \mu\text{m}$ ) and oversized granules were further deformed. Compared to location 3, there was a minor increase in the width of the intermediate size granules (between  $200\text{-}800 \mu\text{m}$ ) at sample location 5 (bottom subplot in Fig. 5.5) with a more uniform aspect ratio. However, the larger granules remained deformed. This can be explained by the high shear and the lack of free space inside the TSG which is very different from high-shear mixers where granules, despite their large sizes, tumble on their free surface and get rounded (Lee et al., 2013).

Furthermore, as the wetted powder is conveyed from the pre-kneading zone to the first kneading zone and further, the number density of the granules shifted towards the right, indicating an increase in the fraction of larger granules and occasionally some breakup at the end (Fig. 5.6 and 5.8). Remarkably, an increasing number of kneading discs not only increased the fraction of larger granules for the downstream sample locations 3 and 5 which were located after the kneading blocks but also at sample location 1, which was located upstream



**Figure 5.5:** Mean, maximum and minimum aspect ratios vs. mean Feret diameter of the granules in the range of 50 to 1600  $\mu\text{m}$  (log scale, x-axis) at location 1 (top subplot), location 3 (middle subplot) and location 5 (bottom subplot) in barrel for the runs performed at different throughputs (10, 25 kg/h), liquid-to-solid ratio (4.58, 6.72% (w/w)), screw speed (500, 900 rpm) and number of kneading discs (4, 12).

of the kneading discs. This suggests that along with the mixing section composed of kneading discs, a significant mixing and granulation also occurs in the upstream section. The material in the mixing section flows more slowly than in the upstream section and hence the built-up material in the flow restricted zone of the barrel is force-mixed with the incoming materials. Lee et al. (2012) have shown that the degree of filling of the 'non-kneading zone' of the granulator increases with an increase in the restriction to the flow. Also, elongation of the granules was observed to decrease along the granulator length and for increasing number of kneading discs (Fig. 5.7 and 5.9). This spherification of granules together with enlargement now allows discussion of the effects of factors as well as their interactions on GSSD.

## **Effect of throughput**

### **Low liquid-to-solid ratio (4.58%) and low screw speed (500 rpm)**

An increase in the throughput from 10 kg/h to 25 kg/h keeping the L/S and screw speed at the lowest level resulted in a minor increase in the granule size for successive sample locations (comparing ID 1 and 3 plots in Fig. 5.6). This effect was clearest for 12 kneading discs, where a small reduction in the amount of fines for sample location 5 occurred. No significant effect on the shape distribution was observed for configurations containing up to 6 kneading discs (comparing ID 1 and 3 plots in Fig. 5.7). For a higher number of kneading discs the elongation of the granules decreased with the progressive sample locations indicating a greater consolidation of granules.

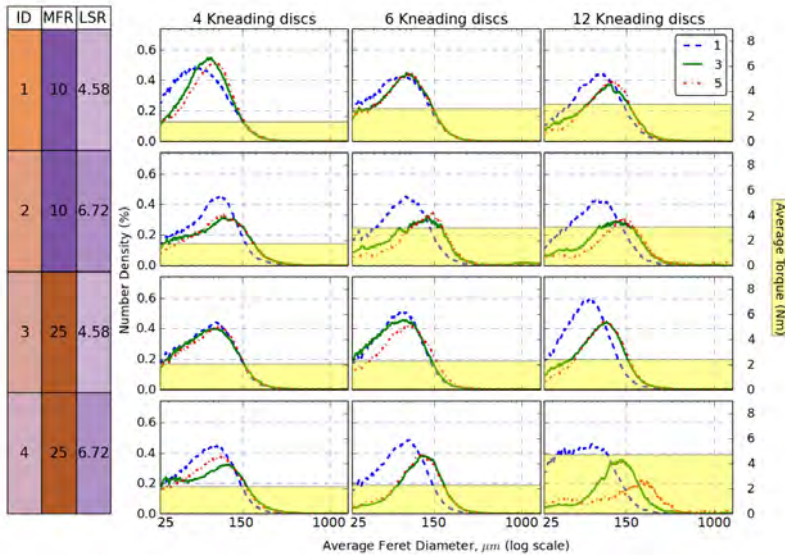
### **High liquid-to-solid ratio (6.72%) and low screw speed (500 rpm)**

At high L/S more granulation liquid enhanced the size enlargement rate processes (such as wetting, nucleation and aggregation), and thereby a shift of GSDs towards higher average diameters was noticed (ID 2 and 4 plots in Fig. 5.6). For up to 6 kneading discs, increased throughput had a trivial influence on granulation, which was reflected by the fact that no change in the GSD was observed. However, a further granule size enlargement at location 5 and a broadening of the distribution were observed when the second kneading block was present (comparing ID 2 and 4 plots for 12 kneading discs in Fig. 5.6). Besides the size, increasing throughput at a high number of kneading discs affected the aspect ratio profile, which shifted towards the right and became narrower for location 3 (ID 2 and 4 plots in Fig. 5.7). However, the higher fill ratio at increased throughput and sluggish flow of more wetted powder in the granulator barrel led to an almost doubled TSG drive torque (ID 4 plots in Fig. 5.6).

### **Low liquid-to-solid ratio (4.58%) and high screw speed (900 rpm)**

Despite good shear mixing at high screw speed, increasing the throughput did not support an increase in the fraction of larger granules due to a low L/S (ID 1 and 3 plots in Fig. 5.8). The increased throughput for the 12 kneading discs configuration showed a reduction in the larger granules after the second kneading block (location 3 and 5 profiles when comparing ID 1 and 3 plots for 12 kneading discs in Fig. 5.8). Besides the reduction in the granule size, the increased throughput did not affect the shape of granules and the profiles for ID 1 and 3 plots in Fig. 5.9 corresponded to the same pattern for an equal number



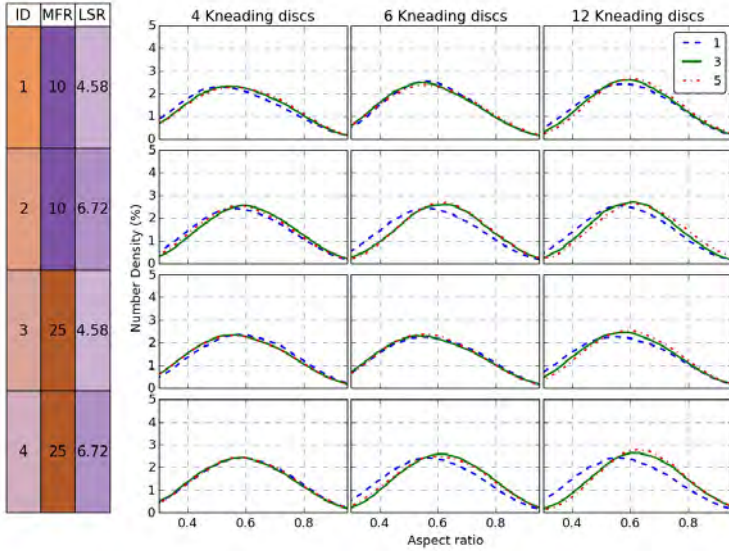


**Figure 5.6:** Number density of the granules (primary y-axis) having an average Feret diameter in the range of 50 to 1500  $\mu\text{m}$  (log scale, shared x-axis) and torque level (secondary y-axis) at different throughputs (10-25 kg/h), liquid-to-solid ratio (4.58-6.72% (w/w)) at low screw speed (500 rpm) [ID: experiment ID, MFR: throughput (kg/h), LSR: liquid-solid ratio (%)].

of kneading discs.

### High liquid-to-solid ratio (6.72%) and high screw speed (900 rpm)

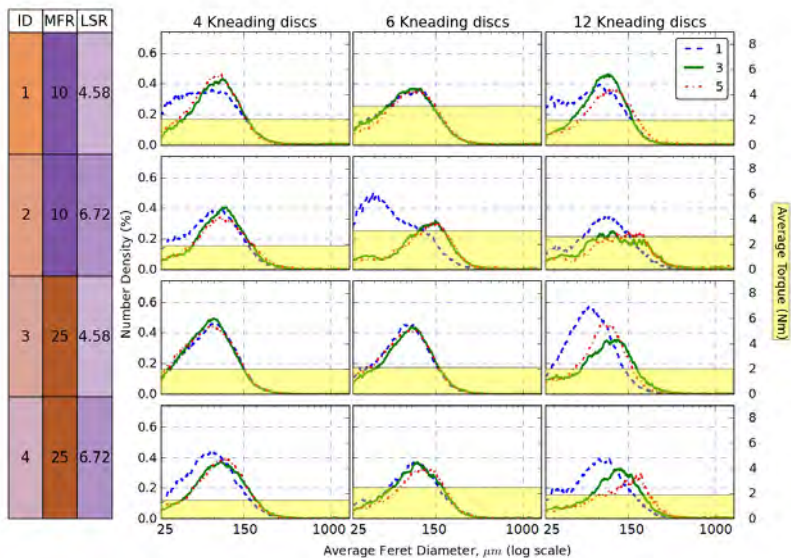
With an increase in throughput at these conditions, granulation was more uniform which led to a clear difference between the GSD profile from sample location 1, 3 and 5 when two kneading blocks were used (comparing ID 2 and ID 4 plots in Fig. 5.8). However, the GSD of location 3 was narrower than at location 5 in the ID 4 plot for 12 kneading discs. The increased throughput only affected the shape of the granules from location 1, where the granulation liquid was distributed to a larger amount of powder available at high throughput. However, due to the high shear-induced mixing at high screw speed, despite the high filling ratio the downstream material was well-mixed thus yielding a more uniform particle aspect ratio distribution for ID 4 plots compared to ID 2 plots in Fig. 5.9. However, for sample locations 3 and 5 the aspect ratio profile



**Figure 5.7:** Number density of the granules (primary y-axis) having an aspect ratio in the range of 0.3 to 1 (shared x-axis) at a different throughput (10-25 kg/h), liquid-to-solid ratio (4.58-6.72% (w/w)) at low screw speed (500 rpm) [ID: experiment ID, MFR: throughput (kg/h), LSR: liquid-solid ratio (%)].

corresponded to the same pattern for an equal number of kneading discs.

The above suggests that increasing throughput is not beneficial without sufficient granulation liquid and shear mixing to make strong bridges between powder particles in the agglomerates. Despite the availability of granulation liquid, when the shear-induced mixing is poor, an inhomogeneous distribution of liquid over the material occurs resulting in a broader GSD. On the other hand, at low L/S, an increase in screw speed leads to a high level of shear mixing and further contributes to the fragility of the granules and thus increased attrition and breakage. Although an increase in throughput requires a higher torque, this issue can be solved by increasing the screw speed during granulation which increases the conveying rate and reduces the load on the screws. At high shear and high L/S, the wet granules are easy to deform leading to a more uniform shape. However, due to the higher filling of the channels of the screws and the increased consolidation at high throughput, attrition of the wet mass between the screws and barrel wall may increase, as observed by Dhenge et al. (2011).



**Figure 5.8:** Number density of the granules (primary y-axis) having an average Feret diameter in the range of 50 to 1500  $\mu\text{m}$  (log scale, shared x-axis) and torque level (secondary y-axis) at different throughputs (10-25 kg/h), liquid-to-solid ratio (4.58-6.72% (w/w)) at high screw speed (900 rpm) [ID: experiment ID, MFR: throughput (kg/h), LSR: liquid-solid ratio (%)].

## Effect of liquid-to-solid ratio

### Low throughput (10 kg/h) and low screw speed (500 rpm)

When the L/S was increased at low levels of throughput and screw speed, the degree of aggregation increased (comparing ID 1 and 2 in Fig. 5.6). With an increase in the number of kneading discs, the measured torque and shear mixing increased and the GSD shifted towards higher granule sizes at sample locations 3 and 5 (ID 2 plot in Fig. 5.6). However, no narrowing of the size distribution at sample location 5 was observed. An additional kneading block showed only a slight contribution to the aggregation when comparing the number based GSD profile at sample location 3 and 5 in the ID 2 plots of Fig. 5.6. This also happened due to the fact that bigger granules are created by aggregation of many small particles, thereby resulting in a visible drop in the number of small size granules, but only a small increase in the bigger ones. The increase in

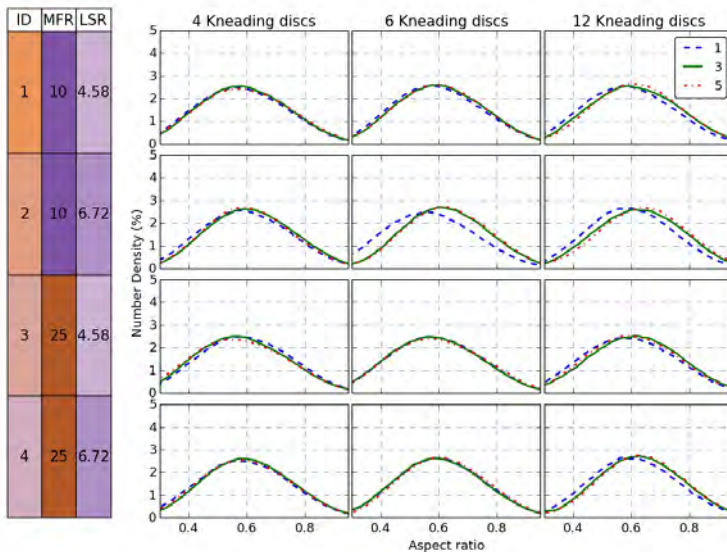
L/S also reduced the granule elongation for the screw configurations with 6 and 12 kneading discs at sample locations 3 and 5 (comparing ID 1 and 2 in Fig. 5.7). Altogether it can be confirmed that the additional kneading block had a minor contribution in this case, both in terms of granule enlargement and the spherification of granules.

### **High throughput (25 kg/h) and low screw speed (500 rpm)**

When the granulation was performed at high throughput and a low screw speed, an increase in L/S increased the degree of aggregation (comparing ID 3 and 4 plots in Fig. 5.6). However, the most remarkable change was observed for the screw configuration with 12 kneading discs when the GSD profiles of the three sample locations were clearly segregated by the second kneading block in the TSG. Moreover, the aspect ratio profiles at higher L/S shifted towards the right and became narrower in ID 4 compared to ID 3 plots of Fig. 5.7, indicating an increased aspect ratio and uniformity of the granule shape. However, the torque of the TSG drive increased significantly due to the high fill ratio and sluggish flow of wetted powder inside the granulator barrel.

### **Low throughput (10 kg/h) and high screw speed (900 rpm)**

With the increase in L/S at the low throughput and high screw speed, there was only a minor increase in granule size for the screw configuration with 4 kneading discs (comparing ID 1 and 2 plots in Fig. 5.8). However, increasing the number of kneading discs increased the aggregation level due to which the GSD shifted towards a larger diameter. The second kneading block showed only a small contribution to the aggregation level as can be observed from profiles from sample locations 3 and 5 in ID 2 plots of Fig. 5.8. This may be due to the lack of unwetted powder in the granulator to support further agglomeration. Besides, the additional granulation liquid encouraged the formation of more spherical granules in successive sample locations of the TSG suggesting a higher level of consolidation of the granules (comparing ID 1 and 2 plots in Fig. 5.9). However, the shape distributions of samples before and after the second kneading block were similar. This indicates that, at a very low fill level, the second kneading block played a minor role in changing the shape of the granules.



**Figure 5.9:** Number density of the granules (primary y-axis) having an aspect ratio in the range of 0.3 to 1 (shared x-axis) at different throughputs (10-25 kg/h), liquid-to-solid ratio (4.58-6.72% (w/w)) at high screw speed (900 rpm) [ID: experiment ID, MFR: throughput (kg/h), LSR: liquid-solid ratio (%)].

### High throughput (25 kg/h) and high screw speed (900 rpm)

At high throughput more material was available inside the TSG, but an increase in screw speed caused a reduction in the fill level and improved mixing. However, at a lower number of kneading discs, a considerable reduction of distributive mixing of the powder and the granulation liquid and consequent aggregation occurred, leading to minor shifts in GSD between locations 1, 3 and 5 (comparing ID 3 and 4 plots in Fig. 5.8). When the number of kneading discs was increased, the wetted powder was well mixed despite a lower fill level of the barrel and hence agglomerated, leading to an increase in granule size. For the screw configuration with 12 kneading discs, the most significant difference between all three locations was observed, which can be attributed to the presence of an additional kneading block between sampling location 3 and 5 along with the one between sample location 1 and 3. An increase in the number of kneading discs also caused an increase in the number density of high aspect ratio granules (comparing ID 3 and 4 plots in Fig. 5.9). Moving from a low to a high number of kneading discs, for the location 1, 3 and 5 the aspect ratio distributions were very similar. This indicates that shear-induced

consolidation occurred in the early stage of the granulation (near location 1) and the aggregation and the consolidation of the granules took place simultaneously.

Overall, more granulation liquid at increased L/S enhances wetting, nucleation and aggregation, i.e. granule enlargement rate processes (Litster and Ennis, 2004). However, an increased L/S can only improve the agglomeration level when the mixing is also increased. An increase in screw speed causes a reduction in the fill level of the wetted material and an increase in the shear leading to improved mixing. Especially at high screw speed the axial mixing inside the granulator increases significantly (section 4.4). In this study, a higher L/S also affected the shape of the granules along the length and the produced granules grew to be more spherical. This outcome is in accordance with results reported by Dhenge et al. (2012b) comparing samples collected at the granulator output only. However, the torque of the TSG drive increases significantly due to the high fill ratio and sluggish flow of wetted powder in the granulator barrel, which can be reduced by increasing the conveying rate of the screw at high screw speed.

## **Effect of combined change in throughput and liquid-to-solid ratio**

### **Low screw speed (500 rpm)**

When both throughput and the L/S were increased at low screw speed, there was less difference between the GSD from sample locations 1 and 3 for a low number of kneading discs due to the lack of mixing (comparing ID 1 and 4 plots in Fig. 5.6). However, a progressive mixing in the axial direction occurred due to the shear induced during the conveying of the wet powder, hence changing the morphology in terms of reduction in the fraction of smaller granules and an increase in the fraction of larger granules at sample location 3 and 5 in the ID 4 plot for 4 kneading discs in Fig. 5.6. For the screw configuration with 12 kneading discs, most distinctly separate distributions for the three sample locations were observed. However, the number density of small granules also increased with spatial progress indicating that, beyond the consolidation, breakage was an important size reduction phenomenon and competed with the aggregation process in the second kneading block of the TSG under these conditions. Also, at a low number of kneading discs, the shape distribution of the sample locations 1, 3 and 5 were similar (comparing ID 1 and ID 4 plots in Fig. 5.7). For an increasing number of kneading discs, an increase in the aspect ratio of granules from location 3 and 5 caused the shape distribution of the locations 1 and 3 samples to be more distinct, while the difference between locations 3 and 5 samples remained low.

### **High screw speed (900 rpm)**

When the screw speed was increased, for 4 kneading discs the difference between the downstream sample profiles from locations 3 and 5 was small (plot ID 4 in Fig. 5.8). With 6 kneading discs the restrictive forces started playing a role, which resulted in the formation of more stable GSD even before the material entered the first kneading block (plot ID 4 in Fig. 5.8). However, in lack of adequate distributive mixing of wetted powder, there was only a minor difference between sample location 3 and 5. When a second kneading block was added between sampling location 3 and 5 in the screw, the powder with high moisture content was distributively mixed and hence agglomerated further (plot ID 4 in Fig. 5.8). This led to GSD profiles, which were separated for all the three sample locations. Also, unlike the observations at low screw speed (ID 4 plot for 12 kneading discs in Fig. 5.6), the number density for the lower particle size did not increase with the spatial progress for high screw speed indicating that sufficient mixing occurred to support the aggregation process at location 5 in the TSG barrel (ID 4 plot for 12 kneading discs in Fig. 5.7). The suitability of this condition was also reflected in the shape dynamics as the increase in number of kneading discs only caused a minor increase in the aspect ratio distributions (comparing ID 1 and ID 4 plots in Fig. 5.9). For both a low and a high number of kneading discs, for the location 1, 3 and 5 the aspect ratio distribution were quite similar regardless of the throughput. This indicates that consolidation of the granules went well along with the aggregation during the conveying of the granules in the TSG barrel.

These results suggest that increased mixing is required when the throughput and the L/S are high. Since the mixing of the wetted powder inside the TSG is mainly distributive, the most effective mixing in this condition can be obtained by increasing the number of kneading discs. Besides, a high shear and a low fill level due to the increased conveying rate at high screw speed can lead to a very efficient mixing in the TSG barrel (Vercruyse et al., 2012). These results also suggest that at increased shear first the wetted granules' shape changes through consolidation, only after which the breakage occurs.

### **Effect of increase in screw speed**

At low throughput and L/S, when the screw speed was increased from 500 rpm (ID 1 plot of Fig. 5.6) to 900 rpm (ID 1 plot of Fig. 5.8), there was no significant shift in the GSDs. Only the measured torque level decreased for 12 kneading discs due to reduction in hindrance to the flow at increased conveying rate and low filling ratio at high screw speed. Comparing the shape dynamics, the distribution of shape followed a consistent pattern due to a lower fill ratio

and good mixing in the barrel. With an increasing number of kneading discs, there was an increase in the aspect ratio due to an accumulated level of shear (ID 1 plots of Fig. 5.7 and 5.9).

At a low throughput and a high L/S, an increased screw speed assisted early aggregation of the wetted powder, which is reflected by an increase in the fraction of larger granules for all three sample locations (comparing ID 2 plots of Fig. 5.6 and 5.8). The addition of more kneading discs further increased the agglomeration level and a successive reduction in the amount of fines. Moreover, at increased screw speed together with an increase in the number of kneading discs, the granules became more spherical (comparing ID 2 plots of Fig. 5.7 and 5.9). It can be assumed that increased shear caused a greater consolidation of granules and consequently an increased sphericity, while making squeezed-out liquid available to a further granulate leading to the further shift of the GSD towards larger diameters.

However, when the feed rate was high and the L/S was low, an increase in the screw speed resulted in an early aggregation of the particles with minimal number of kneading discs (comparing ID 3 plots in Fig. 5.6 and 5.8). The addition of more kneading discs to the screw caused a reduction in the amount of fines. However, for the configuration with 12 kneading discs there was a reduction in the number density of larger particle sizes at successive sample locations indicating breakage of larger granules induced by the second kneading block (ID 3 plot for 12 kneading discs in Fig. 5.8). This is likely due to availability of insufficient liquid to make strong bridges between the particles in the granules, which was also reflected in the aspect ratio where no significant change in the shape distribution was observed due to lack of additional particle growth processes (comparing ID 3 plots in Fig. 5.7 and 5.9).

The effect of an increase in screw speed at high levels of throughput and L/S was discussed in section 5.3.2. The major contribution of increasing the screw speed at high throughput and L/S was the reduction in granulator torque, without affecting the GSD. This is desirable at manufacturing scale from a productivity point of view where operation at high throughput is a prerequisite.

These comparisons suggest that along with the distributive mixing by the kneading discs, the shear-induced mixing by increasing screw speed is another important factor in mixing. However, increasing the screw speed reduces the mean residence time of the wet powder in the barrel. Hence, a competitive relationship exists between the shear mixing in the barrel and the residence time of the wetted powder, both of which are desired to support granulation rate processes. Except for the granules which are brittle due to lack of sufficient



granulation liquid, the shape distribution at high shear remains the same compared to low shear conditions. This suggests that the shape of granules largely depends on the design of the screws and not on the shear level.

## 5.4 Conclusions

This study showed that a balanced mixing is important to change the granule characteristics through aggregation and breakage mechanisms along with the consolidation of the particles. The fill ratio in the barrel is an important factor both because it affects the torque required by the granulator drive, and it plays a major role in changing the size and shape of the particles. Increasing throughput is beneficial only when sufficient granulation liquid and shear mixing is present to make strong agglomerates. An increase in throughput causes a higher torque, which can be resolved by increasing the screw speed. The deformation of wet granules is easy and granules with a more uniform shape are produced. A number of competing mechanisms, such as aggregation, consolidation and breakage occur in the process. Although this study provided a detailed insight regarding the process, the experimental data produced only semi-quantitative insight into which of these mechanisms were dominant. Unlike experimental results, where only the collected data are available, mechanistic models are more transparent in the sense that any and all of the intermediate data can be observed after simulation (given a thoroughly validated model is available). Therefore the results obtained from this study will now be used as the basis for the development of a mechanistic model to further improve our understanding of the granulation process in a TSG.

---

## Experimental investigation linking granulation performance with residence time and granulation liquid distributions in twin-screw granulation

---

### Summary

The residence time in a twin screw granulator is short. Thus, the solid-liquid mixing must be achieved quickly by appropriate arrangement of transport and kneading elements in the granulator barrel allowing the production of granules with a particle size distribution appropriate for further downstream processing. In this study, the impact of process (feed rate, liquid-to-solid ratio and screw speed) and equipment parameters (number of kneading discs and stagger-angle) on the residence time (distribution), the granulation liquid-powder mixing and the resulting granule size distributions (GSDs) during twin-screw granulation were investigated. Residence time and axial mixing information was extracted from tracer maps and the solid-liquid mixing was quantified from moisture maps, obtained by monitoring the granules at the granulator outlet using near infra-red chemical imaging (NIR-CI). The granule size distribution was measured using the sieving method. The screw speed most dominantly influenced the mean residence time, which decreased with increasing screw speed. Interaction of material throughput with the screw speed and with the number of kneading discs caused most variation in the studied responses including residence time and mixing capacity. At a high screw speed, granulation yield (granules with diameter between 150-1400  $\mu\text{m}$ ) improved due to high axial mixing. However, increasing material throughput quickly lowers the yield due to insufficient solid-liquid mixing. Similarly, increasing liquid-to-solid ratio (L/S) resulted in more

oversized granules, which further increased at higher throughput. Although an increasing number of kneading discs was found to be critical for achieving a uniform distribution of the granulation liquid, the granulation performance was hampered due to insufficient solid-liquid mixing capacity of the current kneading discs which is essential for wet granulation. Thus, a balance between material throughput and screw speed should be strived for in order to achieve a specific granulation time and solid-liquid mixing for high granulation yield. Additionally, more efforts are needed both in modification of the screw configuration as well as the geometry of the mixing elements to improve the mixing capacity of twin-screw granulator (TSG). The results from the current experimental study improved the understanding regarding the interplay between granulation time and the axial and solid-liquid mixing responsible for the granulation performance in twin-screw wet granulation.

*Keywords:* residence time distribution, axial mixing, NIR chemical imaging, solid-liquid mixing

## 6.1 Introduction

The granulation time in a TSG (which is generally between 2 and 40 seconds) and is measured as the  $\bar{t}$ , is much shorter compared to the granulation time available in a typical batch granulator, which is in the order of minutes (see Chapter 7). Thus, the solid-liquid mixing in the TSG must be achieved in a short period by appropriate arrangement of transport and kneading elements in the granulator barrel allowing the production of granules with a GSD suitable for further downstream processing. Therefore, it is interesting to investigate how different process and equipment settings lead to changes in the residence time distribution (RTD), axial and solid-liquid mixing which consequently lead to a certain granulation yield. This is particularly important as it could be concluded from an earlier study that a residence time increase beyond a certain threshold is the result of a change in flow regime inside the TSG, transitioning from mixed flow to plug-flow (see section 4.4 of Chapter 4). As the plug flow regime is unfavourable for mixing which is ultimately required for wet granulation, a detailed study investigating the link between mixing and transport characteristics in the TSG and the granulation performance is required.

Experimental investigation of twin-screw granulation RTD and its impact on granulation performance has already been of interest for several other researcher groups. Dhenge et al. (2010) measured the RTD using the sampling cup method under different processing conditions and showed that process parameters such as screw speed and L/S have a vital influence on the residence time. The

same RTD measurement approach was applied by El Hagrasy et al. (2013b) to estimate the effect of changes in formulation properties such as raw material composition as well as granulation liquid properties such as viscosity on the granule properties. However,  $\bar{t}$  for a typical screw design is between 2-40 s which is in the order of the sampling time in the sampling cup method, making this method unsuitable for TSG studies (Li et al., 2014). In a remarkable attempt, Lee et al. (2012) obtained the RTD for TSG using positron emission particle tracking (PEPT) to study the axial mixing of the processed material inside the TSG barrel, which is essential information for the optimisation of the obtained granule properties. Although this technique is very powerful, the single-particle tracking method also suffers from major challenges as discussed in Chapter 7. Recently, Li et al. (2014) used a visual technique based on digital video recording to measure RTD as a function of screw elements during twin-screw granulation. Results from this study indicated a significant increase in  $\bar{t}$  and a narrowing of RTD with larger kneading blocks. The study questioned the role of the kneading block as mixing zone which is atypical since RTD can only be used to quantify axial mixing. Mixing of solid-liquid is typically driven by a combination of both axial and transverse mixing inside the TSG. Thus, this cannot be investigated solely from an RTD study. However, only a small number of investigations have attempted to quantitatively describe the influence of process parameters on solid-liquid mixing performance (Vercruyse et al., 2013b). This is because of the lack of suitable techniques allowing detailed local flow characterisation in systems such as the TSG, especially due to their opacity. Vercruyse et al. (2013b) applied an image data collection method based on near infrared (NIR) chemical imaging to evaluate the influence of the liquid addition method, screw configuration, moisture content and barrel filling degree on the moisture homogeneity during twin-screw granulation. Applying the same measurement approach, a tracer (theophylline anhydrate) was injected in the granulator and monitored to investigate the RTD of the tracer inside the barrel as a function of screw speed, material throughput and number as well as stagger angle of the kneading discs in the screw configuration of the TSG. Model-based analysis of these experimental data was also performed to further investigate the mixing and flow behaviour inside the TSG (Kumar et al., 2015). However, a relation between the residence time, the axial mixing and the solid-liquid mixing, all responsible for the shape of the granule size distribution, is still not established.

In this study, NIR chemical imaging was used as analytical technique to simultaneously and qualitatively and quantitatively characterise the flow and axial mixing of tracer material as well as the mixing of the two phases, i.e. solid formulation material and granulation liquid, as function of process parameters

(screw speed, material throughput and liquid-to-solid ratio) and equipment parameters (number and stagger angle of kneading discs in screw configuration) of the twin-screw granulation. Since residence time and its distribution, as well as solid-liquid mixing dictate the final granulation yield, the resulting GSD was also measured to understand the overall influence of different flow and mixing conditions.

## 6.2 Materials and methods

### 6.2.1 Pharmaceutical model formulation and twin screw granulation

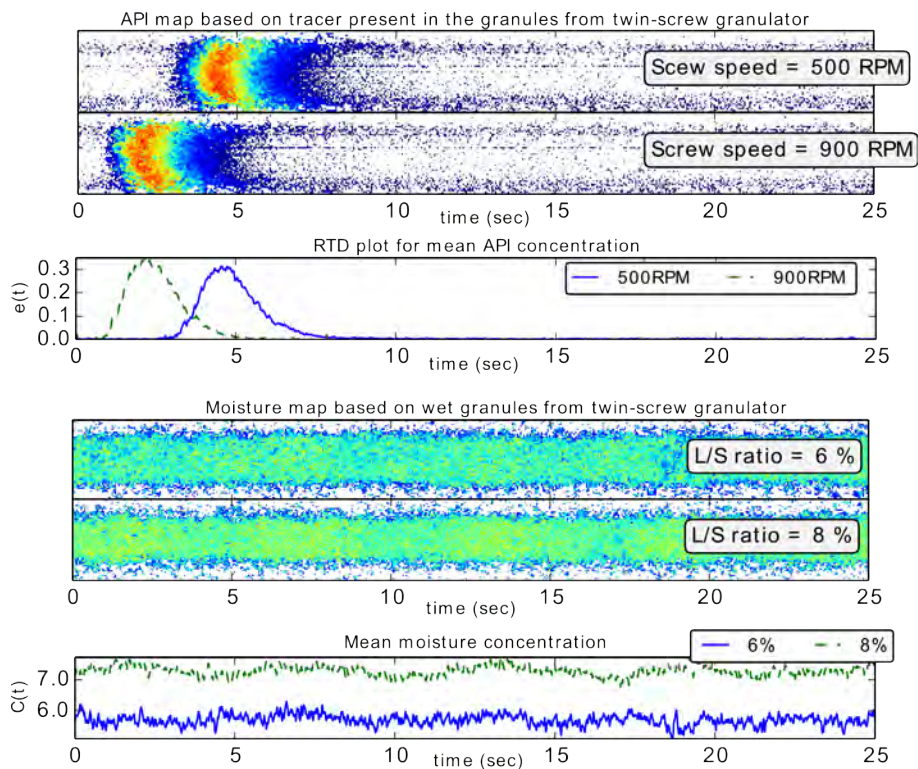
$\alpha$ -Lactose monohydrate (Pharmatose 200M, Caldic, Hemiksem, Belgium) was used as a model excipient. Distilled water was added as granulation liquid which was mapped in the granules for liquid distribution. To evaluate the residence time of material inside the barrel, theophylline anhydrate (Farma-Química Sur, Malaga, Spain) was used as tracer component. Granulation experiments were performed using a 25 mm diameter co-rotating twin screw granulator, the granulation module of the ConsiGma-25 unit (GEA Pharma Systems, Collette™, Wommelgem, Belgium) (See Chapter 3, section 3.1 for granulator details).

#### Experimental design

A full factorial experimental design was performed to evaluate the influence of screw speed (500-900 rpm), material throughput (10-25 kg/h), L/S (6-8%), number (4, 6 and 12) and stagger angle (30° and 60°) of the kneading discs in the screw configuration on the RTD and axial mixing of the material. Three center point experiments were performed as well, resulting in  $48 + 3 = 51$  experiments.

At the outlet of the granulator, the near infrared chemical imaging (NIR-CI) system was used to measure solid-liquid mixing and the theophylline dynamics (see Fig. 4.1 in Chapter 4). A 25 s chemical imaging measurement without tracer injection for each design experiment (run) was used to measure the spatial distribution of the granulation liquid which was calculated using the band ratio method explained in section 6.2.2. For the residence time measurements, anhydrous theophylline (2% (w/w) of the material throughput per minute, corresponding to 3.33, 5.83 and 8.33 g for throughputs of 10, 17.5 and 25 kg/h respectively) was spiked. Since it took 5 s for the conveyor belt to move from below the granulator output to the location of the spectral image collection, the chemical imaging measurements were started 5 s after injecting the tracer (theophylline) for each experiment. Thus, the first frame of the spectral image

corresponded to the instant of theophylline addition. The spatial distribution of theophylline during the 25 s measurement was calculated with the spectral matched filter (SMF) method (section 6.2.2).



**Figure 6.1:** Representation of an active pharmaceutical ingredient (API)-map and a moisture map, the corresponding mean temporal profile, which was translated into the corresponding residence time distribution and moisture distribution for the twin screw granulator at fixed material throughput (25 kg/h), number of kneading discs (6), stagger angle (60°) and different screw speeds.

## 6.2.2 NIR chemical imaging and Extraction of relevant information from spectral data

For this study the same NIR chemical imaging setup was used as discussed in section 4.3.2 of Chapter 4. The hyperspectral images were first post-processed to remove the background via partial least squares discriminant analysis (PLS-DA) classification as discussed in section 4.3.2. In the second step, the NIR spectra in the remaining pixels corresponding to the granules were subjected to semi-quantitative analysis of theophylline content and moisture content. In both

cases, the spectral range was narrowed to 1100-2200 nm and the spectra were subjected to the standard normal variate (SNV) pretreatment to eliminate the additive baseline offset variations and multiplicative scaling effects in the spectra which may be caused by experimental conditions such as shadowed regions near large granules and possible differences in granule density. Subsequently, a measure for the theophylline level was obtained for RTD using the SMF method which provides a highly selective response for the target analyte. A measure for the moisture level was obtained for studying solid-liquid mixing using the band ratio method (Fig. 6.1) (Vercruyssen et al., 2013b). The NIR chemical imaging measurement setup and extraction of relevant information from chemical images was discussed in more detail by Vercruyssen et al. (2013b) and is schematically shown in Fig. 4.1 of Chapter 4.

### Estimation of RTD and axial mixing efficiency

Conventionally, a RTD is obtained by injecting a pulse of tracer into the system at the inlet, and the residence time function,  $e(t)$ , is calculated as

$$e(t) = \frac{c(t)}{\int_0^{\infty} c(t)dt} \quad (6.1)$$

where  $c(t)dt$  is the concentration of the tracer at the outlet between  $t$  and  $t + \Delta t$ . In this study, the exit age distribution of the tracer molecule (theophylline) was derived from the tracer concentration  $c_i$  (as estimated using the SMF method) between  $t$  and  $t + \delta t$  in the temporal profile of the discrete tracer map (top of Fig 6.1) calculated as

$$e(t) = \frac{c_i}{\sum_{i=1}^t c_i \Delta t} \quad (6.2)$$

This tracer map was transformed into the exit age distribution curve, i.e. the RTD based on the mean tracer concentration,  $e(t)$  between  $t$  and  $t + dt$  (RTD plot in Fig 6.1), which was then used to calculate the mean residence time  $\bar{t}$ , normalised variance  $\sigma_{\bar{t}}^2$  and Péclet number  $Pe$  as detailed in section 4.3.3 of Chapter 4.

### Estimation of moisture distribution

A large amount of chemical imaging data were collected resulting in spatio-temporal moisture maps of wet granules for each experimental run (Fig. 6.1). The liquid-solid mixing can be seen as a process in which a complex liquid exchange network between particles of the processed material is generated. The pixel intensity values in the moisture maps are indicative of this liquid exchange level or distribution. The statistical phenomena on uncertainty of the pixel

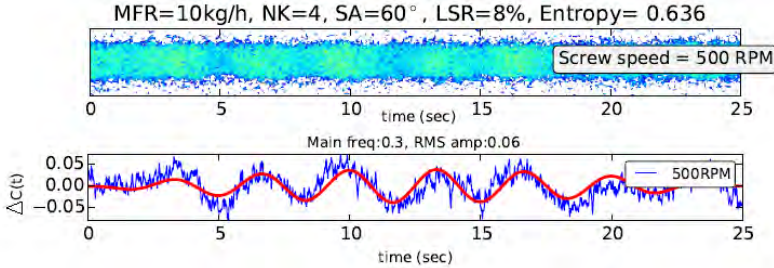
intensity at a randomly selected point on the moisture map can be quantified as Shannon entropy (Guida et al., 2010) given by (eq. 6.3),

$$H(X) = \sum_{j=1}^n P(X_j) \log_{256}(1/P(X_j)) = - \sum_{j=1}^n P(X_j) \log_{256} P(X_j) \quad (6.3)$$

where  $X$  is the value of the pixel index  $j$  and  $n$  is total number of pixels in the moisture map. The Shannon entropy, which is used in Information Theory, thus appears to be a useful parameter for describing the mixing efficiency in a system (Guida et al., 2010). Since the moisture maps were not calibrated for quantitative moisture content determination, entropy was selected to evaluate the liquid distribution. Entropy only envisages the distribution itself and not the values that pixel intensity may take. In this study, the logarithm to the base 256 was applied, as the 8-bit moisture map allows displaying the moisture distribution using 256 different intensities. Since a progression in mixing causes an increase in uncertainty of pixel intensity transitions in the moisture map, a mixing index (MI) based on such an uncertainty was defined as:

$$\text{MI} = - \frac{1}{\log_{256}(n)} \sum_{j=1}^n P(X_j) \log_{256} P(X_j) \quad (6.4)$$

The mixing index (MI) value lies between 0 and 1 indicating "no mixing" and "perfect mixing" of the granulation liquid, respectively.



**Figure 6.2:** The FFT algorithm was used to remove noise from the mean moisture profiles, allowing the identification of the most dominant frequency band and corresponding amplitude.

Since the MI is derived from the bulk solid-liquid mixing outcome, hereby completely avoiding the dynamics of the mixing process which lead to variations in mean moisture content in the granules produced at different times, an additional method based on calculation of frequency and amplitude of variations in the mean profile of the moisture content was used to quantify the perturbations in the solid-liquid mixing (Fig. 6.2). The fast Fourier transform (FFT) of the



mean moisture profile was performed to remove noise and only extract the main frequency and its amplitude value for every moisture mean profile curve (Cooley and Tukey, 1965). An increase in either the frequency or corresponding amplitude, indicated conditions leading to higher fluctuations.

### 6.2.3 Sieving test for particle size analysis

The GSD of the granule samples, collected at the outlet of the TSG during each experiment, was determined using the sieve analysis method (Retsch VE 1000 sieve shaker (Haan, Germany)). Granule samples (100 g) were placed on a shaker for 5 min. at an amplitude of 2 mm using a series of sieves (150, 250, 500, 710, 1000, 1400 and 2000  $\mu\text{m}$ ). The amount of granules retained on each sieve was determined. All granule batches were measured in triplicate. The fractions  $<150$ , 150-1000 and  $>1000$   $\mu\text{m}$  were defined as the amount of fines, fraction of interest for tableting (yield) and oversized fraction, respectively.

### 6.2.4 Quantification of effects and interactions of factors

The factor effects upon the responses from the experimental design derived from the CI-data and granule size measurements were estimated. Since multiple responses ( $\bar{t}$ ,  $\sigma_{\theta}^2$ , Pe, moisture entropy and GSD) were determined, it was helpful to fit a model simultaneously representing the variation of all responses to the variation and interactions of the factors. Therefore, using the Modde 10.1 software (Umetrics, Umeå, Sweden), partial least squares (PLS) modelling taking all responses simultaneously into account, was employed.

The effect plots are used to display the change in the response (y-axis) when each process factor (screw speed [RPM], material throughput [MFR], L/S [LSR], number of kneading discs [NK] and stagger angle [SA]) varies from its low to its high level, keeping all other factors at their center values of the interval (Fig.6.4 – 6.10). The y-axis indicates the estimated effect which has a value of twice the corresponding coefficients of the regression model. For each factor, the uncertainty of the effect is indicated by the 95% confidence interval error bar. When an interaction effect prevails, the synergistic or antagonistic effect of one factor depends on the level of another factor. The interaction effect represents the synergy or antagonism between two factors in explaining a response. In these plots the effects of factors on the response are sorted from the largest to the smallest. The factors and interaction terms with insignificant effect (those where the confidence interval includes zero) were removed from the model (Eriksson et al., 2000). Additionally, the interaction plot was used to display the predicted change in the response when one factor varies, and the second factor is set at both its low and high level, all other factors being set

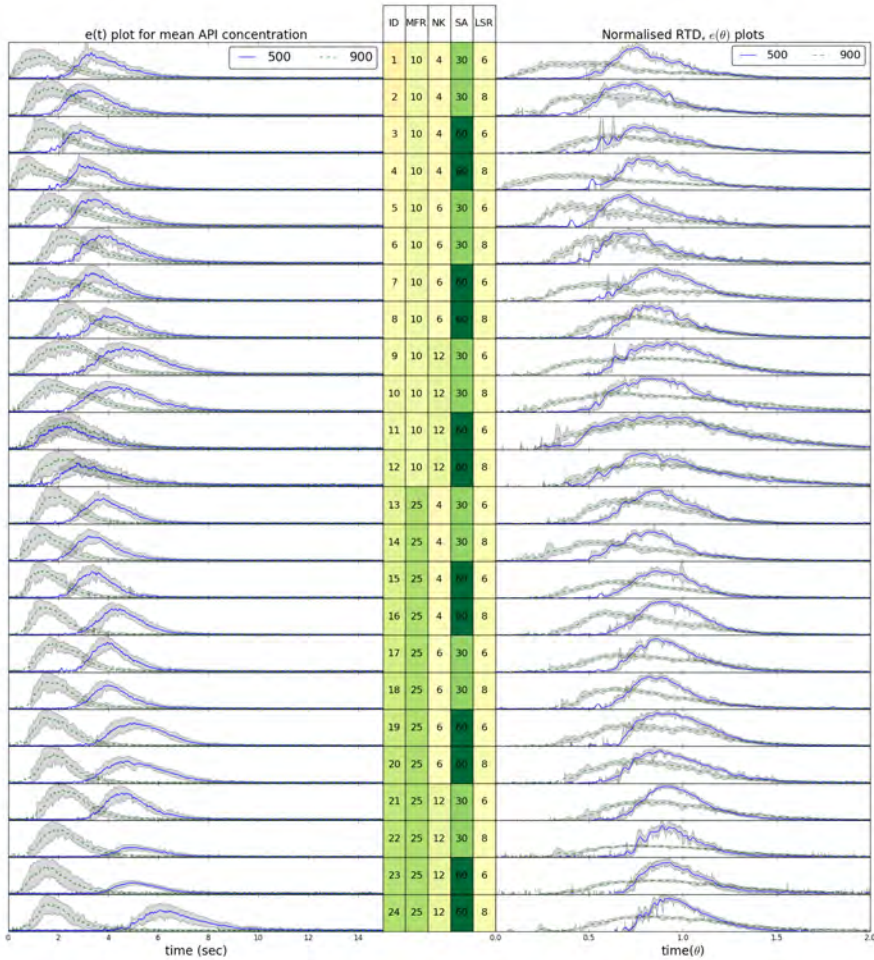
on their centre value. When in such a plot the two lines are parallel one can conclude that there is no interaction between the two factors, whereas when they cross each other there is a strong interaction.

## 6.3 Results and discussion

The performed design of experiments resulted in 51 residence time profiles (Fig. 6.3), and solid-liquid mixing and granulation performance results (see the overview of the performed experiments and obtained responses in Appendix B Table B.2). The power input variation was indicated by the measured torque in the granulator drive and the granulation time variation was expressed by the  $\bar{t}$  (Fig. 6.4). The variation in axial mixing was derived from the width of the normalised RTD, i.e. the  $\sigma_{\theta}^2$  and the change in relative magnitude of convective and dispersive transport capacities was given by Pe (Fig. 6.7). The change in solid-liquid mixing of the bulk material was quantified as effect on MI. The frequency and amplitude of the mean moisture profiles quantified the dynamics in the solid-liquid mixing in the TSG (Fig. 6.9). To understand the role of process and screw design parameters on granulation performance, it is important to first discuss the observed effects of the factors on these responses (section 6.3.1-6.3.4). This will feed the detailed discussion to link granulation time and mixing performance with the resulting granulation yield in the follow-up section 6.3.5.

### 6.3.1 Change in torque at different process conditions

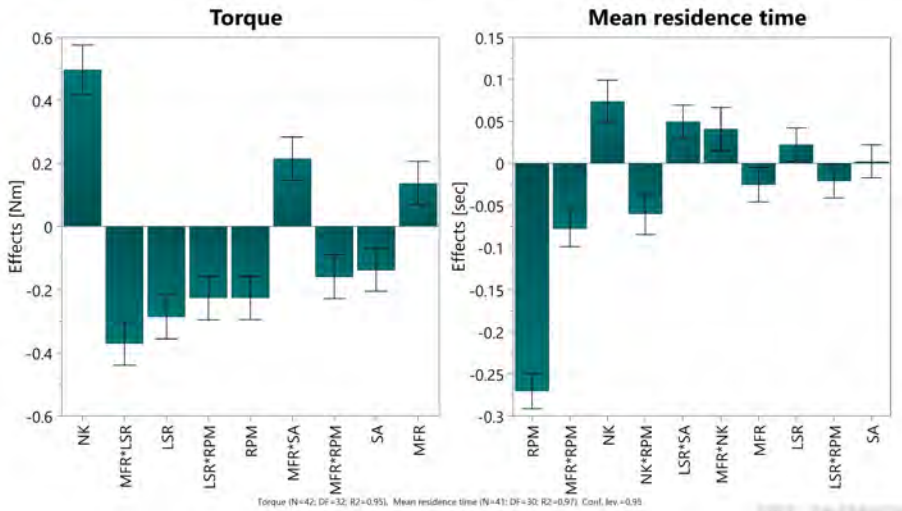
The torque of the granulator drive indicates the energy input to the granulation process by the motor drive. In this study, all the factors originating from the screw configuration and process conditions had a significant influence on the measured torque level (Fig. 6.4). This is in accordance with earlier studies on the effect of changing the process parameters on the torque level (Dhenge et al., 2010; Verduyck et al., 2015; Kumar et al., 2014b). An increase in the number of kneading discs most significantly increased the torque level and an increase in L/S most significantly reduced the torque level. An increase in the material throughput resulted in higher torque. However, the material throughput had a significant interaction with L/S [LSR\*MFR] (Fig. 6.5a). At a low material throughput increasing L/S resulted in an increased torque, whereas at a high material throughput increasing L/S resulted in a significant reduction in the torque. An increase in the screw speed led to a reduction of the torque. However, due to the interaction between L/S and the screw speed [LSR\*RPM], a reduction in screw speed at a high L/S resulted in a sharp increase in the torque level compared to low L/S (Fig. 6.5b). Increasing stagger angle resulted



**Figure 6.3:** The age distribution (left) and normalised RTD (right) profiles with a shaded region denoting the standard deviation at different screw speed (500, 900 RPM) during various experiments (ID) using twin screw granulation [SA: stagger angle ( $^{\circ}$ ), NK: number of kneading discs (-), MFR: material throughput (kg/h), LSR: liquid-solid ratio (%)].

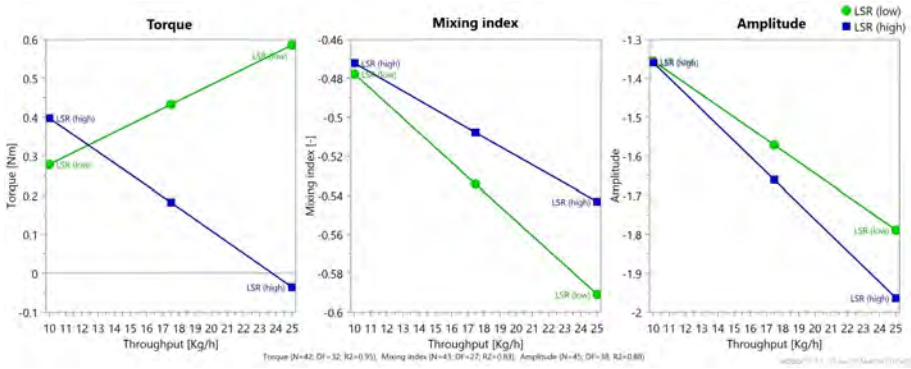
in a reduction of torque. However, this effect was found to be more observed at a low material throughput. At high material throughput, an elevated flow restriction by increasing stagger angle resulted in an increased torque level (Fig. 6.5c). The interaction between the material throughput and screw speed [MFR\*RPM], which impacts the fill ratio, resulted in a reduction of the torque when both screw speed and material throughput were increased simultaneously

(Fig. 6.6a). At a low material throughput, this interaction did not exist. The highest torque level (12.41 N.m) was observed at a throughput of 25 kg/h, L/S of 6%, screw configuration with 12 kneading discs at 60° and screw speed of 500 rpm. The torque level was lowest (0.38 N.m) at a throughput of 25 kg/h, L/S of 8%, screw configuration with 4 kneading discs at 30° and screw speed of 900 rpm.

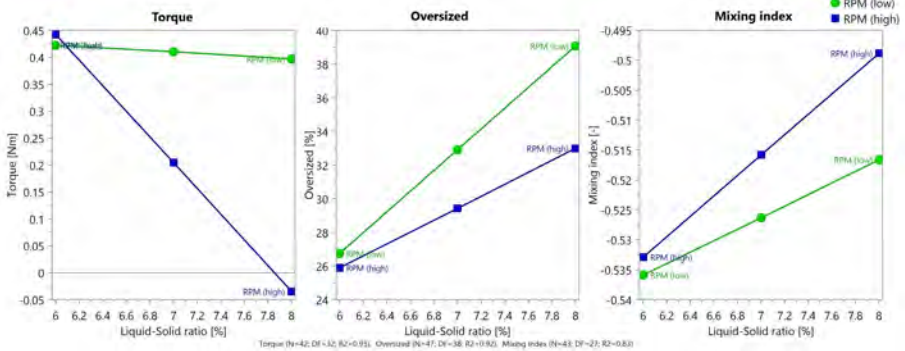


**Figure 6.4:** Effects plots showing predicted changes in the measured torque and  $\bar{t}$  when factors, number of kneading discs (NK) [4, 6, 12], screw speed (RPM) [500-900 rpm], throughput (MFR) [10-25 kg/h], liquid-to-solid ratio (LSR) [6-8%] and stagger angle (SA) [30-60°], vary from low to the high level, while keeping the other factors at their average.

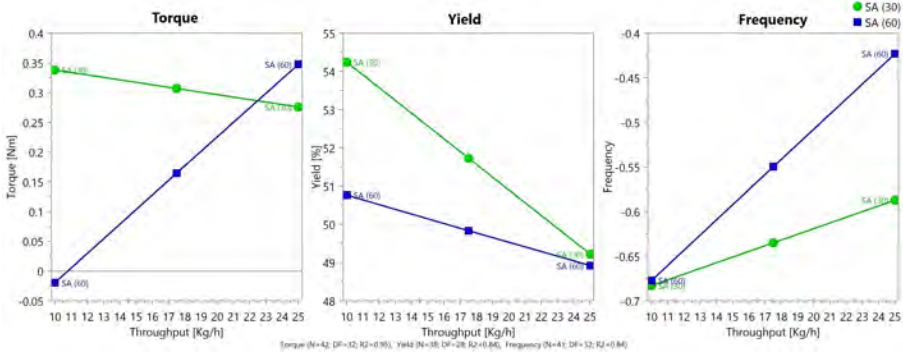
These observations suggest that the load on the screws (based on screw speed and material throughput) and the flow restriction (based on number of kneading discs and stagger angle) dictate the torque level of the granulator drive. Besides, at low barrel fill ratio, i.e. when the flow inertia is low, an increased moisture content at higher L/S causes sluggish flow and consequently higher torque. However, at a high throughput when more material is present, the inertial force is high and increasing L/S lubricates the granular flow leading to a reduction of the torque. The observed significant influence of all the factors on the torque level also suggests that the energy input to the system varied significantly for all the changes in process parameters. Thus, the studied experimental domain was suitable to investigate the effects of equipment and process parameters on other responses.



(a) Predicted changes in the measured torque, MI and amplitude of the mean moisture profile.



(b) Predicted changes in the measured torque, oversized fraction of granules (>1400 μm) and mixing index (MI).



(c) Predicted changes in the measured torque, yield fraction (>150 μm to <1400 μm) of granules and frequency of the mean moisture profile.

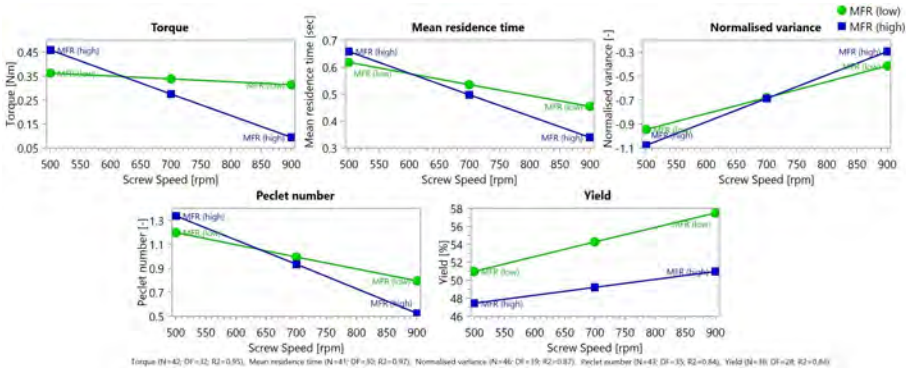
**Figure 6.5:** Predicted changes in the responses due to interaction (i) between the liquid-to-solid ratio (L/S) and material throughput [MFR\*LSR], (ii) between the liquid-to-solid ratio (L/S) and screw speed [LSR\*RPM] and (iii) between the material throughput and stagger angle [MFR\*SA] in the screw configuration.

### 6.3.2 Granulation time at different process conditions

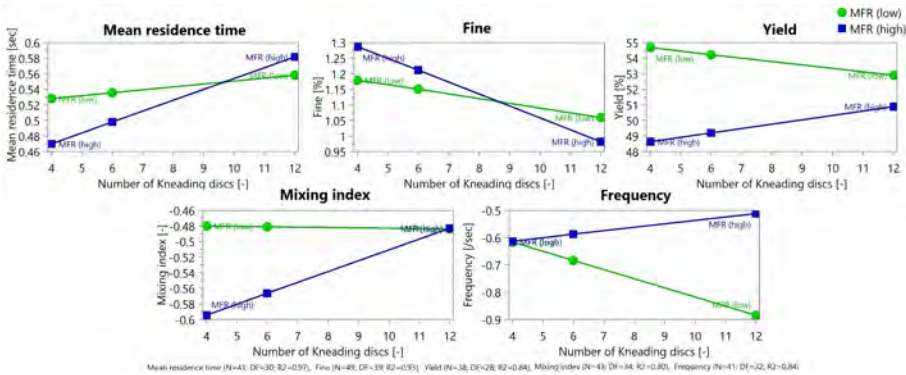
The granulation time in the TSG measured as  $\bar{t}$  was most influenced by the screw speed and the number of kneading discs (Fig. 6.4). An increase in the screw speed resulted in a lower  $\bar{t}$ , i.e. the RTD profiles consistently shifted to the left in Fig. 6.3, whereas an increase in number of kneading discs led to an increase in the residence time. Increasing material throughput resulted in a reduction in the  $\bar{t}$ , which was also observed in earlier studies (Kumar et al., 2014b; Dhenge et al., 2011). Additionally,  $\bar{t}$  was significantly reduced by the interaction between material throughput and screw speed [MFR\*RPM] (Fig. 6.6a). At a high fill ratio (i.e., increasing throughput at low screw speed) this interaction effect was dampened, but at lower fill ratio (i.e., increasing throughput at high screw speed), the  $\bar{t}$  reduced significantly. An opposite effect on  $\bar{t}$  was detected when more kneading discs were included in the screw configuration. An interaction between the number of kneading discs and the material throughput [MFR\*NK] resulted in a significant reduction in the  $\bar{t}$  when increasing the material throughput at a lower number of kneading discs (Fig. 6.6b).

Similarly, due to a significant interaction between the number of kneading discs and screw speed [NK\*RPM], the  $\bar{t}$  reduced when either the number of kneading discs was reduced at a low screw speed or screw speed was increased at a high number of kneading discs. Interestingly, an increasing L/S, which lowered the torque level of the granulator, resulted in an increase in  $\bar{t}$ . Although the effect of change in L/S on  $\bar{t}$  was not very dominant, an increased sluggishness of powder at high L/S and elevated flow restriction at higher stagger angle interacted to raise the  $\bar{t}$ . The maximum  $\bar{t}$  (6.88 sec) was observed at a throughput of 25 kg/h, L/S of 8%, screw configuration with 12 kneading discs at 60° and screw speed of 500 rpm. The minimum  $\bar{t}$  (1.61 sec) was observed at a throughput of 10 kg/h, L/S of 8%, screw configuration with 4 kneading discs at 60° and screw speed of 900 rpm.

These results suggest that at a given process condition, the required residence time for a good mixing and high granulation yield can mainly be achieved by either choosing the number of kneading discs in the screw configuration before starting the granulation process or by changing the screw speed during the process. Also, the reduction in  $\bar{t}$  at low fill ratio indicates a synergy between throughput force and the drag force in the mixed flow condition. The lowering of torque level at a high L/S despite an increase in  $\bar{t}$ , i.e. more material inside the granulator, confirms that the granulation liquid at high fill ratio had a lubricating effect on the screw rotation without increasing the conveying rate.



(a) Predicted changes in the measured torque, mean residence time, Pe and yield fraction (>150  $\mu\text{m}$  to <1400  $\mu\text{m}$ ) of granules, mixing index (MI) and frequency of the mean moisture profiles.



(b) Predicted changes in the mean residence time, and fine (<150  $\mu\text{m}$ ) and yield fractions (>150  $\mu\text{m}$  to <1400  $\mu\text{m}$ ) of granules.

**Figure 6.6:** Predicted changes in the responses due to interaction (a) between the material throughput and screw speed [MFR\*RPM] and (b) between material throughput and number of kneading discs [MFR\*NK] in the screw configuration.

### 6.3.3 Mixing at different process conditions

#### Axial mixing

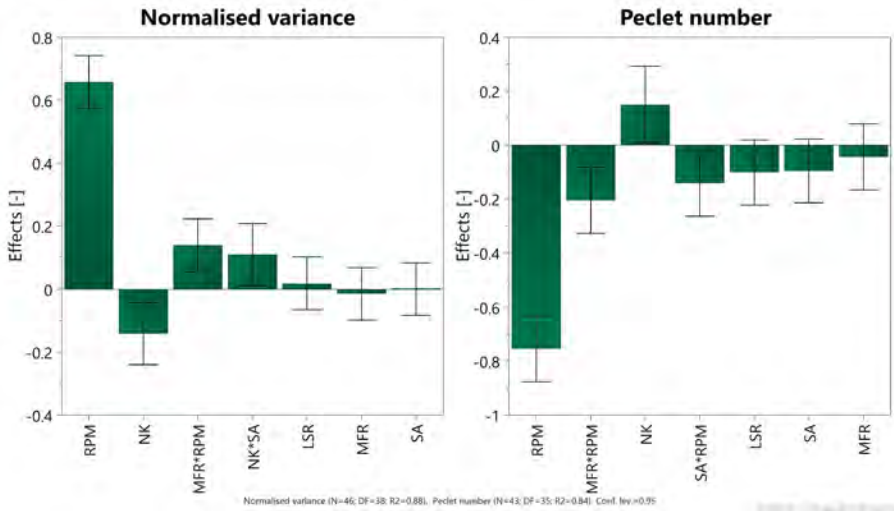
The axial mixing during the bulk flow inside the granulator was quantified as  $\sigma_{\theta}^2$  and Pe (Fig. 6.7). Increasing the screw speed resulted in an increase in  $\sigma_{\theta}^2$ , whereas a higher number of kneading discs resulted in reduced  $\sigma_{\theta}^2$ . Visually this is reflected in a broadening of the RTD with increasing screw speed (Fig. 6.3). The opposite effect on the RTD profile was observed with increasing number of kneading discs. Similar results were also obtained in our previous experimental (Chapter 4) and model-based study (will be discussed in Chapter 7) (Kumar et al., 2014b, 2015). Besides, an interaction between material throughput and

the screw speed was observed such that increasing the screw speed at a high material throughput, i.e. lowering the fill ratio, resulted in a high  $\sigma_\theta^2$  (Fig. 6.6a). However, keeping the material throughput at a high level when the screw speed was reduced resulted in a lower  $\sigma_\theta^2$  compared to the condition with low throughput and low screw speed. The largest  $\sigma_\theta^2$  (0.84) was observed at a throughput of 25 kg/h, L/S of 6%, screw configuration with 4 kneading discs at 60° and screw speed of 900 rpm. In contrast, the minimum  $\sigma_\theta^2$  (0.05) was observed at a throughput of 25 kg/h, L/S of 8%, screw configuration with 12 kneading discs at 60° and screw speed of 500 rpm.

Beside  $\sigma_\theta^2$  quantifying mainly dispersive transport, the Pe, which is the ratio of convective to dispersive transport in a system, was also directly influenced by the screw speed and the number of kneading discs. An increase in the screw speed resulted in the dominance of dispersive over convective transport phenomena, whereas the opposite effect was observed for increasing the number of kneading discs. Also, similar to  $\sigma_\theta^2$ , the interaction between material throughput and the screw speed resulted in a fast reduction in Pe, i.e. dispersive transport increased when the screw speed was increased at a high throughput (Fig. 6.6a). This similarity in the effect of different factors on  $\sigma_\theta^2$  and Pe suggests that the dispersive transport changed was much larger than on convective transport up on variations in the factors. At a low throughput, i.e. lower barrel filling, the observed increase in dispersive transport was lower compared to a high material throughput. Due to a significant interaction between stagger angle and screw speed, increasing screw speed resulted in a rapid decline in Pe at higher stagger angle (60°) compared to lower stagger angle (30°). The largest Pe (36.66) was observed at a throughput of 25 kg/h, L/S of 8%, screw configuration with 12 kneading discs at 60° and screw speed of 500 rpm. In contrast, the minimum Pe (0.55), which is lower than 1 indicating that the dispersive transport length was longer than the barrel size and exceeded the convective transport within the granulator barrel at a throughput of 25 kg/h, L/S of 6%, screw configuration with 4 kneading discs at 60° and screw speed of 900 rpm.

These observations suggest that the flow regime inside the granulator is controlled both by the screw design and the process conditions. Due to the change in the hindrance to the axial flow by the fully filled zones around the kneading discs, dispersive transport was less efficient for a high number of kneading discs. Increasing the throughput force and drag force by the increasing material throughput and screw speed simultaneously and consequently a low fill ratio led to an increase in the wall slippage resulting in more axial mixing in the TSG.



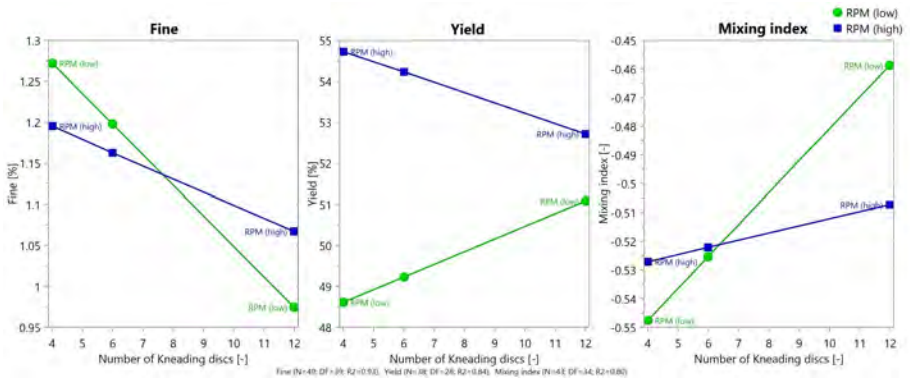


**Figure 6.7:** Effects plots showing predicted changes in the  $\sigma_{\theta}^2$  and Pe when factors, number of kneading discs (NK) [4, 6, 12], screw speed (RPM) [500-900 rpm], throughput (MFR) [10-25 kg/h], liquid-to-solid ratio (LSR) [6-8%] and stagger angle (SA) [30-60°], vary from a low to a high level, while keeping the other factors at their center point value.

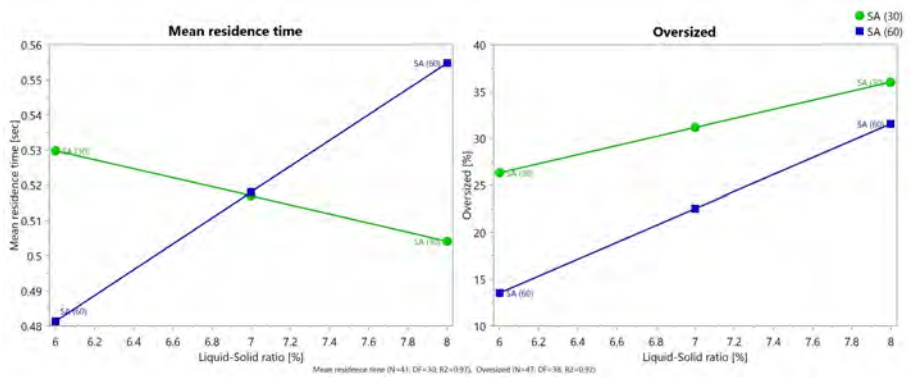
### Solid-liquid mixing

The solid-liquid mixing in the bulk mixture was quantified as MI and its dynamics during continuous granulation were quantified as frequency and amplitude of the mean moisture profile of each run. According to the effect plot for the MI, the bulk mixing was most significantly reduced by the increase in material throughput (Fig. 6.9). In contrast, increasing the number of kneading discs significantly increased the bulk mixing, which is reflected by an increase in the mixing index. Also the throughput and the number of kneading discs interacted [MFR\*NK] significantly leading to an increase in the MI at a high throughput by the increasing number of kneading discs (Fig. 6.6b). Additionally, MI increased significantly at a high L/S. The effect of a change in L/S also had significant interaction with the changes in material throughput. An increase in the material throughput at low L/S resulted in a lower MI than when a high L/S is applied. The effect of change in the screw speed was not significant on the MI but its interaction with the change in the number of kneading discs resulted in a significant reduction in MI when the screw speed was increased at high number of kneading discs (Fig. 6.8a). The stagger angle did not affect the MI significantly. The highest MI (0.39) was observed at a throughput of 25 kg/h, L/S of 8%, screw configuration with 12 kneading discs at 30° and screw speed of 500 rpm. In contrast, the minimum MI (0.13) was observed at a

throughput of 25 kg/h, L/S of 8%, screw configuration with 4 kneading discs at 60° and a screw speed of 900 rpm.



(a) Predicted changes in the mean residence time, and fine (<150  $\mu\text{m}$ ) and yield fractions (>150  $\mu\text{m}$  to <1400  $\mu\text{m}$ ) of granules.

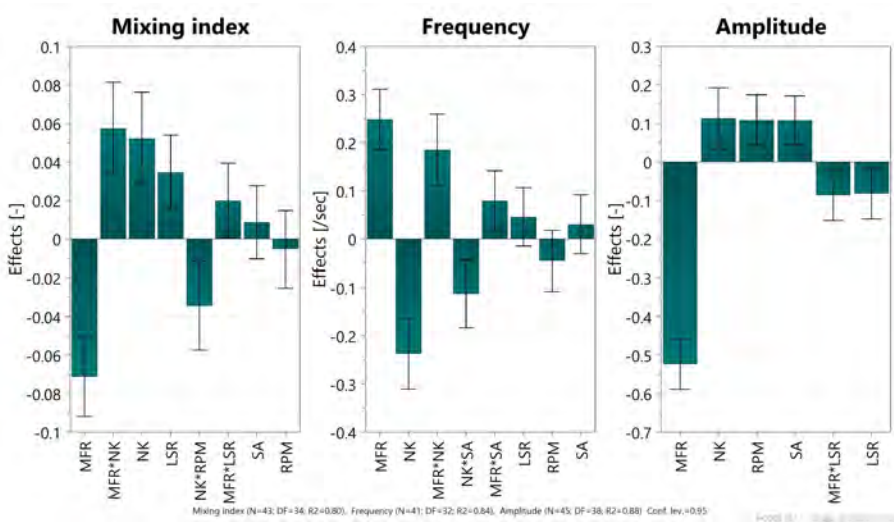


(b) Predicted changes in the mean residence time, and oversized granule fraction (>1400  $\mu\text{m}$ ).

**Figure 6.8:** Predicted changes in the responses due to interaction (a) between number of kneading discs and screw speed [NK\*RPM], and (b) between liquid-to-solid ratio and stagger angle between kneading discs [LSR\*SA] in the screw configuration.

The effect plot for the frequency of mean moisture profile showed that, similar to the bulk mixing, increasing the material throughput increased the frequency of the mean moisture profile, i.e. indicating inferior solid-liquid mixing. The opposite effect occurred when the number of kneading discs increased (Fig. 6.9). Also, an interaction between the throughput and number of kneading discs [MFR\*NK] significantly influenced MI. An increase in the material throughput at a high number of kneading discs resulted in an increase in the frequency, thus more variations in the dynamic profile, which is opposite to the observation for

the bulk mixing as indicated by MI (Fig. 6.6b). Additionally, due to a significant interaction between the material throughput and stagger angle [MFR\*SA], the frequency of the mean moisture profile increased more rapidly by the increasing throughput at a high stagger angle (60°) compared to a low stagger angle (30°) between kneading discs (Fig. 6.5c). Moreover, the interaction between the stagger angle and number of kneading discs in the screw configuration at a low number of kneading discs resulted in an increase in frequency when the stagger angle was increased. The opposite was observed when the stagger angle was increased at a high number of kneading discs. The change in L/S, screw speed and stagger angle had no significant effect on the variation frequency.



**Figure 6.9:** Effects plots showing predicted changes in the Shannon entropy based mixing index (MI), frequency and amplitude of the mean moisture profiles when factors, number of kneading discs (NK) [4, 6, 12], screw speed (RPM) [500-900 rpm], throughput (MFR) [10-25 kg/h], liquid-to-solid ratio (LSR) [6-8%] and stagger angle (SA) [30-60°], vary from a low to a high level, while keeping the other factors at their center point value.

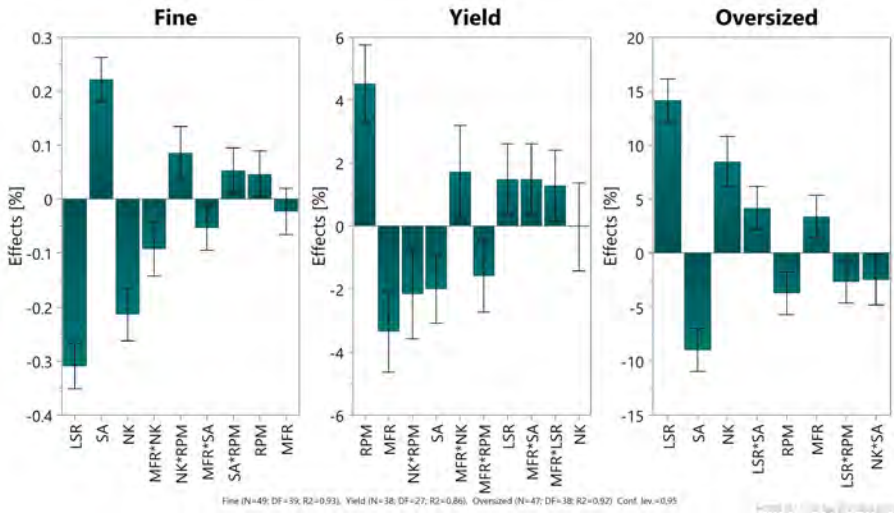
The effect plot for the amplitude of the mean moisture profile also showed that similar to the bulk mixing, the material throughput most significantly resulted in a decrease in the degree of variation. However, increase in the number of kneading discs, screw speed and stagger angle equally resulted in an increase in the variation and, hence, a higher amplitude. A high L/S caused a reduction in the extent of fluctuation, i.e. a lower amplitude. Due to the interaction between the material throughput and L/S [MFR\*LSR], an increase in the L/S resulted

in a lower amplitude when the material throughput was increased.

These results suggest that although a high material throughput and a high screw speed are desired for process efficiency, their exclusive increase may cause inefficient solid-liquid mixing which will result in an inferior granulation yield. Similarly, an increase in the number of kneading discs should be considered to obtain good solid-liquid mixing by reducing both the rate and degree of variations in the moisture content of the granules. Also, at a higher L/S, bulk mixing is better and the degree of variation is less, indicating that a proper amount of liquid addition is also required for good distribution of the liquid during granulation.

### 6.3.4 GSD at different process conditions

In order to understand the effect of each factor on the GSD, the sieved granules were classified in three fractions (fine ( $<150\ \mu\text{m}$ ), yield ( $150\text{-}1400\ \mu\text{m}$ ) and oversized fraction ( $>1400\ \mu\text{m}$ )) (Fig. 6.10). An increase in L/S and number of kneading discs resulted in a lower amount of fines in the produced granules. On the other hand, an increase in the stagger angle and screw speed led to more fines in the granules. Although material throughput independently had no significant influence on the fines fraction, a significant interaction between material throughput and the number of kneading discs [MFR\*NK] resulted in a more rapid reduction in the amount of fines with increasing number of kneading discs at high throughput (Fig. 6.6b). Also, the two factors with an opposite effect on fines i.e., the number of kneading discs and the screw speed interacted significantly [NK\*RPM]. The amount of fines at a low number of kneading discs and a high screw speed was less, but the opposite was observed when high screw speed was applied along with high number of kneading discs (Fig. 6.8a). The maximum amount of fines (55%) was observed at a throughput of 10 kg/h, L/S of 6%, screw configuration with 12 kneading discs at  $30^\circ$  and a screw speed of 900 rpm. In contrast, the smallest amount of fines (4.9%) was observed at a throughput of 25 kg/h, L/S of 8%, screw configuration with 12 kneading discs at  $30^\circ$  and a screw speed of 500 rpm.



**Figure 6.10:** Effects plots showing predicted changes in the fines (>150 μm), yield [150-1400 μm] and oversized (>1400 μm) fractions of the resulting GSD produced when factors, number of kneading discs (NK) [4, 6, 12], screw speed (RPM) [500-900 rpm], throughput (MFR) [10-25 kg/h], liquid-to-solid ratio (LSR) [6-8%] and stagger angle (SA) [30-60°], vary from a low to a high level, while keeping the other factors at their center point value.

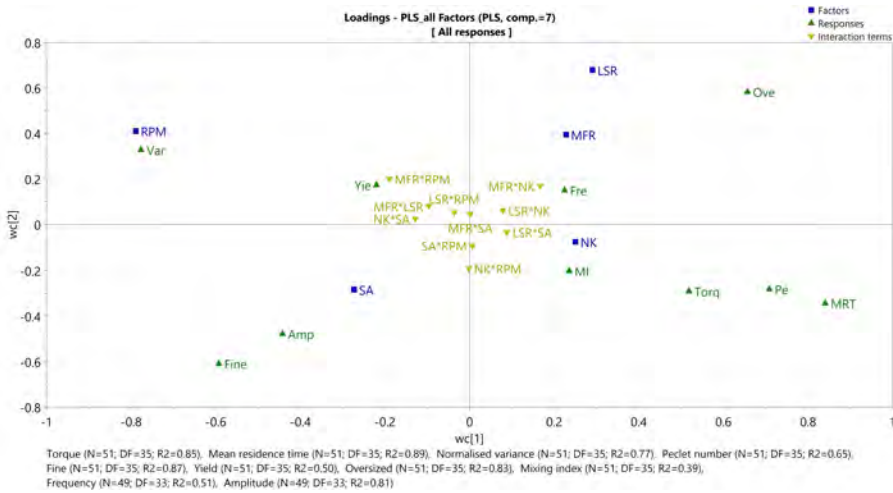
The yield fraction was most significantly influenced by the screw speed and the material throughput (Fig. 6.10). A higher screw speed resulted in an increase of the yield fraction, whereas increasing the material throughput resulted in a reduction of the yield fraction. Additionally, an increase in stagger angle resulted in a reduction in the yield fraction and the opposite was observed when L/S was increased. A strong interaction between the number of kneading discs and the screw speed resulted in a decrease in the yield fraction when the number of kneading discs was increased at a high screw speed (Fig. 6.8a). The yield fraction increased when the number of kneading discs was increased at low screw speed. This indicates that an increase in the mechanical shear beyond a certain extent is not favourable to the granulation yield. Similarly, due to interaction between material throughput and number of kneading discs [MFR\*NK], more yield fraction granules were produced when the number of kneading discs was increased at high throughput (Fig. 6.6b). The change in yield fraction was also influenced by the interaction of material throughput with stagger angle and the screw speed. Increasing the throughput at lower stagger angle resulted in a drastic reduction in the yield fraction (Fig. 6.5c). Increasing the screw speed at a low throughput increased the yield fraction more than operation at a high throughput (Fig. 6.6a). The highest yield fraction (61.8%

when the fines and oversized fractions were 18.5 and 17.9 % respectively) was observed at a throughput of 25 kg/h, L/S of 6%, screw configuration with 12 kneading discs at 60° and a screw speed of 500 rpm. In contrast, the lowest yield fraction (41.7% when the fines and oversized fractions were 4.9 and 53.4 % respectively) was observed at a throughput of 25 kg/h, L/S of 8%, screw configuration with 12 kneading discs at 30° and a screw speed of 500 rpm.

The effect plot for the oversized fraction shows that the additional liquid at a high L/S significantly increased the amount of oversized granules (Fig. 6.10). Similarly, increasing the number of kneading discs and the material throughput also resulted in the favoured production of oversized granules. This suggests ineffective mixing by the kneading discs despite an increase in the number of kneading discs. However, increasing stagger angle and screw speed lowered the oversized fraction. An interaction between L/S and stagger angle resulted in a rapid increase in the oversized fraction at low L/S when the stagger angle was reduced from 60° to 30° (Fig. 6.8b). Additionally, the interaction between L/S and screw speed resulted in a reduction in the oversized fraction at high L/S when the screw speed was increased (Fig. 6.5b). The highest amount of oversized granules fraction (53%) were observed at a throughput of 25 kg/h, L/S of 8%, screw configuration with 12 kneading discs at 30° and a screw speed of 500 rpm. The smallest oversized granule fraction (3%) was observed at a throughput of 10 kg/h, L/S of 6%, screw configuration with 12 kneading discs at 30° and a screw speed of 900 rpm.

### 6.3.5 Link between granulation time, mixing and yield

The purpose of granulation process design and optimisation is to maximize the process efficiency, i.e. maximising the yield fraction. The results discussed so far (section 6.3.1-6.3.4) suggest a correlation between the granulation time, mixing and the GSD. This was also reflected by the PLS loadings plot (Fig. 6.11). The measured torque of the granulator drive indicating power input to the system,  $Pe$  quantifying the axial mixing,  $MI$  quantifying the solid-liquid mixing and  $\bar{t}$  quantifying average time spent by the material inside the granulator are positively correlated as can be seen in the loadings plot. On the other hand, all the three size fractions (fine, yield and oversized granules fractions) are located in different regions suggesting that they have different important contributing factors. Also, the desired condition for the responses such as a high residence time, a good axial as well as solid-liquid mixing and resulting high yield fraction are favoured by different factors. Therefore, the connections between different factors and responses requires detailed discussion.



**Figure 6.11:** Scatter plot with PLS loadings of the two first model dimensions

As discussed in the introduction, due to the short residence time, the major challenge in twin-screw wet granulation is to achieve proper solid-liquid mixing in the shortest distance along the granulator screw to allow more time for other constitutive mechanisms of granulation to shape the final distribution. For this purpose, kneading discs were used in the TSG which improved solid-liquid mixing both by increasing the bulk mixing and reducing the frequency of deviations in the moisture content of the granules (Fig. 6.9). A high number of kneading discs also resulted in relatively longer residence time. Despite this improvement in mixing and time, increasing the number of kneading discs did not significantly contribute to increasing the yield fraction (Fig. 6.10). Additionally, increasing the L/S had no significant contribution to increasing the desired yield fraction since most of the additional liquid resulted in the formation of oversized granules. This evidently indicates that despite the contribution of kneading discs in the solid-liquid mixing, the required quality of mixing inside the TSG barrel was still unachieved. Since the highest torque level (12.4 N.m) was also observed by the screw configuration with 12 kneading discs at 60° and screw speed of 500 rpm, further increase in the number of kneading discs will for sure increase the bulk mixing, but on the other hand significantly limit the operational ranges of the process settings. Therefore, more efforts should be done to modify the TSG screw configuration both using conventional (conveying and kneading elements) as well as non-conventional screw elements with modified geometries (Vercruyse et al., 2015; Sayin et al., 2015; Meier et al., 2015).

Increasing the screw speed not only lowered the torque, allowing greater flexibility in choosing process settings but also most significantly increased the

yield fraction of the granules despite smaller  $\bar{t}$ . However, mixing at a high screw speed was more dispersive as indicated by Pe than the bulk mixing indicated by MI (Fig. 6.7 and 6.9). Due to this, the fines fraction increased as well. Increasing the material throughput (which will be the ultimate target in industrial production) quickly changed the flow regime inside the granulator which consequently reduced the yield fraction. Moreover, beside reducing the axial mixing, an increasing material throughput also reduced the bulk mixing which was mostly driven by the distributive mixing by the kneading discs. Since the number of kneading discs significantly interacts both with material throughput and screw speed, keeping the number of kneading discs at a fixed level, a balance between material throughput and screw speed should be strived for in order to achieve required granulation time, axial mixing and solid-liquid mixing for a high granulation yield. Moreover, although increasing stagger angle had negative effect on yield fraction, since increasing the stagger angle and screw speed simultaneously, lowered both fines and the oversized fraction in the granules produced, the higher stagger angle ( $60^\circ$ ) should be used in the screw configuration.

Additionally, considering the inability of experimental studies in visualising and measuring the effects of screw configuration and elements on powder flow, mixing and granulation rate processes at particle-scale, further studies based on application of mechanistic modelling tools, such as discrete element simulations and population balance modelling should be performed to improve the understanding of the governing constitutive mechanisms of twin-screw wet granulation process.

## 6.4 Conclusions

NIR chemical imaging was shown to be an adequate tool for simultaneous characterisation of the material flow, axial mixing and bulk mixing analysis during twin-screw granulation. This also allowed investigating the effect of RTD and solid-liquid mixing on the resulting GSD to better understand the overall influence on different flow and mixing conditions. According to the study, an interaction between screw speed, the material throughput, liquid-to-solid ratio, number of kneading discs and stagger angle led to variation in the residence time as well as mixing capacity. At a high screw speed, despite high axial mixing leading to reduction of the oversized ( $>1400 \mu\text{m}$ ) fraction and a higher yield fraction, a low residence time resulted in increase in the fine ( $<150 \mu\text{m}$ ) fraction. Similarly, increasing L/S led to more oversized granules, which increased further at higher throughput. This indicated insufficient solid-liquid mixing capacity of



the current kneading discs which is ultimately required for good granulation performance. Similarly, at high throughput improper solid-liquid mixing resulted in more oversized particles. Thus, a balance between material throughput and screw speed should be looked for to achieve required granulation time and solid-liquid mixing for high granulation yield. Additionally, more efforts are needed to modify the screw configuration as well as geometry changes of the mixing elements to improve the mixing capacity of the TSG. The results from this experimental study improved the understanding regarding the interplay between granulation time, the axial and the solid-liquid mixing responsible for the granulation yield. However, only empirical qualitative insight is gained, not detailed quantitative insight. Therefore, application of mechanistic modelling tools, such as discrete element simulations and population balance modelling, need to be further explored for further detailed investigation of material flow, mixing and their impact on granulation yield during twin-screw granulation.

## PART III

Continuous granulation system:  
Model-based analysis of residence time,  
mixing and particle size evolution in a  
twin-screw granulator



## Conceptual framework for model-based analysis of residence time distribution in twin-screw granulation

---

**Redrafted from:** Ashish Kumar, Jurgen Vercruyse, Valérie Vanhoorne, Maunu Toiviainen, Pierre-Emmanuel Panouillot, Mikko Juuti, Chris Vervaeet, Jean Paul Remon, Krist V. Gernaey, Thomas De Beer, Ingmar Nopens, Conceptual framework for model-based analysis of residence time distribution in twin-screw granulation, *European Journal of Pharmaceutical Sciences*, Volume 71, 2015, Pages 25-34.

### Summary

Till now, experimental data has been used to determine the residence time distribution (RTD) during twin-screw granulation. In this study, a conceptual model based on classical chemical engineering methods is proposed to better understand and simulate the residence time distribution in a twin-screw granulator (TSG). The experimental data were compared with the proposed most suitable conceptual model to estimate the parameters of the model and to analyse and predict the effects of changes in number of kneading discs and their stagger angle, screw speed and material throughput on residence time. An important finding from this study was that the presence of a kneading block in the screw configuration acts as a plug-flow zone inside the granulator. Furthermore, it was found that a balance between the throughput force and conveying rate is required to obtain a good axial mixing inside the twin-screw granulator. Although the material transport and mixing behaviour can be different for other formulations, the experimental data collection and modelling methods applied

in this study are generic and can be adapted to other formulations.

## 7.1 Introduction

In a TSG, which features short residence times, mixing of the respective powder and liquid phase and particle enlargement is achieved by the modular/interchangeable configuration of the screw design. However, due to the difficulties to visualise the material flow in the barrel, little efforts have been made towards understanding the RTD and mixing of material inside the TSG barrel. As for experimental process visualisation, the efforts toward predictive modelling of the RTD in TSG are sparse compared to other fields employing extrusion based systems, such as the food and polymer industries (Gao et al., 2012). This is mainly due to the difficulties in defining the intrinsic physico-chemical properties of the formulation mixture in the opaque and high-shear process environment of the TSG as discussed in Chapter 2. Solving local mass balances is complex, therefore drastically simplified hypotheses are required. Kumar et al. (2013b) presented a one-dimensional transport model based on screw geometry and material characteristics. However, conceptual flow modelling is another approach, in which the transport process is modelled as a combination of ideal reactors, the plug-flow reactor (PFR) having no axial mixing and the  $n$  having perfect axial mixing. Originally derived for chemical reactors, different types of single and multi-stage models and their applications have been widely discussed in the literature (Levenspiel, 1999; Puaux et al., 2000; Fogler, 2006; Kumar et al., 2008a). For a non-ideal flow system, the conceptual model used for RTD modelling generally consists of combinations of a plug flow fraction  $p$ , a finite number of continuously stirred tank reactors in series  $n$  with stagnant pockets or dead volume fractions  $d$  to closely represent the flow pattern. This approach was also adopted by Lee (2013) to explain the experimental RTDs obtained from positron emission particle tracking (PEPT) measurements in a continuous TSG.

However, to our best knowledge, a systematic evaluation of the performances of different conceptual models for their ability to describe flow and transport in a TSG for a broad spectrum of process conditions is still not available. Therefore, the objective of this study was to compare some of the existing conceptual models based on goodness-of-fit between the calibrated model and the experimental data, in order to identify the most suitable model configuration for describing the RTD in a TSG. Furthermore, the effect of input variables, screw configuration (number and stagger angle of kneading discs) and fill ratio (governed by screw speed and material throughput), was analysed by simulating the calibrated model.

## 7.2 System analysis and model formulation

### 7.2.1 Continuous wet-granulation using TSG

The TSG consists of a barrel enclosing two co-rotating self-wiping screws. At the entrance, raw materials are fed into the transport zone and the granulation liquid is added via two nozzles, one for each screw, before the material reaches the mixing zone which consists of kneading discs (Fig. 3.2). The modular structure of the screws allows changing the number of kneading discs and hence, the length of the mixing zone. The powder is hence wetted by the granulation liquid in this region. Further down, since the granulation occurs by a combination of capillary and viscous forces binding particles in the wet state, the wetted material is distributed, compacted and elongated by the kneading discs of the mixing zones, changing the particle morphology from small (microstructure) to large (macrostructure). It is believed that the material is mixed, compacted and chopped to form irregular and porous granules by the succeeding transport elements and kneading blocks (Vercruyssen et al., 2012). The rotation of the screws conveys the material in axial direction through the different zones of the TSG by the drag and flow-induced displacement forces and thus causing mixing and granulation. The rheological behaviour of the material also changes based on liquid-to-solid ratio (L/S) (Althaus and Windhab, 2012).

### 7.2.2 Experimental determination of RTD

Details of the experimental procedure for twin-screw wet granulation and determination of RTD has been discussed in section 4.3 of chapter 4. See chapter 3, section 3.1 for granulator details.

### 7.2.3 Estimation of RTD from experimental data

A RTD was derived by injecting a pulse of tracer into the system at the inlet, and the residence time function,  $e(t)$ , was calculated as

$$e(t) = \frac{c(t)}{\int_0^{\infty} c(t)dt} \quad (7.1)$$

where  $c(t)dt$  is the concentration of the tracer at the outlet between time points  $t$  and  $t + dt$ . This tracer map was then transformed into the exit age distribution curve, i.e. the RTD based on the mean tracer concentration,  $e(t)$  between  $t$  and  $t + dt$ , which was then used to calculate the mean residence time  $\bar{t}$  as the ratio

of the first and the zeroth moment using equation

$$\bar{t} = \frac{\int_0^{\infty} t.e(t)dt}{\int_0^{\infty} e(t)dt} \quad (7.2)$$

The RTD shape and  $\bar{t}$  thus obtained were used to obtain the normalised residence time as  $e(\theta) = \bar{t}.e(t)$ , where dimensionless time,  $\theta = t/\bar{t}$ .

#### 7.2.4 Theoretical models for RTD in TSG

In the previous experimental studies, the RTDs obtained for TSG showed intermediate flow characteristics between the two ideal cases, the perfectly-mixed flow and the plug flow (Lee, 2013; Kumar et al., 2014b). Therefore, models for non-ideal flow have to be used to describe the material flow inside the TSG. Major considerations for the selection of a flow model are, the physical significance of the model and the number of adjustable parameters. In order to have a physical significance, the model structure should be able to characterise the real process through its parameters. In this study, three model candidates were selected to simulate the RTD of the twin-screw granulator: the tanks-in-series (TIS) model without a plug-flow volume fraction, the TIS with a plug-flow volume fraction and the TIS including a plug-flow volume fraction and dead zones (Fig. 7.1). The TIS model without a plug-flow volume fraction is a one-parameter flow model expressed as (Levenspiel, 1999)

$$e(\theta) = \frac{n(n\theta)^{n-1}}{(n-1)!} \exp(-n\theta) \quad (7.3)$$

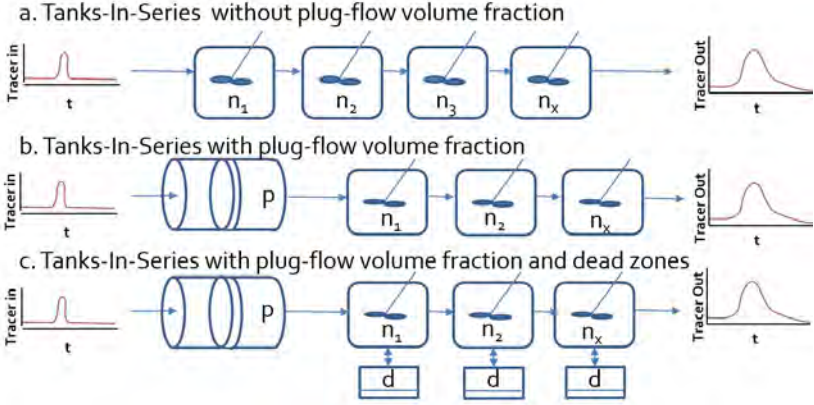
where,  $n$  is the number of continuously stirred tank reactors. The closer the  $n$  value to unity, the higher the degree of mixing, and vice-versa. The TIS model containing a  $p$  as well is a three-parameter flow model given by (Levenspiel, 1999)

$$e(\theta) = \frac{b[b(\theta - p)]^{n-1}}{(n-1)!} \exp[-b(\theta - p)] \quad (7.4)$$

where,  $p = \frac{t_{min}}{\bar{t}}$  and,  $b = \frac{n}{1-p}$

where,  $t_{min}$  is the minimum residence time and  $p$  is the fraction of the volume of the TSG that is assumed to correspond to the plug-flow volume fraction. For the TIS model with both  $p$  and  $d$ , which is a four-parameter flow model, the calculation of  $e(\theta)$  and the  $p$  in eq. 7.4 remains the same, whereas the  $b$  is modified as (Kumar et al., 2008a)

$$b = \frac{n}{(1-p)(1-d)} \quad (7.5)$$



**Figure 7.1:** Schematic diagram of three conceptual models based on non-ideal flow for the RTD in a TSG with a series of continuously stirred tank reactors (a) without a plug-flow volume fraction , (b) with a plug-flow volume fraction , and (c) with plug-flow volume fraction and dead zones.

where,  $d$  is the dead zone of continuously-stirred tank reactors indicating the fraction of material which is either excessively back-mixed or spend much longer time than  $\bar{t}$  in the stagnant pockets that exist in the TSG. Normally, this material spends more than twice the  $\bar{t}$ , and the average velocity is much smaller compared to the well mixed region, leading to a long tail in the RTD. Hence, the four parameters that are present in these models are  $\bar{t}$ ,  $n$ ,  $p$  and  $d$ .

Regarding the number of adjustable parameters, the heuristic rule is to use the model with the lowest number of parameters. Since the TIS model with both  $p$  and  $d$  contained four adjustable parameters, practical identifiability was studied in order to verify the reliability of parameter estimates and their functional relation. The collinearity analysis was used to detect practical identifiability problems over the complete parameter space  $\mathbf{S}$ . Columns of a matrix  $\mathbf{S}$  are called near collinear if there exists a vector  $\beta$  such that  $\|\beta\| \neq 0$  and  $S\beta \approx 0$ . The collinearity among columns  $\mathbf{S}_k = 1, 2, \dots, m$ , of  $\mathbf{S}$  was tested by inspecting the smallest eigenvalue  $\lambda_m$  of the normalised sensitivity matrix,  $\tilde{\mathbf{S}}$ . For details see Brun et al. (2001). Finally, the collinearity index,  $\gamma$  was calculated as

$$\gamma = \frac{1}{\min_{\|\beta\|=0} \|\tilde{\mathbf{S}}\beta\|} = \frac{1}{\sqrt{\lambda_m}} \quad (7.6)$$

A high collinearity index indicates correlation among the parameters. Parameter subsets with collinearity index smaller than 5 are considered as identifiable and collinearity index values above 20 are considered non-identifiable (Brun et al.,



2001).

### 7.2.5 Parameter estimation

$\bar{t}$  and  $p$  were estimated from the RTD measurement data using eqs. 7.2 and 7.4 respectively. The estimation of the other two parameters of different TIS models,  $n$  and  $d$  was done using the residual sum of squares (RSS) as an objective function (eq. 7.7), which was minimised. In order to find the global minimum of the objective function, the "brute force" method was used, which computes the objective function's value at each point of a multidimensional grid of points, to arrive at the global minimum of the function. This multidimensional grid contained ranges of  $n$  (1 to 10),  $p$  (0 to 0.75) and  $d$  (0 to 0.75) with linear step length of 1, 0.005 and 0.005, respectively. Later, to obtain a more precise (local) minimum near brute's best gridpoint, the downhill simplex algorithm was used applying the result of "brute force" minimization as initial guess (Nelder and Mead, 1965).

$$\text{RSS} = \sum (e(\theta)_{\text{exp}} - e(\theta)_{\text{sim}})^2 \quad (7.7)$$

### 7.2.6 Model analysis

The RSS values were obtained by comparing experimental data,  $e(\theta)_{\text{exp}}$  with the simulated data,  $e(\theta)_{\text{sim}}$  of the conceptual models presented in section 7.2.4 (Fig. 7.2, 7.3, eq. 7.7). Two different techniques are used to find if the model is adequate to describe the RTD and hence transport and mixing inside the TSG. First, the coefficient of determination ( $R^2$ ) was used, which is a statistical measure of how well the simulated data points approximate the real measurement data points. Acceptable values of  $R^2$  (close to 1) imply that the respective model defines the true behaviour of the system. Second, RSS was used which is a measure of the discrepancy between the experimental data and an estimation model. A small RSS indicates a close fit of the model to the data.

The calculations for parameter estimation and model analysis were performed using the Python programming language, employing built-in functions in scientific libraries NumPy and SciPy (Jones et al., 2001). If a conceptual framework for RTD could demonstrate a high  $R^2$  value and RSS for a broad spectrum of process conditions, this would form a strong indication that the model is suitable and thus can be used for interpolation in the experimental domain.

## 7.3 Results and Discussion

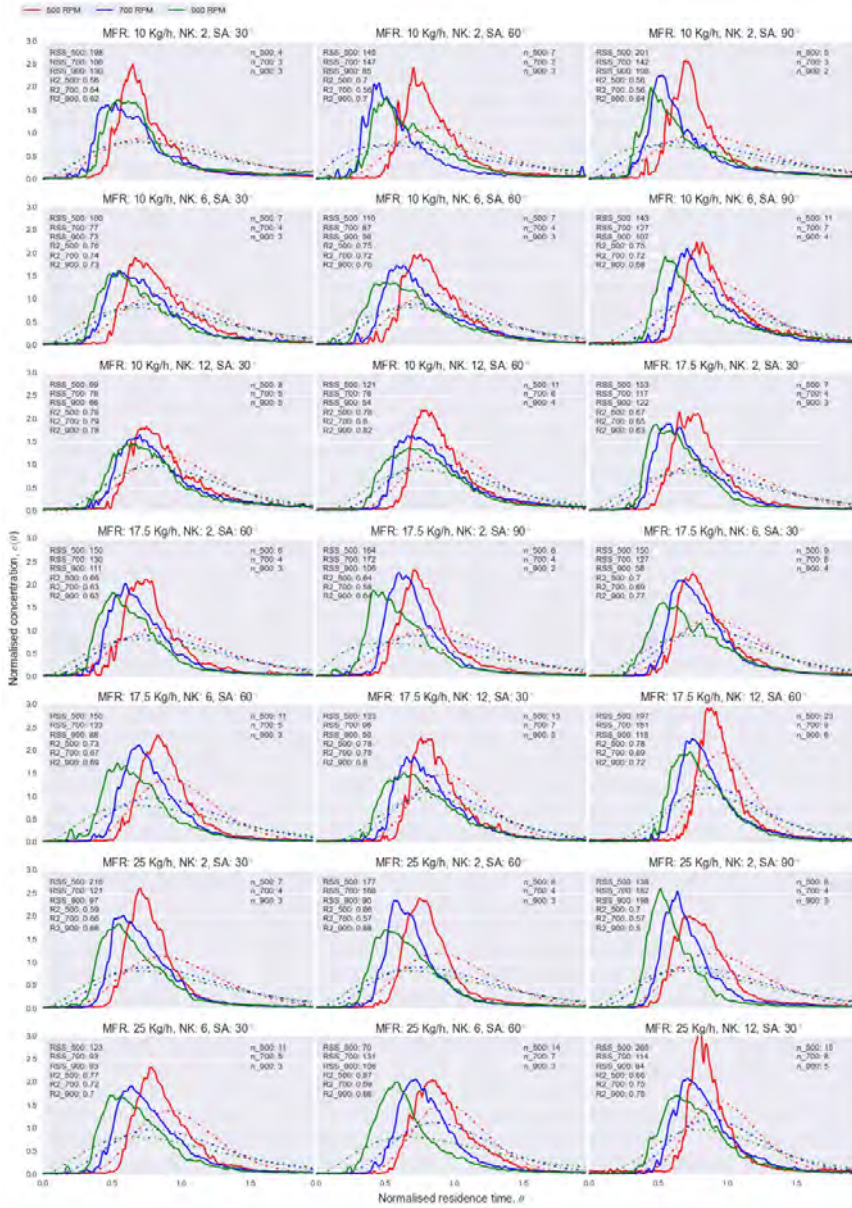
### 7.3.1 Comparison of models based on the goodness-of-fit

#### Tanks-in-series (TIS)

This model allowed estimation of the axial mixing of the bulk material stream under a non-ideal mixing condition in terms of  $n$  (eq. 7.3) (Levenspiel, 1999). The RSS between the experimental data and the model prediction was calculated for the  $n$  values ranging from 1–50. The parameter  $n$  that gave the least RSS varied from 2 to 30 for the different runs (Fig. 7.2). The  $n$  increased with an increase in  $\bar{t}$ . An increase in number and stagger angle of kneading discs and a reduction in screw speed led to an increase in the  $\bar{t}$ . However, there was a significant lack of fit obtained for this model as the  $R^2$  for the different runs for this model varied from 0.50–0.94. Also, the RSS was found to be between 54–265. This suggests that this model structure was not suitable to conceptually describe the RTD in the TSG. The high value of  $n$  estimated by this model also indicates that axial mixing in the TSG was non-ideal. Therefore, in order to improve accuracy in simulating the flow behaviour of the material in the TSG,  $p$  was needed to be introduced in the TIS model (eq. 7.4). In lack of axial mixing, the flow in  $p$  rely on the conveying rate only. Hence, it is a cause of delay in the appearance of the tracer in the outlet.

#### TIS with plug-flow volume fraction

This model structure contained two physically significant parameters ( $p$  and  $n$ ) thus allowing the quantification of the plug-flow volume fraction along with the degree of mixing, respectively. As for the TIS without a plug-flow volume fraction, the estimated parameters of the TIS with a plug-flow volume fraction also suggest a deviation from the ideal-plug and mixed flow behaviour in the TSG. Including the  $p$  as model component caused a significant reduction in the value of  $n$ , which now ranged between 2–21. The value of  $p$  for different runs were obtained between 0.2–0.65. The existence of a plug-flow regime was clearly identified by this model, and resulted in a lower RSS and higher  $R^2$  ranges compared to the TIS without a plug-flow volume fraction. The RSS and the  $R^2$  were obtained between 42–305 and 0.73–0.97, respectively. However, as the fit between the experimental and predicted RTDs was poor, this model failed to represent the mixing properly resulting in an exceptionally low value of  $n$  for all the runs (Fig 7.3). This situation arises when there are dead or stagnant pockets in the system along with the dispersion effects leading to a long tail in the RTD (Fogler, 2006). Therefore, for a further change in the model structure the conceptual model proposed by Kumar et al. (2008a) including the  $p$  and  $d$



**Figure 7.2:** Experimental (—) vs. predicted (-.-) RTD by a TIS model at different screw speed (500, 700, 900 RPM), material throughput (10-25 kg/h), number of kneading discs (2, 6, 12) and stagger angle (30-90°) [SA: stagger angle (°), NK: number of kneading discs (-), MFR: material throughput (kg/h)].

was used to define the RTD in the TSG (eq. 7.5).

### **TIS with plug-flow volume fraction and dead-zones**

This model allowed estimation of  $p$  and degree of mixing in terms of a finite  $n$  having  $d$  (Fig. 7.1). A significant improvement in the fit between the experimental and estimated RTD data was established by introducing the  $d$  in the model structure (Fig. 7.4). The RSS for different runs varied from 5 to 60 and the  $R^2$  between 0.93 and 0.99, which is much better than observed for the other model structures. This also suggests that the TIS model with  $p$  and  $d$  is the most suitable to conceptually define RTD in the TSG and can flexibly reflect the behaviour of the system in the domain of the experiment. The obtained  $p$  values are found between 0.2–0.65, similar to the TIS model with  $p$  only. The values of  $n$  and  $d$  ranged from 2 to 6 and from 0.01 to 0.54, respectively. Due to a very good fit between the experimental and estimated RTD by this model, the calculated values for the parameters can be reliably used for characterisation of residence time and mixing in the TSG.

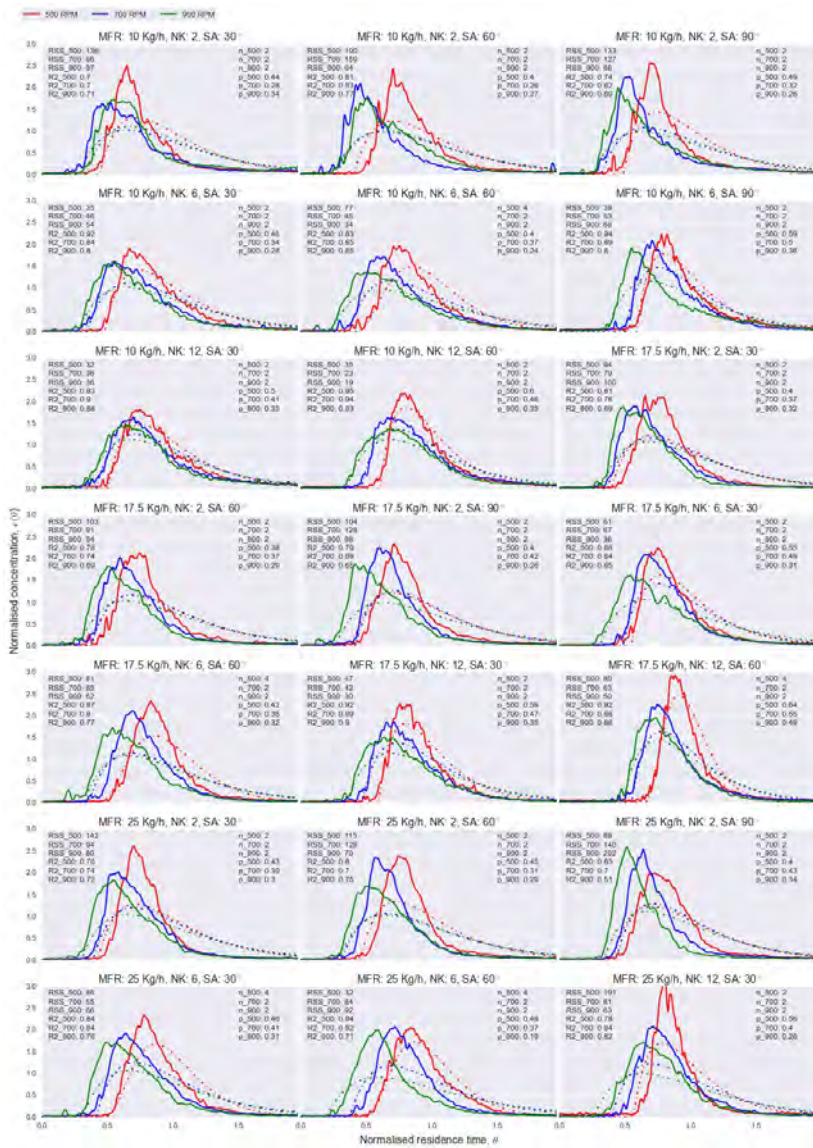
Therefore, based on the parameters estimated by this model, further detailed analysis of the twin-screw granulation system will be presented in the next section. A complete list of parameter sets, RSS and  $R^2$  values at different process conditions for all three model configurations is provided in Appendix C, Table C.1.

### **7.3.2 Analysis of RTD using TIS model with plug-flow and dead-volume fractions**

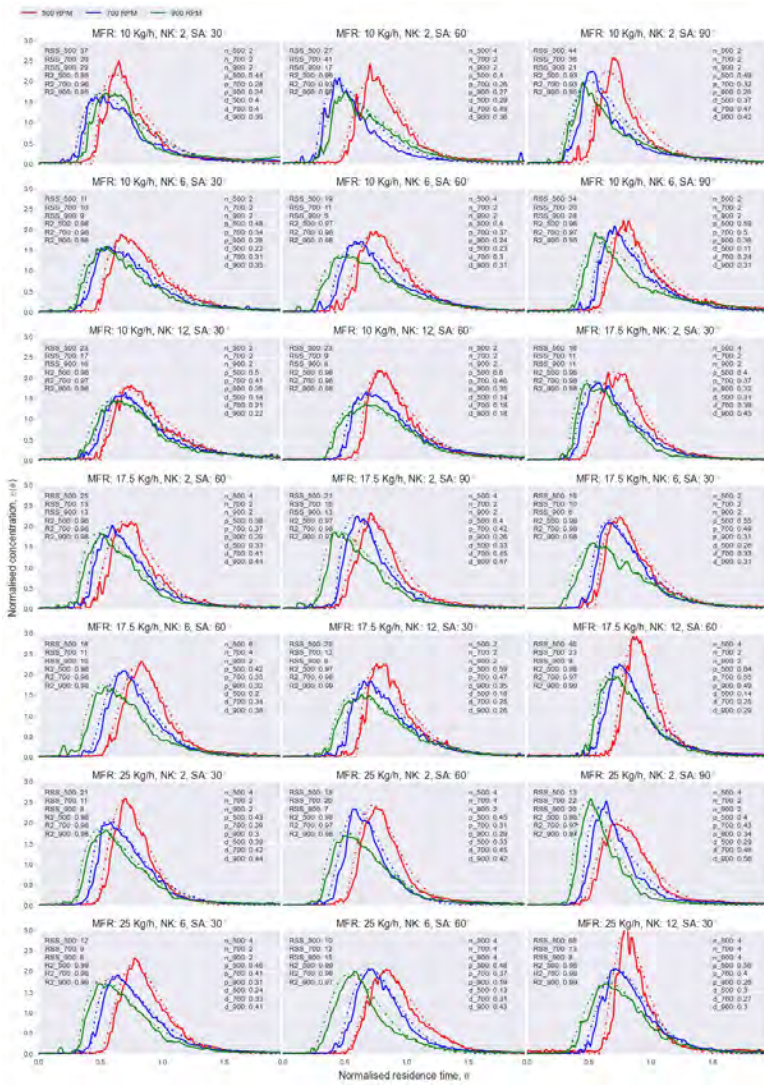
Prior to a comprehensive analysis of modeling results, it is indispensable to know the reliability of the parameter estimates. Although only certain numerically estimated parameter combinations for the model could closely reproduce the experimental RTD of the process, ignoring the dependencies among the estimated parameters may lead to an identifiability problem and meaningless estimates which severely reduces the prediction power of the model. Therefore, practical identifiability was analysed globally over the complete parameter space by the collinearity analysis. The collinearity index (eq. 7.6) was found to be 1.87, which is sufficiently low to suggest that there was no significant interrelation between parameters.

### **Effect of process settings on plug-flow volume fraction in the TSG**

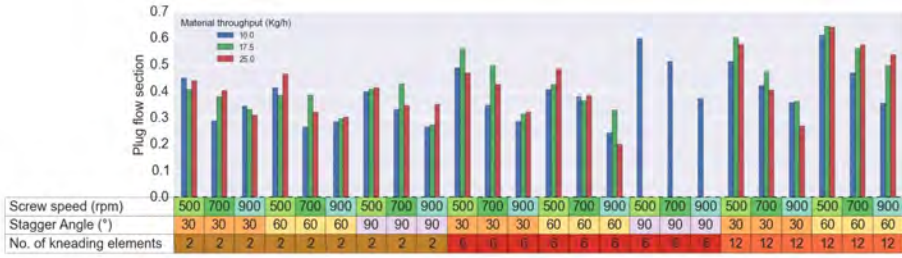
The effect of material throughput (10-25 kg/h) on  $p$  was very low for a lower number of kneading discs, however, for 6 and 12 kneading discs, the plug-flow



**Figure 7.3:** Experimental (—) vs. predicted (---) RTD by a TIS with plug-flow volume fraction model at different screw speed (500, 700, 900 RPM), material throughput (10-25 kg/h), number of kneading discs (2, 6, 12) and stagger angle (30-90°) [SA: stagger angle (°), NK: number of kneading discs (-), MFR: material throughput (kg/h)].



**Figure 7.4:** Experimental (—) vs. predicted (-.-) RTD by a TIS with plug-flow and dead-volume fractions model at different screw speed (500, 700, 900 RPM), material throughput (10-25 kg/h), number of kneading discs (2, 6, 12) and stagger angle (30-90°) [SA: stagger angle (°), NK: number of kneading discs (-), MFR: material throughput (kg/h)].



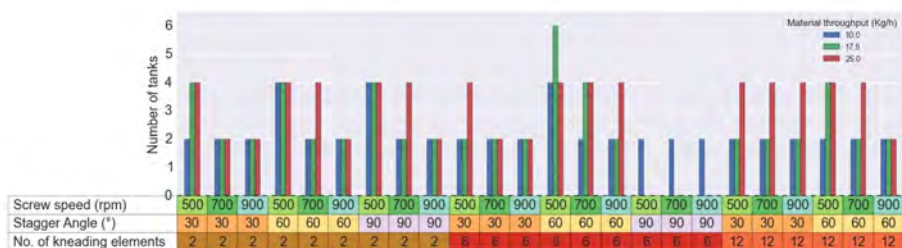
**Figure 7.5:** Effects of change in the process conditions on the plug-flow volume fraction as predicted by the TIS model with plug-flow volume fraction and dead zones.

volume fraction increased with an increase in material throughput (Fig. 7.5). Similarly, increasing the number of kneading discs caused an increase in  $p$  in the TSG. Also, the effect of a change in stagger angle was less prominent for a low number of kneading discs. However, for 6 and 12 kneading discs, the plug-flow volume fraction increased significantly when stagger angle increased from  $30^\circ$  to  $60^\circ$  and then to  $90^\circ$ . The effect of screw speed was most dominant, and therefore,  $p$  always reduced with the increase in the screw speed (500 to 700 and 900 rpm) irrespective of other process settings.

These results suggest that kneading blocks in the TSG screws act like a plug-flow region and the fill ratio in this region is critical. An increase in material throughput led to a high fill ratio due to a higher material flux, whereas the increase in screw speed increased conveying rate leading to reduction in the fill ratio. Since the  $p$  is the ratio between  $t_{min}$  and  $\bar{t}$  (eq. 7.4), and since we know from a previous experimental study (Chapter 4) that an increasing material throughput and screw speed cause a reduction in  $\bar{t}$ , it can be inferred that an increase in material throughput causes a relatively greater reduction in  $\bar{t}$  than  $t_{min}$  (narrowing of the RTD) and hence a higher  $p$ . However, when the screw speed was increased the relative reduction in  $t_{min}$  was greater than  $\bar{t}$  (broadening of the RTD), leading to a lower  $p$ . Hence, material throughput and screw speed, despite having the same effect on  $\bar{t}$ , have an opposite influence on the axial mixing.

### Effect of process settings on axial mixing in the TSG

Mixing of the material within the shortest possible granulator length is of key importance in TSG. Beside the indirect measurement of axial mixing in terms of the ratio between  $t_{min}$  and  $\bar{t}$ , in the TIS model with  $p$  and  $d$  the axial mixing is directly quantified in terms of  $n$ . The trend of change in  $n$  at various process



**Figure 7.6:** Effects of change in the process conditions on the number of TIS as predicted by the TIS model with plug-flow volume fraction and dead zones.

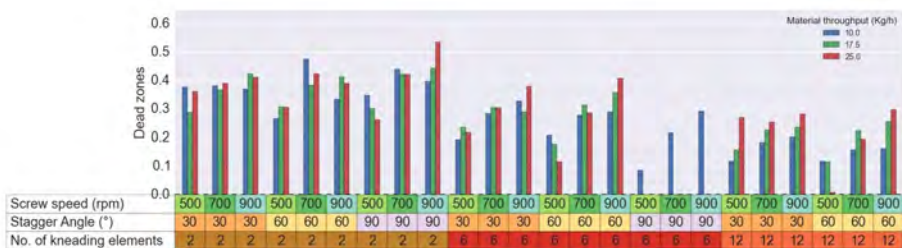
settings suggests that the level of axial mixing was most dominantly controlled by the screw speed (Fig. 7.6). At a low screw speed (500 rpm), the value of  $n$  was mostly 4 compared to the experiments with a high screw speed (900 rpm) where it was 2. Also, a high material throughput along with a low screw speed, i.e., the high fill ratio condition, led to reduction in axial mixing. At a high material throughput, an increase in the number of kneading discs from 2 to 6 and then to 12 as well as a change of the stagger angle ( $30^\circ$  to  $60^\circ$ ) also caused a reduction in the axial-mixing level despite a high screw speed (900 rpm), and the  $n$  increased to 4. The runs for  $90^\circ$  stagger angle could not be performed due to low axial mixing, which caused jamming of the granulator. However, an increase in the screw speed to its maximum (900 rpm) mostly resulted in resetting of the axial mixing to the same level ( $n = 2$ ).

These results suggest that material throughput and screw speed together dictate the axial mixing. Therefore, a balance between the throughput force and conveying rate is needed to obtain good axial mixing inside the TSG. At a high conveying rate, material throughput can be increased without loss in mixing, however, an increase beyond the conveying capacity of the screw may lead to a sudden change in flow regime to plug-flow and complete jamming of the granulator (see section 4.4.2 of Chapter 4).

### Effect of process settings on dead zones in the TSG

Although axial mixing reflected by broadening of the RTD is necessary to compensate for process variations (see Chapter 4), the excessive broadening in the tail region of the RTD may also result from a stagnant region and excessive back mixing inside the TSG. Such a desirable region may lead to build-up of material in long runs and is therefore estimated by the  $d$  in the model. The value of  $d$  was primarily influenced by the screw speed and the number of kneading discs (Fig. 7.7). When the number of kneading discs increased in





**Figure 7.7:** Effects of change in the process conditions on the dead-volume fractions inside the TSG barrel as predicted by the TIS model with plug-flow volume fraction and dead zones.

the screw configuration,  $d$  decreased monotonically. Furthermore, an increase in screw speed caused a reduction in  $d$ . In contrast, for a higher number of kneading discs (6 and 12), an increase in material throughput caused an increase in  $d$ . This change is once again related to the higher throughput force by the increased material flux.

These results indicate that the kneading blocks, which normally work under a more filled channel condition than the transport screws, prevent excessive back-mixing in the TSG. Also, increasing fill ratio reduces the stagnant region and consequently lowers the dead zone inside the mixed flow section of the TSG. However, when the slippage rate increases due to an increase in screw speed, there is a greater possibility of back-mixing, hence an increase in  $d$ . Also, the conveying force helps in clearing the flow in the kneading blocks leading to more back-mixing.

Beside the modelling and system identification owing to a good agreement between the simulated and the experimental RTD data, this study also established that the combination of modelling and dedicated experimental data collection is very effective for gaining an improved insight into the transport and mixing characteristics of material in the TSG. The presented results from this study may not necessarily translate to other formulations due to the likely difference in the granulation behaviour of different formulations (such as microcrystalline cellulose and dibasic calcium phosphate), model scope is limited to this formulation. However, the method used in this study (both data collection and modelling) is generic and can be repeated for other excipients. Once this knowledge is further built for different excipients, the observations from these studies can be compared for similarities between specific excipients and apply the knowledge in a generic model that will be able to predict all of the tested formulations, thereby reducing the dependence on experimental study.

The knowledge gained from this study can now be used as the basis for future extensive numerical simulation of flow and transport in the TSG using discrete element method (DEM). The, DEM requires enormous numerical and computational effort due to the large number of equations, the strong coupling between various physical processes and the difficulties to resolve boundaries of the flow domain in the intermeshing twin-screw involved. However, these models are necessary for complete understanding of the multiphase flow and mixing of wetted powder such as local residence time and impact speed of colliding granules in the screw zones, which are important for understanding the granulation mechanism in the TSG. Until an extensive DEM model is developed, the best-fit conceptual model consisting of algebraic equation to describe a plug flow in series with a finite number of constantly stirred tank reactors having dead volume fractions can be applied for representation of the RTD in a TSG with a reasonable accuracy along with simplicity and computational advantages.

## 7.4 Conclusions

In this study, a systematic evaluation of the performance of three different conceptual models for the description of the RTD in a TSG has been performed. The suitability of the model framework was examined using the statistical difference between the experimental and estimated RTD for runs with different screw configurations and process settings. The TIS model assuming  $p$  in series with a finite  $n$  with  $d$  was found to be the most suitable conceptual model for describing the experimentally measured RTD in a TSG. As estimated by this model, the kneading block in the screw configuration significantly stimulates the plug-flow transport of material inside the granulator. Furthermore, the results showed that mixing and  $d$  are generally affected by the fill level inside the TSG barrel, thus a good balance between the throughput force and the conveying rate is necessary for a good axial mixing and reduction in the stagnant regions inside the TSG. The steady-state models consisting of algebraic equations rather than the physical models containing differential equations, achieve a reasonable accuracy in representation of the RTD along with the simplicity of implementation and computational advantages. Therefore, the conceptual TIS model describing RTD as a plug flow in series with a finite number of constantly stirred tank reactors having dead volume fractions was suggested for improved understanding the mixing and transport of material in the TSG. Future experiments and modelling studies should investigate the effect of other formulations with significantly different raw material properties.



---

## Model-based characterisation of granule size evolution in a twin-screw granulation system for continuous solid dosage manufacturing

---

**Extended from:** Ashish Kumar, Krist V. Gernaey, Thomas De Beer, Ingmar Nopens, Model-based characterisation of twin-screw granulation system for continuous solid dosage manufacturing, *Computer Aided Chemical Engineering*, Volume 37, 2015, Pages 2165-2170

### Abstract

The screw used in a twin-screw granulator (TSG) has a modular structure and achieves mixing in a short time by a combination of screw design and alignment, and process settings (e.g. feed rate, screw speed, etc.). Therefore, an understanding of the dominating granulation sub-processes and the change in granule size distribution and dynamics along the twin-screw granulator barrel as the function of individual screw modules and their interaction, is necessary for the optimisation and control of the granulation process. Mechanistic models that incorporate the understanding of the underlying granulation mechanisms can be used to gain knowledge about the granulation system both under steady state and dynamic conditions. In the study, the constitutive mechanisms of a granulation process such as growth, aggregation and breakage are included in a population balance model (PBM) framework. This was done for the different mixing zones of a continuous TSG containing kneading elements. The rate processes which are considered dominant in the kneading element regions of the granulator, i.e. aggregation and breakage, were included in the model. Based on an experimentally determined inflow granule size distribution and

mean residence time of the granulator, predictions of the outflow granule size distribution were made using the PBM. The experimental data was used for calibrating the model for individual screw modules in the TSG. The granule size distribution (GSD) dynamics at different process conditions and in successive screw sections as predicted by the calibrated model provided an improved insight into behaviour of the system. The results showed that, by choosing appropriate process conditions, the successive kneading blocks lead to a granulation regime-separation inside the TSG. The first kneading block after wetting caused an increase in the aggregation rate, which was reduced after the second kneading block. In contrast, the breakage rate increased successively along the length of the granulator. Getting insight into the physical separation between the granulation regimes is promising for future design and advanced control of the continuous granulation process.

## 8.1 Introduction

A TSG achieves mixing and granulation by a complex interplay between the screw configuration (e.g. number and stagger angle of the kneading discs) and process settings (e.g. feed rate, screw speed, etc.) to produce granules in a short time (typically, in order of seconds). Thus, an understanding of this complex process is required to optimise and control this new technology. In recent years, experimental studies on twin-screw granulation have been widely pursued. The available studies primarily focused on the effect of process variables (such as screw configuration, material throughput, screw speed etc.) (Vercruyssen et al., 2012; Dhenge et al., 2011; Thompson and Sun, 2010) and formulation properties (El Hagrasy et al., 2013b; Dhenge et al., 2013) on "granule properties at the outlet" of the TSG due to the opacity of the multiphase system. Thus, little is known about the effect of these variables on the evolution and kinetics of granule formation in the TSG and the resulting granule structure. Without this, the system remains a black box and its understanding is hampered. In a recent study, however, the GSD evolution along the TSG screw was experimentally mapped in order to understand the dominant constitutive mechanisms of a granulation system such as growth, aggregation and breakage (Kumar et al., 2014b). Despite the fact that, such measurements provide a semi-quantitative insight regarding the GSD at discrete time steps, it still is difficult to apply in process design applications. Moreover, process development causes plenty of costs in continuous processing due to absence of batches and the requirement for on-line and in-line instrumentation (the process analytical technology (PAT) tools), which are more expensive than traditional analysing methods in batch production (Schaber et al., 2011). This calls for application of mathematical tools, which can efficiently simulate, predict and analyse the twin-screw wet

granulation for better process understanding.

Population balance equations (PBEs) are a frequently used mathematical tool to describe particulate processes such as granulation (Kumar et al., 2013a). An extensive review of the applications of such equations to particulate systems in engineering is given by Ramkrishna (2000). Barrasso et al. (2013) used a multi-component PBM for tracking the liquid content and porosity of each particle size class during twin-screw granulation. The experimental data from El Hagrasy et al. (2013b) was used in this study. It consists of samples collected from the granulator outlet and therefore a lumped-parameter approach was adopted for the development of the model. Furthermore, Barrasso et al. (2015a) applied bi-directional coupling between particle scale discrete element method (DEM) and PBM for achieving a more mechanistic description of a twin-screw wet granulation process. The model showed sensitivities to the screw configuration, process parameters such as screw speed, liquid-to-solid ratio as well as material properties such as binder viscosity and pore saturation. Despite the fact that the bi-directional coupling between DEM and PBM to evaluate collision frequencies and liquid distribution was proved to be an excellent proof-of-concept of mechanistic modelling of granulation processes, it is computationally very expensive and requires many particle-scale assumptions, which demand further validation. Due to this, there is still very little understanding regarding the primary driving mechanisms and function of screw components in the twin-screw wet granulation. Thus, a combination of experimental and mathematical techniques/approaches is required.

In this study, the principal constitutive mechanisms of a granulation system such as growth, aggregation and breakage were included in a PBM framework to track particle size evolution through different mixing zones of a continuous TSG. Based on an experimentally determined inflow GSD (Kumar et al., 2014b) and mean residence time  $\bar{t}$  (Kumar et al., 2014a) of the granulator, predictions of the outflow GSD were made. The experimental data was used for calibrating the model for individual screw modules in the TSG at different process conditions. The results from the calibrated model were used to understand the role of mixing zones and the influence of their location in the screw, and this for different process conditions.

## 8.2 Materials and methods

### 8.2.1 Population balance model for TSG

A TSG consists of a wetting zone and several mixing zones containing a finite number of kneading elements, which significantly drive the solid-liquid mixing and hence the granulation process. For the mathematical description of a TSG with two mixing blocks, the compartmentalisation into two well-mixed zones for simulation solved the challenge of inhomogeneous distribution of particle properties along the TSG length. This inhomogeneity exists due to the geometry of the screw as well as the position of the liquid addition ports. Introducing an external coordinate can be another possibility to model this inhomogeneity, but that will require implementation of the DEM together with population balances which is computationally challenging. In order to model the change in GSD across the individual mixing zone, these mixing zones were assumed to be well mixed systems. The granulation rate processes which are considered to be dominant in the kneading element regions of the granulator, i.e. aggregation and breakage, were included in a PBM framework, which can be represented as:

$$\begin{aligned} \frac{\partial n(t, x)}{\partial t} = & \frac{Q_{in}}{V} n_{in}(x) - \frac{Q_{out}}{V} n_{out}(x) + \frac{1}{2} \int_0^x \beta(t, x - \varepsilon, \varepsilon) n(t, x - \varepsilon) n(t, \varepsilon) d\varepsilon \\ & - n(t, x) \int_0^\infty \beta(t, x, \varepsilon) n(t, \varepsilon) d\varepsilon + \int_0^\infty b(x, \varepsilon) S(\varepsilon) n(t, \varepsilon) d\varepsilon \\ & - S(x) n(x, t) \end{aligned} \quad (8.1)$$

where,  $n(t, x)$  is the number density function of particle volume  $x$  as the internal coordinate at time  $t$ ,  $Q_{in}$  and  $Q_{out}$  were inflow and outflow of the material based on throughput and  $V$  was the volume of the mixing zone. Assuming the material transport across the mixing zone to occur at a steady state, inflow and outflow can be eliminated from Eq. 8.1. Moreover, the GSD of the inflow to the second mixing/transport zone was assumed to be same as the GSD of the outflow from the first mixing zone.

#### Aggregation and breakage kernels

The primary challenge for using PBE is to model the kinetics of the twin-screw granulation process in  $\beta(t, x, \varepsilon)$  and  $b(x, \varepsilon)$ , because of their strong dependence on the time and in a fairly complex way on operating parameters and material properties. The aggregation kernel  $\beta(t, x, \varepsilon)$  is a product of two factors, aggregation efficiency  $\beta_0(t)$  and collision frequency  $\beta(x, \varepsilon)$  i.e.,

$$\beta(t, x, \varepsilon) = \beta_0(t) \beta(x, \varepsilon) \quad (8.2)$$

The aggregation efficiency  $\beta_0(t)$  depends on effect of process and equipment settings on kinetic energy of particles, their trajectories and several other mechanical properties of the particles such as orientation and surface structure. Generally  $\beta_0(t)$  is assumed to remain constant with respect to time and size independent (Rao, 2009). The collision frequency  $\beta(x, \varepsilon)$  is mostly assumed to be a function of particles size. For the sake of simplicity, the constant aggregation kernel ( $\beta(t, x, \varepsilon) = \beta_0$ ) describing the frequency that particles with diameter  $\varepsilon$  and  $x - \varepsilon$  collide to form a particle of size  $x$  was used in this study.

Same as aggregation kernel, the breakage kernel is also composed of two components, breakage function  $b(x, y)$  and selection function  $S_0$ . The breakage function  $b(x, y)$  is a probability density function for the formation of particles of size  $x$  after breakage of particle of size  $y$ . For the breakage process, the quadratic selection function,  $S(y) = S_0(y)^\mu$  was used in which  $S_0$  and  $\mu$  are chosen to be positive rate constants. The breakage function,  $b(x, y)$  originally proposed for the ball milling operation by Austin (2002) (eq. 8.3), which is an operation involving particles in high-shear like twin-screw wet granulation, describes the daughter size distribution  $x$  from the breakup of a particle of size  $y$  was used.

$$b(x, y) = \frac{\frac{\phi\gamma x^{\gamma-1}}{y^\gamma} + \frac{(1-\phi)\alpha x^{\alpha-1}}{y^\alpha}}{\frac{\phi\gamma}{\gamma+1} + \frac{(1-\phi)\alpha}{\alpha+1}} \quad (8.3)$$

where  $\gamma$ ,  $\phi$  and  $\alpha$  are dimensionless material constants. The term  $\phi$  is called the weight parameter to quantify the mass content of the first breakage distributions. The exponents  $\gamma$  and  $\alpha$  represent the width of the fragment distributions  $\phi$  and  $1 - \phi$ , respectively.

## 8.2.2 Numerical solution of PBM

In this study, a sectional method known as the cell average technique (CAT) was applied to solve the PBE (Kumar et al., 2006). It has been shown numerically that CAT is very accurate and efficient, as it prevents over-prediction of number density for the large particles and limits a diverging behaviour of higher moments, which are critically important. The CAT is consistent with the first two moments and the scheme can be generalized to conserve any two moments (Kumar et al., 2006). For this study, the zeroth moment which is proportional to total number of particles and first moment which is proportional to total mass were calculated. The numerical solution scheme can be briefly described as follows:

1. *Domain discretisation*: First, the computational domain  $]0, d_{max}]$  is fixed and the truncated equation is obtained from eq. 8.1 by replacing  $\infty$  by  $d_{max}$ . In order to accommodate particles of a wide size range with



a minimal number of bins, a logarithmic grid with  $I = 50$  bins was used for the discretisation of internal coordinates, such that bin  $\Delta_i := [d_{i-1/2}, d_{i+1/2}]$ , where  $i = 1$  to  $I$ , with  $d_{I+1/2} = 3000 \mu\text{m}$ , which is the maximum granule size under consideration for this study. The *pivot* for each bin is calculated as  $d_i = (x_{i-1/2}, x_{i+1/2})/2$ , where the particle distributions within bin  $\Delta_i$  are considered to be represented by a point mass. According to the mid point rule, they are second order quadrature points.

2. *Computation of birth and death rates:* The discrete events such as aggregation and breakage which can occur at arbitrary locations in the discretised domain lead to change in the particle size and that adds or removes particle in the  $i$ th bin of the domain is termed as birth and death, respectively. Since both aggregation and breakage processes are considered to take place together in the mixing zones, the discrete birth and death rates for the combined processes are considered by algebraically summing the total birth and death rates in a bin, i.e.,

$$\begin{aligned} \frac{dN_i}{dt} &= B_{agg,i}^{mod} + B_{break,i}^{mod} - D_{agg,i} - D_{break,i} \\ &= B_{agg+break,i}^{mod} - D_{agg+break,i} \end{aligned} \quad (8.4)$$

where  $B_{agg+break,i}^{mod}$  and  $D_{agg+break,i}^{mod}$  represent the modified birth and death rates of particles in the  $i$ th bin due to aggregation and breakage respectively. The discrete birth and death rates can be obtained by substituting a Dirac-delta representation of the number density  $n(t, x) \approx \sum_{i=1}^I N_i \delta(x - x_i)$  into the continuous form of total birth and death rates in each bin. Thereby  $B_{agg,i}$ ,  $B_{break,i}$ ,  $D_{agg,i}$ ,  $D_{break,i}$  are calculated as :

$$B_{agg,i} = \sum_{\substack{j \geq k \\ x_{i-1/2} \leq (x_j + x_k) < x_{i+1/2}}} \left(1 - \frac{1}{2} \delta_{j,k} N_j N_k\right) \quad (8.5)$$

The net flux of volume  $V_{agg,i}$  into the  $i$ th bin as a result of aggregations between particles is therefore given by

$$V_{agg,i} = \sum_{\substack{j \geq k \\ x_{i-1/2} \leq (x_j + x_k) < x_{i+1/2}}} \left(1 - \frac{1}{2} \delta_{j,k} N_j N_k\right) (x_j + x_k) \quad (8.6)$$

The death rate,  $D_{agg,i}$  is calculated as:

$$D_{agg,i} = N_i \sum_{k=1}^I \beta_{i,k} N_k \quad (8.7)$$

The discrete birth  $B_{break,i}$  and death  $D_{break,i}$  due to breakage events in the  $i$ th bin are computed by the following expressions:

$$B_{break,i} = \sum_{k \geq i} N_k(t) S_k \int_{x_{i-1/2}}^{p_k^i} b(x, x_k) \quad (8.8)$$

and,

$$D_{break,i} = S_i N_i(t) \quad (8.9)$$

where,  $p_k^i$  is defined as

$$p_k^i = \begin{cases} x_i, & \text{if } k = i \\ x_{i+1/2} & \text{otherwise} \end{cases} \quad (8.10)$$

Similar to the net flux of volume  $V_{agg,i}$ , the discrete volume flux in the  $i$ th bin due to birth by breakage is given by

$$V_{break,i} = \sum_{k \geq i} N_k(t) S_k \int_{x_{i-1/2}}^{p_k^i} x b(x, x_k) dx \quad (8.11)$$

The total birth and death rates in the  $i$ th bin are then calculated as

$$B_{agg+break,i} = B_{agg,i} + B_{break,i} \quad (8.12)$$

and,

$$D_{agg+break,i} = D_{agg,i} + D_{break,i} \quad (8.13)$$

3. *Computation of average volume in bins:* For the consistency of two moments, the net birth in the  $i$ th bin is calculated using the volume average of all newborn particles due to aggregation and breakage within three neighbouring bins,  $(i - 1)$ th,  $i$ th and  $(i + 1)$ th. Thus, the average volume of the particles in each bin is calculated as

$$\bar{v}_i = \frac{V_{agg,i} + V_{break,i}}{B_{agg,i} + B_{break,i}} \quad (8.14)$$

If the average volume  $\bar{v}_i$  matches with the respective size of the bin  $x_i$

then the total birth  $B_i$  can directly be assigned to the node  $x_i$ . However, this is rarely possible and hence the total particle birth  $B_{agg+break,i}$  is reassigned based on the position of the average value to the neighbouring nodes such that the total number and mass remain conserved.

4. *Birth modification:* As the volumes of the newborn particles due to aggregation and/or breakage may lie between the bins of the logarithmic grid, the CAT allocates these particles into the corresponding bins. The modified birth term for this purpose is calculated

$$\begin{aligned}
B_{agg+break,i}^{mod} = & B_{agg+break,i-1} \lambda_i^- (\bar{v}_{i-1}) H(\bar{v}_{i-1} - x_{i-1}) \\
& + B_{agg+break,i} \lambda_i^- (\bar{v}_i) H(x_i - \bar{v}_i) \\
& + B_{agg+break,i} \lambda_i^+ (\bar{v}_i) H(\bar{v}_i - x_i) \\
& + B_{agg+break,i-1} \lambda_i^+ (\bar{v}_{i+1}) H(x_{i+1} - \bar{v}_{i+1}) \quad (8.15)
\end{aligned}$$

where, the discontinuous Heaviside step function  $H$  is defined as

$$H = \begin{cases} 1, & \text{if } x > 0 \\ 1/2 & \text{if } x = 0 \\ 0 & \text{if } x < 0 \end{cases} \quad (8.16)$$

and the function used for the distribution of particles is given as

$$\lambda^\pm(x) = \frac{x - x_{i\pm 1}}{x_1 - x_{i\pm 1}} \quad (8.17)$$

Thus, the modified birth rate  $B_{agg+break,i}^{mod}$  is consistent with the first two moments. There is no need to modify the death term since particles are just removed from the grid points and therefore the formulation remains consistent with all moments due to discrete death  $D_{agg+break,i}$ .

5. *Solving ordinary differential equations (ODEs):* The values of  $B_{agg+break,i}^{mod}$  and  $D_{agg+break,i}$  were substituted in eq. 8.4. The obtained set of ODEs were solved simultaneously for each bin using the higher order LSODE (Livermore Solver for Ordinary Differential Equations) routine from the Odespy package (Langtangen and Wang, 2014). The LSODE is an adaptive solver based on a variable order backward differentiation formulas (BDF) code, allowing order specification. So, the maximum order was specified as 5 and the time steps were getting adjusted throughout the solution process to meet the prescribed absolute error tolerance ( $1 \times 10^{-6}$ ).

### 8.2.3 Model parameter estimation

The experimental data provided evidence that the aggregation and breakage are the dominant mechanisms in twin-screw granulation (for details see Chapter 5) and a model framework was developed to include these phenomena. However, various parameters in this model are unknown and can vary based on process settings and material properties. Experimental data of volume distributions of granule samples from various locations inside the granulator (Fig. 5.2) were used to estimate values of five model parameters: three dimensionless material constants,  $\gamma$ ,  $\phi$  and  $\alpha$  and the aggregation constant  $\beta_0$  and the selection function constant  $S_0$ . Based on available literature, the selection function constant  $\mu$  was fixed at 0.33. The estimation of these parameters was done by minimising the root mean square error (RMSE) as an objective function (eq. 8.18):

$$\text{RMSE} = \sqrt{\frac{\sum_{i=1}^I (N_{sim,i} - N_{exp,i})^2}{n}} \quad (8.18)$$

where  $N_{sim,i}$  and  $N_{exp,i}$  are the simulated and experimentally measured number density values for  $I$  bins of the granule size range. In order to find the global minimum of the objective function, the "brute force" method was used, which computed the objective function's value at each point of a multidimensional grid of points, to arrive at the global minimum of the function. This multidimensional grid contained physically sound ranges of  $\beta_0$  (1e-5, 0.4),  $S_0$  (0.001, 3.5),  $\alpha$  (3.3e-6, 1),  $\gamma$  (1.6e-4, 5) and  $\phi$  (0.01, 1.5) with linear step length of 0.005, 0.005, 0.000005, 0.05 and 0.05, respectively. Later, to obtain a more precise (local) minimum, the downhill simplex algorithm was used applying the estimation result of brute force minimization as initial guess (Nelder and Mead, 1965). The estimated parameter ranges from brute force minimization were also useful to check any correlations between estimated parameters, as well as to determine the confidence interval of the fitted parameters using bootstrap estimation (Efron and Tibshirani, 1986). In the Bootstrap estimation 25 randomly picked residuals  $R_{syn}$  from the least RMSE fitting using estimated parameters was used to generate 50 synthetic datasets from the experimental data  $N_{exp}$ , such that

$$N_{syn,i} = N_{exp,i} + R_{syn,i} \quad (8.19)$$

The  $N_{syn,i}$  was again fitted using the same algorithm which minimises the RMSE for the actual experimental data  $N_{exp,i}$  as discussed before. The 50 bootstrap parameter sets thus obtained were used to calculate the 95% confidence interval (CI) as,

$$CI_{95\%} = \mu \pm 1.96\sigma \quad (8.20)$$

by calculating the mean  $\mu$  and standard deviation  $\sigma$  of each parameter in the

bootstrap parameter sets. The implementation of the PBM solution method, model parameter estimation and bootstrap estimation were performed using the Python which is a simple yet powerful programming language, employing built-in functions in scientific libraries NumPy and SciPy (Oliphant, 2007).

## 8.2.4 GSD experimental data for model calibration

The granulation data was obtained by granulating a premix of  $\alpha$ -Lactose monohydrate (Pharmatose 200M, Caldic, Hemiksem, Belgium) and Polyvinylpyrrolidone (PVP) (Kollidon<sup>®</sup> 30, BASF, Ludwigshafen, Germany) (ratio: 97.5/2.5, w/w) with distilled water. Granulation experiments were performed using a 25 mm diameter co-rotating twin screw granulator, the granulation module of the ConsiGma-1 unit (GEA Pharma Systems, Collette<sup>™</sup>, Wommelgem, Belgium).

The experiments were performed to evaluate the influence of number of mixing zones with kneading discs ( $1\times 6$  and  $2\times 6$ ), screw speed (500 and 900 rpm), at a high throughput (25 kg/h) and liquid-to-solid ratio (L/S) (6.72% (w/w) based on wet mass). For each run, samples were collected from different locations inside the barrel by opening the barrel after stopping the process running at steady state (Fig. 5.2 in Chapter 5). Sample location 1 was just prior to the first kneading block, sample location 2 on the first kneading block, sample location 3 was between the first and second kneading block, sample locations 4 and 5 were on and right after the second kneading block. The sample preparation and analysis are discussed in detail in section 5.2 of Chapter 5. For the first block, the experimentally obtained volume-based GSD from location 3 was used for the calibration of a model for which simulation was initialised using the GSD for sample location 1. Similarly, for the second block, the volume-based GSD from sample location 5 was used for the calibration of the model for which simulation was initialised using the GSD for sample location 3 as a starting point. When the GSD span is presented as 25%, 50% and 75% quartiles, a shift in the quartiles indicated a change in the amount of a certain size fraction and a dominance of the related constitutive mechanism. Hence a detailed reasoning regarding the sample locations and measurement methods can be obtained in the experimental study of Chapter 5 that served as basis for this modelling work.

## 8.3 Results and discussion

### 8.3.1 Parameter estimation for predictive modelling

Both for the screw configuration with  $1\times 6$  and  $2\times 6$  kneading elements, for the runs at low (500 rpm) and high (900 rpm) screw speed, experimentally measured

GSD from location 1, 3 and 5 in Fig. 5.2 were used for model calibration. In order to quantitatively represent these trends in the simulations, the unknown rate parameters of the aggregation and Austin breakage kernels were estimated by comparing the simulation results with experimental data. The estimated model parameters and their confidence intervals (95 %) estimates for the simulation of a granulator with one mixing zone at low (500 rpm) and high (900 rpm) screw speeds are listed in table 8.1. The error estimates (RMSE and  $R^2$ ) are mentioned in Fig. 8.2 and 8.3. Furthermore, the estimated parameters for the numerical computations and their confidence intervals (95%) for a granulator with two mixing zones at low (500 rpm) and high (900 rpm) screw speeds are listed in table 8.2.

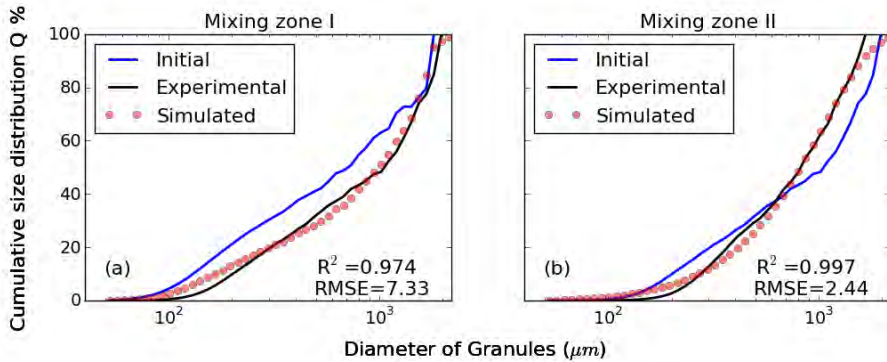
**Table 8.1:** Estimated model parameters with corresponding confidence intervals (95%) at low (500 rpm) and high (900 rpm) screw speeds and for one mixing zone followed by the transport zone (II) of the granulator.

Screw speed	Low		High	
	Mixing	Transport	Mixing	Transport
$\beta_0$	1.05E-03 $\pm$ 1.17E-04	3.12E-01 $\pm$ 1.16E-02	2.36E-04 $\pm$ 4.07E-05	2.95E-01 $\pm$ 1.19E-02
$S_0$	3.01E-02 $\pm$ 2.18E-03	3.30E+00 $\pm$ 3.18E-01	5.10E-02 $\pm$ 2.25E-03	1.18E+00 $\pm$ 2.37E-02
$\alpha$	6.01E-02 $\pm$ 5.53E-06	1.65E-07 $\pm$ 1.94E-08	1.86E-04 $\pm$ 4.49E-06	1.14E-06 $\pm$ 9.30E-07
$\gamma$	5.21E-01 $\pm$ 8.07E-02	4.24E-01 $\pm$ 1.19E-03	8.28E-01 $\pm$ 1.31E-02	3.07E-01 $\pm$ 3.13E-03
$\phi$	9.73E-01 $\pm$ 4.51E-02	7.20E-01 $\pm$ 6.54E-03	4.07E-01 $\pm$ 2.98E-03	5.34E-01 $\pm$ 7.29E-03

The low RMSE and high  $R^2$  values for all the screw speeds and mixing zones indicate that numerical results were in excellent agreement with the experimental data for each location inside the granulator (Fig. 8.1 and in Appendix C Fig. C.1 and C.2). However the solutions were subject to different optimal model parameters for each section. This suggests that the different sections of the granulator at different process condition behave differently.

**Table 8.2:** Estimated model parameters with corresponding confidence intervals (95%) at different screw speeds and for two mixing zones (I, II) of the granulator.

Screw speed	Low		High	
	Mixing I	Mixing II	Mixing I	Mixing II
$\beta_0$	3.02E-03 $\pm$ 1.47E-04	1.95E-01 $\pm$ 4.56E-02	8.97E-02 $\pm$ 3.36E-03	4.99E-02 $\pm$ 1.80E-02
$S_0$	2.53E-02 $\pm$ 5.91E-03	7.99E-01 $\pm$ 4.35E-02	3.11E-02 $\pm$ 2.25E-03	5.72E-01 $\pm$ 3.55E-02
$\alpha$	1.13E-05 $\pm$ 8.83E-06	6.11E-01 $\pm$ 3.19E-02	1.26E-03 $\pm$ 3.29E-04	4.38E-01 $\pm$ 9.30E-02
$\gamma$	4.05E+00 $\pm$ 7.60E-01	3.81E-03 $\pm$ 2.18E-04	2.63E-01 $\pm$ 9.02E-03	4.49E-02 $\pm$ 3.78E-03
$\phi$	1.03E+00 $\pm$ 2.31E-01	5.43E-02 $\pm$ 2.24E-03	1.18E+00 $\pm$ 3.89E-01	1.50E-02 $\pm$ 2.13E-03



**Figure 8.1:** Fit between simulated and experimental particle size distribution for TSG with two mixing zones (I, II) of the granulator at low screw speed.

### 8.3.2 Simulated dynamic behaviour in the mixing zones of the TSG

#### Screw configuration with one mixing zone

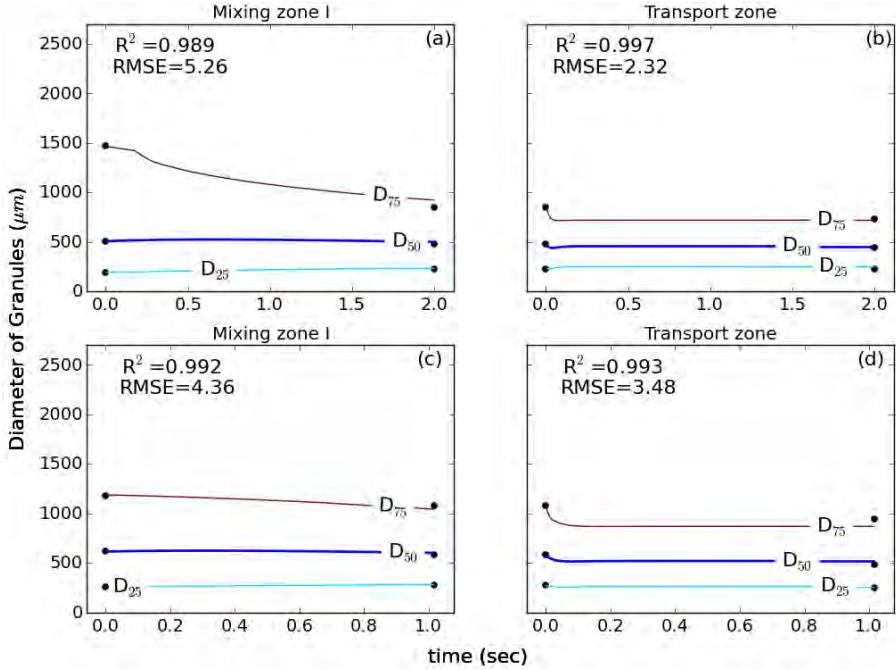
In this process condition, the mixing zone was placed between location 1 and 3. So, the downstream material from the mixing zone was conveyed between location 3 and 5 by the transport elements without any further distributive mixing by the kneading elements.

#### At a low screw speed

The simulation results for a screw configuration with one mixing zone showed that at a low screw speed, the mixing zone between location 1 and 3 was mainly involved in breakage of over-wetted lumps after the wetting of the powder immediately before location 1 (Fig. 8.2.a). This was indicated by the sharp reduction in the  $D_{75}$  of the simulated dynamic trends of the GSD. The  $D_{50}$  remained fairly constant and the  $D_{25}$  increased slightly when the material passed the first mixing zone. As the fill ratio is high due to the high throughput (25 kg/h) and the low screw speed (500 rpm), the mechanical shear and distributive mixing by the kneading elements caused breakage of over-wetted lumps.

In the follow-up section with transport elements (between location 3 and 5), the material was conveyed, but was only slightly mixed (Fig. 8.2.b). This led to a minor reduction in the oversized fraction. However, no further change in the other fractions was observed. After an initial slight reduction, all the quartile values of the GSD remained constant as the material passed the first mixing zone. This was also reflected by the minor reduction in the oversized

granules (>1000  $\mu\text{m}$ ) the in the inflow and outflow GSD as shown in Fig. C.1.b (Appendix C). This suggests that without mechanical mixing further granulation cannot be achieved under these process conditions.



**Figure 8.2:** Experimental ( $\bullet$ ) and simulated ( $\text{—}$ ) trends for dynamic change in quartiles of the GSD ( $D_{25}$ ,  $D_{50}$ ,  $D_{75}$ ) at low (a and b) and high (c and d) screw speeds for the mixing zone (a and c) and transport zone (b and d) of TSG.

### At a high screw speed

When the screw speed is increased from 500 to 900 rpm the fill ratio inside the barrel is reduced (Fig. 8.2.c). In the simulation of the high screw speed condition, this was reflected in a more uniform change in GSD. The larger over-wetted lumps broke when the material passed the first mixing zone. This was reflected by reduction in the  $D_{75}$  of the simulated dynamic trends of the GSD. Moreover, the  $D_{50}$  and the  $D_{25}$  values increased slightly which indicated an improved granulation compared to that at a low screw speed. This also suggests that conditions favouring very high filling of the barrel are desirable for the twin-screw granulation process.

In the subsequent section of the TSG, despite the fact that mechanical mixing by



the kneading discs was not present between location 3 and location 5, the higher shear due to increased screw speed resulted further granulation as inferred (Fig. 8.2.d). Therefore, there was little increase in the  $D_{25}$  values between location 3 and location 5. Moreover, some breakage of the oversized fraction as indicated by the reduction in the  $D_{75}$  value of the dynamic GSD trend.

## **Screw configuration with two mixing zones**

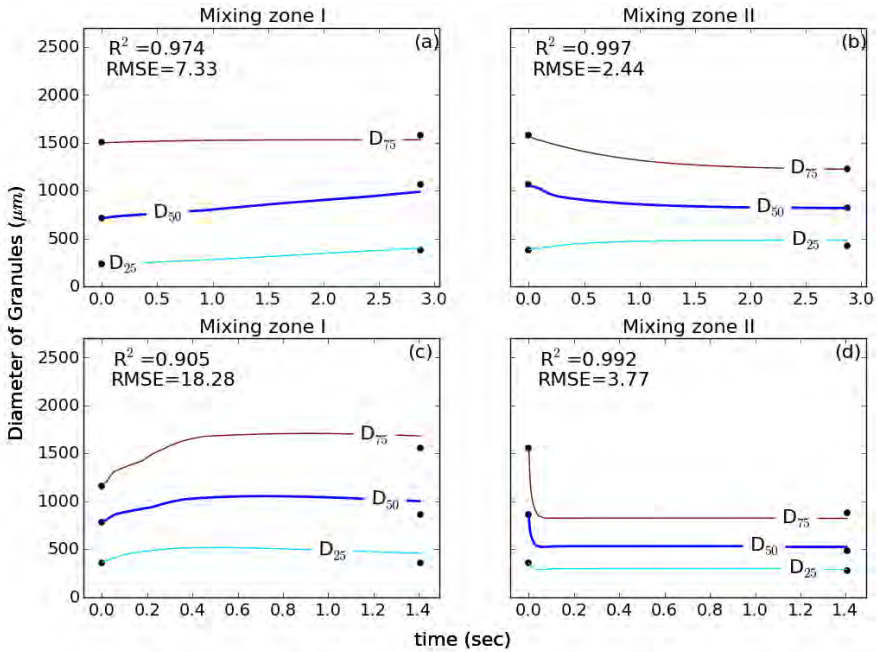
### **At a low screw speed**

The simulation results for a screw configuration with two mixing zones showed that when the screw speed was low (Fig. 8.3.a), the  $D_{75}$  remained constant whereas the  $D_{25}$  and  $D_{50}$  increased when the material passed the first mixing zone. This indicates that the primary role of the first kneading block at this condition was supporting the aggregation leading to formation of larger granules. Moreover, a clear difference between the simulated trends in Fig. 8.3.a and Fig. 8.2.a illustrate that the presence of the second mixing zone also affects the granulation dynamics in the upstream mixing zones. This was also suggested by the experimental study presented in section 5.3.2 of Chapter 5.

The second mixing zone at this condition caused breakage of the larger granules leading to reduction in  $D_{50}$  as well together with  $D_{75}$  (Fig. 8.3.b). However, the  $D_{25}$  value of the GSD increased by the mixing in the second zone at this condition. This indicates toward a mixed regime in the second mixing zone of the TSG where both aggregation and breakage compete with each other. This situation is similar to high shear mixers where granulation regimes co-exist and thus it is difficult to control granulation. Moreover, the barrel at this condition was highly filled due to the low screw conveying rate at low screw speed leading to less space for material to get distributed. This was also the reason why in the experimental study this condition led to an undesirably high level of torque (see Chapter 5).

### **At a high screw speed**

The simulation of the high screw speed condition showed a significant change in the granulation behaviour in the two mixing zones (Fig. 8.3.c and d). Unlike the case with low screw speed, when the material passed through the first mixing zone at this condition all the quartiles of the GSD increased (Fig. 8.3.c). This indicates that aggregation was the most dominant mechanism under these conditions in this mixing zone, while the level of breakage was very low leading to no reduction in any fraction with time. However, when the material was introduced to the second kneading block, the quartile values  $D_{75}$  and  $D_{50}$  dropped significantly, which indicates that breakage occurred as the dominant



**Figure 8.3:** Experimental ( $\bullet$ ) and simulated ( $\text{—}$ ) trends for dynamic change in quartiles of the GSD ( $D_{25}$ ,  $D_{50}$  and  $D_{75}$ ) at low (a and b) and high (c and d) screw speeds for first (a and c) and second (b and d) mixing zones.

mechanism in the second mixing zone (Fig. 8.3.d). This observation by process simulation is very important as it established that the successive kneading blocks led to a granulation regime-separation inside the twin-screw granulator under this condition. The mixing of the wetted powder in the first kneading block caused an increase in the aggregation rate, which was reduced after the second kneading block. However, the breakage rate increased successively along the length of the granulator. Such a physical separation between the granulation regimes is promising for future design of granulation system. Moreover, a properly calibrated and validated model for such a condition can be used for and advanced control of the continuous granulation process.

## 8.4 Model application and future development

As per the results shown above, the proposed PBM framework can be used for building improved process knowledge regarding mixing zones of the continuous twin-screw granulation process at steady-state. Also, it was established by

the discretised PBM that the process and equipment variables were linked to the time evolution of the GSD in the TSG. The results from the calibrated model also elucidated the regime separation phenomena under certain process conditions. This hints towards a potential decomposition of the twin-screw granulation system, allowing to simulate the complete granulator by switching between different granulation mechanisms.

However, an application model requires the model to completely capture the essential dynamics involved in the twin-screw granulation process. To completely describe the granulator dynamics, the coupling between two PBMs for individual mixing blocks, i.e. a two-stage granulator model is required. The model used in this study was a one dimensional (i.e. considering granule size only) PBM (eq. 8.1) limited to one stage only, and the experimental data was used to extract the aggregation and breakage rates for individual blocks of the granulator at a certain condition (Table 8.1 and 8.2). Therefore, the link between process variables and the constant parameters of the rate kernels need to be explored, which can be used to predict the result of the granulation process within the experimental window of the design of experiments used for the parameter estimation (Sanders et al., 2009).

Furthermore, in order to further improve the model, future work should focus on introducing the wetting kinetics in the model framework and to obtain particle flux data and collision frequencies using DEM to avoid the parameter estimation by model inversion. Additionally, dedicated mechanistic kernels for the twin-screw granulation can be developed in order to improve the sensitivity of the model towards the change in process conditions and other field parameters. Finally, a validated model can be used to define the design space of the process for the future optimization and model-based control of the granulation process.

## 8.5 Conclusions

A 1-D PBM including aggregation and breakage subprocesses for a continuous twin-screw granulation process was presented. Unknown model parameters and their 95% confidence range were estimated using experimentally measured particle size distributions from inside the granulator and a brute force calibration method. The calibrated model was subsequently used as a predictive tool within the experimental space. The results showed strong agreement with experimental data. This approach is the better way forward for the development of twin-screw granulation models as multiple factors of the TSG leading to an experimental output can now constrain the model during calibration. Further analysis

revealed that, at high screw speed, the successive kneading blocks can lead to the dominance of different constitutive granulation mechanisms inside the twin-screw granulator. The ability to achieve a physical separation between the granulation regimes inside the granulator can be promising for future design and advanced control of the continuous granulation process using the twin-screw granulator. Furthermore, the study suggested that a model-based approach can be adopted to develop a better understanding of twin-screw granulation processes. A validated model can ultimately be used to define the design space of the process to facilitate process optimization and model-based control.



## PART IV

Continuous granulation system:  
Scale-independent analysis of particle  
size evolution in a twin-screw granulator



---

## Development of a process map: an step towards regime map for steady-state high shear wet twin screw granulation

---

**Redrafted from:** Ashish Kumar, Jens Dhondt, Jurgen Vercruyssen, Fien De Leersnyder, Valérie Vanhoorne, Chris Vervaet, Jean Paul Remon, Krist V. Gernaey, Thomas De Beer, Ingmar Nopens, Development of regime map for steady-state high shear wet twin-screw granulation, 7th International Granulation Workshop, Sheffield, UK, 2015.

### Summary

Twin-screw granulator (TSG) allows the manipulation of size and properties of the granules by adjusting the binder addition method, the number and stagger angle of the kneading elements in the screw configuration, the granulation barrel temperature, the liquid addition rate, the powder feed rate and the screw speed. Multiple studies based on modifications of parameters both related to equipment and process have appeared in the last decade. However, most of these studies performed on twin-screw granulation are limited to a certain design and scale of the TSG. For each configuration and scale, there is a different energy (torque) requirement for the rotation of the screws and hence resulting different particle size distribution. In this study, in order to improve the understanding about the granulation process and to comprehend the applicability and limits of the process variables in a scale independent manner, the regime theory was applied. For this purpose,  $\alpha$ -lactose monohydrate was granulated with distilled water containing polyvinylpyrrolidone (PVP) (2.5%, w/w) as binder. A TSG with a screw configuration consisting of one or two kneading zones of six kneading



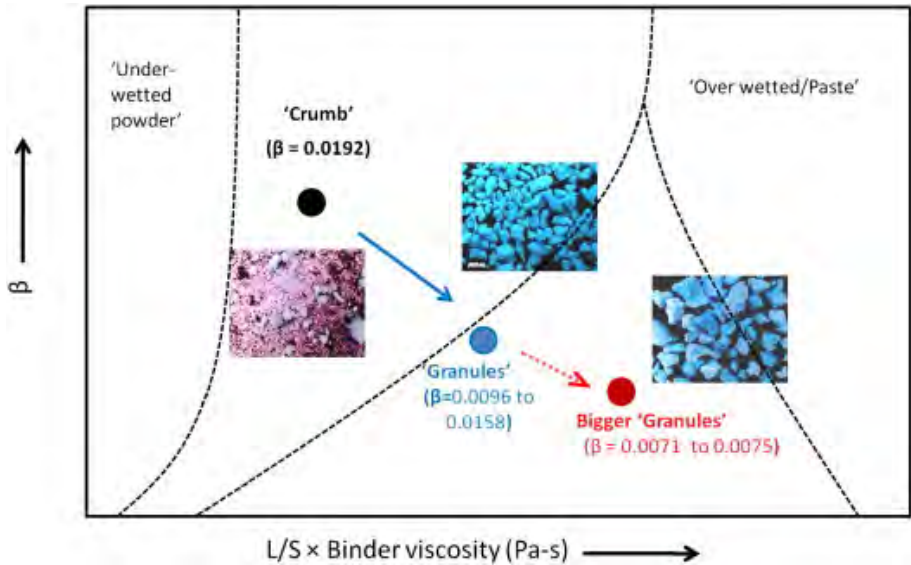
elements each ( $1\times 6$  and  $2\times 6$ , respectively), at a stagger angle of  $60^\circ$ , was used. The specific mechanical energy (SME) which involves the combination of screw speed, material throughput and torque required to rotate the screws was correlated with the applied liquid-to-solid ratio. The study suggested that, although increasing liquid-to-solid ratio (L/S) strongly drives the granule size distribution towards a large mean granule size, increasing the energy input to the system can be effectively used to lower the mean granule size and also narrow the width of the size distribution.

## 9.1 Introduction

Several researchers have investigated various aspects of TSG including the effect of key formulation variables (Dhenge et al., 2012b, 2013; Fonteyne et al., 2014; El Hagrasy et al., 2013b), screw configurations (Djuric, 2008; El Hagrasy and Litster, 2013; Sayin et al., 2015; Thompson and Sun, 2010; Vercruyssen et al., 2015) and process settings (Vercruyssen et al., 2013a; Dhenge et al., 2011). However, all these studies have been performed using granulators with different dimensions leading to differences in the scale and limits of variations in the parameters across studies.

In order to improve the understanding regarding the granulation process and to comprehend the applicability and limits of variables, the regime theory is applied. A regime theory is presented as a map which semi-quantitatively explains the variation in granulation behaviour during operation (Litster and Ennis, 2004). By developing a regime map, it becomes possible to correlate the input variables of the process and equipment with the granule characteristics (Tu et al., 2009). The mechanistic basis derived from a regime map is better than data-driven models, and the granulation design space can be determined more effectively with fewer experiments (Kayrak-Talay et al., 2012). Initially, regime maps were introduced for nucleation and granule growth behaviour (Hapgood et al., 2003; Iveson et al., 2001a,b; Rough et al., 2005). Later, an equipment specific granulation regime map resolving general effects of parameters such as impeller speed and liquid-to-solid (L/S) ratio in a high shear granulator was proposed by Tu et al. (2009).

To extend this approach of knowledge development to the twin-screw granulation process, Dhenge et al. (2012b, 2013) developed two regime maps for the TSG, first with a twin-screw containing conveying elements only and the other in which both conveying and mixing elements were present. Both these regime maps mapped the granulation characteristics as under-wetted, nuclei, crumb, granules and over-wetted or paste based on the relation between the



**Figure 9.1:** Granule growth regime map for twin screw granulation by Dhenge et al. Dhenge et al. (2012b).

modified deformation value and the pore saturation. The modified deformation value was calculated as  $\beta = \frac{T}{V} \times \frac{1}{\tau}$ , where  $T$ ,  $V$ ,  $\tau$  are torque (Nm), volume of material in the barrel ( $\text{m}^3$ ) and the strength of the granules (MPa), respectively. The pore saturation was assumed to be a function of  $L/S$  and viscosity of the granulation liquid, i.e.  $L/S \times \text{viscosity}$ . Dhenge et al. Dhenge et al. (2013) observed that without mixing zone the wet, big, loose and weak agglomerates termed as nuclei were produced in different amounts based on the deformation values ( $\beta$ ). It was suggested in the other regime map by Dhenge et al. Dhenge et al. (2012b) that a transition of regimes can be achieved by applying changes in the screw configuration and the process conditions (Fig. 9.1). Tu et al. Tu et al. (2013), following the earlier approach of building a regime map for a high shear granulator Tu et al. (2009), also proposed a regime map for a co-rotating TSG. The studied parameters were  $L/S$  ratio, screw speed and screw configuration. Hereby, reduction in screw speed led to an increased fill level of the TSG barrel which showed a direct correlation with an increase of frictional force and torque. Similarly, an increase in the  $L/S$  ratio correlated with a high fill level and torque. Depending on the screw configuration three regimes were suggested: granulation, extrudate and blocked regime. Granules with a large size and narrow granule size distribution (GSD) were obtained for increased binder addition and screw speed and using a screw configuration that provided sufficient mixing Tu et al. (2013). However, unlike dimensionless numbers used

in all the previous work on development and parameters with intensive property used by Dhenge et al. Dhenge et al. (2012b, 2013), the regime map by Tu et al. Tu et al. (2013) used scale-dependent parameters, such as screw speed and torque, for the development of this regime map. This further extends the current limitation of regime maps from uncomprehended regime boundaries for a range of materials to their inapplicability in explaining a TSG process with a different screw diameter, which does not operate under similar operational conditions. Also, a bi-modal GSD was obtained for several runs reported in this study. Thus, using only the mean granule size is not valid for granule size characterisation in many of the reported experimental conditions. The regime maps proposed by Dhenge et al. Dhenge et al. (2012b, 2013) and Tu et al. Tu et al. (2013) also indicated that a significant effort is still needed to identify the controlling parameters of twin-screw granulation at different process and equipment settings in order to propose a granulation regime map.

In the current study, the effect of four input variables (screw configurations (1×6 and 2×6 kneading discs), liquid-to-solid ratio (8-10 %), powder feed rate (10-25 kg/h), and screw speed (500-900 rpm)) on the GSD was evaluated. Afterwards, GSD results were used for mapping of granulation regimes during changes in process parameters. Scale-independent parameters (SME, L/S) were chosen to expand the applicability to multiple scales of TSGs.

## 9.2 Materials and methods

### 9.2.1 Pharmaceutical model formulation and twin screw granulation

$\alpha$ -lactose monohydrate (Pharmatose 200M, DFE-Pharma, Caldic, Hemiksem, Belgium) was used as a model excipient and PVP (Kollidon<sup>TM</sup>30, BASF, Ludwigshafen, Germany) was used as a binder. An aqueous PVP solution (2.5 %, w/w) was used as granulation liquid. Granulation experiments were performed using a 25 mm diameter co-rotating twin screw granulator, the granulation module of the ConsiGma-25 unit (GEA Pharma Systems, Collette<sup>TM</sup>, Wommelgem, Belgium) (See Chapter 3, section 3.1 for granulator details).

### 9.2.2 Experimental design

The experimental range for the performed screening design was determined by carrying out preliminary tests. The studied process variables include powder

feed rate (10, 17.5, 25 kg/h), liquid addition (8, 9 and 10 %), screw configuration (1×6 and 2×6 kneading discs) and screw speed (500, 700 and 900 rpm). Granules were collected at the outlet of the TSG and oven dried for 24 h at 40 °C. A full-factorial experimental design, with 54 experiments, was used to evaluate the influence of the different process variables upon the granulation process and the GSD. The experimental data were fitted using the most appropriate multiple linear regression (MLR) model (using Modde 9.0 software by Umetrics, Umeå, Sweden) Eriksson (2008). 4D Contour plots were made to display the responses for the four varying factors simultaneously.

### 9.2.3 Determination of torque and specific mechanical energy

To evaluate the granulation process, the torque on the screws at the work segment was recorded (1s interval). After steady-state was reached, the torque values were averaged. These represent the energy required to rotate the screws in the barrel, and represent the frictional forces on the material during processing. The SME, which is a scale-independent measure of energy introduced to the system during the granulation process, was calculated as follows

$$\text{SME (kJ/kg)} = \text{motor rating} \times \% \text{ torque} \times \frac{\text{RPM}_{\text{oper}}}{\text{RPM}_{\text{max}}} \times \frac{\text{gearbox efficiency}}{\text{material throughput}} \quad (9.1)$$

where the TSG had a motor rating (MR) of 2.2 kW and a maximum screw speed,  $\text{RPM}_{\text{max}}$  of 1000 RPM. The operational screw speed,  $\text{RPM}_{\text{oper}}$  and material throughput (kg/h) varied based on the processing setting. The gearbox of a TSG transmits energy from the motor to the screws, and is hence critical for achieving the desired screw speed and energy input. Based on the technical specification of the granulator drive (POSITWIN, Brevini Power Transmission), the gearbox efficiency is set at 0.98 (PIV Drives GmbH, 2014).

### 9.2.4 Particle size analysis

For each experiment, the GSD was determined using the sieve analysis method (Retsch VE 1000 sieve shaker, Haan, Germany). Granule samples (100 g) were placed on a shaker for 5 min at an amplitude of 2 mm using a series of sieves (150, 250, 500, 710, 1000, 1400 and 2000  $\mu\text{m}$ ). The amount of granules retained on each sieve was determined. All granule batches were measured in triplicate. The fractions <150, 150-1400 and >1400  $\mu\text{m}$  were defined as the amount of fines, useful fraction for tableting or yield fraction and oversized fraction, respectively. Also, three quartile values ( $D_{25}$ ,  $D_{50}$  and  $D_{75}$ ), corresponding to the 25, 50 and 75 percentiles respectively of the obtained GSD were calculated to build

the regime map. The width of the GSD was measured as percentile ratio, a relative measure of the distribution width ( $D_{75}/D_{25}$ ). The percentile ratio value approaches unity as the distribution becomes narrower.

## 9.2.5 Spatial interpolation and verification

The 'natural neighbour interpolation' method based on Delaunay triangulation was used for the spatial interpolation in the granulation regime map Sibson (1981). This has advantages over simpler methods of interpolation (such as nearest-neighbour interpolation), as it provides a smoother approximation to the underlying function. The basic equation in 2D is given as:

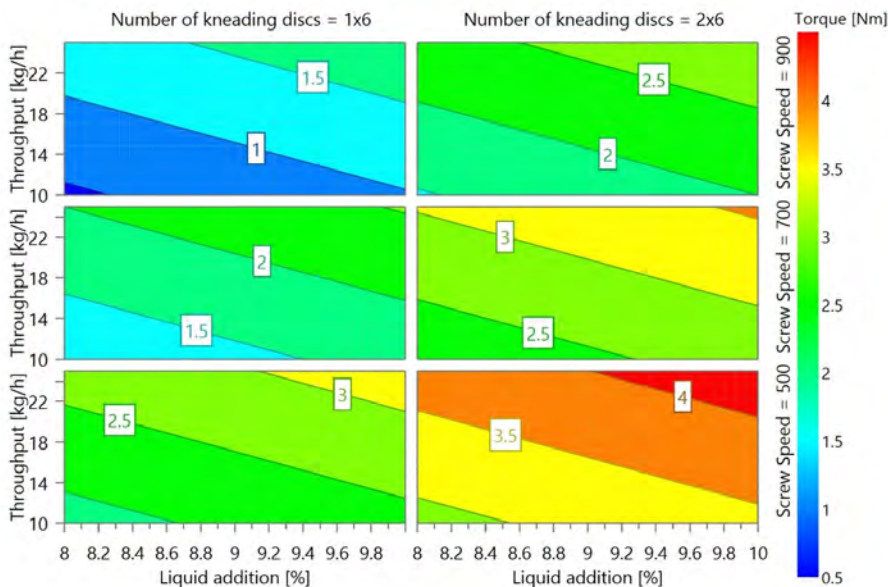
$$G(x, y) = \sum_{i=1}^n w_i f(x_i, y_i) \quad (9.2)$$

where  $G(x, y)$  is the estimate for the (L/S, SME) ranges,  $w_i$  are the weights and  $f(x_i, y_i)$  are the known granule size values at  $L/S_i, SME_i$ . The weights,  $w_i$ , were calculated by finding how much of each of the surrounding areas is taken when inserting  $(x, y)$  into the tessellation. To assess the accuracy of the interpolation, 14 measured points were removed from the known input (total 54 points), and the regime map was re-created using the remaining points. The root mean square error (RMSE) of the predicted values in the regime map with the removed measured points and the actual values was calculated and normalised to quantify the accuracy.

## 9.3 Results and discussion

### 9.3.1 Effect on torque

The highest torque values were obtained at maximal fill ratio of the barrel (i.e., low screw speed and high throughput) together with the highest restriction to the material flow by using the  $2 \times 6$  configuration (Figure 9.2). Low screw speed led to low conveying rate, whereas high material throughput resulted in high load on the screws. Furthermore, increased L/S ratio was causing sluggish flow of the material and using a second kneading block on the granulator screws resulted in a high restriction to the material flow. On the other hand, the torque level dropped when the screw speed was increased or when either throughput or L/S was reduced.



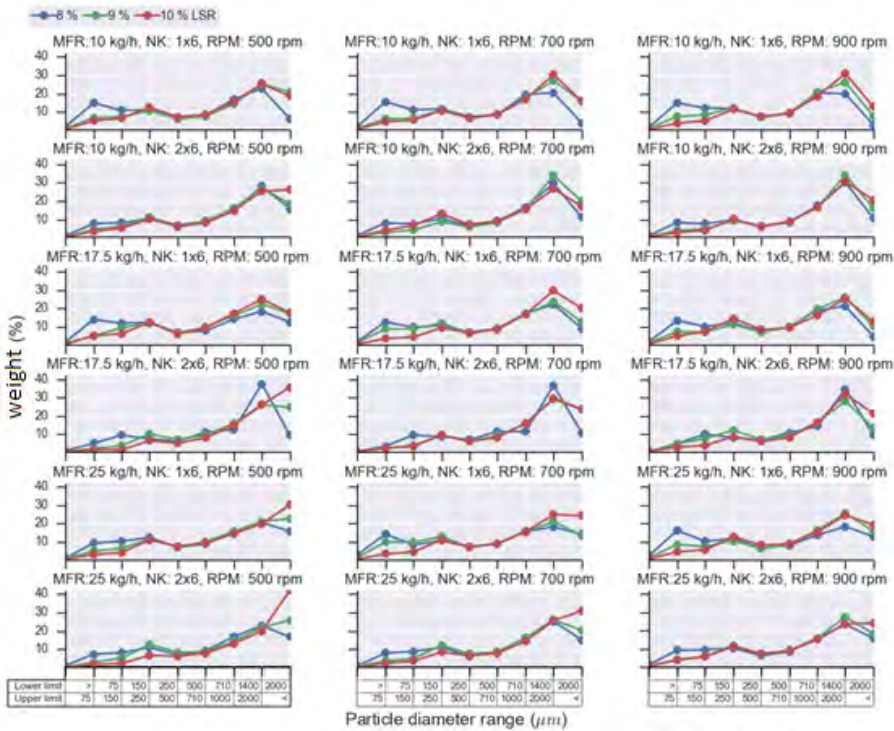
**Figure 9.2:** Change in the torque level at different screw speeds (500, 700, 900 rpm), material throughputs (10-25 kg/h), number of kneading discs (1×6, 2×6) and stagger angle (60°) during twin-screw granulation.

### 9.3.2 Effect on granule size distribution

An increase in L/S ratio caused reduction in fines and an increase in the oversized fraction (Figure 9.3). The effect of changing L/S ratio on GSD was most evident for the runs performed at low screw speed. However, the yield fraction was least affected by the additional granulation liquid (i.e., at high L/S). Hence, other process parameters play a critical role in increasing the yield fraction. A brief analysis of the effect of various process parameters under study on each size fraction is presented below.

#### Effect on fines

A higher amount of fines was produced by using the screw configuration with 1×6 kneading discs (Figure 9.4). Furthermore, at increased L/S ratio as well as at increased throughput a reduction in the amount of fines was obtained. For the screw configuration with 2×6 kneading discs the amount of fines mostly remained at a low level due to better mixing of powder and granulation liquid. An increase in screw speed from 500 to 900 rpm caused an increase in fines at low L/S ratio due to attrition of bigger granules caused by the higher impact of the screws at high screw speed. This occurred together with an increased weakness

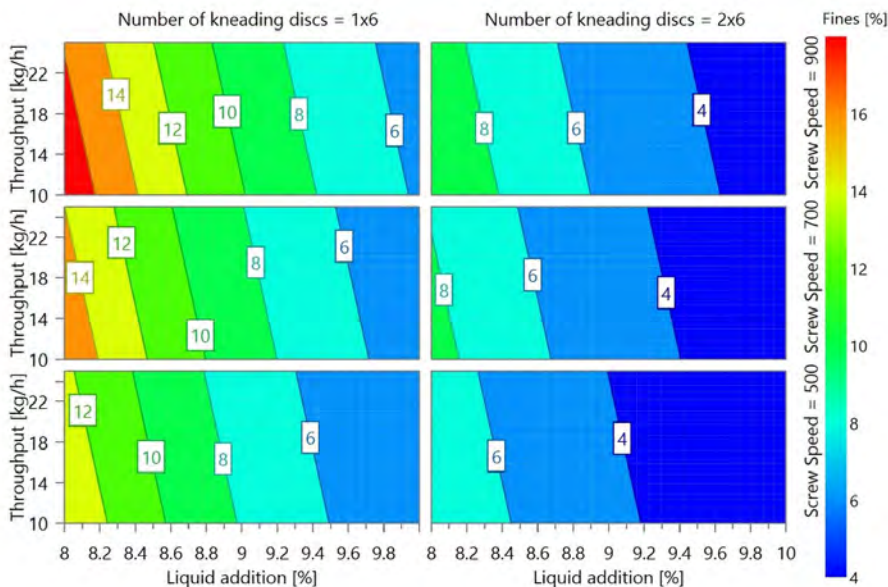


**Figure 9.3:** GSD at different screw speeds (500, 700, 900 rpm), material throughputs (10-25 kg/h), number of kneading discs (1×6, 2×6), stagger angle (60°) and liquid-to-solid ratio (8-10 %) [MFR: material throughput (kg/h), NK: number of kneading discs (-), RPM: screw speed (rpm), liquid-to-solid ratio [LSR]].

of the granules because of their low liquid content. Furthermore, if fines are created they will not stick to other granules because of lack of granulation liquid at the surface of these granules. In contrast, fines that are created at high L/S ratio can still be captured again because of the presence of granulation liquid at the surface.

### Effect on yield fraction

The yield fraction of the granules remained low despite higher mechanical shear caused by the additional kneading block present in the screw configuration with 2×6 kneading discs. However, an increase in the yield fraction was observed by the increasing screw speed for both screw configurations suggesting that along with good mixing, shear breaking of bigger lumps is desirable for a higher yield fraction. Beside a lower amount of fines, an increase in L/S ratio also reduced



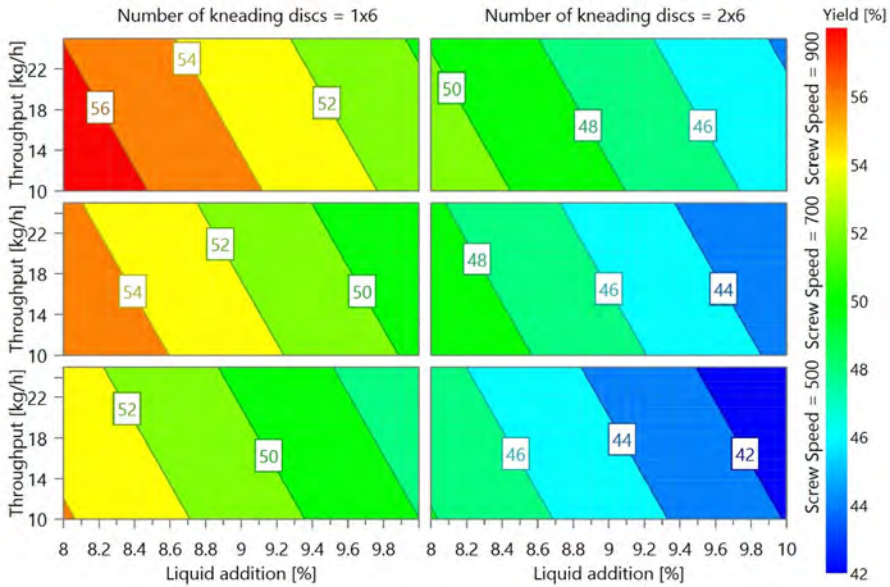
**Figure 9.4:** Change in fines fraction ( $<150 \mu\text{m}$ ) in the granules produced at different screw speeds (500, 700, 900 rpm), material throughputs (10-25 kg/h), number of kneading discs ( $1\times 6$ ,  $2\times 6$ ) and stagger angle ( $60^\circ$ ).

the yield fraction. This indicates that additional granulation liquid directly contributed to formation of oversized granules. Therefore, the basic granulation mechanism of growth by nucleation followed by aggregation as observed in high-shear mixers is not the primary mechanism of the twin-screw granulation to control the yield. Breakage of oversized lumps is required to achieve a high yield inside a TSG. Additionally, when the screw speed was low, an increase in L/S ratio showed only a minor influence on the yield fraction (causing less mixing between the powder and the granulation liquid) for both the screw configurations despite a change in the material throughput. An increase in throughput otherwise caused a reduction in yield fraction. This was again due to inferior mixing at high fill ratio. An increase in screw speed lowered the fill ratio due to higher conveying rate, and thus increased the yield fraction.

### Effect on oversized fraction

Although twin-screw granulation always resulted in a large fraction of oversized granules, increasing the L/S ratio, i.e., adding more granulation liquid, contributed most to the formation of the oversized granule fraction (Figure 9.6). When a restriction to the material flow was introduced by the additional kneading block in the screw configuration with  $2\times 6$  kneading discs combined with



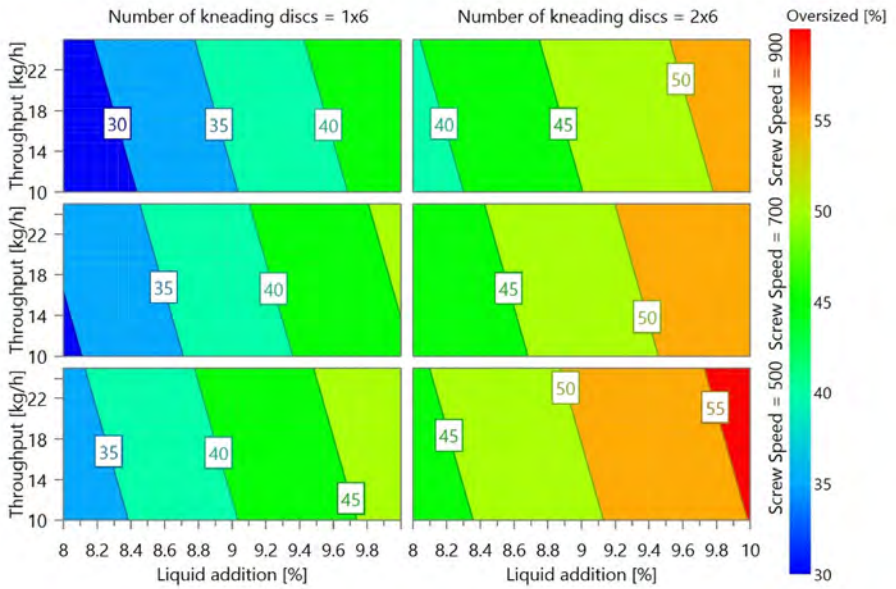


**Figure 9.5:** Change in yield fraction (150 - 1400  $\mu\text{m}$ ) in the granules produced at different screw speeds (500, 700, 900 rpm), material throughputs (10-25 kg/h), number of kneading discs (1x6, 2x6) and stagger angle (60°).

a high amount of granulation liquid, more oversized granules were obtained. However, an increase in the screw speed decreased the amount of oversized granules produced to a certain extent. This was due to a reduction in the fill ratio and an improved shear mixing of the formulation mixture and the granulation liquid. For the same reason, an increase in throughput causing a high fill ratio yielded an increased oversized fraction in the produced granules.

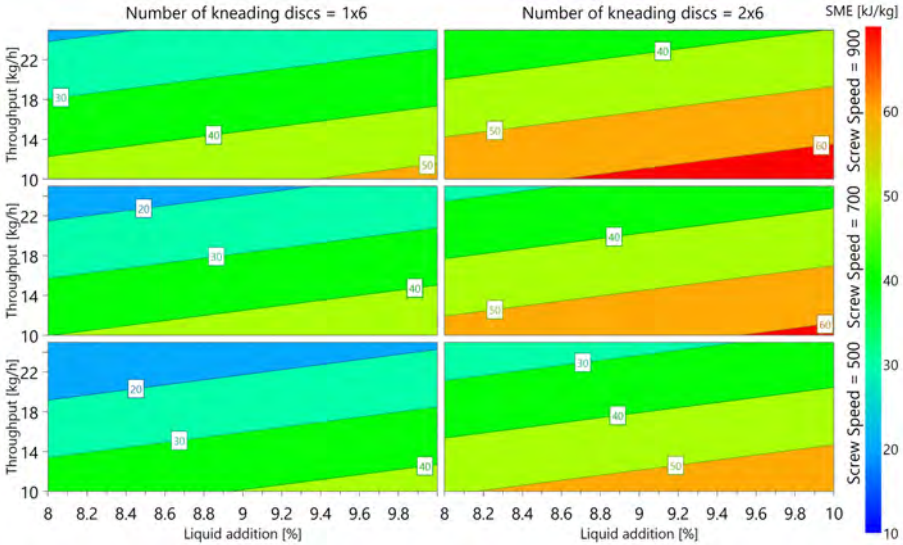
### 9.3.3 Effect on SME level

The SME is a direct measure of the amount of power being introduced by the motor into each kilogram of material being processed inside the TSG. A gradual increase in screw speed led to a gradual increase in the SME level (Figure 9.7). However, for fixed process settings (screw speed and throughput), the change in screw configuration caused major changes in the SME levels such that their range for the screw with 2x6 kneading discs was much higher than for the 1x6 kneading discs screw configuration. Beside screw configuration and speed, other process parameters such as material throughput and L/S ratio also affected the SME level. An increase in the material throughput resulted lowering of SME input whereas an increase in L/S ratio contributed to the restriction to the



**Figure 9.6:** Change in oversized fraction ( $>1400\ \mu\text{m}$ ) in the granules produced at different screw speeds (500, 700, 900 rpm), material throughputs (10-25 kg/h), number of kneading discs ( $1\times 6$ ,  $2\times 6$ ) and stagger angle ( $60^\circ$ ).

material flow inside the granulator, hence changing the load on the screws and energy input to the material. Due to these encompassing characteristics of the SME it was used along with L/S ratio to characterize the granulation regime in the TSG in the next section.

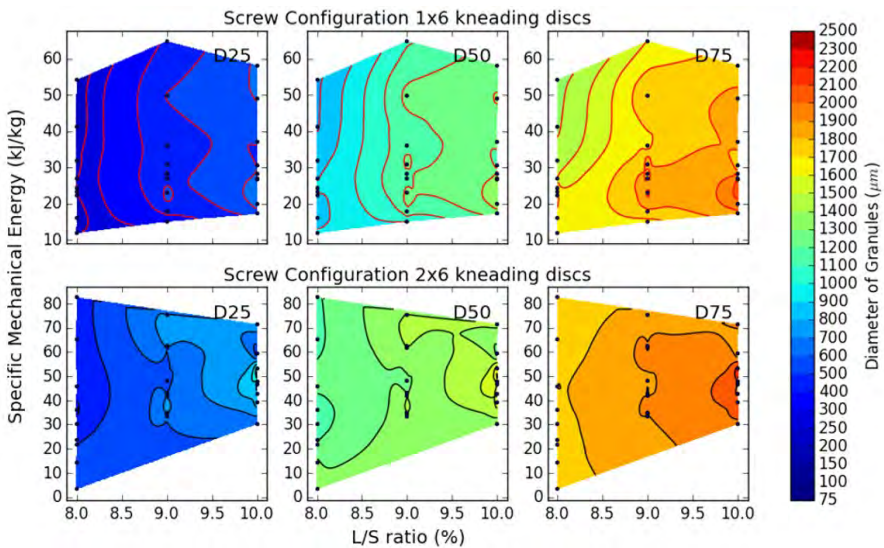


**Figure 9.7:** Change in specific mechanical energy input level at different screw speeds (500, 700, 900 rpm), material throughputs (10-25 kg/h), number of kneading discs (1×6, 2×6) and stagger angle (60°) during twin-screw granulation.

### 9.3.4 Regime map based on GSD, L/S and SME

The regime maps for the  $D_{25}$ ,  $D_{50}$  and  $D_{75}$  for 1×6 and 2×6 screw configurations are shown in Figure 9.8. The accuracy of the interpolated map was tested and the normalised RMSD for the  $D_{25}$ ,  $D_{50}$  and  $D_{75}$  regime map of the 1×6 screw configuration was found to be 3.36, 1.83 and 0.48, respectively. The normalised RMSD for the  $D_{25}$ ,  $D_{50}$  and  $D_{75}$  regime map of the 2×6 screw configuration was found to be 3.05, 1.30 and 0.07, respectively. The effect of changes in L/S ratio and SME inputs on GSD is given in this regime map. Both are scale-independent parameters and expand the applicability of the results to multiple scales of the TSG (i.e. different screw diameter). The  $D_{25}$  values ranged from 300 to 600  $\mu\text{m}$  in case of the 1×6 screw configuration for all SME and L/S ratio levels. However, when additional kneading discs were used (2×6) leading to better mixing, a high SME input and L/S ratio caused a further increase in the  $D_{25}$  value (up to 900  $\mu\text{m}$ ). This indicates that besides increased liquid and energy

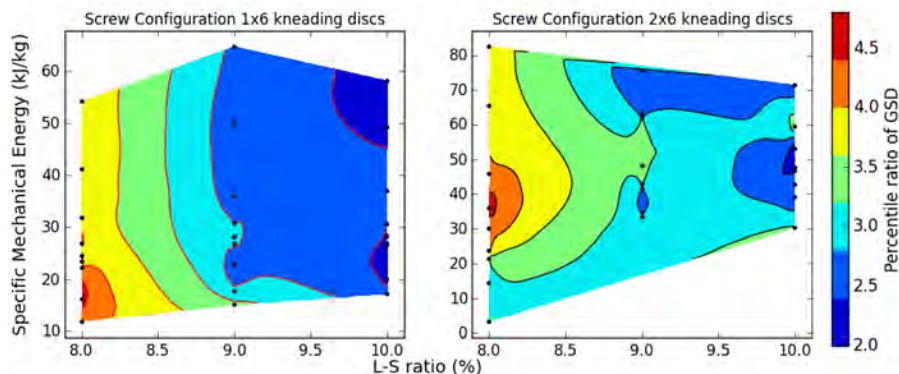
input, the screw configuration is important in reducing the amount of fines during granulation. The maps for  $D_{50}$  indicate the central tendency of the GSD during changes in the twin-screw granulation process parameters. These maps indicate that for the intermediate ranges of L/S ratio (8.5 - 9.5 %) and the SME input (4-10 kJ/kg), the central tendency of the GSD remained similar. The  $2\times 6$  screw configuration led to bigger granules and thus higher  $D_{75}$  values for all levels of SME and L/S ratio, compared to the  $1\times 6$  configuration. For the latter,  $D_{75}$  values corresponded with the oversized fraction ( $> 1400 \mu\text{m}$ ) at medium to high L/S ratio and at increased SME input. However, an increase in SME at low L/S ratio caused a reduction in  $D_{75}$  values towards the yield fraction size range (150-1400  $\mu\text{m}$ ). At 10 % liquid addition, a minimum of 520  $\mu\text{m}$  in the  $D_{25}$  plot and a maximum of 2200  $\mu\text{m}$  in the  $D_{75}$  plot was observed. Such a width in granule size indicates that it is better to use a lower liquid addition. In this regard, 8 to 9 % liquid addition was most optimum, with the particle size ranging from 370-1800 and 490- 2010  $\mu\text{m}$  respectively.



**Figure 9.8:** Regime map indicating change in percentile values ( $D_{25}$ ,  $D_{50}$ ,  $D_{75}$ ) of the granule size distribution with change in L/S ratio and specific mechanical energy input.

As indicated in Figure 9.8, a higher L/S ratio contributed to the formation of oversized granules instead of increasing the yield. Therefore, measurement of the width of the size distribution is critical to understand the regime supporting an increase of the yield fraction. The percentile ratio map for both screw configurations ( $1\times 6$  and  $2\times 6$ ) indicated that the percentile ratio reduced at higher L/S ratio (Figure 9.9). Except for a high L/S ratio, the width of the

distribution (percentile ratio) also reduced with an increase in the SME level, indicating that shear-driven and energy intensive granulation mechanisms such as attrition and breakage play a major role in twin-screw granulation.

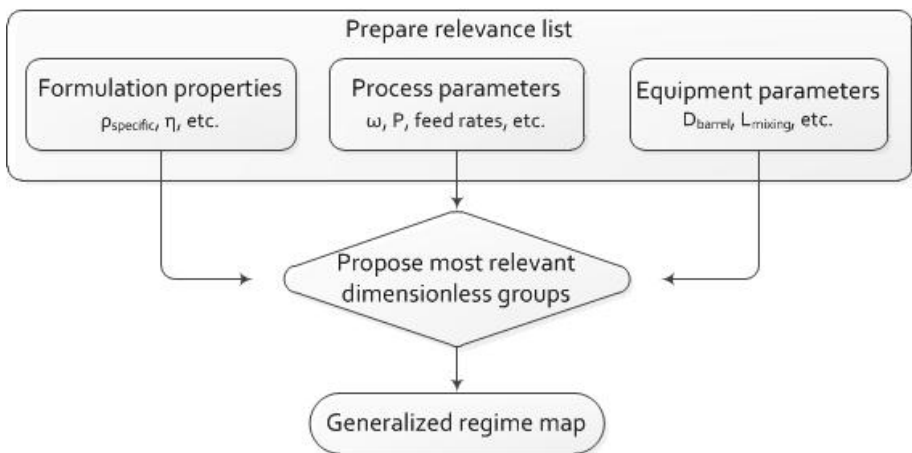


**Figure 9.9:** Change in the percentile ratio ( $D_{75}/D_{25}$ ) of granule size distribution with change in L/S ratio and specific mechanical energy input.

Based on these results, it is clear that the throughput and screw speed should be increased simultaneously to further improve the granulation yield results. By this, a favourable fill level can be achieved and the torque values are also at an optimum level, thus creating the desired level of energy input to the TSG. The liquid addition should be kept at an intermediate level as a low liquid addition produces a low amount of usable granules whereas higher L/S ratio causes higher torque values. The regime map can be used as a guidance for process optimization or up-scaling of new formulations. Despite the scale-independence of parameters (SME, L/S ratio) expanding the applicability to multiple scales of TSGs, more regime maps for other formulations are necessary due to the likely differences in the granulation behaviour of different excipients. Furthermore, other process variables, such as stagger angle between kneading discs in the screw could be investigated. In order to improve the understanding of the granulation process and the regime map, process knowledge should be further developed both under steady state and dynamic conditions. For this purpose, application of mechanistic models incorporating the underlying mechanisms in the model framework is suggested. A validated model thus obtained can potentially be used to define the design space of the process for the future optimization of the twin-screw granulation process.

## 9.4 Future development: from process map to regime map

The present process map can be used as a guidance for process optimization or scale-up of new formulations. However, additional experiments on a large scale granulator should be performed to verify the scale-independency of the developed process map. Moreover, the formulation properties and operating variables that control wet granulation behaviour in a TSG are strongly coupled as evidenced by different results obtained from various studies performed at different process conditions. Despite the scale-independence of parameters (SME, L/S ratio), more process maps for formulations with significantly different raw material properties are necessary due to their likely differences in the granulation behaviour. While these process maps will progress our understanding regarding the mechanisms that control granule attributes, for a reliable and more generalised regime map the most relevant dimensionally homogeneous terms, i.e. dimensionless groups should be identified (Fig. 9.10). This is done by preparation of a "relevance-list" which contains parameters originating from formulation, equipment and process. For details regarding such an approach the reader is referred to Zlokarnik (2011).



**Figure 9.10:** Step required to develop a generalised granulation regime map for twin-screw granulation

Additionally, in order to improve the understanding of the wet granulation process using TSG, process knowledge should be further developed both under steady state and dynamic conditions. For this purpose, application of mechanistic models incorporating the underlying mechanisms in the model framework is suggested Iveson et al. (2001a). A validated model thus obtained can potentially

be used to define the design space of the process for the future optimization of the twin-screw granulation process.

## 9.5 Conclusions

In this study, development of a scale-independent wet granulation process map was presented. This granulation process map revealed that, although increasing the liquid-to-solid ratio strongly drives the granule size distribution of the product towards a large mean granule size, by increasing the energy input to the granulator the mean granule size can be effectively lowered and also the size distribution can be narrowed. Building such process maps for a range of formulations, the most relevant granulation mechanisms and dimensionless groups should be identified to propose a generalised regime map in the future. With the aim of further process knowledge buildup, the GSD evolution along the length of the screws inside the TSG should be experimentally and theoretically mapped in order to understand the dominant constitutive mechanisms (such as growth, aggregation and breakage) of a twin-screw granulation system.

---

## Micro-scale modelling of wet granulation in a twin-screw granulator

---

**Extended from:** Ashish Kumar, Stefan Radl, Johannes G. Khinast, Krist V. Gernaey, Thomas De Beer, Ingmar Nopens, Detailed simulation of particle and liquid distribution in the mixing zone of a twin-screw granulator, In: AIChE annual meeting 2015.

### Summary

Solid-liquid mixing in high shear wet granulation (HSWG) in a twin-screw granulator (TSG) is difficult to understand experimentally due to opacity of the multi-phase system and very fast dynamics (typically few seconds). In this study, discrete element method (DEM) based simulations of a short quasi-two-dimensional simulation domain are performed, incorporating models for liquid bridge formation, rupture, as well as the effect of the bridges on inter-particle forces. Based on the knowledge gained from these simulations, the time evolution of particle flow and liquid distribution in the kneading section of a twin-screw wet granulation process was simulated. The study showed that agglomeration is a rather delayed process which takes place once the excess liquid from the particle surface is transferred to the primary liquid bridges which re-distribute the liquid to make more liquid bridges and hence granules. Moreover, the transfer of liquid from the particle surface to capillary bridges which resulted in initialisation of agglomeration was observed to be most dominant in the intermeshing region of the mixing region of the TSG.



## 10.1 Introduction

An accurate description of aggregation and breakage processes are of wide interest in the field of HSWG. This interest is fuelled by the need of rational process design, i.e., the production of granules with the desired quality and maximum yield. Many mechanistic models in the frame of so-called population balance models (PBMs) have been developed to describe the aggregation and breakage rates (see section 2.2.1 of Chapter 2). However, these expressions involve rate terms, referred to as *rate kernels*, which often require the specification of different material properties, such as wetness, porosity and yield strength. Typically, the PBMs require closures for (i) collision rates, (ii) particle collision velocities, or data on other particle-scale phenomena. Additionally, material fluxes (i.e., the axial and radial velocities) need to be described for an accurate dynamic simulation of the mixing process. Unfortunately, this particle-scale information, known to be dependent on process parameters, equipment geometry, or material properties cannot be directly computed. Hence, a common strategy is to calibrate these unknown parameters, required in the rate kernels, using experimental data (for details see Chapter 8). However, despite calibration, such models have limited applicability due to the lack of predictive capabilities outside of their experimental domain (Barrasso et al., 2015a). This is unsatisfactory, especially in case one aims at using the model for process optimization, or to design a different granulator geometry on this basis.

In contrast, DEM is a micro-scale framework that tracks individual particles, or granules, as they move through space and time. This highly-accurate physical modeling tool can provide details on the flow of particles or granules (section 2.2.1 of Chapter 2). This information, e.g., collision rates and velocity profiles, can then be fed into the rate kernels, incorporating effects due to current process parameters, the equipment geometry, and material properties. Based on the level of detail put into a DEM-based simulation, this can further be classified as (i) a particle-scale or (ii) a granule-scale simulation, serving different applications.

The "particle-scale" simulations can be used for the direct investigation of mixing phenomena on the individual particle level, including for example liquid bridges. Thus each particle (and liquid bridge if desired) is tracked and treated as separate entity. Previous attempts of particle-scale simulations include the work of Lian et al. (1998) and McCarthy (2003). However, the result of the tracking of each particle is also that simulations become considerably more computationally expensive compared to the granule-scale DEM-based simulations as a large number of entities (i.e., particles) have to be tracked.

DEM-based simulations that track individual granules (i.e., ensembles of particles) are frequently used (Sen et al., 2012b; Barrasso et al., 2015b,a). This type of simulations are referred to as "granule-scale", since phenomena on the scale of the granules, typically with a size of 100 to 1,000  $\mu\text{m}$ , can be predicted. The advantage of these simulations is that a comparably small number of entities (i.e., granules) has to be tracked, and granules are allowed to break or aggregate. This opens the door for investigating the effect of the actual geometry of a TSG. Moreover, variations in granule properties, such as porosity and liquid content, are often accounted for in this type of DEM simulations using empirical correlations, e.g., the coefficient of restitution or Young's modulus (Sarkar and Wassgren, 2009). Closures for mechanisms such as aggregation, breakage and consolidation, which cause changes in particle size and other properties, need to be provided in granule-scale DEM simulations. Therefore, often a multi-scale approach is suggested where DEM data is collected and used within a PBM by either one-directional or bidirectional coupling (Cameron and Wang, 2009). Most of the multi-scale studies, such as Gantt et al. (2006) used one-directional coupling of DEM with PBM to evaluate mechanistic aggregation kernels. Goldschmidt et al. (2003) used DEM simulations to solve a PBM for fluidised bed spray granulation, replacing small particles with larger ones as they successfully aggregate. Bouffard et al. (2012) used DEM results to evaluate a spatial transfer in a compartmental PBM. Sen et al. (2012b) have used DEM to complete the compartmental model, using flux data from DEM simulations as input to the PBM. Additionally, Reinhold and Briesen (2012) developed a coupled PBM-DEM model for wet granulation, using DEM simulations to evaluate a mechanistic aggregation rate kernel. Recently, Barrasso et al. (2015b) implemented bi-directional coupling between PBM and DEM to evaluate collision frequencies and liquid distribution as a proof-of-concept, and Sen et al. (2014) combined this work with a computational fluid dynamics model to simulate fluidized bed granulation. Furthermore, Barrasso et al. (2015a) applied bi-directional coupling between particle scale DEM and PBM in case of a twin-screw wet granulation process. The model showed sensitivities to the screw configuration, process parameters such as screw speed, liquid-to-solid ratio as well as material properties such as binder viscosity and pore saturation. However, this bi-directional coupling of a PBM-DEM model for wet granulation depends on the assumption that liquid is distributed evenly with respect to particle volume, which is not the case as shown experimentally by Vercruyssen et al. (2013b). In fact, achieving a homogeneous distribution of liquid which largely controls the constitutive mechanisms of the twin-screw granulation is the primary requirement for driving the granulation process towards the required state. Therefore, investigating the drivers for particle and liquid mixing in TSG

is key to the understanding of the twin-screw wet granulation process.

In this chapter, in order to investigate the particle and liquid mixing in the mixing zones of a TSG, the focus of the simulations was to first track individual particles in a short quasi-two-dimensional simulation domain, incorporating models for liquid bridge formation, rupture, as well as the effect of the bridges on inter-particle forces. Subsequently, the same simulation approach was applied to the mixing zone of the TSG and the effect of process parameters on particle and liquid mixing rate was investigated.

## 10.2 Particle scale modelling approach

### 10.2.1 Particle flow model

Computer simulations using the discrete element method were performed using the software package LIGGGHTS (Kloss et al., 2012). In a dense particle system forces acting on a particle can be decomposed into body force  $F_i^b$  of a particle  $i$  and contact force  $F_{ij}^{con}$  and cohesion force  $F_{ij}^{coh}$  between particles  $i$  and  $j$ . The interaction of the granular flow with the surrounding air has been neglected in this work due to the high particle fill ratio. The so-called soft-sphere method, in which collisions are modeled as enduring contacts, was used. The overlap between particles over a few time steps is used to model the deformation of the particles and the contact forces are a function of these overlaps (further details on this were already given in section 2.2.1 of Chapter 2).

A linear spring dashpot model was used to model normal and tangential contact forces between particles (Cundall and Strack, 1979). Based on these forces, the trajectories of individual particles were computed using Newton's equation of translational and rotational motions. Thus, the force acting on particle  $i$ , from particle  $j$  can be decomposed into a normal component  $\mathbf{F}_i^{c,n}$  and a tangential component  $\mathbf{F}_i^{c,t}$ , which are given by:

$$\mathbf{F}_i^{c,n} = k_n \delta \mathbf{n}_{ij} - \eta_n \mathbf{v}_{ij}^n \quad (10.1)$$

$$\mathbf{F}_i^{c,t} = -k_t \mathbf{u}_{ij}^t - \eta_t \mathbf{v}_{ij}^t \quad (10.2)$$

where,  $\mathbf{u}_{ij}^t$  is the tangential overlap and  $\delta$  is the normal overlap between particles  $i$  and  $j$ :

$$\delta = r_i + r_j - |\mathbf{r}_i^* + \mathbf{r}_j^*| \quad (10.3)$$

Considering Newton's third law, particle  $j$  experiences the same force as particle

$i$  but in the opposite direction. The characteristic contact time  $t_c$  is given by

$$t_c = \pi/\omega \quad (10.4)$$

where,

$$\omega = \sqrt{k_n/m_{\text{eff}} - \eta_n^2/(4m_{\text{eff}}^2)} \quad (10.5)$$

This contact time sets the time step  $\Delta t$  for the integration of Newton's equation of motion. The restitution coefficient  $e_n$  which is the ratio of relative velocities of the particle after and before collision (Luding, 1998), can be approximated for low value of  $e_n$  as:

$$e_n = \exp\left(\frac{-\pi\eta_n}{m_{\text{eff}}\sqrt{4k_n/m_{\text{eff}} - \eta_n^2/m_{\text{eff}}^2}}\right) \quad (10.6)$$

## 10.2.2 Liquid bridge model

When the granulation liquid, i.e. the liquid phase, is added to a dry mass of powder particles in the TSG, the surface of the particles is wetted and the liquid on particle surface is distributed between the particles in contact. Liquid distribution in the moving dense particle system progresses due to liquid transfer both by particle–particle collisions and convective transport caused by the particle motion induced by the throughput force of incoming material and the drag force of the rotating screws. Depending on the ratio between solid and liquid volume, different wetting states are achieved as shown in Table A.1 of Appendix A. The cohesive forces between the wetted particles strongly depend on the exact shape of the liquid bridge and the pressure difference between the gas and liquid phase. The stability of a liquid bridge between two particles and its rupture thus mechanistically dictates the macroscopic granulation status. For simulating cohesive forces the capillary force model by Mikami et al. (1998) was used. In case of bridge formation, model C considering the stretching and rupture of the bridge was used for liquid tracking (Mohan et al., 2014). In this model, when wet particles touch each other, a certain fraction of the liquid on the particle surface  $\phi_{tr}$  was exchanged at a finite rate  $Q_{tr}$  calculated as

$$Q_{tr,i} = -\frac{c_f}{t_{\text{ref}}}(L_{p,0}\phi_{tr} - V_b) \quad (10.7)$$

where,  $c_f$  is a dimensionless filling rate coefficient and  $t_{\text{ref}}$  is the reference liquid bridge filling time calculated as

$$t_{\text{ref}} = \frac{r_{\text{eff}}\mu_l}{\sigma_l}, \text{ where } r_{\text{eff}} = \frac{2r_i r_j}{(r_i + r_j)^2} \quad (10.8)$$

and,

$$\phi_{tr} = 1 - \sqrt{1 - \frac{r_j^2}{(r_i + r_j)^2}} \quad (10.9)$$

For a more detailed discussion regarding the liquid transfer model the reader is referred to the study by Mohan et al. (2014).

### Liquid loading, bridge volume fraction & liquid bridge coordination number

In a granulator, liquid is added to a specific region of the granulator and it is later distributed by the shear. The amount of liquid load on the particles present in the liquid addition region can be calculated as

$$Q_{lod} = \frac{Q_i}{n_{p,liq}} t_{exp} \quad (10.10)$$

At the steady state condition, the liquid bridge volume is given by

$$V_b = \frac{1}{2}(L_{pi} + L_{pj})\phi_{tr} \quad (10.11)$$

Thus, the fraction of liquid transferred from the total added liquid to the liquid bridge, i.e. the liquid bridge volume fraction was calculated as:

$$V_{bf} = \frac{\sum_{i=1}^{n_p} V_b}{\sum_{i=1}^{n_p} (V_{bi} + L_{pi})} \quad (10.12)$$

As the liquid tracking model accesses the per-particle liquid content, the number of liquid bridges and the number of particle-particle contacts at each time step was also tracked. This information can be used to compute a liquid bridge coordination number, i.e. the average number of liquid bridges per particle as:

$$\bar{Z}_b = \frac{2 \sum_{i=1}^{n_p} n_{b,i}}{n_p} \quad (10.13)$$

## 10.2.3 Simulation set-up and input parameters

### Simple shear flow condition

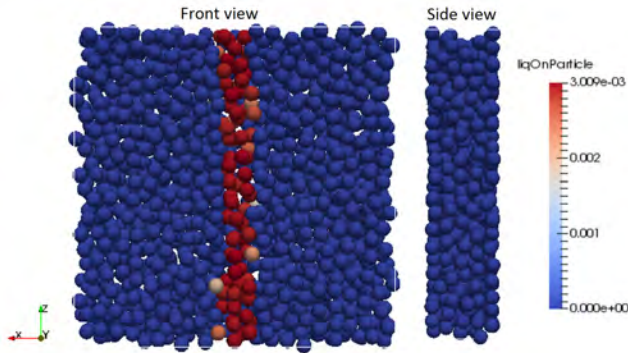
In order to investigate the solid-liquid mixing under well-controlled flow conditions, an assembly of about 1500 mono-disperse particles (the exact number changed based on the fill ratio) of diameter  $d_p$  and density  $\rho_p$  were placed in a periodic box of equal length and width ( $H/d_p = 20$ ) at particle volume fractions of 0.4 (Fig. 10.1). A homogeneous shear flow, with the shear gradient pointing

in the x-direction was applied using Lees–Edwards boundary conditions (Lees and Edwards, 1972). The y-direction was chosen to be the spanwise direction. In such a setup wall effects can be completely avoided since each point in the simulation domain is statistically identical. The dimensionless shear rate (eq. 10.14), which is defined as the ratio of a characteristic deformation time of the particles and a characteristic shearing time, was used to characterize the shearing rate:

$$\gamma^* = \gamma d_p^{3/2} / \sqrt{k_n / \rho_p} \quad (10.14)$$

For soft particles,  $\gamma^* > 10^{-1}$  (Chialvo et al., 2012), thus the simulations were carried out for a fixed  $\gamma^*$  of  $3.5 \times 10^{-3}$ .

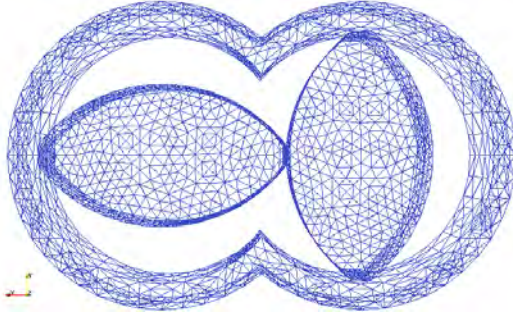
A gradient of liquid content on the particles was imposed in the central zone of  $2d_p$  width in the periodic box (unless stated otherwise), both in positive and negative y-directions (see Fig. 10.1). The liquid content of the particles in this zone was fixed, while keeping other particles initially dry (i.e., the liquid content on the particle and the bridge volume were set to zero). The liquid content on the particles was defined based on a dimensionless reference film thickness  $\epsilon = h_0 / r_{\text{eff}}$  where,  $h_0$  is proportional to the reference liquid content on the particles  $L_{p,0} = d_p^2 \pi h_0$ . A typical snapshot of such a simulation at initial condition  $t_0$  is presented in Fig. 10.1. Other simulation parameters are listed in Table 10.1. The experimentally measured applicable range for  $\alpha$ -lactose monohydrate particles were applied to assign values for mechanical properties, such as Young’s Modulus and Poisson ratio of the solid particles (Perkins et al., 2007) and properties of water were applied to assign values for physical properties like viscosity of the granulation liquid in the simulations.



**Figure 10.1:** Setup used for the simple shear simulation (front and side views; the red coloured particles indicate the wetting zone).

## Mixing zone of TSG

In order to investigate the mixing of granulation liquid and formulation powder in the mixing zone of the TSG, DEM simulations were performed using the approach discussed in section 10.2 and knowledge gained from the base case of the simple shear flow condition (section 10.2.3). A 3D CAD model for the kneading discs and barrel was created in SALOME based on the geometry of the screws which were used in the TSG of the ConsiGma-25 unit (GEA Pharma Systems, Collette™, Wommelgem, Belgium) (Fig. 10.2). The triangulated surface mesh (STL) was created using Gmesh. The screws were rotated at a fixed speed, and approximately 46000 mono-disperse particles of diameter  $d_p$  and density  $\rho_p$  were placed in the free space between the fixed-mesh of the barrel and the rotating-mesh of two kneading discs. Periodic boundary conditions were imposed in the axial direction of the mixing section, i.e. particles that exit the computational domain in this direction are re-inserted on the opposite side.



**Figure 10.2:** The 3D STL mesh for the kneading discs and barrel used for TSG mixing zone simulation.

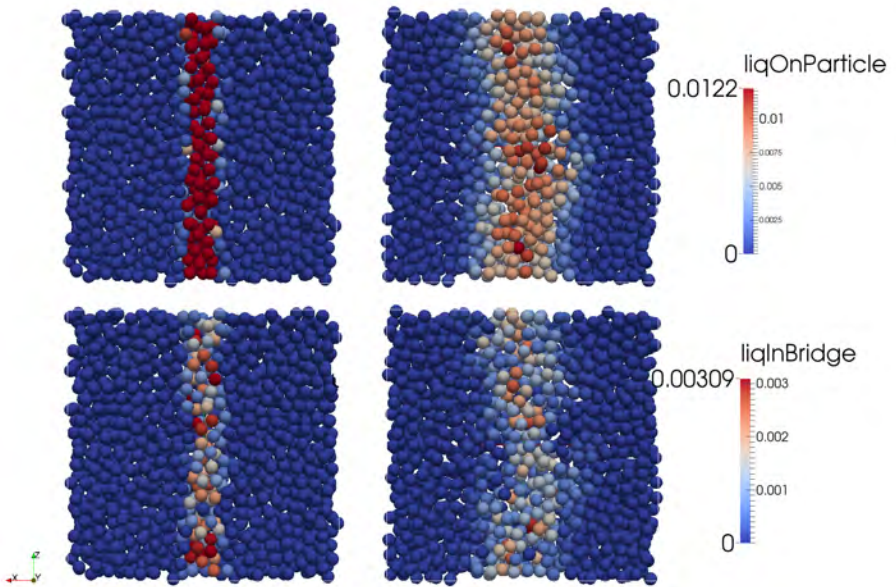
**Table 10.1:** Summary of input parameters used in particle-scale modelling.

Quantity	Symbol	Value	Unit
Particle diameter	$d_p$	$1.0 \times 10^{-4}$	[m]
Young's modulus	Y	$3.45 \times 10^9$	[N/m <sup>2</sup> ]
Initial particle velocity	$v_x, v_y$	1, 0.1	[m/s]
Coefficient of restitution	$e_n$	0.9	[-]
Coefficient of friction	$\mu$	0.1	[-]
Poisson ratio	$\nu$	0.45	[-]
Surface tension of liquid (water)	$\gamma_l$	0.001	[J/m <sup>2</sup> ]
Viscosity of liquid (water)	$\mu$	$8.90 \times 10^{-4}$	[kg/m.s]
Film thickness	$h_0/r_{\text{eff}}$	$1.0 \times 10^{-2}$	[-]
Dimensionless filling rate coefficient	$c_f$	1	[-]

## 10.3 Results and discussion

### 10.3.1 Solid-liquid mixing in a simple shear flow condition

The solid-liquid mixing in a dense particle system was first investigated by the DEM simulation for a sheared assembly of particles discussed in section 10.2.3. Shearing of particles resulted in convective transport of liquid between particles observed as liquid distribution as well as transfer of liquid from the particle surface to the liquid bridges which results in the formation of agglomerates (Fig. 10.3).



**Figure 10.3:** Transfer of liquid from particle surface (top left) to other particles by convective transport (top right) and transfer of liquid from particle surface to liquid bridges between particles by conductive transport before (bottom left) and after shearing (bottom right).

In order to investigate the effect of changes in the bulk density and fill ratio of the powder bed inside the granulator barrel by means of a simple shear flow simulation, the volume fraction of the particles was modified. To investigate the effect of liquid addition rate during granulation, the dimensionless liquid load on the particles  $Q_{lod}$  in the wetting zone was changed. The effect of liquid addition method at one point or two points which basically affects the width of the addition zone was investigated by changing the width of the wetting zone.



Response of all these investigations on mixing and granulation was recorded in terms of change in the average number of liquid bridges per particle  $\bar{Z}_b$  and the volume fraction of liquid in bridges  $V_{bf}$ . An increase in  $\bar{Z}_b$  indicates an increase in aggregation level. Normally, the trends for  $\bar{Z}_b$  and  $V_{bf}$  should follow the same pattern. However, a change in their relation indicates dominance of convective or conductive transport during wet granulation. Moreover, increase in the screw speed leads to increase in the shear level which was investigated by increasing the applied shear to the particle assembly in the shear box.

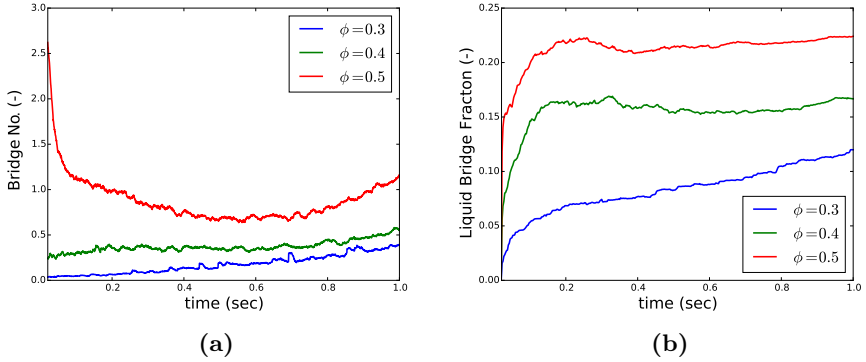
### **Effect of change in volume fraction of particles**

The filling ratio inside the TSG varies significantly due to changes in the screw speed, material throughput and flow restriction by the kneading elements. To understand the effect of a difference in fill ratio by the simple shear flow simulation the volume fraction of the particles was changed from 0.3 to 0.5. Increasing the fill ratio resulted in a larger number of particles in the wetting zone (Fig. 10.1). This directly resulted in more liquid bridges at a high fill ratio at the start of the simulation (Fig. 10.4a). However, as the shearing progressed  $\bar{Z}_b$  increased for conditions with lower volume fractions ( $\phi = 0.3, 0.4$ ) whereas for the high volume fraction ( $\phi = 0.5$ ) it first reduced and then equilibrated to finally gain some increase. The volume fraction of liquid in bridges  $V_{bf}$  also showed the same patterns where the liquid bridge fraction was higher for higher  $\phi$ , and it always remained so compared to the lower  $\phi$  despite shearing. However, while  $V_{bf}$  equilibrated as shearing progressed for a higher volume fraction ( $\phi = 0.4, 0.5$ ), it kept on increasing for a lower volume fraction ( $\phi = 0.3$ ). Additionally, at a high fill fraction, the  $\bar{Z}_b$  decreased by initial shearing, whereas  $V_{bf}$  increased. This indicates shear elongation, thus a larger amount of liquid in the capillary bridges followed by the breakage of these bridges.

The results indicate that at a high fill ratio the breakage mechanism dominates over agglomeration which results in redistribution of the liquid. However, at a low fill ratio agglomeration is the dominant mechanism in granulation. In order to keep both agglomeration and breakage as active mechanisms of granulation during simulation, in the remainder of this chapter  $\phi$  has been fixed to the intermediate level ( $\phi = 0.4$ ) unless stated otherwise.

### **Effect of change in liquid loading on particles**

In a granulator, the amount of liquid loaded on the first wetted particles in the wetting zone changes when the liquid addition rate or the fill fraction is changed. The shear mixing distributes these differently liquid-loaded particles to proceed to a certain granulation end-point. This was simulated by increasing the liquid



**Figure 10.4:** Changes in (a) average number of liquid bridges per particle  $\bar{Z}_b$  and (b) volume fraction of liquid in bridges  $V_{bf}$  when the particle volume fraction  $\phi$  was increased from 0.3 to 0.5.

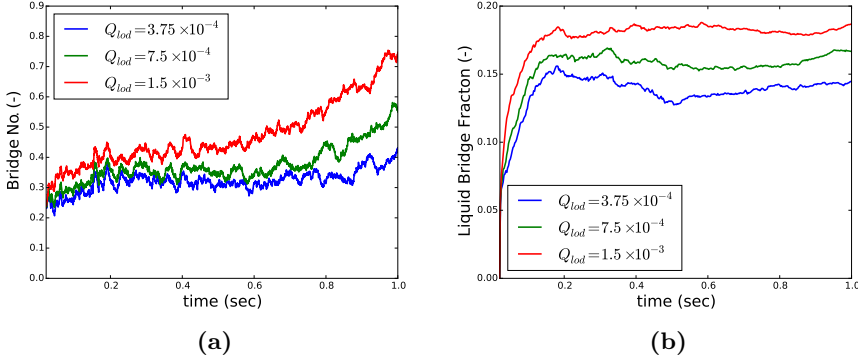
loading of the particles in the wetting zone  $Q_{lod}$  (eq. 10.10). The effect of an increase in liquid loading resulted in an increase both of  $\bar{Z}_b$  and  $V_{bf}$  (Fig. 10.5). At a low  $Q_{lod}$  ( $3.75 \times 10^{-4}$ ), after an initial increase,  $\bar{Z}_b$  equilibrates at a certain level and later started increasing (Fig. 10.5a). However, at higher levels of  $Q_{lod}$  ( $7.5 \times 10^{-4}$ ,  $1.5 \times 10^{-3}$ )  $\bar{Z}_b$  kept on increasing. Interestingly, although  $V_{bf}$  had already achieved equilibration (Fig. 10.5b),  $\bar{Z}_b$  kept on increasing.  $\bar{Z}_b$  increased further at high shear and this elevation was more pronounced at higher  $Q_{lod}$ .

This indicates that when more liquid is available, the liquid present on the particle surface quickly gets transferred to the liquid bridges. At low liquid loading, in the attempt of forming more bridges by changing rearrangement, some liquid is returning to the particle surface. However, in case of particles with higher liquid loading the initial liquid bridges rearranged themselves to form more bridges without returning the liquid to the particle surface.

### Effect of change in liquid addition zone width

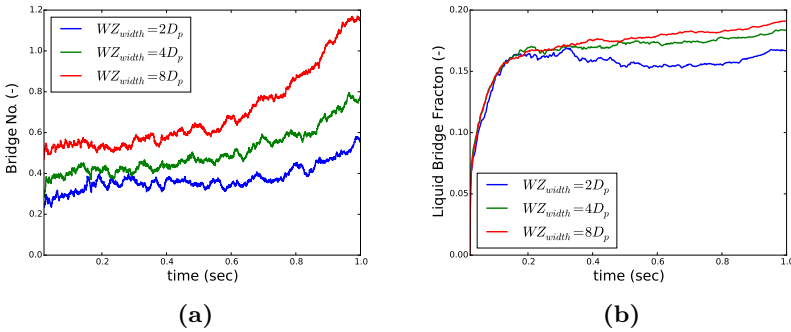
The width of the wetting zone in the granulator, including its effect on the liquid distribution inside the granulator, is an important parameter when designing a granulator. This becomes especially crucial in case of TSG, since these granulators come with one or two liquid addition ports depending on the manufacturer. This will influence the wetting zone. Changing the width of the wetting zone in the granulator while keeping the liquid flux constant allowed investigation of this effect.

Despite a drastic increase in the wetting zone width  $WZ_{width}$  from  $2d_p$  to



**Figure 10.5:** Changes in (a) average number of liquid bridges per particle  $\bar{Z}_b$  and (b) volume fraction of liquid in bridges  $V_{bf}$  when the liquid loading on particles  $Q_{lod}$  was increased.

$8d_p$ , the qualitative behaviour of the liquid bridge fraction evolution remained similar (Fig. 10.6). However, as the shearing time increases, in case of a narrower wetting zone the liquid present in the bridges is returned to the particle surface indicating dominance of convective transport of liquid (Fig. 10.6a). When the wetting zone was wide there was a slight increase in  $\bar{Z}_b$  indicating an increase in the volume of liquid present in bridges. This also translated in  $V_{bf}$  but the effect was delayed. While  $\bar{Z}_b$  increased initially,  $V_{bf}$  showed a very limited increase for the narrower wetting zone (Fig. 10.6b). However,  $\bar{Z}_b$  increased when  $V_{bf}$  was already in equilibrium for all three different wetting zone widths tested. This increase was more pronounced for larger wetting zones.



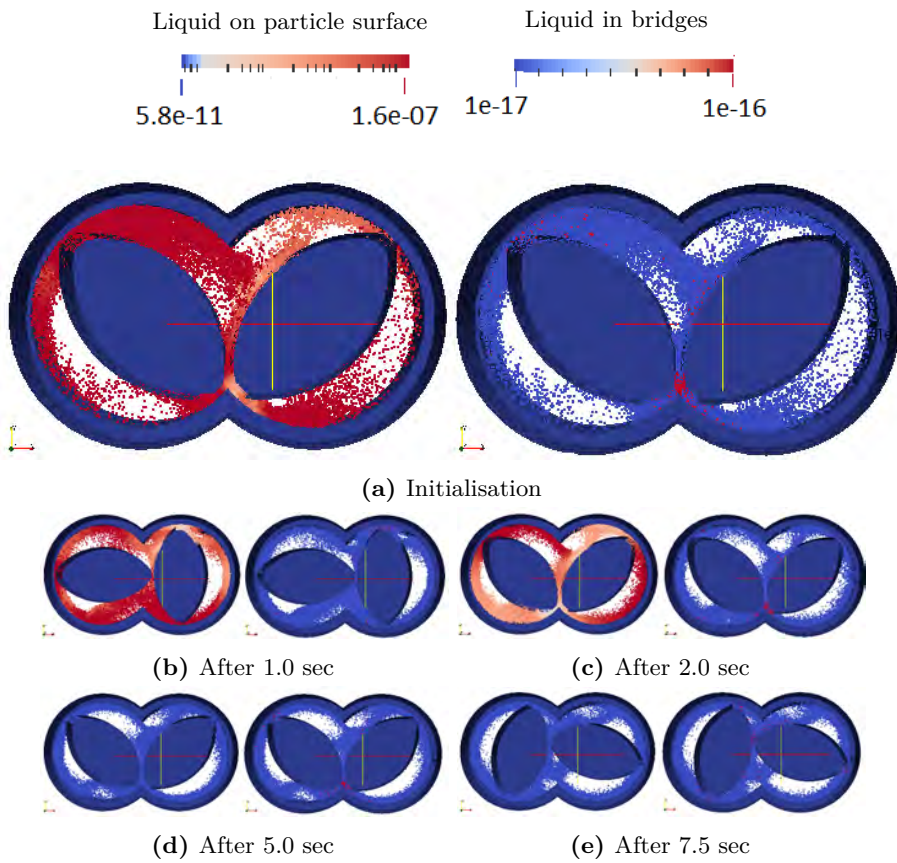
**Figure 10.6:** Changes in (a) average number of liquid bridges per particle  $\bar{Z}_b$  and (b) volume fraction of liquid in bridges  $V_{bf}$  when the wetting zone width  $WZ_{width}$  was increased keeping the flux of liquid addition constant.

These results once again suggest that the liquid present on the particle surface is quickly transferred to the liquid bridges. The liquid in the bridges is subsequently redistributed due to the rearrangement of particles (caused by shear), resulting in larger number of liquid bridges. The results also suggest that the liquid addition to a wider area provides a clear benefit in terms of more liquid bridges per particle which is beneficial for granulation.

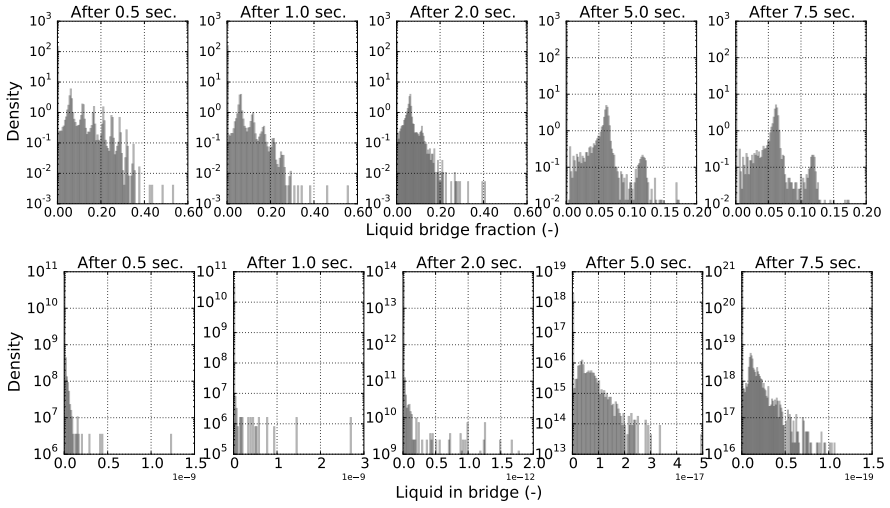
### 10.3.2 Solid-liquid mixing in the mixing zone of TSG

To investigate the solid liquid mixing in the mixing zone of a TSG, DEM simulations were performed using the set-up illustrated in Fig. 10.2. About 46,000 particles were introduced, and the simulation was pre-sheared for 0.5 seconds after the wetting of particles. This was done to obtain a random initial particle and liquid configuration (Fig. 10.9a and 10.7a). Subsequently, the time evolution of the liquid transfer from the surfaces of particles to the bridges between particles (liquid bridge fraction,  $V_{bf}$ ) and the liquid content present in the particle bridges  $V_b/V_p$  caused by the collisions and subsequent flow (due to rotation of two kneading discs) was tracked (Fig. 10.8). The effect was change in of the liquid-to-solid ratio (L/S) during twin-screw granulation was investigated by changing the liquid loading  $Q_{lod}$  on the particles from a standard level of  $7.5 \times 10^{-4}$  (Fig. 10.7, left side) and a ten times higher level of  $7.5 \times 10^{-3}$  (Fig. 10.7, right side).

In the base case scenario (i.e., using the default liquid loading) it was observed that the liquid was quickly transferred from the liquid surface to the liquid bridges (Fig. 10.7 and top plots in Fig. 10.7). Moreover, despite a reduction in liquid volume on the particle surfaces, the number of liquid bridges did not increase rapidly (bottom plots in Fig. 10.7). This observation was similar in the case of the simple shear flow simulation. This indicates that initial capillary bridges between particles imbibe more liquid volume, leading to either agglomerates or fines in the initial steps. Furthermore, the inter-meshing region was observed to be the most active solid-liquid mixing region where liquid bridges form more often (see snapshot for liquid in bridge Fig. 10.7c). The liquid in primary bridges was later distributed with progress in time, leading to formation of more bridges (between 5 and 7.5 seconds in bottom plot of Fig. 10.8). This again shows that the primary liquid bridges mostly resulted in over-wetted lumps, from which liquid was squeezed under shear leading to a sizeable number of liquid bridges between the particles with lower volumes.



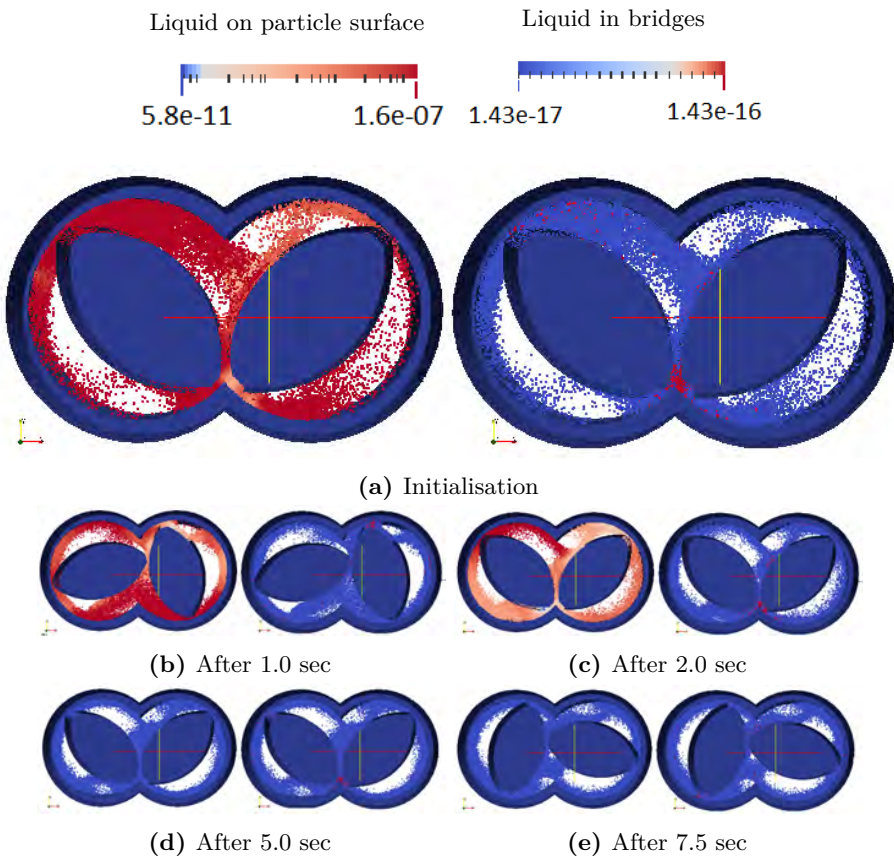
**Figure 10.7:** Changes in volume of liquid on particle surface (left side snapshot in each sub-plot) and liquid in bridges (right side snapshot in each sub-plot) when two kneading discs were co-rotating at 100 rpm and at a  $Q_{lod}$  of  $7.5 \times 10^{-4}$ .



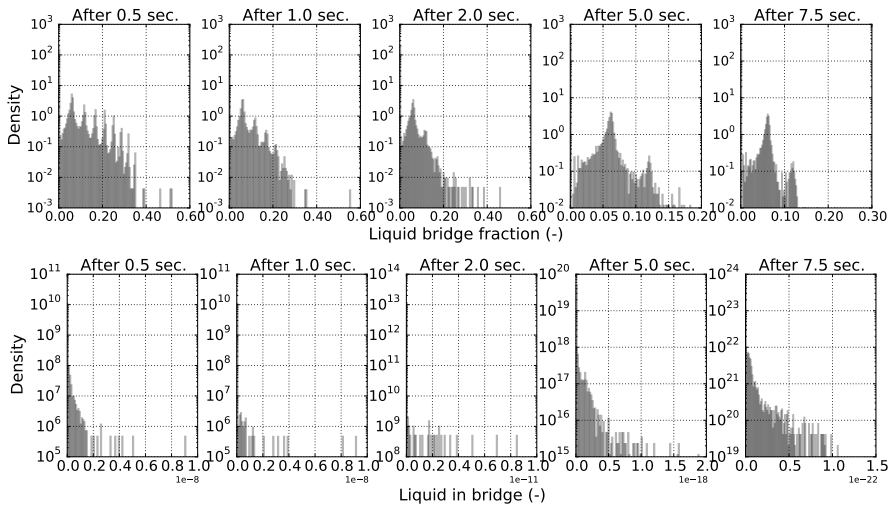
**Figure 10.8:** Histograms showing changes in volume fraction of liquid in bridges  $V_{bf}$  (top row) and the liquid content present in the particle bridges  $V_b/V_p$  when two kneading discs were co-rotating at 100 rpm and at a  $Q_{lod}$  of  $7.5 \times 10^{-4}$ .

As discussed in the case of simple shear simulation, the amount of liquid loaded on the first wetted particles in the wetting zone changes when the liquid addition rate is changed during the twin-screw granulation. These differently liquid-loaded particles require shear to distribute the liquid. This was simulated for the mixing zone of the granulator by a ten times increase in the liquid loading of the particles ( $Q_{lod}$  of  $7.5 \times 10^{-3}$ ) in TSG simulation (Fig. 10.9) compared to the previous case with default liquid loading. Although an increase in the liquid loading resulted in similar volume fraction of liquid in bridges  $V_{bf}$  (top row Fig. 10.8 and 10.10), the liquid content present in the particle bridges  $V_b/V_p$  increased at high  $Q_{lod}$  (bottom row of Fig. 10.10). This suggests that increasing the liquid addition rate to the granulator increased both liquid present on the particle surfaces as well as the liquid in the bridges between the particles. Moreover, the number density of these highly filled liquid bridges at high  $Q_{lod}$  remained same as in the case of low  $Q_{lod}$  (bottom row of plots for 0.5 to 2.0 seconds in 10.8 and 10.10). This again confirms for the mixing zone of the TSG that the liquid transferred from particle surfaces was not contributing to agglomeration as a first step, and the primary liquid bridges were mostly over-wetted lumps, from which water was squeezed under shear. Thus, same as with the case with standard  $Q_{lod}$ , liquid in the primary bridges was later distributed by the continuous shearing. Since more liquid was present in these bridges, the spread of liquid from these bridges resulted formation of more bridges (bottom plots for 5 to 7.5 seconds in Fig. 10.10) at high liquid loading.

Additionally, similar to low  $Q_{lod}$ , the liquid present on the particle surface at high  $Q_{lod}$  was mostly transferred to the liquid bridges when the wetted powder was compressed between the closely inter-meshing kneading discs (right snapshot in Fig. 10.9a).



**Figure 10.9:** Changes in volume of liquid on particle surface (left side snapshot in each sub-plot) and liquid in bridges (right side snapshot in each sub-plot) when two kneading discs were co-rotating at 100 rpm and a default  $Q_{lod}$  of  $7.5 \times 10^{-3}$ . The plots below every snapshot indicate the volume of liquid on particle and volume of liquid in bridge for each particle in the system.



**Figure 10.10:** Histograms showing changes in volume fraction of liquid in bridges  $V_{bf}$  (top row) and the liquid content present in the particle bridges  $V_b/V_p$  when two kneading discs were co-rotating at 100 rpm and at a high  $Q_{lod}$  of  $7.5 \times 10^{-3}$ .

The results from this study suggest that the agglomeration is a delayed process, which is followed by an equilibration of the liquid available on the particle surfaces. The results from this study are preliminary though. A more detailed study is required to further explore the exact mechanisms. Nevertheless, this modelling technique can be very useful for detailed investigation of mixing of solid particles and the way the liquid is included and spread over the particles. Since every particle in the simulation is tracked, the velocity and contact frequency information can be extracted to be subsequently used in a population balance equation (PBE) for a more mechanistic simulation with local insight and verification with dynamically measured granule size distributions (GSDs).

## 10.4 Conclusions

This chapter presented a theoretical analysis of the particle and liquid mixing based on particle-scale DEM simulations. In the initial simulations individual particles in a small quasi-two-dimensional simulation domain were tracked. Liquid bridge formation, rupture, as well as the effect of the bridges on inter-particle forces were simulated. Furthermore, a similar simulation approach was applied to the mixing zone of the TSG and the effect of process parameters on particle and liquid mixing rate was investigated. The preliminary results from this study demonstrate the potential of this method. A more detailed



study is to be performed for detailed investigation of solid-liquid mixing in TSG. Since every particle in the simulation is tracked, the velocity and contact frequency information can be extracted. This allows a future development of more mechanistic kernels to be used in PBE for more realistic simulation of the process.

## PART V

General discussion, conclusions and  
perspectives



The work presented in previous parts of the thesis showed how experimental and theoretical modelling based approaches can be applied to describe the wet granulation of pharmaceutical granules in a twin-screw granulator that is part of a fully continuous pharmaceutical manufacturing process. In this chapter the results presented are discussed in a global perspective leading to the main conclusions of the work and a number of suggestions for further developments in the field of twin-screw granulation.



## General discussion

---

### 11.1 Summary

In this chapter, the results of this thesis are discussed in view of fulfilling the objectives as defined in Chapter 3, with specific focus on how the results have improved the overall understanding regarding the pharmaceutical twin-screw granulation processes. The results obtained for transport, mixing and granulation, both experimental and the theoretical, are discussed altogether. It was shown that there is a strong interaction between the process and screw parameters, which dictate both the granulation time and mixing degree inside the twin-screw granulator (TSG). Similarly, granulation regimes along the TSG barrel length can be spatially separated and controlled through changes in screw configuration by capitalising the modular structure of the screw, and by introducing a change in process conditions which dictates the mixing and transport inside the barrel. Finally, strengths and remaining gaps are discussed, suggesting the direction of future research.

### 11.2 Introduction

The twin-screw granulation is an emerging continuous wet granulation technique, which allows great flexibility in equipment design and choosing process variables. However, little is in fact known about how process settings affect the evolution and kinetics of granule formation and the resulting granule structure. Thus, a need exists to acquire more fundamental understanding of the continuous granulation processes. Improved process understanding can result in improvements in equipment design, process control and processing efficiency. The main aim of this research was therefore to develop a mechanistic description of the continuous

twin-screw wet granulation process by combining experimental and theoretical modelling based approaches. The presented studies in the previous chapters demonstrated that the experimental results when linked to the theoretical model provided the fundamental basis and detailed description to the time, mixing and constitutive mechanisms of the twin-screw wet granulation. They were focused on elucidating various aspects of wet-granulation in a TSG such as granulation time, mixing and particle size evolution. The overall understanding that has been developed within this PhD project is discussed with this perspective in mind.

## 11.3 Material transport and mixing

The study towards the first objective, which was set to characterise the material flow and mixing inside the granulator confirmed that both the process (material throughput and screw speed) and equipment parameters (number of kneading discs and the stagger angle) affect the residence time and mixing (Chapter 6), and therefore understanding their relation is critical to achieve the desired granulation yield.

### 11.3.1 Granulation time

The most promising feature about the twin-screw wet granulation is the ability to process a high material throughput with a short residence time (typically few seconds) (as observed in Chapter 4). Although from a productivity point of view, this time gain with respect to batch granulation which takes minutes to hours, is preferred, its implications on the extent of the granulation rate processes and consequently the granulation yield can be unfavourable (El Hagrasy et al., 2013b). This is because, within this limited time frame, both homogeneous distribution of granulation material (esp., the solid-liquid mixing) and different rate processes of granulation such as aggregation and breakage have to occur to produce a final granule size distribution (GSD). Thus, the main aim of process design for achieving a high granulation yield in continuous twin-screw granulation should be to keep the residence time sufficiently longer than the mixing time of the material transported across the granulator barrel.

The experimental study to investigate residence time distribution (RTD) in TSG presented in Chapter 4 showed that the screw speed most significantly changes the residence time during operation. This is mainly related to the increased conveying rate at a high screw speed. Previous studies also showed that a high conveying rate of the rapidly moving twin-screw reduces the mean residence time  $\bar{t}$  (Dhenge et al., 2010; Lee et al., 2012). By sequentially changing

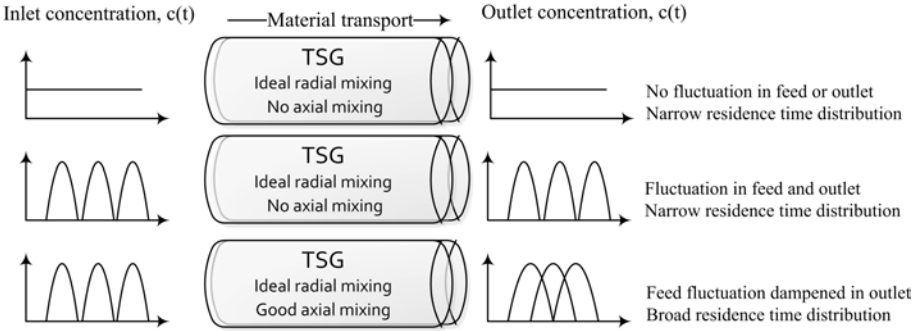
the process parameters and the screw configuration it was demonstrated that not only the parameters independently affect the residence time, but their interaction strongly changes in the flow regime inside the granulator, which drives the residence time of the material (Fig. 4.6). The flow restriction caused by an increasing number of kneading discs at a high screw speed increases  $\bar{t}$  by increasing the plug flow component in the TSG. Thus, if the distributive mixing is insufficient, the changes in the flow regime inside the granulator also lead to reduced efficiency. Moreover, increasing the stagger angle or reducing the screw speed for a screw configuration with a high number of kneading discs quickly changes the flow regime to a critical plug flow level, leading to granulator jamming. Similarly, material throughput is reported as a parameter leading to reduction in the  $\bar{t}$  at a high throughput (Dhenge et al., 2011), which was also confirmed by the study in Chapter 4. This is mainly attributed to the increased throughput force of the material leading to a low  $\bar{t}$ . However, this study also demonstrated the limits of this hypothesis in terms of effect reversal, i.e. an increase in  $\bar{t}$  with increasing material throughput at high fill degree conditions. It was shown that the extra conveying rate is limited by the conveying capacity of the screws which cannot be increased inexhaustibly by an increasing material throughput.

### 11.3.2 Mixing

The mixing inside the TSG is related to the functional role of the screw configuration as well as the induced shear by the rotating screws based on the process setting. The bulk mixing is classified as axial and radial based on direction of spread in the granulator barrel. In the high-shear environment of the TSG, a good radial mixing is required to ensure a homogeneous distribution with a constant material throughput (top scheme in Fig. 11.1). However, in case of variations in the material and process inputs, which is inevitable in a pharmaceutical manufacturing environment (Sochon et al., 2010), lack of axial mixing will lead to the same amount of variability in the outlet (middle scheme in Fig. 11.1). A good axial mixing in addition to the radial mixing during granulation in TSG is thus required to avoid the effect of any inhomogeneities at the inlet on the produced granules (bottom scheme in Fig. 11.1). Feeding rates of the granulation material, the screw speed and the screw configuration can be independently chosen to achieve the desired mixing level of the material both in terms of axial mixing (Chapter 4) as well as bulk mixing of solid and liquid (Chapter 6). The RTD exhibited by the system yields distinctive evidence both regarding the average time spent by the material and the degree of axial mixing occurring within the system, and thus is one of the most informative characterisation methods of the system (Levenspiel, 1999). On the other hand, the knowledge of solid-liquid mixing requires detailed investigation of wet



granules produced from the TSG.



**Figure 11.1:** Radial and axial mixing as a function of the material feeding characteristics and the RTD in a TSG.

### Axial mixing

Broadening of the RTD indicates axial mixing as discussed in Chapter 4 and 6. The normalisation of this width gives normalised variance  $\sigma_{\theta}^2$ , whereas the ratio of RTD width and the delay in onset of RTD gives Péclet number  $Pe$ . As the conveying rate increases at a higher screw speed, the axial mixing increased which was quantified by the rise in  $\sigma_{\theta}^2$  (Fig. 4.7) and lowering of  $Pe$  (Fig. 4.8). At a low filling condition with reduced material feed rate and few kneading discs axial mixing increased. However, at high fill conditions increasing screw speed only reduced  $\bar{t}$  without increasing the axial dispersion as flow becomes plug flow like, which was also indicated by a high  $Pe$ . At a low screw speed the  $Pe$  increased sharply with feed rate, number of kneading elements and stagger angle indicating a transition to plug flow when the throughput exceeds the conveying capacity. These results were different from the results presented by Dhenge et al. (2010) and Lee et al. (2012), who investigated RTD at a lower screw speed and material throughput with a granulator containing a smaller diameter screw and suggested that the extent of axial mixing is similar regardless of the screw speed, feed rate and screw configuration. This contradiction forms an indication towards influence of screw geometry, scale and process parameters on the axial mixing, and thus requires further investigations using granulators of different scales.

### Solid-liquid mixing

Mixing powders together with liquid is a challenging task in a TSG as the mixing time domain is limited and cannot be extended beyond a certain limit

for the reasons discussed in section 11.3.1. The liquid bridges between the powder particles result in aggregation of particles to produce larger granules. Thus, a homogeneous liquid distribution within the powder is desired both to initialise the wet granulation and to obtain granules exhibiting a narrow GSD. An uneven liquid distribution was suggested as the cause of a broad GSD and lump formation using a TSG by El Hagrasy et al. (2013b). Vercruyssen et al. (2013b) also pointed towards the importance of the dosing systems on the solid-liquid mixing in a TSG. In this study, it was observed that the periodicity of two peristaltic pumps used for the liquid addition resulted in significant variation in the solid-liquid mixing, which reduced when the pump head orientation was set to out-of-phase. Similar deviation can also occur due to the fluctuations in the powder dosing feeder. The solid-liquid mixing was quantified in Chapter 6 as the mixing index (MI) of the bulk granules and the mixing dynamics was quantified as frequency and amplitude of variations in the mean moisture profile of each run. The study suggested that the increasing number of kneading discs improves the liquid distribution in the material after TSG, which was also observed earlier by Vercruyssen et al. (2013b). However, the present study also demonstrated that despite improvement in the bulk solid-liquid mixing by the increasing number of kneading discs, the required quality of mixing inside the TSG barrel was still not achieved, which led to a broad GSD. Further increase in the number of kneading discs may indeterminately improve the bulk mixing, but will limit the feasible operating ranges of the process settings by increasing the plug-flow fraction in the transport profile leading to an undesired high torque level. Therefore, along with the efforts to modify the TSG screw configuration using conventional screw elements (conveying and kneading elements), efforts should also be done to explore non-conventional screw elements with modified geometries. Some efforts in this direction such as application of distributive mixing elements by Sayin et al. (2015), screw mixing elements by Vercruyssen et al. (2015) and distributive flow elements by Meier et al. (2015) have already shown positive results in terms of a more narrower GSD. The study presented in Chapter 6 also showed that, although a high material throughput and a high screw speed are desired for process efficiency, their exclusive increase causes inefficient solid-liquid mixing which is not desirable.

## 11.4 Granule size evolution

Beside the time and mixing, the field conditions (such as shear, free liquid and fill ratio) inside the granulator lead to dominance of one constitutive granulation mechanism over others, resulting in a certain quality of granules at the TSG outlet. At the same time, the process (material throughput and screw speed) and equipment parameters (number of kneading discs and the stagger angle)

not only affect the transport and mixing discussed in section 11.3, but also the field conditions. Therefore, it was important to diagnose both the spatial evolution of particle size in the TSG (Chapter 5) as well as the link between residence time, solid-liquid mixing and the GSD (Chapter 6).

### 11.4.1 Granule size and shape dynamics

The knowledge regarding the primary shaping mechanisms behind the particle size and shape distribution during wet granulation in the TSG is more limited compared to the high shear mixers due to the opacity of the granulator (Dhenge et al., 2012b; El Hagrasy and Litster, 2013). Operation of a TSG in which the barrel could be opened to collect samples from several locations inside the TSG barrel allowed a detailed experimental investigation of the granule size and shape dynamics in the granulator (Fig. 5.2 in Chapter 5). One of the key observations was that an increasing number of kneading discs in the screw configuration not only increased the fraction of larger granules for the downstream sample locations 3 and 5 which were located after the kneading blocks but also at sample location 1, which was located upstream of the kneading block. This suggests that along with the distributive mixing by the kneading block of the screw and dispersive mixing by the slippage of material at a high screw speed, the built-up material before the "flow-restricted" kneading zone is force-mixed with the incoming materials due to the throughput force. The results also suggested that the increasing throughput is beneficial and can lead to an increased amount of larger granules in the successive mixing zone only when sufficient granulation liquid is present to make strong agglomerates. However, a further granule size enlargement was observed which also corresponded with broadening of the distribution after the second kneading block (comparing ID 2 and 4 plots for 12 kneading discs in Fig. 5.6). This suggests a mixed granulation regime, i.e., along with aggregation, size reduction mechanisms such as attrition and breakage also take place in the second kneading block. Moreover, spherification of granules was observed along the granulator length and for an increasing number of kneading discs (Fig. 5.7 and 5.9). El Hagrasy and Litster (2013) also reported a greater consolidation due to chopping-off of the edges of the brittle and elongated granules in the second kneading block of the TSG.

### 11.4.2 Link between RTD, liquid distribution and GSD

Different size fractions in the produced granules dominate based on the residence time, axial as well as solid-liquid mixing, and field conditions. Therefore, these interrelations were investigated to discover the residence time and mixing settings which resulted in a high granulation yield. Furthermore, the influence

of process settings which lead to variation in residence time and mixing and can be applied to efficaciously steer the GSD profile were investigated. An increase in number of kneading discs and liquid-to-solid ratio (L/S) are generally suggested parameters to increase the granulation yield in the TSG (El Hagrasy and Litster, 2013; Dhenge et al., 2012a; Thompson, 2015). However, increasing these parameters results in a broad GSD (El Hagrasy et al., 2013b; Kumar et al., 2014a). The study presented in Chapter 6 showed that an increasing number of kneading discs did not significantly contribute to increasing the yield fraction, despite improvement in bulk solid-liquid mixing and an increase in the residence time (Fig. 6.10). Moreover, the yield fraction did not change significantly by increasing the L/S since most of the additional liquid resulted in the formation of oversized granules. Instead, the yield fraction reduced significantly by an increasing material throughput which is ultimately linked to the reduced residence time due to a higher throughput force as well as an inferior solid-liquid mixing which is mostly driven by the distributive mixing by the kneading discs. This evidently suggests that the yield fraction of granules in the GSD obtained by the TSG is low due to inferior performance of the kneading discs in the solid-liquid mixing. Thus, other mixing element configurations should be explored as discussed in 11.3.2.

## 11.5 Model-based analysis

A mechanistic understanding of transport of material and the kinetics of granulation in a TSG can be developed and improved by theoretical models which are closely coupled with experimental data as discussed in the introductory Chapter 1. Such a model can provide a detailed information about several crucial process parameters which cannot be easily measured and thus far correlated with in-line dynamic torque which is a 0-dimensional measurement, leading to a very limited process knowledge. Thus, the data from an experimental study on RTD was used to identify the most suitable conceptual model and apply it in order to improve the knowledge regarding material transport in a TSG (Chapter 7). Similarly, the data from the experimental investigation of RTD was used along with experimental data regarding the GSD evolution in a TSG to propose and calibrate a modelling framework based on a population balance model (PBM) for the mixing zones of the TSG (Chapter 8).

### 11.5.1 Modelling RTD

The conceptual modelling based on a tanks-in-series (TIS) approach allows identification of different flow components based on ideal flow reactors. In the plug-flow component the convective transport is larger than the dispersive

transport and in the well-mixed component indicated by a continuously stirred tank reactor (CSTR) the dispersive transport dominates and dead zones occur where the material transport was either excessively back-mixed or spent much longer time than the  $\bar{t}$  in the stagnant pockets that exist in the TSG (Chapter 7). The study suggested that the mixing zones containing the kneading elements support the plug-flow transport in the TSG. The excess of material in this region also prevents the back-mixing inside the granulator hence decreasing the size of the dead zone. The thickness of the slip layer of material which forms against the barrel wall at a low shear condition supports an increase in the plug-flow component and an increase in the dead fraction. Thus, either a high throughput force by increasing throughput or increasing the shear level by a high screw speed reduces the plug-flow component leading to more axial mixing in the TSG. This finding was of significant importance since the earlier studies always assumed TSG as a plug-flow device such that increasing throughput leads to an increased plug-flow fraction (Dhenge et al., 2010). As the TSG was assumed as a plug-flow system, it was also believed that the level of back-mixing in the TSG is low. The results about the increasing amount of axial mixing and its excess leading to the dead fraction confirms that a significant back mixing occurs in the TSG. The axial mixing reflected by broadening of the RTD is necessary to compensate for process variations as discussed in section 11.3.2, however, the excessive broadening leading to a long tail region of the RTD as reflected by a dead zone should be avoided to control the traceability of the material as it moves on to the next unit operation.

### 11.5.2 Tracking GSD using PBM

The experimental study provided local information regarding the GSD (Chapter 5), however the fundamental basis, i.e. mechanistic understanding of the shift in the GSD within different locations of the barrel and at different process conditions was missing. The PBM framework developed and calibrated in Chapter 8 linked the experimental measurements with the constitutive mechanisms of the granulation, namely aggregation and breakage, which are expected to dominate in the mixing zones of the TSG. The modular structure of TSG is always targeted and the screw configuration is modified during the experimental studies to render a regime separated state of granulation (El Hagrasy and Litster, 2013). However, in practice a regime-separation was never demonstrated earlier. In the study presented in Chapter 8, it was shown that along with the screw configuration, the regime separation also requires suitable process conditions. It was observed in this study that at a high material throughput and for a screw configuration with two mixing zones, the low screw speed resulted in a mixed granulation regime, i.e. aggregation and breakage occurred simultaneously in the second mixing zone. However, increasing the screw speed for the same con-

figuration and condition resulted in separation of the aggregation and breakage between the two mixing zones of the granulator. Such a diagnosis of the process to achieve a "regime-separated" state is important as that would allow improved control over granule properties compared to the conventional batch granulation equipment like high shear mixers in which all granulation sub-processes occur simultaneously.

## 11.6 Towards a generic twin-screw granulation knowledge

By performing a number of separate experiments on a TSG, one can render the behaviour or regime of the twin-screw wet granulation process for a certain granulator setting (Fig. 9.3). With the aid of this regime map, more insight into the granulation processes may be gained and the expected behaviour of the process can be predicted (Chapter 9). This should eventually lead to improved design and control of the twin-screw granulation processes (Litster and Ennis, 2004). Additionally, as the understanding regarding the TSG process is improving with experimental and model-based studies, there is also a need to reduce the dependence of the model on the experimental data by adopting more mechanistic models. This is especially required when the aim is to optimise the process, or the design of the equipment in terms of change in granulation material or change in screw geometry. Therefore, efforts were done to simulate the mixing of solid and liquid at particle scale in the mixing zone of the TSG using the discrete element method (DEM) (Chapter 10).

### 11.6.1 Regime map approach

The flexibility of the TSG in choosing process and equipment parameters to achieve desired size and properties of the granules makes twin-screw granulation a potential technology. This has also led to a wide range of studies with focus on adjusting parameters such as binder addition method, number and stagger angle of kneading elements in the screw configuration, granulation barrel temperature, liquid addition rate, powder feed rate and screw speed (Dhenge et al., 2011; Vercruyssen et al., 2012; El Hagrasy et al., 2013b; Djuric, 2008) and at different scales (Djuric et al., 2009). In the study presented in Chapter 9, to comprehend the applicability and limits of the process variables in a scale independent manner for improved understanding about the twin-screw granulation process, the regime theory was applied. The specific mechanical energy (SME) which involves the combination of screw speed, material throughput and torque required to rotate the screws was correlated with the applied liquid-to-solid

ratio. The study suggested that, although increasing L/S strongly drives the GSD towards a large mean granule size, increasing the energy input to the system can be effectively used to lower the mean granule size and also narrow the width of the size distribution. This observation also corresponds with the observation regarding solid-liquid mixing in Chapter 6 where an increased shear by the high screw speed and increasing number of kneading discs resulted in an improved mixing and a higher yield fraction. However, due to the inherent flexibility in design and operation of the TSG which allows more than one process setting to produce the same effect, different regime maps for two different screw configurations (1×6 and 2×6 kneading discs) were made to reduce such possibility.

## 11.6.2 Particle-scale simulation using DEM

As the twin-screw granulation technology is fairly new, not only the mechanism of granulation is relatively unknown but also the changes in design need to be explored to obtain efficiency as discussed in section 11.3.2 and 11.4.2. This calls for a modelling approach which can inherently consider the effects caused by both the geometry of the TSG as well as the field conditions. The DEM was therefore applied to understand the solid-liquid mixing by tracking each particle as well as the liquid exchange network, i.e. the liquid distribution inside the system was also tracked. However, as these simulations are computationally very expensive, simulation of the dense particle system in the complete TSG was impossible within the time frame of this PhD. Therefore, a more tractable and equally powerful approach was adopted by simulating the particle system first in a well-defined quasi two dimensional simulation domain and then transferring this approach to the mixing element section of the TSG to unravel the fundamentals of solid-liquid mixing (Chapter 10). Pursuing this approach led to a novel finding that the solid liquid mixing starts with a quick transfer of liquid from the particle surface to bridges and these thick bridges later redistribute the liquid to form more bridges. As this reallocation of liquid bridges is a delayed event it can safely be deduced that the agglomeration cannot be achieved earlier without quicker wetting of the particles. The visualisation of DEM data also suggested that mixing the liquid bridge formation is most dominant in the inter-meshing region of the kneading elements. Providing access to complete detail of the particle dynamics, this approach can be very useful for extensive analysis of the twin-screw granulation system.

## 11.7 Strengths and limitations of the current approach

The integrated approach adopted in this thesis used the strengths of both methodologies, experimental and theoretical, for in-depth investigation of twin-screw granulation. This allowed understanding the limitations and advantages of such an approach while investigating the complex process of twin-screw wet granulation. The rheo-kinetics of material in the TSG cannot be visualised easily by experimental studies. On the other hand, rigorous modelling of material transport and kinetics in a TSG requires the closure of particle velocity profiles, a multi-particle multiphase interaction model, a mechanistic definition of granulation sub-processes and all the complex moving geometry of the screw channels. Since such an approach is the more complex and less efficient, and if applied can give acceptable results only for specific zones of the TSG, the adopted integrated approach can be believed to be the best possible approach to understand the twin-screw granulation process at this moment. In this thesis the experimental measurements were used both for conceptualisation and calibration of models which were later used for further diagnosis of transport and kinetics in a TSG. Therefore the presented model results are more realistic and complement the description outlined by the experiments.

The studies performed for this thesis relied on a simple placebo formulation based on  $\alpha$ -lactose monohydrate to verify each hypothesis. Lactose is a very commonly used filler for granulation (Chan and Heng, 2005) and a commonly used excipient in tablets (Rowe et al., 2009) which are the most popular forms for drug administration. Thus a broad spectrum of formulations with similar properties should show a similar behaviour as discussed above. However, it can be expected that water insoluble fillers, such as microcrystalline cellulose and dibasic calcium phosphate, will have a different granulation behaviour. As the method used for this work (both data collection and modelling) is generic, it can be repeated for other excipients with a significantly behaviour. Beside, although this work investigates the mechanistic link between the transport, mixing and wet granulation in the TSG in terms of change in GSD, the link for other critical quality attributes (CQAs) such as granule density and friability, which also required detailed investigation in the twin-screw granulation process, is still missing. Furthermore, the kinetics of wetting, despite being a key constitutive mechanism of granulation, were not considered in the PBM framework presented in this thesis. This was mainly due to lack of a mechanistic description of the wetting process. In order to fill these gaps and to make the most use of the advancements made by the current work, several directions for future research are discussed in the next chapter.





---

## General conclusions

---

The overall objective of this dissertation was to develop a mechanistic understanding of the pharmaceutical twin-screw wet granulation process to be used in a continuous solid dosage manufacturing process. Through a series of experimental and theoretical studies, various aspects of this objective have been achieved as extensively discussed in Chapter 11. The knowledge that was obtained leads to several conclusions, which are summarised here.

### 12.1 Granulation time and mixing quality

The residence time distribution (RTD) analysis has shown that changes in experimental conditions can lead to very different flow regimes, and the argument that the twin-screw granulator (TSG) shows a plug flow mixing characteristic is an oversimplification of transport characteristics in TSG and hence needs to be revised. According to the study conducted in the frame of this thesis, the variations in screw rotation speed, material throughput, liquid-to-solid ratio, number of kneading discs and stagger angle not only have direct influence on the residence time of the material in the barrel but also change the axial mixing during twin-screw granulation. Increased screw speed led to a lower mean residence time  $\bar{t}$  and wider RTD, i.e. more axial mixing. Increasing the powder feed rate increases  $\bar{t}$  via a higher throughput force while increasing liquid-to-solid ratio (L/S) increases  $\bar{t}$  by raising the sluggishness or inertia of the material in the barrel. The screw geometry was one of the important factors affecting the axial mixing, which was convincingly diagnosed by the RTD model.

Examining the suitability of the model framework for describing the experimentally measured RTD in a TSG, large variations in the flow regime within the TSG were found through the tanks-in-series (TIS) model containing all

three components, i.e. the plug-flow fraction  $p$  in series with a finite number of continuously stirred tank reactors  $n$  with dead zones  $d$ . This was found to be the most suitable conceptual model for describing RTD in a TSG. This steady-state model consisting of algebraic equations instead of a physical model containing differential equations, achieved a reasonable accuracy in representation of the RTD despite the simplicity of implementation and obvious computational advantages of the investigated approach. The model showed that the kneading block in the screw configuration significantly stimulates the plug-flow transport of material inside the granulator. Additionally, the mixing and  $d$  are generally affected by the fill level inside the TSG barrel, thus a good balance between the throughput force and the conveying rate is necessary for a good axial mixing and reduction of the stagnant regions inside the TSG.

The solid-liquid mixing analysis indicates that the current kneading discs provide insufficient solid-liquid mixing capacity which aggravates at a high material throughput resulting in broad granule size distributions (GSDs). Currently, increasing the screw speed lowers the fill ratio and supports the mixing by axial transport. Thus, a balance between material throughput and screw speed should be looked for to achieve the required solid-liquid mixing within the residence time for a high granulation yield. Additionally, more efforts should be put into both the modification of the screw configuration as well as the geometry of the mixing elements in order to improve the mixing capacity of the TSG. Additionally, application of mechanistic modelling tools, such as discrete element simulations should be further explored for rigorous investigation of material flow and mixing during twin-screw granulation.

## 12.2 GSD transformation by TSG

From the experimental study to understand the GSD evolution in the TSG barrel it can be concluded that an increasing throughput is beneficial only when sufficient granulation liquid and shear mixing is present to make strong agglomerates. An increase in the number of kneading discs significantly contributes to granulation. However, at a high throughput, more liquid addition and a high number of kneading discs result in a higher torque, and also a broader GSD. The fill ratio in the barrel is an important factor both because it affects the torque required by the granulator drive, and because it plays a major role in changing the size and shape of the particles. Increasing the screw speed lowers the torque and reduces the width of the GSD but can also result in lowering of the yield due to a low granulation time.

The deformation of wet granules is easy and granules with a more uniform shape are produced at higher L/S. Although this study provided a detailed insight regarding the process and suggested a number of competing mechanisms, such as aggregation, consolidation and breakage occurring across the kneading block, the experimental data produced only yield semi-quantitative insight into which of these mechanisms were dominant. However, a 1-D population balance model (PBM) framework including aggregation and breakage subprocesses was proposed and the model parameters were calibrated using the experimentally measured GSD inside the granulator. The calibrated model was then used as a predictive tool within the experimental space. The analysis of the simulation data revealed that, at high screw speed, the successive kneading blocks can lead to the dominance of different constitutive granulation mechanisms inside the TSG. An ability to achieve a physical separation between the granulation regimes inside the granulator can be promising for future design and advanced control of the continuous granulation process using the TSG. The study suggested that a model-based approach can be adopted to develop a better understanding of twin-screw granulation processes. Moreover, the approach of experimental calibration and validation is the better way forward for the development of twin-screw granulation models as multiple factors of the TSG leading to a specific experimental output can now constrain the model during calibration. A validated model can ultimately be used to define the design space of the process to facilitate process optimization and model-based control.

From the study linking residence time, mixing and resulting GSD it can be concluded that a broad GSD of granules produced by a TSG is linked with insufficient solid-liquid mixing capacity of the current kneading discs which is ultimately required for good granulation performance. Due to this suboptimal solid-liquid mixing, the granulation performance of the TSG tested in the frame of this thesis can only be improved at lower fill ratio of the GSD. However, efforts should be made to improve the mixing capacity of the TSG by modifying the screw geometry. Moreover, application of mechanistic modelling tools, such as discrete element simulations and population balance modelling, need to be further explored for further detailed investigation of both, the material transport and mixing and their impact on the constitutive mechanisms of granulation which ultimately decide the yield during twin-screw granulation.

## 12.3 Overall conclusion

From the presented studies in this dissertation, it has been identified that:

1. A systematic framework and scientific approach is necessary to utilise efficiently the opportunity provided by the regulators to increasingly

rely on the science- and risk-based holistic development of processes and products for commercialisation.

2. A critical analysis of complex pharmaceutical processes is possible by combination of modelling and measurement studies.
3. Mechanistic and data-driven modelling approaches have great joint prospects and can play an important role in process design, optimisation and control of critical quality parameters in pharmaceutical granulation, but they require a high degree of reliability and development to achieve the target of simulating and investigating real-time quality control for complex unit operations such as granulation.
4. Furthermore, rigorous calibration and validation is required for the granulation models to more accurately represent granulation conditions measured in the field. This is important to maintain the predictive power of the model which, if lost, leads to poor, unreliable decisions based on the model predictions.

---

## Perspectives & future work

---

Although this dissertation covers a large spectrum of studies several gaps still remain and need further research. Additionally, promising research avenues for development and implementation of continuous wet granulation in the pharmaceutical sector were also identified.

1. The granulation data based on simple placebo formulation was used in this dissertation to verify the hypothesis. It can be easily expected that water insoluble fillers, such as microcrystalline cellulose, will have a different flow and granulation behaviour in the twin-screw granulator (TSG). For example, much more water might be needed in the granulation process as no strong solid bridges will be formed. Similarly, weaker liquid bridges based on capillary forces will be formed when water insoluble fillers are used. Therefore, future experiments and modelling studies should investigate the effect of other formulations with significantly different raw material properties.
2. The modular structure of the TSG is a central issue which is captured in the modelling and measurement techniques applied to the TSG. Understanding the changes in the granules properties requires extensive measurement of granule properties beyond the granule size distribution (GSD) such as porosity and moisture distribution along the screw geometry. Such data should be applied together with a multivariate population balance model (PBM) for exploration of more detailed local information about granulation mechanisms.
3. A rigorous calibration and validation of such a multivariate granulation model is required to predict the granulation characteristics more accurately.

4. To further improve the granulation model, future work should focus on introducing the wetting kinetics in the model framework and to obtain particle flux data and collision frequencies using the discrete element method (DEM) to avoid the parameter estimation by model inversion as this only leads to empiricism. Additionally, dedicated mechanistic kernels for the twin-screw granulation can be developed in order to improve the sensitivity of the model towards the change in process conditions and other field parameters.
5. The available modelling methods show performance limitations as the dimensions of the model are increased. This motivates the need to develop more reliable and computationally efficient numerical methods to provide solutions which can be applied for on-line model-based control.
6. A single simple model cannot determine the complex granulation behaviour in a TSG with shifting granulation regimes. Therefore, different parts of the granulation process are described by different mechanistically based structural models. Although such a model is useful in process understanding, a fully integrated compartmental PBM capturing effects of different modules of the screw should be developed for an application model.
7. With the aim of further process knowledge build-up, the GSD evolution along the length of the screws inside the TSG should be experimentally and theoretically mapped in order to understand the dominant constitutive mechanisms (such as growth, aggregation and breakage) of a twin-screw granulation system.
8. The rigorous approach for the modelling of the transport, mixing and granulation of material in a TSG based on first principles is, although more complex and less efficient, very useful for closure of particle scale phenomena, based on the multiple inter-particle and particle-wall forces which can be utilised in a mesoscale model like PBM to predict the granulation mechanism for specific zones of the screw.
9. The twin-screw granulation solves the scale-up challenge by the flexibility towards the amount of material processed per run. However, the scaling of the TSG is not completely overruled to meet the demands at commercial manufacturing level. Therefore additional experiments on a small and large scale granulator should be performed to derive scale-up rules and the scale-dependence of the granulation regime in the TSG.
10. The twin-screw granulation process is one of the unit operations in the continuous solid dosage manufacturing. Hence, similar experimental

and model-based analyses should be applied for all unit processes. The calibrated and validated models thus obtained should be implemented in a flowsheet simulation model.

11. The main remaining challenge in the area of continuous processing and twin-screw granulation though lies in the development of new measurement techniques, which are able to measure the fundamental granule properties, preferably *in situ*. Following extensive research conducted on software sensor technology in the last few years, also in other related fields facing the challenge of opaque multiphase system, it becomes more and more attractive for the industry to use software sensors in real applications. As the concept of a software sensor is to replace the more complex direct measurement by a suitable algorithm to calculate the desired quantity from other easily measurable data with pre-existing hardware sensors, the development of mechanistic models which describe the relationships of different parameters in a system, and conceptual models representing the system behaviour in terms of the relationship between input and output can promote the further development in this area.





---

## Bibliography

---

- Abberger, T. (2007). Population balance modelling of granulation. In A.D. Salman, M. J. H. and Seville, J. P. K., editors, *Handbook of Powder Technology*, volume Volume 11, chapter 24, pages 1109–1186. Elsevier Science B.V.
- Adetayo, A. A. and Ennis, B. J. (1997). Unifying approach to modeling granule coalescence mechanisms. *AIChE J.*, 43(4):927–934.
- Adetayo, A. A., Litster, J. D., Pratsinis, S. E., and Ennis, B. J. (1995). Population Balance Modeling of Drum Granulation of Materials with Wide Size Distribution. *Powder Technol.*, 82(1):37–49.
- Althaus, T. O. and Windhab, E. J. (2012). Characterization of wet powder flowability by shear cell measurements and compaction curves. *Powder Technol.*, 215-216:59–65.
- am Ende, M. T., Bharadwaj, R., Garcia-Munoz, S., Ketterhagen, W., Prpich, A., and Doshi, P. (2010). *Process Modeling Techniques and Applications for Solid Oral Drug Products*, pages 633–662. John Wiley & Sons, Inc.
- Antonyuk, S., Khanal, M., Tomas, J., Heinrich, S., and Mörl, L. (2006). Impact breakage of spherical granules: Experimental study and DEM simulation. *Chem. Eng. Process.*, 45(10):838–856. Particulate Processes A Special Issue of Chemical Engineering and Processing.
- Austin, L. G. (2002). A treatment of impact breakage of particles. *Powder Technol.*, 126(1):85 – 90.
- Bakalis, S., Fryer, P. J., and Parker, D. J. (2004). Measuring velocity distributions of viscous fluids using positron emission particle tracking (pept). *AIChE J.*, 50(7):1606–1613.
- Barigou, M. (2004). Particle Tracking in Opaque Mixing Systems: An Overview of the Capabilities of PET and PEPT. *Chem. Eng. Res. Des.*, 82(9):1258–1267.
- Barrasso, D., Eppinger, T., Pereira, F. E., Aglave, R., Debus, K., Bermingham, S. K., and Ramachandran, R. (2015a). A multi-scale, mechanistic model of a wet granulation process using a novel bi-directional PBM-DEM coupling algorithm. *Chem. Eng. Sci.*, 123(0):500 – 513.
- Barrasso, D., Hagrasy, A. E., Litster, J. D., and Ramachandran, R. (2015b). Multi-dimensional population balance model development and validation for a twin screw granulation process. *Powder Technol.*, 270, Part B(0):612 – 621.
- Barrasso, D. and Ramachandran, R. (2012). A comparison of model order reduction techniques for a four-dimensional population balance model describing multi-component wet granulation processes. *Chem. Eng. Sci.*, 80:380–392.
- Barrasso, D., Tamrakar, A., and Ramachandran, R. (2015c). Model order reduction of a multi-scale pbm-dem description of a wet granulation process via ANN. *Procedia Eng.*, 102(0):1295 – 1304. New Paradigm of Particle Science and Technology Proceedings of The 7th World Congress on Particle Technology.
- Barrasso, D., Walia, S., and Ramachandran, R. (2013). Multi-component population balance modeling of continuous granulation processes: A parametric study and comparison with experimental trends. *Powder Technol.*, 241(0):85 – 97.
- Betz, G., Bürgin, P. J., and Leuenberger, H. (2003). Power consumption profile analysis and tensile strength measurements during moist agglomeration. *Int. J. Pharm.*, 252(1-2):11–25.
- Biggs, C. A., Sanders, C., Scott, A. C., Willemse, A. W., Hoffman, A. C., Instone, T., Salman, A. D., and Hounslow, M. J. (2003). Coupling granule properties and granulation rates in high-shear granulation. *Powder Technol.*, 130(1-3):162–168.
- Bigio, D. and Stry, W. (1990). Measures of mixing in laminar flow. *Polym. Eng. Sci.*, 30(3):153–161.
- Bouffard, J., Bertrand, F., and Chaouki, J. (2012). A multiscale model for the simulation of granulation in rotor-based equipment. *Chem. Eng. Sci.*, 81:106–117.
- Braumann, A., Goodson, M. J., Kraft, M., and Mort, P. R. (2007). Modelling and validation of granulation with heterogeneous binder dispersion and chemical reaction. *Chem. Eng. Sci.*,

62(17):4717–4728.

- Braumann, A. and Kraft, M. (2010). Incorporating experimental uncertainties into multivariate granulation modelling. *Chem. Eng. Sci.*, 65(3):1088–1100.
- Braumann, A., Kraft, M., and Mort, P. R. (2010a). Parameter estimation in a multidimensional granulation model. *Powder Technol.*, 197(3):196–210.
- Braumann, A., Man, P. L. W., and Kraft, M. (2010b). Statistical Approximation of the Inverse Problem in Multivariate Population Balance Modeling. *Ind. Eng. Chem. Res.*, 49(1):428–438.
- Bridgwater, J. (2012). Mixing of powders and granular materials by mechanical means - a perspective. *Particuology*.
- Brun, R., Reichert, P., and Künsch, H. R. (2001). Practical identifiability analysis of large environmental simulation models. *Water Resour. Res.*, 37(4):1015–1030.
- Cameron, I. T. and Wang, F. Y. (2007). Process systems engineering applied to granulation. In A.D. Salman, M. J. H. and Seville, J. P. K., editors, *Handbook of Powder Technology*, volume Volume 11, chapter Chapter 11, pages 499–552. Elsevier Science B.V.
- Cameron, I. T. and Wang, F. Y. (2009). Granulation Process Modeling. In *Handbook of Pharmaceutical Granulation Technology*, chapter 24, pages 498–537. Informa Healthcare.
- Cameron, I. T., Wang, F. Y., Immanuel, C. D., and Stepanek, F. (2005). Process systems modelling and applications in granulation: A review. *Chem. Eng. Sci.*, 60(14):3723–3750.
- Camp, T. R. and Stein, P. C. (1943). Velocity gradients and internal work in fluid motion. *J. Boston Soc. Civ. Eng.*, 85:219–237.
- Cervera-Padrell, A. E., Skovby, T., Kiil, S., Gani, R., and Gernaey, K. V. (2012). Active pharmaceutical ingredient (API) production involving continuous processes - a process system engineering (PSE)-assisted design framework. *Eur. J. Pharm. Biopharm.*, 82(2):437–456.
- Chakraborty, J. and Kumar, S. (2007). A new framework for solution of multidimensional population balance equations. *Chem. Eng. Sci.*, 62(15):4112–4125.
- Chan, E. L., Reynolds, G. K., Gururajan, B., Hounslow, M. J., and Salman, A. D. (2013). Blade granule bed stress in a cylindrical high shear granulator: Online measurement and characterisation. *Chem. Eng. Sci.*, 86:38–49.
- Chan, L. W. and Heng, P. (2005). Drug substance and excipient characterization. *Handbook of Pharmaceutical Granulation Technology*, page 79.
- Chaudhury, A., Armenante, M. E., and Ramachandran, R. (2015). Compartment based population balance modeling of a high shear wet granulation process using data analytics. *Chemical Engineering Research and Design*, 95(0):211 – 228.
- Chialvo, S., Sun, J., and Sundaresan, S. (2012). Bridging the rheology of granular flows in three regimes. *Phys. Rev. E*, 85:021305.
- Chiruvella, R. V., Jaluria, Y., Karwe, M. V., and Sernas, V. (1996). Transport in a twin-screw extruder for the processing of polymers. *Polym. Eng. Sci.*, 36(11):1531–1540.
- CHMP (2012). Guideline on Real Time Release Testing (formerly Guideline on Parametric Release). Technical report, European Medicines Agency.
- Choi, Y. J., McCarthy, M. J., McCarthy, K. L., and Davis, C. A. (2004). MRI for process analysis: co-rotating twin screw extruder. *J. Process Anal. Chem.*, 9(2):72–84.
- Cleary, P. W. and Sinnott, M. D. (2008). Assessing mixing characteristics of particle-mixing and granulation devices. *Particuology*, 6(6):419–444.
- Cooley, J. W. and Tukey, J. W. (1965). An algorithm for the machine calculation of complex Fourier series. *Math. Comput.*, 19:297–301.
- Cryer, S. A. (1999). Modeling agglomeration processes in fluid-bed granulation. *AIChE J.*, 45(10):2069–2078.
- Cundall, P. A. and Strack, O. D. L. (1979). A discrete numerical model for granular assemblies. *Geotechnique*, 29(1):47–65.
- Darelius, A., Brage, H., Rasmuson, A., Bjorn, I. N., and Folestad, S. (2006). A volume-based multi-dimensional population balance approach for modelling high shear granulation. *Chem. Eng. Sci.*, 61(8):2482–2493.
- Darelius, A., Rasmuson, A., Björn, I. N., and Folestad, S. (2005). High shear wet granulation modelling - a mechanistic approach using population balances. *Powder Technol.*, 160(3):209–218.
- De Beer, T., Burggraave, A., Fonteyne, M., Saerens, L., Remon, J. P., and Vervaet, C. (2011). Near infrared and Raman spectroscopy for the in-process monitoring of pharmaceutical production processes. *Int. J. Pharm.*, 417(1-2):32–47.
- Dhanarajan, A. P. and Bandyopadhyay, R. (2007). An energy-based population-balance approach to model granule growth and breakage in high-shear wet granulation processes. *AAPS Pharm-SciTech*, 8(3):E66.
- Dhenge, R. M., Cartwright, J. J., Doughty, D. G., Hounslow, M. J., and Salman, A. D. (2011).

- Twin screw wet granulation: Effect of powder feed rate. *Adv. Powder Technol.*, 22(2):162 – 166.
- Dhenge, R. M., Cartwright, J. J., Hounslow, M. J., and Salman, A. D. (2012a). Twin screw granulation: Steps in granule growth. *Int. J. Pharm.*, 438(1-2):20–32.
- Dhenge, R. M., Cartwright, J. J., Hounslow, M. J., and Salman, A. D. (2012b). Twin screw wet granulation: Effects of properties of granulation liquid. *Powder Technol.*, 229:126–136.
- Dhenge, R. M., Fyles, R. S., Cartwright, J. J., Doughty, D. G., Hounslow, M. J., and Salman, A. D. (2010). Twin screw wet granulation: Granule properties. *Chem. Eng. J.*, 164(2-3):322–329. Pharmaceutical Granulation and Processing.
- Dhenge, R. M., Washino, K., Cartwright, J. J., Hounslow, M. J., and Salman, A. D. (2013). Twin screw granulation using conveying screws: Effects of viscosity of granulation liquids and flow of powders. *Powder Technol.*, 238:77–90.
- Diemer, R. and Olson, J. (2002). A moment methodology for coagulation and breakage problems: Part 3—generalized daughter distribution functions. *Chem. Eng. Sci.*, 57(19):4187–4198.
- Djuric, D. (2008). *Continuous granulation with a twin-screw extruder*. Cuvillier Verlag.
- Djuric, D., Van Melkebeke, B., Kleinebudde, P., Remon, J. P., and Vervaet, C. (2009). Comparison of two twin-screw extruders for continuous granulation. *Eur. J. Pharm. Biopharm.*, 71(1):155–160.
- Drumm, C., Attarakih, M. M., and Bart, H.-J. (2009). Coupling of CFD with DPBM for an RDC extractor. *Chem. Eng. Sci.*, 64(4):721–732.
- Efron, B. and Tibshirani, R. (1986). Bootstrap methods for standard errors, confidence intervals, and other measures of statistical accuracy. *Stat. Sci.*, 1(1):pp. 54–75.
- El Hagrasy, A. S., Cruise, P., Jones, I., and Litster, J. D. (2013a). In-line size monitoring of a twin screw granulation process using high-speed imaging. *J. Pharm. Innov.*, 8(2):90–98.
- El Hagrasy, A. S., Hennenkamp, J. R., Burke, M. D., Cartwright, J. J., and Litster, J. D. (2013b). Twin screw wet granulation: Influence of formulation parameters on granule properties and growth behavior. *Powder Technol.*, 238:108–115.
- El Hagrasy, A. S. and Litster, J. D. (2013). Granulation rate processes in the kneading elements of a twin screw granulator. *AIChE J.*, 59(11):4100–4115.
- Ennis, B. J. (2010). Theory of Granulation: An Engineering Perspective. In *Handbook of Pharmaceutical Granulation Technology*, pages 6–58.
- Eriksson, L. (2008). *Design of Experiments: Principles and Applications*. Umetrics.
- Eriksson, L., Johansson, E., Kettaneh-Wold, N., Wikström, C., and Wold, S. (2000). *Design of Experiments -Principles and Applications*. Umetrics Academy.
- Faure, A., Grimsey, I. M., Rowe, R. C., York, P., and Cliff, M. J. (1999). Process control in a high shear mixer- granulator using wet mass consistency: The effect of formulation variables. *J. Pharm. Sci.*, 88(2):191–195.
- FDA, U. (2004). PAT Guidance for Industry - Framework for Innovative Pharmaceutical Development, Manufacturing and Quality Assurance. Technical report.
- Fogler, H. (2006). *Elements Of Chemical Reaction Engineering*. Pearson international edition. Prentice Hall Professional Technical Reference.
- Fonteyne, M. (2014). *Development and validation of process analytical methods for a continuous pharmaceutical manufacturing process of tablets based on wet granulation*. PhD thesis, Ghent University.
- Fonteyne, M., Soares, S., Vercruyse, J., Peeters, E., Burggraeve, A., Vervaet, C., Remon, J. P., Sandler, N., and De Beer, T. (2012). Prediction of quality attributes of continuously produced granules using complementary pat tools. *Eur. J. Pharm. Biopharm.*, 82(2):429–436.
- Fonteyne, M., Vercruyse, J., Diaz, D. C., Gildemyn, D., Vervaet, C., Remon, J. P., and De Beer, T. (2013). Real-time assessment of critical quality attributes of a continuous granulation process. *Pharm. Dev. Technol.*, 18(1):85–97.
- Fonteyne, M., Vercruyse, J., Leersnyder, F. D., Snick, B. V., Vervaet, C., Remon, J. P., and Beer, T. D. (2015). Process analytical technology for continuous manufacturing of solid-dosage forms. *TrAC Trends in Analytical Chemistry*, 67(0):159 – 166.
- Fonteyne, M., Wickström, H., Peeters, E., Vercruyse, J., Ehlers, H., Peters, B.-H., Remon, J. P., Vervaet, C., Ketolainen, J., Sandler, N., Rantanen, J., Naelapää, K., and De Beer, T. (2014). Influence of raw material properties upon critical quality attributes of continuously produced granules and tablets. *Eur. J. Pharm. Biopharm.*, 87(2):252 – 263.
- Freireich, B., Li, J., Litster, J., and Wassgren, C. (2011). Incorporating particle flow information from discrete element simulations in population balance models of mixer-coaters. *Chem. Eng. Sci.*, 66(16):3592–3604.
- Fries, L., Antonyuk, S., Heinrich, S., Dopfer, D., and Palzer, S. (2013). Collision dynamics in fluidised bed granulators: A DEM-CFD study. *Chem. Eng. Sci.*, 86:108–123.

- Fukushima, E. (1999). Nuclear magnetic resonance as a tool to study flow. *Annu. Rev. Fluid Mech.*, 31(1):95–123.
- Gantt, J. A., Cameron, I. T., Litster, J. D., and Gatzke, E. P. (2006). Determination of coalescence kernels for high-shear granulation using DEM simulations. *Powder Technol.*, 170(2):53–63.
- Gantt, J. A. and Gatzke, E. P. (2005). High-shear granulation modeling using a discrete element simulation approach. *Powder Technol.*, 156(2-3):195–212.
- Gao, Y., Muzzio, F. J., and Ierapetritou, M. G. (2012). A review of the Residence Time Distribution (RTD) applications in solid unit operations. *Powder Technol.*, 228:416–423.
- Gao, Y., Vanarase, A., Muzzio, F., and Ierapetritou, M. (2011). Characterizing continuous powder mixing using residence time distribution. *Chem. Eng. Sci.*, 66(3):417–425.
- Garth, C., Middel, A., and Hagen, H. (2011). CFD Simulation of Liquid-Liquid Extraction Columns and Visualization of Eulerian Datasets. In *Visualization of Large and Unstructured Data Sets: Applications in Geospatial Planning, Modeling and Engineering-Proceedings of IRTG 1131 Workshop 2011*, volume 27, pages 59–70. Schloss Dagstuhl–Leibniz-Zentrum fuer Informatik.
- Gautam, A. and Choudhury, G. S. (1999). Screw configuration effects on residence time distribution and mixing in twin-screw extruders during extrusion of rice flour. *J. Food Process Eng.*, 22(4):263–285.
- Gernaey, K. V., Cervera-Padrell, A. E., and Woodley, J. M. (2012). A perspective on PSE in pharmaceutical process development and innovation. *Comput. Chem. Eng.*, 42:15–29.
- Gernaey, K. V. and Gani, R. (2010). A model-based systems approach to pharmaceutical product-process design and analysis. *Chem. Eng. Sci.*, 65(21):5757–5769.
- Ghebre-Selassie, I. and Martin, C. (2003). *Pharmaceutical extrusion technology*, volume 133. CRC Press.
- Gimbun, J., Nagy, Z. K., and Rielly, C. D. (2009). Simultaneous quadrature method of moments for the solution of population balance equations, using a differential algebraic equation framework. *Ind. Eng. Chem. Res.*, 48(16):7798–7812.
- Goldschmidt, M. J. V. (2001). *Hydrodynamic modelling of fluidised bed spray granulation*. PhD thesis.
- Goldschmidt, M. J. V., Weijers, G. G. C., Boerefijn, R., and Kuipers, J. A. M. (2003). Discrete element modelling of fluidised bed spray granulation. *Powder Technol.*, 138(1):39–45.
- González-Montellano, C., Ramirez, A., Gallego, E., and Ayuga, F. (2011). Validation and experimental calibration of 3D discrete element models for the simulation of the discharge flow in silos. *Chem. Eng. Sci.*, 66(21):5116–5126.
- Guida, A., Nienow, A. W., and Barigou, M. (2010). Shannon entropy for local and global description of mixing by lagrangian particle tracking. *Chem. Eng. Sci.*, 65(10):2865–2883.
- Guideline, I. H. T. (2006). Guidance for Industry: Q10 quality systems approach to pharmaceutical CGMP regulations. Technical report, ICH Expert Working Group.
- Guideline, ICH Harmonised Tripartite (2005). Quality Risk Management. Technical report, ICH Expert Working Group.
- Guideline, ICH Harmonised Tripartite (2012). Development and Manufacture of Drug Substances. Technical report, ICH Expert Working Group.
- Guo, Z., Ma, M., Wang, T., Chang, D., Jiang, T., and Wang, S. (2011). A Kinetic Study of the Polymorphic Transformation of Nimodipine and Indomethacin during High Shear Granulation. *AAPS PharmSciTech*, 12(2):610–619.
- Hansuld, E. M., Briens, L., Sayani, A., and McCann, J. A. B. (2012). Monitoring quality attributes for high-shear wet granulation with audible acoustic emissions. *Powder Technol.*, 215-216:117–123.
- Hapgood, K. P., Litster, J. D., and Smith, R. (2003). Nucleation regime map for liquid bound granules. *AIChE J.*, 49(2):350–361.
- Hassanpour, A., Pasha, M., Susana, L., Rahmanian, N., Santomaso, A. C., and Ghadiri, M. (2013). Analysis of seeded granulation in high shear granulators by discrete element method. *Powder Technol.*, 238:50–55. Special Issue: 5th International Granulation Workshop Granulation across the length scale 2011.
- Heinrich, S., Peglow, M., Ihlow, M., Henneberg, M., and Mörl, L. (2002). Analysis of the start-up process in continuous fluidized bed spray granulation by population balance modelling. *Chem. Eng. Sci.*, 57(20):4369–4390.
- Herrmann, H. J. and Luding, S. (1998). Modeling granular media on the computer. *Continuum Mech. Therm.*, 10(4):189–231.
- Hill, P. J. and Ng, K. M. (1995). New discretization procedure for the breakage equation. *AIChE J.*, 41(5):1204–1216.
- Horsthuis, G., Vanlaarhoven, J., Vanrooij, R., and Vromans, H. (1993). Studies on upscaling parameters of the Gral high shear granulation process. *Int. J. Pharm.*, 92(1-3):143–150.

- Hounslow, M. J. (1990). A Discretized Population Balance for Continuous Systems at Steady-State. *AIChE J.*, 36(1):106–116.
- Hounslow, M. J. (1998). The population balance as a tool for understanding particle rate processes. *Kona*, 16:179–193.
- Hounslow, M. J., Pearson, J. M. K., and Instone, T. (2001). Tracer studies of high-shear granulation: II. Population balance modeling. *AIChE J.*, 47(9):1984–1999.
- Huang, J., Kaul, G., Utz, J., Hernandez, P., Wong, V., Bradley, D., Nagi, A., and O’Grady, D. (2010). A PAT approach to improve process understanding of high shear wet granulation through in-line particle measurement using FBRM C35. *J. Pharm. Sci.*, 99(7):3205–3212.
- ICH Harmonised Tripartite Guideline (2009). Pharmaceutical development, Q8 (R2). Technical report, Maryland: ICH, Federal Register.
- Immanuel, C. D. and Doyle, F. J. (2003). Computationally efficient solution of population balance models incorporating nucleation, growth and coagulation: application to emulsion polymerization. *Chem. Eng. Sci.*, 58(16):3681–3698.
- Immanuel, C. D. and Doyle, F. J. (2005). Solution technique for a multi-dimensional population balance model describing granulation processes. *Powder Technol.*, 156(2-3):213–225.
- Ingram, G. D. and Cameron, I. T. (2005). Formulation and comparison of alternative multiscale models for drum granulation. *Comput. Aided Chem. Eng.*, 20:481–486.
- Ingram, G. D. and Cameron, I. T. (2010). Dynamic Multiscale Modeling - An Application to Granulation Processes. In *Process Systems Engineering*, pages 35–65. Wiley-VCH Verlag GmbH & Co. KGaA.
- Ingram, G. D., Cameron, I. T., and Hangos, K. M. (2004). Classification and analysis of integrating frameworks in multiscale modelling. *Chem. Eng. Sci.*, 59(11):2171–2187.
- Iveson, S. M., Litster, J. D., Hapgood, K., and Ennis, B. J. (2001a). Nucleation, growth and breakage phenomena in agitated wet granulation processes: a review. *Powder Technol.*, 117(1):3–39.
- Iveson, S. M., Wauters, P. A., Forrest, S., Litster, J. D., Meesters, G. M., and Scarlett, B. (2001b). Growth regime map for liquid-bound granules: further development and experimental validation. *Powder Technol.*, 117(1):83 – 97. Granulation and Coating of Fine Powders.
- Jones, E., Oliphant, T., Peterson, P., et al. (2001). SciPy: Open source scientific tools for Python. [Online; accessed 2014-06-29].
- Jørgensen, A. C. et al. (2004). *Increasing process understanding of wet granulation by spectroscopic methods and dimension reduction tools*. University of Helsinki.
- Kadlec, P., Gabrys, B., and Strandt, S. (2009). Data-driven Soft Sensors in the process industry. *Comput. Chem. Eng.*, 33(4):795–814.
- Kapur, P. C. (1972). Kinetics of granulation by non-random coalescence mechanism. *Chem. Eng. Sci.*, 27(10):1863–1869.
- Kapur, P. C. and Fuerstenau, D. W. (1969). A Coalescence Model for Granulation. *Ind Eng Chem, Process Des Dev*, 8(1):56–61.
- Kariwala, V., Cao, Y., and Nagy, Z. K. (2012). Automatic differentiation-based quadrature method of moments for solving population balance equations. *AIChE J.*, 58(3):842–854.
- Kayrak-Talay, D., Dale, S., Wassgren, C., and Litster, J. (2012). Quality by design for wet granulation in pharmaceutical processing: Assessing models for a priori design and scaling. *Powder Technol.*
- Ketterhagen, W. R., am Ende, M. T., and Hancock, B. C. (2009). Process modeling in the pharmaceutical industry using the discrete element method. *J. Pharm. Sci.*, 98(2):442–470.
- Kloss, C., Goniva, C., Hager, A., Amberger, S., and Pirker, S. (2012). Models, algorithms and validation for opensource dem and cfd-dem. *Progress in Computational Fluid Dynamics, an International Journal*, 12(2-3):140–152.
- Kohlgrüber, K. and Bierdel, M. (2008). *Co-rotating twin-screw extruders: fundamentals, technology, and applications*. Hanser Verlag.
- Koren, B. (1993). *A robust upwind discretization method for advection, diffusion and source terms*. Centrum voor Wiskunde en Informatica Amsterdam.
- Kostoglou, M. (2003). Exact self-similar solutions to the fragmentation equation with homogeneous discrete kernel. *Phys. A*, 320:84–96.
- Kostoglou, M. (2007). Chapter 18 The Linear Breakage Equation: From Fundamental Issues to Numerical Solution Techniques. In Agba D. Salman, M. G. and Michael, J. H., editors, *Handbook of Powder Technology*, volume Volume 12, pages 793–835. Elsevier Science B.V.
- Kostoglou, M. and Karabelas, A. J. (1998). Theoretical analysis of the steady state particle size distribution in limited breakage processes. *Phys. A*, 31(44):8905–8921.
- Kostoglou, M. and Karabelas, A. J. (2001). On the breakage problem with a homogeneous erosion type kernel. *Phys. A*, 34(8):1725–1740.
- Kumar, A., Ganjyal, G. M., Jones, D. D., and Hanna, M. A. (2008a). Modeling residence time

- distribution in a twin-screw extruder as a series of ideal steady-state flow reactors. *Journal of Food Engineering*, 84(3):441 – 448.
- Kumar, A., Gernaey, K. V., De Beer, T., and Nopens, I. (2013a). Model-based analysis of high shear wet granulation from batch to continuous processes in pharmaceutical production – a critical review. *Eur. J. Pharm. Biopharm.*, 85(3, Part B):814 – 832.
- Kumar, A., Gernaey, K. V., De Beer, T., and Nopens, I. (2013b). One dimensional model of the prediction of residence time distribution granulation in a twin-screw granulator. In *6th International Granulation Workshop*.
- Kumar, A., Vercruysee, J., Bellandi, G., Gernaey, K. V., Vervaet, C., Remon, J. P., Beer, T. D., and Nopens, I. (2014a). Experimental investigation of granule size and shape dynamics in twin-screw granulation. *Int. J. Pharm.*, 475(1-2):485 – 495.
- Kumar, A., Vercruysee, J., Toiviainen, M., Panouillot, P.-E., Juuti, M., Vanhoorne, V., Vervaet, C., Remon, J. P., Gernaey, K. V., De Beer, T., and Nopens, I. (2014b). Mixing and transport during pharmaceutical twin-screw wet granulation: Experimental analysis via chemical imaging. *Eur. J. Pharm. Biopharm.*, 87(2):279 – 289.
- Kumar, A., Vercruysee, J., Vanhoorne, V., Toiviainen, M., Panouillot, P.-E., Juuti, M., Vervaet, C., Remon, J. P., Gernaey, K. V., De Beer, T., and Nopens, I. (2015). Conceptual framework for model-based analysis of residence time distribution in twin-screw granulation. *Eur. J. Pharm. Sci.*, 71(0):25 – 34.
- Kumar, J., Peglow, M., Warnecke, G., and Heinrich, S. (2008b). An efficient numerical technique for solving population balance equation involving aggregation, breakage, growth and nucleation. *Powder Technol.*, 182(1):81–104.
- Kumar, J., Peglow, M., Warnecke, G., Heinrich, S., and Morl, L. (2006). Improved accuracy and convergence of discretized population balance for aggregation: The cell average technique. *Chem. Eng. Sci.*, 61(10):3327–3342.
- Kumar, J., Warnecke, G., Peglow, M., and Heinrich, S. (2009). Comparison of numerical methods for solving population balance equations incorporating aggregation and breakage. *Powder Technol.*, 189(2):218–229.
- Kumar, R., Kumar, J., and Warnecke, G. (2011). Numerical methods for solving two-dimensional aggregation population balance equations. *Comput. Chem. Eng.*, 35(6):999–1009.
- Kumar, S. and Ramkrishna, D. (1996a). On the solution of population balance equations by discretization-I. A fixed pivot technique. *Chem. Eng. Sci.*, 51(8):1311–1332.
- Kumar, S. and Ramkrishna, D. (1996b). On the solution of population balance equations by discretization-II. A moving pivot technique. *Chem. Eng. Sci.*, 51(8):1333–1342.
- Kumar, S. and Ramkrishna, D. (1997). On the solution of population balance equations by discretization-III. Nucleation, growth and aggregation of particles. *Chem. Eng. Sci.*, 52(24):4659–4679.
- Kurganov, A. and Tadmor, E. (2000). New high-resolution central schemes for nonlinear conservation laws and convection-diffusion equations. *J. Comput. Phys.*, 160(1):241–282.
- Langtangen, H. P. and Wang, L. (2014). Odespy software package. <https://github.com/hplgit/odespy>.
- Laurent, B. F. C. (2005). Structure of powder flow in a planetary mixer during wet-mass granulation. *Chem. Eng. Sci.*, 60(14):3805–3816.
- Lee, K., Lee, J. H., Yang, D. R., and Mahoney, A. W. (2002). Integrated run-to-run and on-line model-based control of particle size distribution for a semi-batch precipitation reactor. *Comput. Chem. Eng.*, 26(7-8):1117–1131.
- Lee, K. T. (2013). *Continuous granulation of pharmaceutical powder using a twin screw granulator*. PhD thesis, University of Birmingham.
- Lee, K. T., Ingram, A., and Rowson, N. A. (2012). Twin screw wet granulation: the study of a continuous twin screw granulator using Positron Emission Particle Tracking (PEPT) technique. *Eur. J. Pharm. Biopharm.*, 81(3):666–73.
- Lee, K. T., Ingram, A., and Rowson, N. A. (2013). Comparison of granule properties produced using Twin Screw Extruder and High Shear Mixer: A step towards understanding the mechanism of twin screw wet granulation. *Powder Technol.*, 238:91–98.
- Lee, S. M., Park, J. C., Ahn, Y. J., and Lee, J. W. (2005). In-line measurement of residence time distribution in twin-screw extruder using non-destructive ultrasound. *Korea-Aust. Rheol. J.*, 17(2):87–95.
- Lees, A. and Edwards, S. (1972). The computer study of transport processes under extreme conditions. *J. Phy. C*, 5(15):1921.
- Levenspiel, O. (1999). *Chemical Reaction Engineering, 3rd Edition*. John Wiley & Sons.
- Li, H., Thompson, M., and O'Donnell, K. (2014). Understanding wet granulation in the kneading block of twin screw extruders. *Chem. Eng. Sci.*, 113(0):11 – 21.

- Li, J., Freireich, B., Wassgren, C., and Litster, J. D. (2012). A general compartment-based population balance model for particle coating and layered granulation. *AIChE J.*, 58(5):1397–1408.
- Li, J., Tao, L., Dali, M., Buckley, D., Gao, J., and Hubert, M. (2011). The effect of the physical states of binders on high-shear wet granulation and granule properties: A mechanistic approach toward understanding high-shear wet granulation process. part ii. granulation and granule properties. *J. Pharm. Sci.*, 100(1):294–310.
- Lian, G. P., Thornton, C., and Adams, M. J. (1998). Discrete particle simulation of agglomerate impact coalescence. *Chem. Eng. Sci.*, 53(19):3381–3391.
- Litster, J. and Ennis, B. (2004). *The science and engineering of granulation processes*, volume 15. Springer.
- Liu, L. and Litster, J. (2002). Population balance modelling of granulation with a physically based coalescence kernel. *Chem. Eng. Sci.*, 57(12):2183–2191.
- Liu, P. Y., Yang, R. Y., and Yu, A. B. (2013). DEM study of the transverse mixing of wet particles in rotating drums. *Chem. Eng. Sci.*, 86:99–107.
- Luding, S. (1998). Collisions & contacts between two particles. In *Physics of dry granular media*, pages 285–304. Springer.
- Luukkonen, P., Newton, J., Podczeczek, F., and Yliruusi, J. (2001). Use of a capillary rheometer to evaluate the rheological properties of microcrystalline cellulose and silicified microcrystalline cellulose wet masses. *Int. J. Pharm.*, 216(1-2):147–157.
- Maded, L., Falk, L., and Plasari, E. (2003). Modelling of the agglomeration in suspension process with multidimensional kernels. *Powder Technol.*, 130(1-3):147–153.
- Majumder, A., Kariwala, V., Ansumali, S., and Rajendran, A. (2012). Lattice Boltzmann method for population balance equations with simultaneous growth, nucleation, aggregation and breakage. *Chem. Eng. Sci.*, 69(1):316–328.
- Marchisio, D. L. and Fox, R. O. (2005). Solution of population balance equations using the direct quadrature method of moments. *J. Aerosol Sci.*, 36(1):43–73.
- Marchisio, D. L., Vigil, R. D., and Fox, R. O. (2003). Quadrature method of moments for aggregation-breakage processes. *J. Colloid Interface Sci.*, 258(2):322–334.
- Marigo, M., Davies, M., Leadbeater, T., Cairns, D., Ingram, A., and Stitt, E. (2013). Application of positron emission particle tracking (pept) to validate a discrete element method (DEM) model of granular flow and mixing in the turbula mixer. *Int. J. Pharm.*, 446(1–2):46–58.
- Marshall, C. L., Rajniak, P., and Matsoukas, T. (2011). Numerical simulations of two-component granulation: Comparison of three methods. *Chem. Eng. Res. Des.*, 89(5):545–552.
- Marshall, C. L., Rajniak, P., and Matsoukas, T. (2013). Multi-component population balance modeling of granulation with continuous addition of binder. *Powder Technol.*, 236:211–220.
- McCarthy, J. (2003). Micro-modeling of cohesive mixing processes. *Powder Technol.*, 138(1):63 – 67. World Congress of Particle Technology.
- Meier, R., Thommes, M., Rasenack, N., Krumme, M., Moll, K.-P., and Kleinebudde, P. (2015). Simplified formulations with high drug loads for continuous twin-screw granulation. *Int. J. Pharm.*, (0):-.
- Michaels, J. N., Farber, L., Wong, G. S., Hapgood, K., Heidell, S. J., Farabaugh, J., Chou, J. H., and Tardos, G. I. (2009). Steady states in granulation of pharmaceutical powders with application to scale-up. *Powder Technol.*, 189(2):295–303.
- Mikami, T., Kamiya, H., and Horio, M. (1998). Numerical simulation of cohesive powder behavior in a fluidized bed. *Chem. Eng. Sci.*, 53(10):1927 – 1940.
- Mishra, B. K., Thornton, C., and Bhimji, D. (2002). A preliminary numerical investigation of agglomeration in a rotary drum. *Miner. Eng.*, 15(1-2):27–33.
- Mohan, B., Kloss, C., Khinast, J., and Radl, S. (2014). Regimes of liquid transport through sheared beds of inertial smooth particles. *Powder Technol.*, 264(0):377 – 395.
- Moreno-Atanasio, R., Antony, S., and Ghadiri, M. (2005). Analysis of flowability of cohesive powders using distinct element method. *Powder Technol.*, 158(1–3):51–57.
- Mortier, S. (2014). *Modelling the drying behaviour of wet granules in the context of fully continuous pharmaceutical tablet manufacturing*. PhD thesis, Ghent University.
- Muguruma, Y., Tanaka, T., and Tsuji, Y. (2000). Numerical simulation of particulate flow with liquid bridge between particles (simulation of centrifugal tumbling granulator). *Powder Technol.*, 109(1-3):49–57.
- Naik, S. and Chaudhuri, B. (2015). Quantifying dry milling in pharmaceutical processing: A review on experimental and modeling approaches. *J. Pharma. Sci.*, 104(8):2401–2413.
- Nakamura, H., Fujii, H., and Watano, S. (2013). Scale-up of high shear mixer-granulator based on discrete element analysis. *Powder Technol.*, 236:149–156.
- Nandanwar, M. N. and Kumar, S. (2008). A new discretization of space for the solution of multi-dimensional population balance equations. *Chem. Eng. Sci.*, 63(8):2198–2210.



- Nelder, J. A. and Mead, R. (1965). A simplex method for function minimization. *Comput. J.*, 7(4):308–313.
- Nilpawar, A. M., Reynolds, G. K., Salman, A. D., and Hounslow, M. J. (2006). Surface velocity measurement in a high shear mixer. *Chem. Eng. Sci.*, 61(13):4172–4178.
- Oliphant, T. E. (2007). Python for scientific computing. *Comp. Sci. Eng.*, 9(3):10–20.
- Paavola, M. K., El Hagrasy, A. S., Litster, J. D., and J. L. K. (2013). 3D population balance model for continuous twin screw granulator. 32:2077–2082.
- Pandya, J. D. and Spielman, L. A. (1983). Floc Breakage in Agitated Suspensions - Effect of Agitation Rate. *Chem. Eng. Sci.*, 38(12):1983–1992.
- Perkins, M., Ebbens, S. J., Hayes, S., Roberts, C. J., Madden, C. E., Luk, S. Y., and Patel, N. (2007). Elastic modulus measurements from individual lactose particles using atomic force microscopy. *Int. J. Pharm.*, 332(1–2):168 – 175.
- Pinto, M. A., Immanuel, C. D., and Doyle, F. J. (2007). A feasible solution technique for higher-dimensional population balance models. *Comput. Chem. Eng.*, 31(10):1242–1256.
- PIV Drives GmbH (2014). Gearboxes and drive packages for extrusion, compounding and injection moulding machines.
- Pohlman, D. A. and Litster, J. D. (2015). Coalescence model for induction growth behavior in high shear granulation. *Powder Technol.*, 270, Part B(0):435 – 444. 6th International Workshop on Granulation: Granulation across the length scales.
- Poon, J. M.-H., Ramachandran, R., Sanders, C. F., Glaser, T., Immanuel, C. D., III, F. J. D., Litster, J. D., Stepanek, F., Wang, F.-Y., and Cameron, I. T. (2009). Experimental validation studies on a multi-dimensional and multi-scale population balance model of batch granulation. *Chemical Engineering Science*, 64(4):775–786. 3rd International Conference on Population Balance Modelling.
- Propst, C. W. (2009). *Granulation Characterization*, chapter 22, pages 469–486. 3rd editio edition.
- Puaux, J., Bozga, G., and Ainsler, A. (2000). Residence time distribution in a corotating twin-screw extruder. *Chemical Engineering Science*, 55(9):1641 – 1651.
- Qamar, S. and Warnecke, G. (2007). Numerical solution of population balance equations for nucleation, growth and aggregation processes. *Comput. Chem. Eng.*, 31(12):1576–1589.
- Rajniak, P., Stepanek, F., Dhanasekharan, K., Fan, R., Mancinelli, C., and Chern, R. (2009). A combined experimental and computational study of wet granulation in a wurster fluid bed granulator. *Powder Technol.*, 189(2):190–201.
- Ramachandran, R. and Barton, P. I. (2010). Effective parameter estimation within a multi-dimensional population balance model framework. *Chem. Eng. Sci.*, 65(16):4884–4893.
- Ramachandran, R., Immanuel, C. D., Stepanek, F., Litster, J. D., and Doyle, F. J. (2009). A mechanistic model for breakage in population balances of granulation: Theoretical kernel development and experimental validation. *Chem. Eng. Res. Des.*, 87(4A):598–614.
- Ramkrishna, D. (2000). *Population balances: Theory and applications to particulate systems in engineering*. Academic press.
- Rantanen, J., Wikström, H. k., Turner, R., and Taylor, L. S. (2004). Use of In-Line Near-Infrared Spectroscopy in Combination with Chemometrics for Improved Understanding of Pharmaceutical Processes. *Anal. Chem.*, 77(2):556–563.
- Rao, N. N. (2009). *Simulations for modelling of population balance equations of particulate processes using the discrete particle model (DPM)*. PhD thesis, Otto-von-Guericke-Universität Magdeburg, Universitätsbibliothek.
- Reinhold, A. and Briesen, H. (2012). Numerical behavior of a multiscale aggregation models - coupling population balances and discrete element models. *Chemical Engineering Science*, 70(0):165 – 175. 4th International Conference on Population Balance Modeling.
- Reynolds, G. K., Fu, J. S., Cheong, Y. S., Hounslow, M., and Salman, A. D. (2005). Breakage in granulation: A review. *Chem. Eng. Sci.*, 60(14):3969–3992.
- Reynolds, G. K., Le, P. K., and Nilpawar, A. M. (2007). Chapter 1 High shear granulation. In A.D. Salman, M J Hounslow and Seville, J P K, editor, *Handbook of Powder Technology*, volume 11, chapter 1, pages 3–19. Elsevier Science B.V.
- Rimpiläinen, V., Poutiainen, S., Heikkinen, L. M., Savolainen, T., Vauhkonen, M., and Ketolainen, J. (2011). Electrical capacitance tomography as a monitoring tool for high-shear mixing and granulation. *Chem. Eng. Sci.*, 66(18):4090–4100.
- Roggo, Y., Chalus, P., Maurer, L., Lema-Martinez, C., Edmond, A. A., and Jent, N. (2007). A review of near infrared spectroscopy and chemometrics in pharmaceutical technologies. *J. Pharm. Biomed. Anal.*, 44(3):683–700.
- Rough, S., Wilson, D., and York, D. (2005). A regime map for stages in high shear mixer agglomeration using ultra-high viscosity binders. *Adv. Powder Technol.*, 16(4):373 – 386.
- Rowe, R., Sheskey, P., Quinn, M., and Association, A. P. (2009). *Handbook of Pharmaceutical*

- Excipients*. Rowe, Handbook of Pharmaceutical Excipients. Pharmaceutical Press.
- Sakellariou, A., Sawkins, T., Senden, T., and Limaye, A. (2004). X-ray tomography for mesoscale physics applications. *Phys. Stat. Mech. Appl.*, 339(1-2):152–158.
- Sakr, W. F., Ibrahim, M. A., Alanazi, F. K., and Sakr, A. A. (2012). Upgrading wet granulation monitoring from hand squeeze test to mixing torque rheometry. *Saudi Pharm. J.*, 20(1):9–19.
- Sanders, C. F. W., Hounslow, M. J., and Doyle, F. J. (2009). Identification of models for control of wet granulation. *Powder Technol.*, 188(3):255–263.
- Sanders, C. F. W., Willemse, A. W., Salman, A. D., and Hounslow, M. J. (2003). Development of a predictive high-shear granulation model. *Powder Technol.*, 138(1):18–24.
- Sandler, N. and Wilson, D. (2010). Prediction of granule packing and flow behavior based on particle size and shape analysis. *J. Pharm. Sci.*, 99(2):958–968.
- Sarkar, A. and Wassgren, C. R. (2009). Simulation of a continuous granular mixer: Effect of operating conditions on flow and mixing. *Chem. Eng. Sci.*, 64(11):2672–2682.
- Sastry, K. V. S. (1975). Similarity size distribution of agglomerates during their growth by coalescence in granulation or green pelletization. *Int. J. Miner. Process.*, 2(2):187–203.
- Sathyagal, A. N., Ramkrishna, D., and Narsimhan, G. (1995). Solution of inverse problems in population balances-II. Particle break-up. *Comput. Chem. Eng.*, 19(4):437–451.
- Sato, A., Serris, E., Grosseau, P., Thomas, G., Galet, L., Chamayou, A., and Baron, M. (2013). Experiment and simulation of dry particle coating. *Chemical Engineering Science*, 86:164–172. 5th International Granulation Workshop.
- Sato, Y., Nakamura, H., and Watano, S. (2008). Numerical analysis of agitation torque and particle motion in a high shear mixer. *Powder Technol.*, 186(2):130–136.
- Sayin, R., Hagrasy, A. E., and Litster, J. (2015). Distributive mixing elements: Towards improved granule attributes from a twin screw granulation process. *Chemical Engineering Science*, 125(0):165 – 175. Pharmaceutical Particles and Processing.
- Schaber, S. D., Gerogiorgis, D. I., Ramachandran, R., Evans, J. M. B., Barton, P. I., and Trout, B. L. (2011). Economic analysis of integrated continuous and batch pharmaceutical manufacturing: A case study. *Ind. Eng. Chem. Res.*, 50(17):10083–10092.
- Seem, T. C., Rowson, N. A., Ingram, A., Huang, Z., Yu, S., de Matas, M., Gabbott, I., and Reynolds, G. K. (2015). Twin screw granulation – a literature review. *Powder Technol.*, 276(0):89 – 102.
- Sen, M., Barrasso, D., Singh, R., and Ramachandran, R. (2014). A multi-scale hybrid cfd-dem-pbm description of a fluid-bed granulation process. *Processes*, 2(1):89–111.
- Sen, M., Dubey, A., Singh, R., and Ramachandran, R. (2012a). Mathematical development and comparison of a hybrid PBM-DEM description of a continuous powder mixing process. *J. Powder Technol.*, 2013.
- Sen, M., Singh, R., Vanarase, A., John, J., and Ramachandran, R. (2012b). Multi-dimensional population balance modeling and experimental validation of continuous powder mixing processes. *Chem. Eng. Sci.*, 80:349–360.
- Sibson, R. (1981). A brief description of natural neighbour interpolation. *Interpreting multivariate data*, 21.
- Smith, M. and Matsoukas, T. (1998). Constant-number Monte Carlo simulation of population balances. *Chem. Eng. Sci.*, 53(9):1777–1786.
- Sochon, R. P., Zomer, S., Cartwright, J. J., Hounslow, M. J., and Salman, A. D. (2010). The variability of pharmaceutical granulation. *Chem. Eng. J.*, 164(2 - 3):285 – 291. Pharmaceutical Granulation and Processing.
- Spielman, L. A. and Levenspiel, O. (1965). A Monte Carlo treatment for reacting and coalescing dispersed phase systems. *Chem. Eng. Sci.*, 20(3):247–254.
- Štěpánek, F., Rajniak, P., Mancinelli, C., Chern, R., and Ramachandran, R. (2009). Distribution and accessibility of binder in wet granules. *Powder Technol.*, 189(2):376–384.
- Tackenberg, M. W., Krauss, R., Marmann, A., Thommes, M., Schuchmann, H. P., and Kleinebudde, P. (2015). Encapsulation of liquids using a counter rotating twin screw extruder. *Eur. J. Pharm. Biopharm.*, 89(0):9 – 17.
- Talu, I., Tardos, G. I., and Khan, M. I. (2000). Computer simulation of wet granulation. *Powder Technol.*, 110(1-2):59–75.
- Thielmann, F., Naderi, M., Ansari, M. A., and Stepanek, F. (2008). The effect of primary particle surface energy on agglomeration rate in fluidised bed wet granulation. *Powder Technol.*, 181(2):160–168. Particulate Processes in the Pharmaceutical Industry.
- Thompson, M. R. (2015). Twin screw granulation – review of current progress. *Drug Dev. Ind. Pharm.*, 0(0):1–9. PMID: 25402966.
- Thompson, M. R. and Sun, J. (2010). Wet granulation in a twin-screw extruder: Implications of screw design. *J. Pharm. Sci.*, 99(4):2090–2103.

- Tishmack, P. A., Bugay, D. E., and Byrn, S. R. (2003). Solid-state nuclear magnetic resonance spectroscopy—pharmaceutical applications. *J. Pharm. Sci.*, 92(3):441–74.
- Tu, W.-D., Ingram, A., and Seville, J. (2013). Regime map development for continuous twin screw granulation. *Chem. Eng. Sci.*, 87:315–326.
- Tu, W.-D., Ingram, A., Seville, J., and Hsiau, S.-S. (2009). Exploring the regime map for high-shear mixer granulation. *Chem. Eng. J.*, 145(3):505 – 513.
- Vale, H. M. and McKenna, T. F. (2005). Solution of the population balance equation for two-component aggregation by an extended fixed pivot technique. *Ind. Eng. Chem. Res.*, 44(20):7885–7891.
- Van Melkebeke, B. (2009). *Development and evaluation of a continuous granulation technique using a twin-screw extruder*. PhD thesis, Ghent University.
- Van Melkebeke, B., Vervaet, C., and Remon, J. P. (2008). Validation of a continuous granulation process using a twin-screw extruder. *Int. J. Pharm.*, 356(1-2):224–230.
- Vercruyssen, J. (2014). *Innovation in pharmaceutical manufacturing of solid dosage forms via continuous wet granulation*. PhD thesis, Ghent University.
- Vercruyssen, J., Burggraeve, A., Fonteyne, M., Cappuyns, P., Delaet, U., Assche, I. V., Beer, T. D., Remon, J., and Vervaet, C. (2015). Impact of screw configuration on the particle size distribution of granules produced by twin screw granulation. *Int. J. Pharm.*, 479(1):171 – 180.
- Vercruyssen, J., Córdoba Díaz, D., Peeters, E., Fonteyne, M., Delaet, U., Van Assche, I., De Beer, T., Remon, J. P., and Vervaet, C. (2012). Continuous twin screw granulation: Influence of process variables on granule and tablet quality. *Eur. J. Pharm. Biopharm.*, 82(1):205–211.
- Vercruyssen, J., Delaet, U., Assche, I. V., Cappuyns, P., Arata, F., Caporicci, G., Beer, T. D., Remon, J., and Vervaet, C. (2013a). Stability and repeatability of a continuous twin screw granulation and drying system. *Eur. J. Pharm. Biopharm.*, 85(3, Part B):1031 – 1038.
- Vercruyssen, J., Toiviainen, M., Fonteyne, M., Helkimo, N., Ketolainen, J., Juuti, M., Delaet, U., Assche, I. V., Remon, J. P., Vervaet, C., and De Beer, T. (2013b). Visualization and understanding of the granulation liquid mixing and distribution during continuous twin screw granulation using NIR chemical imaging. *Eur. J. Pharm. Biopharm.*, 86(3):383–392.
- Verkoefen, D., A. Pouw, G., M. H. Meesters, G., and Scarlett, B. (2002). Population balances for particulate processes - a volume approach. *Chem. Eng. Sci.*, 57(12):2287–2303.
- Vervaet, C. and Remon, J. P. (2005). Continuous granulation in the pharmaceutical industry. *Chem. Eng. Sci.*, 60(14):3949–3957.
- Wang, F. Y. and Cameron, I. T. (2002). Review and future directions in the modelling and control of continuous drum granulation. *Powder Technol.*, 124(3):238–253.
- Watano, S. (2001). Direct control of wet granulation processes by image processing system. *Powder Technol.*, 117(1-2):163–172.
- Watano, S. (2007). Chapter 10 Online monitoring. In A.D. Salman, M. J. H. and Seville, J. P. K., editors, *Handbook of Powder Technology*, volume Volume 11, pages 477–498. Elsevier Science B.V.
- Watano, S., Numa, E., Miyamoto, K., and Osako, Y. (2000). On-line monitoring of granule growth in high shear granulation by an image processing system. *Chem. Pharm. Bull. (Tokyo)*, 48(8):1154.
- Watano, S., Sato, Y., and Miyamoto, K. (1997). Application of a neural network to granulation scale-up. *Powder Technol.*, 90(2):153–159.
- Whitaker, M., Baker, G. R., Westrup, J., Goulding, P. A., Rudd, D. R., Belchamber, R. M., and Collins, M. P. (2000). Application of acoustic emission to the monitoring and end point determination of a high shear granulation process. *Int. J. Pharm.*, 205(1-2):79–91.
- Wright, H. and Ramkrishna, D. (1992). Solutions of inverse problems in population balances - I. Aggregation kinetics. *Comput. Chem. Eng.*, 16(12):1019–1038.
- Yu, X., Hounslow, M. J., and Reynolds, G. K. (2015). Accuracy and optimal sampling in monte carlo solution of population balance equations. *AIChE Journal*.
- Zhu, H., Zhou, Z., Yang, R., and Yu, A. (2008). Discrete particle simulation of particulate systems: A review of major applications and findings. *Chem. Eng. Sci.*, 63(23):5728–5770.
- Zlokarnik, M. (2011). *Dimensional analysis and scale-up in theory and industrial application*, chapter 1, pages 1–57. Informa Healthcare.

---

## Glossary

---

$\beta$	Aggregation kernel [ $\text{m}^3\text{s}^{-1}$ ].
$b(x, y)$	Breakage function [ $\text{m}^3$ ].
$t_c$	Characteristic contact time [s].
$c_f$	Dimensionless filling rate coefficient [-].
$d$	Lead volume fraction [-].
$d_p$	Particle diameter [m].
$\epsilon$	Dimensionless reference film thickness [-].
$\eta_n$	Normal damping coefficient [Ns/m].
$e_n$	Normal coefficient of restitution [-].
$\eta_t$	Tangential damping coefficient [Ns/m].
$e(t)$	Residence time distribution function, [ $\text{s}^{-1}$ ].
$F_i^b$	body force of a particle $i$ [N].
$F_{ij}^{coh}$	Cohesion force between particle $i$ and $j$ [N].
$F_{ij}^{con}$	Contact force between particle $i$ and $j$ [N].
$\mathbf{F}_i^{c,n}$	Normal component of force acting on particle $i$ [N].
$\mathbf{F}_i^{c,t}$	Tangential component of force acting on particle $i$ [N].
$\gamma$	Shear rate [1/s].
$\gamma^*$	Scaled shear rate [-].
$h$	Total liquid film thickness [m].
$h_0$	Dimensional reference film thickness [m].
$k_n$	Normal spring stiffness [N/m].
$k_t$	Tangential spring stiffness [N/m].
$L_p$	Volume of liquid present on the particle [ $\text{m}^3$ ].
$L_{p,0}$	Reference liquid content on the particles [-].
$m_i$	Mass of the particle [kg].
$\mu_l$	Dynamic viscosity of liquid [Ns/m <sup>2</sup> ].
$\mu$	Liquid viscosity, [ $\text{kgm}^{-1}\text{s}^{-1}$ ].

$n$	Number of continuously stirred tank reactors [-].
$n_p$	Number of particles [-].
$n_{p,liq}$	Number of particles in liquid addition region [-].
$n(x, t)$	Number distribution of particles [-].
$\mathbf{n}_{ij}$	Unit normal vector [-].
$\omega$	Eigen frequency of damped harmonic oscillator [1/s].
$\phi$	Volume fraction of particles [-].
Pe	Péclet number, [-].
$p$	Plug-flow volume fraction, [-].
$\phi_{tr}$	Fraction of liquid on the surface that is transferred into the bridge [-].
$Q_{lod}$	Dimensionless liquid load per particle [-].
$Q_{tr}$	Liquid transfer rate for particle [m <sup>3</sup> /s].
$r$	Radius of the particle [m].
$\mathbf{r}^*$	Position vector of the particle [m].
$\mathfrak{R}_{birth}$	Net formation rates of particles by discrete event aggregation and breakage [s <sup>-1</sup> ].
$\mathfrak{R}_{death}$	Net depletion rates of particles by discrete event aggregation and breakage [s <sup>-1</sup> ].
$r_{eff}$	Effective radius of the particle [m].
$\rho_p$	Scaled shear rate [-].
$S$	Selection function [s <sup>-1</sup> ].
$\sigma_l$	Surface tension of liquid [N/m].
$\sigma_\theta^2$	Normalised variance, [-].
$\sigma_{\bar{i}}^2$	Mean centered variance, [s].
$\gamma_l$	surface tension of the liquid.
$t_{exp}$	Liquid addition time [s].
$\bar{t}$	Mean residence time, [s].
$t_{min}$	Minimum residence time [s].
$t_{ref}$	Reference liquid bridge filling time [s].
$\mathbf{u}_{ij}^t$	Tangential overlap between particles $i$ and $j$ [m].
$V_{bf}$	Liquid bridge volume fraction [-].
$V_p$	Volume of particle [m <sup>3</sup> ].
$\mathbf{v}_{ij}$	Relative particle velocity components [m/s].
$\mathbf{v}_{ij}^n$	Normal relative particle velocity components [m/s].
$\mathbf{v}_{ij}^t$	Tangential relative particle velocity components [m/s].
$x$	Scalar-state variable such as particle size [m, m <sup>3</sup> ].

$\bar{Z}_b$  Average number of liquid bridges per particle [-].



---

## Acronyms

---

AE	acoustic emission.
ANN	artificial neural network.
API	active pharmaceutical ingredient.
CAT	cell average technique.
CFD	computational fluid dynamics.
CM	compartmental model.
cNMC	constant-number Monte Carlo.
CPP	critical process parameter.
CQA	critical quality attribute.
CSTR	continuously stirred tank reactor.
DEM	discrete element method.
DIA	dynamic image analysis.
DQMOM	direct quadrature method of moments.
ECT	Electrical capacitance tomography.
FBRM	focused beam reflectance measurement.
FDA	Food and Drug Administration.
FFT	fast Fourier transform.
FVM	finite volume method.
GSD	granule size distribution.
GSSD	granule size and shape distribution.
HSWG	high shear wet granulation.
ICH	International Conference on Harmonization.
L/S	liquid-to-solid ratio.
LED	light emitting diode.
MI	mixing index.
MLR	multiple linear regression.
MRI	magnetic resonance imaging.



MTR	mixer torque rheometer.
NIR	near infrared.
NIR-CI	near infrared chemical imaging.
NMR	Nuclear magnetic resonance.
ODE	ordinary differential equation.
PAT	process analytical technology.
PBE	population balance equation.
PBM	population balance model.
PCA	principal component analysis.
PEPT	positron emission particle tracking.
PFR	plug-flow reactor.
PIV	particle image velocimetry.
PLS	partial least squares.
PLS-DA	partial least squares discriminant analysis.
PSE	process system engineering.
PVP	polyvinylpyrrolidone.
QbD	Quality by Design.
$R^2$	coefficient of determination.
RMSE	root mean square error.
RSS	residual sum of squares.
RTD	residence time distribution.
RTRT	real time release testing.
SFV	spatial filter velocimetry.
SME	specific mechanical energy.
SMF	spectral matched filter.
SNV	standard normal variate.
ssNMR	solid-state Nuclear magnetic resonance.
TIS	tanks-in-series.
TSG	twin-screw granulator.
VoF	Volume of Fluid.
XRPD	Powder X-ray diffractometry.

---

## Appendices

---



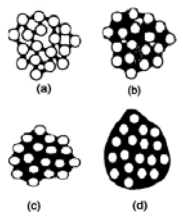

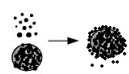
## APPENDIX A

---

Supplementary tables from literature survey

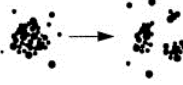
---

**Table A.1:** Constitutive mechanisms of wet granulation and its mathematical description

Mechanism	Particle Formation	Characteristics	Equations
Wetting & Nucleation		<p>(a) Pendular- looks like bridge, but particles not immersed in liquid</p> <p>(b) Funicular- thicker bridges but not completely filled</p> <p>(c) Capillary- particles at edge of cluster not completely wetted by liquid</p> <p>(d) Droplet- all particles completely wet</p>	$\tau_{wetting} = \frac{2V_0^2}{\pi^2 \varepsilon_s^4 r_d^4 R_{pore}} \frac{\mu}{\gamma_{LV} \cos \theta}$ $\frac{\partial n}{\partial t} = B^0 \delta(l - l_0)$
Growth-Aggregation		<ul style="list-style-type: none"> <li>- Successful collision of two particles that result in one larger aggregated particle</li> <li>- When dealing with systems that exhibit aggregation, it is more convenient to use particle volume rather than particle size, since volume is conserved</li> <li>- The success of collisions i.e. aggregation can be a function of particle size, liquid content and powder properties and operational factors such as bed height, powder velocity and shear.</li> </ul>	$\frac{\partial n(x)}{\partial t} = B_{agg}(x) - D_{agg}(x)$ $B_{agg}(x) = \frac{1}{2} \int_0^x \beta(x-y, y) n(x-y, t) n(y, t) dy$ $D_{agg}(x) = n(x, t) \int_0^\infty \beta(x, y) n(y, t) dy$
Growth-Layering		<ul style="list-style-type: none"> <li>- Picking up of smaller particles from the feed onto the surface of larger granules. It is often induced by a rolling action.</li> </ul>	$\frac{\partial n}{\partial t} = \frac{\partial}{\partial x} \left[ n \frac{dx}{dt} \right] (x, t)$

*Continued on next page*

Table A.1 – *Continued from previous page*

Mechanism	Particle Formation	Characteristics	Equations
		<ul style="list-style-type: none"> <li>- It is more convenient to use particle size as the internal coordinate when describing layering or growth.</li> </ul>	
Breakage		<ul style="list-style-type: none"> <li>- Breakage in granulation is a significant issue, being more important in high shear devices.</li> <li>- The complexity of breakage models extends from binary breakage models to full particle</li> </ul>	$\frac{\partial n(x,t)}{\partial t} = \int_0^\infty b(x,y)(y,x-y)S(y)n(y,t)dy - S(x)n(x,t)$

**Table A.2:** Physical modelling approaches in granulation studies

Model	Advantages	Challenges	Ref.
population balance model (PBM)	Simulate a very large number of particles	Semi-mechanistic approach due to lack of process knowledge	Darelius et al. (2005, 2006); Ramachandran et al. (2009); Barrasso and Ramachandran (2012)
discrete element method (DEM)	Mechanistic approach	Computational limitations when very large number of particles	Nakamura et al. (2013)
Hybrid models by combining PBM with DEM	Capable of modelling the complex dynamic mechanisms by bridging micro-scale to meso-scale	Hard to implement due to many many difficulties, for example to measure parameters such as wet granule yield strength, asperity height etc.	Gantt et al. (2006); Sen et al. (2012a)
PBM with Volume of Fluid (VoF) methods	Mechanistic approach; Can provide spatial distribution of binder in wet granule	Hard to implement and requires considerable simplification such as ignoring dynamic change in state of granulation liquid	Štěpánek et al. (2009)

*Continued on next page*

Table A.2 – *Continued from previous page*

Model	Advantages	Challenges	Ref.
PBM with computational fluid dynamics (CFD)	Mechanistic approach; can be used for development of simplified models	Not suitable for dense particle system; ignores particle-particle interaction	Rajniak et al. (2009)
PBM with Compartmental model (CM) and DEM	Improved accuracy of the population balance model when the particle flow is an important parameter	Number of particles is low while stochastic solution methods of PBM are adopted to avoid computational limitations	Bouffard et al. (2012)



**Table A.3:** Summary of chronological evolution of aggregation kernels in the literature

Kernels	Source
Shear kernel $\beta = \beta_0 \cdot \frac{4}{3} G(a_i + a_j)^3$ where $G$ is the local velocity gradient.	(Camp and Stein, 1943)
Size independent kernel $\beta = \beta_0$	(Ingram and Cameron, 2010)
Size dependent kernel $\beta = \beta_0 \frac{(x+x')^a}{(x \cdot x')^b}$	(Kapur, 1972)
Time and size dependent kernel $\beta = \beta_0(t) \cdot \beta^*(x, x')$ where one is a time-dependent and the other a size-dependent function	(Sastry, 1975)
Sequential kernel $\beta = \begin{cases} \beta_0, & t < t_{\text{switch}} \\ \beta_1(x, x'), & t > t_{\text{switch}} \end{cases}$ where $\beta_0$ and $\beta_1$ are constants and $t_{\text{switch}}$ is the time required to reach the final equilibrium size distribution of the first non-inertial stage of granulation.	(Adetayo et al., 1995)
Cut-off kernel $\beta = \begin{cases} \beta_0, & w < w^* \\ 0, & w > w^* \end{cases} \quad \text{where } w = \frac{(x \cdot x')^{a_{AE}}}{(x+x')^{b_{AE}}}$ $a_{AE}, b_{AE}, \beta_0$ are constants and $w^*$ is the critical granule volume.	(Adetayo and Ennis, 1997)
EKE kernel (Equipartition of Kinetic Energy-kernel)	

*Continued on next page*

Table A.3 – Continued from previous page

Kernels	Source
$\beta = \beta_0(x + x')^2 \sqrt{\frac{1}{x^3} + \frac{1}{x'^3}}$	(Hounslow, 1998)
ETM kernel (Equipartition of Translational Momentum kernel)	
$\beta = \beta_0(x + x')^2 \sqrt{\frac{1}{x^6} + \frac{1}{x'^6}}$	(Hounslow, 1998)
physically based kernel	
$\beta = \beta_0 \int_{-\infty}^{St_*} f(\Phi, t) d\Phi$	(Cryer, 1999)
where, $f(\Phi, t)$ is the discrete probability density function.	
Kernel based on the different aggregation mechanisms	
$\beta _{x,x'} = \begin{cases} \beta_1 : \text{for type I and type II coalescence with no permanent deformation} \\ \beta_2 : \text{for type II coalescence with permanent deformation} \\ 0 : \text{for rebound} \end{cases}$	(Liu and Litster, 2002)
Multidimensional kernel	
$\beta = \beta_0 \cdot (x^3 + x'^3) \left( (c_x + c_{x'})^{\alpha_M} \left( 100 - \frac{c_x + c_{x'}}{2} \right)^{\delta_M} \right)^{\alpha_M}$	(Madec et al., 2003)
where $c_x$ and $c_{x'}$ represent the volume percentage of binding agent in the agglomerates $x$ and $x'$ respectively, and $\alpha_M$ and $\delta_M$ are fitted parameters.	
Mechanistic kernel	
$\beta(i, j, t) = \beta_0 \frac{q_{li} - q_{l^*i}}{4\pi((d_i/2))^2((q_{si} + q_{li})/v_i)} - \frac{q_{lj} - q_{l^*j}}{4\pi((d_j/2))^2((q_{sj} + q_{lj})/v_j)}$	(Darelius et al., 2006)
where, $q_{li}$ is the volume of liquid in class $i$ , $q_{l^*i}$ ; the volume of liquid in the voids in class $i$ , and $v_i$ refers to the volume of a single particle in class $i$ .	

**Table A.4:** Summary of chronological evolution of breakage kernels in the literature

Kernels	Source
<p>Semi-empirical breakage kernel</p> $b(x, y)(z) = \frac{P_1 G_{shear}(D(z))^{P_2}}{2}$ <p>where <math>G</math> is the shear rate, <math>D</math> is the particle diameter, and <math>P_1</math> and <math>P_2</math> are adjustable parameters.</p>	<p>(Pandya and Spielman, 1983)</p>
<p>Product and sum-type :</p> $b(x, y)(z) = v \frac{z^{q-1}(1-z)^{q(v-1)-1}}{B(q, q(v-1))}$ $b(x, y)(z) = \frac{z^{q-1}(1-z)^{v-2}}{B(q, v-1)} + (v-1) \frac{(1-z)^{q+v-3}}{B(1, q+v-2)}$ <p>where <math>B</math> is the beta function, <math>v(y) = v(\geq 2)</math> is the number of fragments per breakage event and <math>q &gt; 0</math> is the parameter of the kernel.</p>	<p>(Diemer and Olson, 2002; Hill and Ng, 1995)</p>
<p>Erosion-type kernels:</p> $b(x, y)(z) = \begin{cases} P_1(z) & \text{for } 0 < z < \varepsilon_1 \\ 0 & \text{for } \varepsilon_1 < z < \varepsilon_2 \\ P_2(z) & \text{for } 1-\varepsilon_2 < z < 1 \end{cases} \quad \text{with } \varepsilon_2 \ll 1.$	<p>(Kostoglou and Karabelas, 2001)</p>
<p>Sum of the powers-type kernel:</p> $b(x, y)(z) = \sum_{i=1}^n c_i z^{k_i}$ <p>where <math>k_i \in (-2, \infty)</math>. The coefficients <math>c_i</math> must be such as to conserve the total mass, that is <math>\sum_{i=1}^n \frac{c_i}{k_i+2} = 1</math></p>	<p>(Kostoglou and Karabelas, 1998)</p>
<p>Discrete homogeneous kernels</p>	

*Continued on next page*

Table A.4 – *Continued from previous page*

Kernels	Source
$b(x, y)(z) = \sum_{i=1}^n a_i \delta(z - c_i)$	(Kostoglou, 2003)
<p data-bbox="245 327 573 355">Mechanistic breakage kernel</p> $b(x, y)(z_a) = \sum_{z_a=1}^{z_{a,upper}} \frac{\sigma_{ext}^{particle}(z_a, z_b)}{\sigma_{int}(z_a)} F(z_a) N_a \frac{SA(z_a)}{SA+WA+IA} + \frac{\sigma_{ext}^{wall}(z_a)}{\sigma_{int}(z_a)} \frac{WA}{SA+WA+IA} + \frac{\sigma_{ext}^{impeller}(z_a)}{\sigma_{int}(z_a)} \frac{IA}{SA+WA+IA} + \frac{\sigma_{ext}^{fluid}(z_a)}{\sigma_{int}(z_a)}$ <p data-bbox="245 479 1310 575">where <math>F</math> is the particle density, <math>WA</math> is the total wall surface area, <math>SA</math> is the surface area of an individual particle, <math>IA</math> is the impeller surface area and <math>N_a</math> is Avogadro's constant, <math>z_{a,upper}</math> are the upper limits of the finite volumes in each of the dimensions.</p>	(Ramachandran et al., 2009)

**Table A.5:** State variables in high shear wet-granulation and their modelling and measurement basis

State variable	Measurement basis	Mode#	References	Challenges	Model calibration / validation studies <sup>†</sup>
<i>Material Parameter</i>					
Wettability of the powder by the granulation liquid	Optical tensiometry/ Sessile Drop studies	Off-line	(Litster and Ennis, 2004)	Relies on the consistency of the operator.	PBM (Marshall et al., 2013), DEM (Sato et al., 2013), PBM with VoF (Thielmann et al., 2008)
	Force tensiometers / Washburn method	Off-line	(Litster and Ennis, 2004)	Difficult to separate the effect of contact angle and pore size of powder bed.	
Viscosity and yield stress of liquid	Capillary rheometer	On-line	(Luukkonen et al., 2001)	Difficult to clean.	DEM, PBM (Poon et al., 2009), PBM with VoF (Thielmann et al., 2008)
Flowability	Shear cells	Off-line	(Sandler and Wilson, 2010)	Induced anisotropy can occur during shear.	DEM (Moreno-Atanasio et al., 2005)
<i>Granulation conditions</i>					
Temperature	Resistance thermometer (Pt100)	In-line	(Verduyck et al., 2012)	Spatial variations are neglected, probe fouling.	PBM, DEM, PBM with DEM and CM (Bouffard et al., 2012)

*Continued on next page*

Table A.5 – *Continued from previous page*

State variable	Measurement basis	Mode#	References	Challenges	Model calibration / validation studies <sup>†</sup>
Pressure	Infrared thermometer	In-line	(Tackenberg et al., 2015)	Spatial variations are neglected.	DEM, Hybrid model, PBM with DEM and CM
	Piezoresistive/Piezoelectric Pressure Transmitter	In-line	(Watano, 2007)	Very sensitive to temperature change when at extremes of design range.	
Process time/ Residence time distribution	Telemetric differential pressure sensor	In-line	(Chan et al., 2013)		DEM (Marigo et al., 2013), Hybrid PBM with DEM (Sen et al., 2012a)
	Tracer study	In-line	(El Hagrasy et al., 2013b)	Inconsistent results.	
	positron emission particle tracking (PEPT)	In-line	(Lee et al., 2012; Barigou, 2004)	Reliable, but hard to implement.	
	particle image velocimetry (PIV)	In-line	(Huang et al., 2010)	Not able to measure components along the z-axis (towards to/or away from the camera).	
	Piezoelectric Ultrasonic Transducer	In-line	(Lee et al., 2005)	Very sensitive to temperature change when at extremes of design range.	

*Continued on next page*

Table A.5 – *Continued from previous page*

State variable	Measurement basis	Mode#	References	Challenges	Model calibration / validation studies <sup>†</sup>
Mixing / Shear rate	Impeller tip speed	In-line	(Horsthuis et al., 1993)	Found to be non reproducible.	PBM (Biggs et al., 2003), DEM (Marigo et al., 2013), PBM with DEM and CM (Bouffard et al., 2012)
Impeller torque	Torsionmeter	In-line	(Watano, 2007)	Scale dependent, and not always sensitive enough to characterize the granulation process; can potentially give inaccurate results when sticky materials build up along the granulator wall.	PBM (Biggs et al., 2003), DEM (Sato et al., 2008)
<i>Quality Attributes</i>					
Wet mass consistency	Visual Inspection	At-line	(Sakr et al., 2012)	Relies on the consistency of the operator.	PBM (Darelius et al., 2006)
	mixer torque rheometer (MTR)	In-line	(Faure et al., 1999; Sakr et al., 2012)	No physical basis to establish the measurement, spatial variations are lumped.	

*Continued on next page*

Table A.5 – *Continued from previous page*

State variable	Measurement basis	Mode#	References	Challenges	Model calibration / validation studies <sup>†</sup>
Particle shape/size distribution	Power Consumption	In-line	(Watano, 2007)	Non-reliable: wear and tear of mixer and motor may cause power fluctuations.	PBM (Sanders et al., 2003; Braumann et al., 2007; Van Melkebeke et al., 2008; Ramachandran et al., 2009), DEM (Antonyuk et al., 2006)
	dynamic image analysis (DIA)	On-line	(Watano et al., 2000)	Small portion of bulk material is accessible	
	near infrared (NIR)	On-line/ In-line	(Rantanen et al., 2004)	Size and density information is combined.	
	Optical and scanning electron microscopy	Off-line	(Litster and Ennis, 2004)	Very labour intensive and driven by operator biases.	
	Mechanical Sieving	Off-line	(Vercruysse et al., 2012)	Samples are required to be dried first.	

*Continued on next page*



Table A.5 – *Continued from previous page*

State variable	Measurement basis	Mode#	References	Challenges	Model calibration / validation studies <sup>†</sup>
	Focused beam reflectance measurement (FBRM)	In-line	(Huang et al., 2010; Michaels et al., 2009)	<p>Fouling of the probe was observed during in-process measurements in high shear wet granulation (HSWG) which impeded its reliability as an in-line process analyser. Distribution can be skewed towards the smaller range due to particle orientation which extremely crucial for proper analysis of non-spherical particles. Difficult to discriminate real AE signals from background noise during measurement. Depend very much on scale, cleanliness and usage of equipment, and require frequent recalibration of chemometric models.</p>	
	Laser-diffraction particle size analyser	In-line	Naik and Chaudhuri (2015)		
	acoustic emission (AE) sensors	In-line	(Whitaker et al., 2000)		

*Continued on next page*

Table A.5 – *Continued from previous page*

State variable	Measurement basis	Mode#	References	Challenges	Model calibration / validation studies <sup>†</sup>
Bulk density and porosity	Mercury intrusion psychometry	At-line	(Michaels et al., 2009)	Does not account for closed pores, thus slightly underestimates porosity. Design using tiny amounts of sample is desired. Difficult to discriminate real AE signals from background noise during measurement.	PBM (Darelius et al., 2006), DEM (Moreno-Atanasio et al., 2005)
	ESH Powder Compaction Simulator	In-line	(Michaels et al., 2009)		
	AE sensors	In-line	(Whitaker et al., 2000)		
Moisture content	NIR	At-line/ In-line	(Fonteyne et al., 2012)	Plenty of samples required for calibration purpose.	PBM (Marshall et al., 2013), PBM with VoF (Thielmann et al., 2008), DEM
	magnetic resonance imaging (MRI)	At-line	(Tishmack et al., 2003)	Indirect method, thus requires calibration against a direct method for moisture.	
	Electrical capacitance tomography (ECT)	In-line	(Rimpiläinen et al., 2011)	Interpretations of the tomograms and 3-D sensors	

*Continued on next page*

Table A.5 – *Continued from previous page*

State variable	Measurement basis	Mode#	References	Challenges	Model calibration / validation studies <sup>†</sup>
Drug content uniformity/ Polymorphism	NIR	On-line/ In-line	(Fonteyne et al., 2012)	Robust chemometric models required	PBM (Sen et al., 2012a), DEM (Hasanpour et al., 2013)
	Powder X-ray diffractometry (XRPD)	Off-line	(Guo et al., 2011)	Growth and monitoring of large single granules is very difficult.	
	Raman spectroscopy	In-line/ At-line	(De Beer et al., 2011)	Avoid undesired sample fluorescence and laser fluctuations	
	solid-state Nuclear magnetic resonance (ssNMR) spectroscopy	On-line/ In-line	(Jørgensen et al., 2004)	Not trivial to obtain high-quality spectra	
Granule strength/ friability	Roche type friabilator	Off-line	(Propst, 2009)		DEM (Moreno-Atanasio et al., 2005)

<sup>#</sup> At-line: measurements where the sample is removed, isolated from, and analysed in close proximity to the process stream. On-line: measurements where the sample is diverted from the manufacturing process, and may be returned to the process stream. In-line: measurements (invasive or non-invasive) where the sample is not removed from the process stream (FDA, 2004).

<sup>†</sup> Missing citation indicate that authors could not find suitable calibration/ validation studies.

## APPENDIX B

---

Raw data from experimental studies

---

**Table B.1:** Overview of experimental design runs: factor variables (number of kneading discs, screw speed, throughput and liquid-solid ratio) and responses (Torque,  $F < 150 \mu\text{m}$  (defined as fines),  $150 \mu\text{m} < F < 1000 \mu\text{m}$  (fraction of interest for tableting) and  $F > 1000 \mu\text{m}$  (defined as oversized) granules).

S.No.	NK (-)	SS (RPM)	MFR (kg/h)	LSR (%)	Torque (N-m)	F<150 $\mu\text{m}$ (%)	150- 1000 $\mu\text{m}$ (%)	F>1000 $\mu\text{m}$ (%)
1	2	500	10	4.58	34.95	42.19	22.86	1.38
2	4	500	10	4.58	40.66	37.95	21.39	1.84
3	6	500	10	4.58	38.28	43.77	17.95	2.59
4	12	500	10	4.58	43.2	37.87	18.93	2.92
5	2	900	10	4.58	37.86	46.02	16.11	1.25
6	4	900	10	4.58	43.12	39.53	17.34	2.00
7	6	900	10	4.58	42.78	39.25	17.96	3.06
8	12	900	10	4.58	40.68	37.62	21.7	1.95
9	2	500	25	4.58	36.25	35.66	28.09	1.30
10	4	500	25	4.58	45.79	31.01	23.19	2.02
11	6	500	25	4.58	42.52	37.54	19.93	2.27
12	12	500	25	4.58	45.41	34.69	19.91	2.4
13	2	900	25	4.58	39.87	38.88	21.25	1.55
14	4	900	25	4.58	45.87	36.15	17.98	1.98
15	6	900	25	4.58	43.9	40.89	15.21	2.09
16	12	900	25	4.58	45.07	35.89	19.04	2.02
17	2	500	10	6.72	22.29	39.62	38.10	0.92
18	4	500	10	6.72	22.55	35.65	41.80	1.73
19	6	500	10	6.72	28.49	32.80	38.71	2.97
20	12	500	10	6.72	23.80	34.84	41.36	3.06
21	2	900	10	6.72	23.56	39.75	36.7	1.44
22	4	900	10	6.72	25.70	33.27	41.04	1.89
23	6	900	10	6.72	29.04	34.82	36.15	3.07
24	12	900	10	6.72	22.19	35.15	42.66	2.6
25	2	500	25	6.72	26.14	36.3	37.56	1.24
26	4	500	25	6.72	29.37	32.43	38.21	2.16
27	6	500	25	6.72	33.58	33.71	32.71	2.28
28	12	500	25	6.72	16.10	34.46	49.43	4.7
29	2	900	25	6.72	26.01	44.26	29.73	1.54
30	4	900	25	6.72	30.72	34.44	34.84	1.46
31	6	900	25	6.72	32.58	37.62	29.79	2.46
32	12	900	25	6.72	26.25	31.31	42.44	1.86
33	4	700	17.5	6	22.58	55.90	21.52	1.33
34	4	700	17.5	6	18.52	53.03	28.45	1.32
35	4	700	17.5	6	20.59	55.50	23.92	1.24

**Table B.2:** Overview of experimental design runs performed to study the effect of process parameters on the residence time, axial and solid-liquid mixing and the resulting granule size distribution (GSD) (Chapter 6): factor variables (material throughput [MFR], liquid-solid ratio [LSR], number of kneading discs [NK], stagger angle [SA] and screw speed [SS]) and responses (Torque, mean residence time [MRT], normalised variance [NV], Péclet number [Pe], granules fraction < 150  $\mu\text{m}$  [Fines], 150  $\mu\text{m}$  < granules fraction < 1000  $\mu\text{m}$  [Yield] and granules fraction > 1400  $\mu\text{m}$  [Oversized] granules, mixing index [MI], frequency [Freq.] and amplitude [Amp.] of mean moisture profile).

S.No.	MFR (kg/h)	LSR (%)	NK (-)	SA (°)	SS (rpm)	Torque (N.m)	MRT (sec)	NV (-)	Pe (-)	Fines (%)	Yield (%)	Oversized (%)	MI (-)	Freq (sec)	Amp (-)
1	10	6	4	30	500	2.08	4.07	0.11	16.72	26.1	51.1	23.1	0.342	0.24	0.04
2	25	6	4	30	500	2.77	4.11	0.07	27.68	32.6	46.8	21.0	0.264	0.24	0.01
3	10	8	4	30	500	2.27	3.69	0.14	13.54	13.4	53.2	33.8	0.339	0.24	0.04
4	25	8	4	30	500	2.45	3.85	0.12	15.16	16.9	48.9	34.2	0.252	0.25	0.01
5	10	6	6	30	500	3.15	4.10	0.13	14.47	17.8	48.3	34.3	0.314	0.24	0.04
6	25	6	6	30	500	4.95	4.31	0.07	28.81	22.5	44.7	33.1	0.226	0.04	0.01
7	10	8	6	30	500	2.81	4.49	0.13	14.67	8.9	52.1	39.2	0.319	0.24	0.03
8	25	8	6	30	500	3.75	4.55	0.12	15.80	11.0	51.2	37.9	0.275	0.29	0.01
9	10	6	12	30	500	3.76	5.16	0.07	26.32	15.6	52.0	32.6	0.332	0.12	0.05
10	25	6	12	30	500	8.31	4.99	0.06	34.86	14.0	50.3	36.2	0.275	0.32	0.02
11	10	8	12	30	500	3.18	4.78	0.10	19.51	7.4	51.8	41.1	0.339	0.12	0.06
12	25	8	12	30	500	6.36	5.59	0.08	24.28	4.9	41.7	53.4	0.391	0.14	0.04
13	10	6	4	60	500	0.62	3.46	0.13	13.98	42.9	47.6	9.9	0.297	0.32	0.06
14	25	6	4	60	500	1.41	3.79	0.13	14.50	43.9	43.3	13.0	0.257	0.36	0.02
15	10	8	4	60	500	0.81	3.78	0.17	10.79	23.6	48.6	27.9	0.327	0.30	0.06
16	25	8	4	60	500	1.22	4.73	0.08	24.41	16.8	50.2	33.0	0.275	0.50	0.01
17	10	6	6	60	500	1.37	3.89	0.09	20.18	36.3	52.3	11.9	0.327	0.16	0.06

*Continued on next page*

Table B.2 – Continued from previous page

S.No.	MFR (kg/h)	LSR (%)	NK (-)	SA (°)	SS (rpm)	Torque (N.m)	MRT (sec)	NV (-)	Pe (-)	Fines (%)	Yield (%)	Oversized (%)	MI (-)	Freq (sec)	Amp (-)
18	25	6	6	60	500	5.92	5.47	0.06	32.18	21.4	54.6	24.2	0.237	0.36	0.02
19	10	8	6	60	500	1.81	4.61	0.09	22.28	16.7	46.0	37.7	0.335	0.16	0.03
20	25	8	6	60	500	2.86	5.39	0.08	24.55	7.8	53.6	38.8	0.310	0.40	0.01
21	10	6	12	60	500	1.43	3.51	0.60	1.76	27.1	53.8	19.1	0.349	0.12	0.06
22	25	6	12	60	500	12.41	5.70	0.11	16.71	18.5	61.8	17.9	0.372	0.14	0.03
23	10	8	12	60	500	4.10	4.07	0.27	6.15	13.8	49.0	37.6	0.352	0.12	0.06
24	25	8	12	60	500	3.62	6.88	0.05	36.66	6.8	51.8	41.3	0.294	0.28	0.01
25	10	6	4	30	900	1.85	2.10	0.74	0.96	24.6	56.5	19.3	0.333	0.17	0.06
26	25	6	4	30	900	2.05	2.25	0.22	7.78	27.4	51.5	21.3	0.262	0.06	0.03
27	10	8	4	30	900	1.25	2.37	0.44	3.13	10.8	57.6	31.8	0.342	0.24	0.06
28	25	8	4	30	900	0.38	1.82	0.44	3.19	13.6	53.6	33.3	0.266	0.28	0.02
29	10	6	6	30	900	3.02	2.73	0.49	2.68	16.5	58.7	25.0	0.203	0.24	0.06
30	25	6	6	30	900	4.10	2.52	0.52	2.36	20.2	47.5	32.5	0.190	0.26	0.02
31	10	8	6	30	900	1.87	2.91	0.14	12.86	8.8	59.2	32.3	0.142	0.24	0.05
32	25	8	6	30	900	0.45	2.38	0.51	2.45	11.4	52.0	36.8	0.307	0.06	0.01
33	10	6	12	30	900	1.91	2.71	0.28	5.86	55.1	42.1	3.0	0.308	0.12	0.05
34	25	6	12	30	900	7.43	2.60	0.20	8.85	13.2	50.3	36.6	0.287	0.34	0.02
35	10	8	12	30	900	4.29	2.39	0.21	8.19	8.2	53.8	38.2	0.340	0.14	0.07
36	25	8	12	30	900	1.15	2.40	0.34	4.70	7.9	49.8	42.5	0.310	0.24	0.01
37	10	6	4	60	900	0.52	1.99	0.24	7.33	37.1	54.7	8.3	0.355	0.21	0.05
38	25	6	4	60	900	0.84	2.09	0.84	0.55	40.1	48.0	12.0	0.244	0.12	0.06
39	10	8	4	60	900	0.58	1.61	0.54	2.21	21.6	54.1	24.3	0.346	0.32	0.07

Continued on next page

Table B.2 – *Continued from previous page*

S.No.	MFR (kg/h)	LSR (%)	NK (-)	SA (°)	SS (rpm)	Torque (N.m)	MRT (sec)	NV (-)	Pe (-)	Fines (%)	Yield (%)	Oversized (%)	MI (-)	Freq (sec)	Amp (-)
40	25	8	4	60	900	0.39	2.04	0.61	1.72	24.8	52.5	23.1	0.131	0.17	0.02
41	10	6	6	60	900	1.27	2.42	0.37	4.05	36.5	56.8	7.2	0.332	0.19	0.05
42	25	6	6	60	900	4.58	2.05	0.36	4.26	33.5	50.1	16.9	0.218	0.36	0.02
43	10	8	6	60	900	1.32	3.06	0.16	11.12	15.9	54.0	30.3	0.335	0.19	0.05
44	25	8	6	60	900	0.42	2.38	0.56	2.08	21.2	47.9	31.0	0.301	0.35	0.02
45	10	6	12	60	900	1.71	2.81	0.35	4.48	51.8	45.1	3.4	0.300	0.04	0.27
46	25	6	12	60	900	10.89	2.14	0.71	1.13	28.3	50.5	19.6	0.183	0.32	0.03
47	10	8	12	60	900	1.67	2.78	0.26	6.43	14.8	57.1	28.4	0.349	0.12	0.07
48	25	8	12	60	900	1.54	2.41	0.59	1.85	15.5	52.7	31.3	0.271	0.28	0.03
49	17.5	7	6	60	700	1.58	3.35	0.15	15.15	25.1	48.7	27.4	0.329	0.38	0.02
50	17.5	7	6	60	700	1.34	3.29	0.17	11.01	23.6	50.3	26.2	0.323	0.35	0.02
51	17.5	7	6	60	700	1.69	2.94	0.12	10.42	22.6	47.2	28.3	0.311	0.20	0.02





## APPENDIX C

---

Parameters estimations results for RTD model and PBM

---

**Table C.1:** Estimated model parameters ( $p$ ,  $n$  and  $d$ ), residual sum of squares (RSS) and coefficient of determination ( $R^2$ ) values for different runs for tanks-in-series (TIS) model, tanks-in-series (TIS) model with plug-flow volume fraction (PFR+TIS) and TIS model with plug-flow volume fraction and dead zones (PFR+(TIS+DFR)).

ID	MFR	NK	SA	RPM	$\bar{t}$	$t_{min}$	TIS			TIS+PFR				PFR+(TIS+DFR)				
							n	RSS	$R^2$	n	PF	RSS	$R^2$	n	PF	DF	RSS	$R^2$
1	10	2	30	500	1.9	0.60	4	198	0.56	2	0.44	136	0.70	2	0.45	0.38	34	0.95
2	10	2	30	700	1	0.35	3	106	0.64	2	0.28	87	0.70	2	0.29	0.38	19	0.96
3	10	2	30	900	1.3	0.37	3	130	0.62	2	0.34	97	0.71	2	0.34	0.37	27	0.95
4	10	2	60	500	2.5	0.93	7	146	0.70	2	0.40	101	0.81	4	0.41	0.27	25	0.96
5	10	2	60	700	0.8	0.37	2	147	0.56	2	0.26	159	0.53	2	0.26	0.48	38	0.93
6	10	2	60	900	1	0.33	3	86	0.70	2	0.27	64	0.77	2	0.28	0.33	16	0.96
7	10	2	90	500	2.2	0.88	5	201	0.56	2	0.49	134	0.74	4	0.40	0.35	42	0.94
8	10	2	90	700	1	0.32	3	143	0.56	2	0.32	127	0.62	2	0.33	0.44	33	0.93
9	10	2	90	900	0.8	0.33	2	108	0.64	2	0.26	87	0.69	2	0.26	0.40	20	0.95
10	10	6	30	500	2.4	0.49	7	100	0.76	2	0.48	35	0.92	2	0.49	0.19	11	0.98
11	10	6	30	700	1.3	0.34	4	77	0.74	2	0.34	47	0.84	2	0.35	0.28	10	0.98
12	10	6	30	900	1	0.33	3	73	0.73	2	0.28	54	0.80	2	0.29	0.33	9	0.98
13	10	6	60	500	2.7	0.79	7	110	0.75	4	0.40	78	0.83	4	0.41	0.21	18	0.97
14	10	6	60	700	1.4	0.34	4	88	0.72	2	0.37	46	0.85	2	0.38	0.28	11	0.98
15	10	6	60	900	0.8	0.29	3	57	0.76	2	0.24	35	0.85	2	0.24	0.29	5	0.98
16	10	6	90	500	4.6	1.93	11	144	0.75	2	0.59	40	0.94	2	0.60	0.09	32	0.96
17	10	6	90	700	2.9	0.73	7	127	0.72	2	0.50	53	0.89	2	0.51	0.22	19	0.97
18	10	6	90	900	1.7	0.41	4	107	0.68	2	0.36	69	0.80	2	0.37	0.29	26	0.95
19	10	12	30	500	3.3	0.70	8	99	0.78	2	0.50	32	0.93	2	0.51	0.12	22	0.96
20	10	12	30	700	2.3	0.47	5	76	0.79	2	0.41	36	0.90	2	0.42	0.18	17	0.97

*Continued on next page*

Table C.1 – *Continued from previous page*

ID	MFR	NK	SA	RPM	$\bar{t}$	$t_{min}$	TIS			PFR+TIS				TIS+PFR+DFR				
							n	RSS	R <sup>2</sup>	n	PF	RSS	R <sup>2</sup>	n	PF	DF	RSS	R <sup>2</sup>
21	10	12	30	900	1.8	0.43	5	66	0.78	2	0.35	37	0.88	2	0.36	0.20	15	0.96
22	10	12	60	500	4.2	1.93	11	121	0.78	2	0.60	35	0.95	2	0.61	0.12	22	0.98
23	10	12	60	700	2.4	0.44	6	76	0.80	2	0.46	23	0.94	2	0.47	0.16	9	0.98
24	10	12	60	900	1.6	0.39	4	55	0.82	2	0.35	20	0.93	2	0.36	0.16	8	0.98
25	17.5	2	30	500	2.2	1.72	7	154	0.67	2	0.40	95	0.81	4	0.41	0.29	15	0.98
26	17.5	2	30	700	1.3	0.84	4	117	0.65	2	0.37	80	0.76	2	0.38	0.37	10	0.98
27	17.5	2	30	900	1	0.54	3	123	0.63	2	0.32	101	0.69	2	0.33	0.42	10	0.98
28	17.5	2	60	500	2.1	1.75	6	151	0.66	2	0.38	103	0.78	4	0.39	0.31	24	0.96
29	17.5	2	60	700	1.3	0.86	4	131	0.63	2	0.37	92	0.74	2	0.38	0.38	13	0.98
30	17.5	2	60	900	0.9	0.44	3	112	0.63	2	0.29	94	0.69	2	0.30	0.41	12	0.98
31	17.5	2	90	500	2.3	1.89	6	165	0.64	2	0.40	104	0.79	4	0.41	0.30	20	0.97
32	17.5	2	90	700	1.5	1.18	4	172	0.58	2	0.42	129	0.69	2	0.43	0.42	15	0.98
33	17.5	2	90	900	0.7	0.37	2	107	0.64	2	0.26	98	0.65	2	0.27	0.44	12	0.97
34	17.5	6	30	500	2.7	2.19	9	150	0.70	2	0.55	62	0.88	2	0.56	0.24	19	0.98
35	17.5	6	30	700	1.9	1.38	6	128	0.69	2	0.49	67	0.84	2	0.50	0.31	10	0.98
36	17.5	6	30	900	0.9	0.44	4	59	0.77	2	0.31	36	0.85	2	0.32	0.29	6	0.98
37	17.5	6	60	500	3.4	2.82	11	151	0.73	4	0.42	81	0.87	6	0.43	0.18	17	0.98
38	17.5	6	60	700	1.8	1.39	5	134	0.67	2	0.35	85	0.80	4	0.37	0.31	11	0.99
39	17.5	6	60	900	0.9	0.46	3	89	0.69	2	0.32	62	0.77	2	0.33	0.36	10	0.98
40	17.5	12	30	500	3.6	2.99	13	134	0.78	2	0.59	47	0.92	2	0.60	0.16	24	0.97
41	17.5	12	30	700	2.2	1.46	7	97	0.75	2	0.47	42	0.89	2	0.47	0.23	11	0.98
42	17.5	12	30	900	1.4	0.61	5	57	0.80	2	0.35	31	0.90	2	0.36	0.24	6	0.99

*Continued on next page*

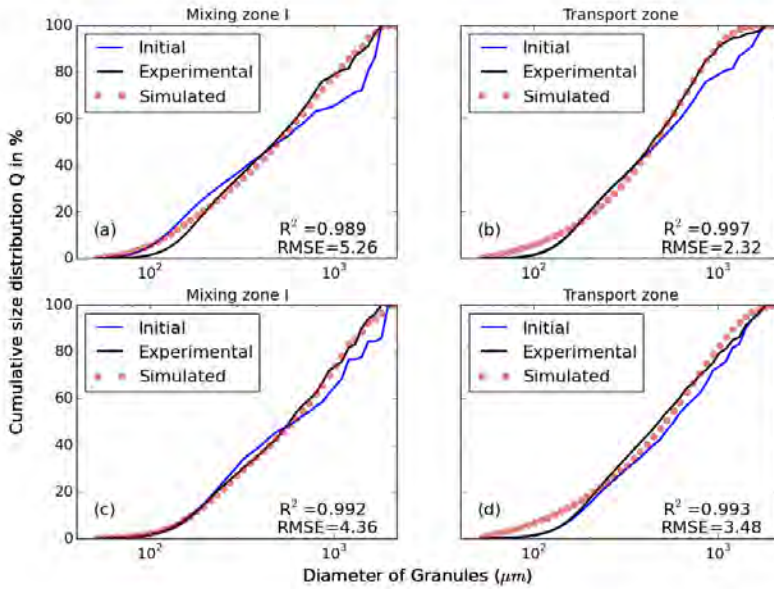
Table C.1 – *Continued from previous page*

ID	MFR	NK	SA	RPM	$\bar{t}$	$t_{min}$	TIS			PFR+TIS				TIS+PFR+DFR				
							n	RSS	R <sup>2</sup>	n	PF	RSS	R <sup>2</sup>	n	PF	DF	RSS	R <sup>2</sup>
43	17.5	12	60	500	5.6	5.06	23	198	0.78	4	0.64	80	0.92	4	0.65	0.12	38	0.98
44	17.5	12	60	700	3	2.44	8	161	0.69	2	0.55	63	0.88	2	0.56	0.22	22	0.97
45	17.5	12	60	900	2.2	1.48	6	119	0.72	2	0.49	51	0.88	2	0.50	0.26	8	0.99
46	25	2	30	500	2.2	0.37	7	216	0.59	2	0.43	143	0.76	4	0.44	0.36	19	0.98
47	25	2	30	700	1.3	0.31	4	121	0.66	2	0.39	95	0.74	2	0.40	0.39	11	0.98
48	25	2	30	900	0.8	0.26	3	98	0.66	2	0.30	80	0.72	2	0.31	0.41	7	0.98
49	25	2	60	500	2.5	0.39	8	177	0.66	2	0.45	115	0.80	4	0.46	0.31	17	0.98
50	25	2	60	700	1.4	0.31	4	169	0.57	2	0.31	129	0.70	4	0.32	0.42	18	0.98
51	25	2	60	900	0.8	0.27	3	91	0.68	2	0.29	70	0.75	2	0.30	0.39	6	0.99
52	25	2	90	500	2.4	0.40	8	138	0.70	2	0.40	89	0.83	4	0.41	0.26	12	0.99
53	25	2	90	700	1.5	0.33	4	183	0.57	2	0.43	141	0.70	4	0.35	0.42	21	0.98
54	25	2	90	900	0.9	0.29	3	198	0.50	2	0.34	203	0.51	2	0.35	0.54	18	0.97
55	25	6	30	500	2.9	0.43	11	124	0.77	4	0.46	86	0.84	4	0.47	0.22	11	0.99
56	25	6	30	700	1.4	0.30	5	94	0.72	2	0.41	55	0.84	2	0.43	0.30	9	0.98
57	25	6	30	900	0.9	0.26	3	83	0.70	2	0.31	67	0.76	2	0.32	0.38	6	0.99
58	25	6	60	500	3.6	0.51	14	70	0.87	4	0.48	33	0.94	4	0.48	0.12	10	0.99
59	25	6	60	700	2	0.36	7	131	0.69	2	0.37	84	0.82	4	0.38	0.29	12	0.98
60	25	6	60	900	0.9	0.28	3	106	0.66	2	0.19	93	0.71	4	0.20	0.41	14	0.97
61	25	12	30	500	4.3	1.03	15	265	0.66	2	0.56	192	0.78	4	0.58	0.27	60	0.96
62	25	12	30	700	2.4	0.39	8	114	0.75	2	0.40	81	0.84	4	0.41	0.25	12	0.98
63	25	12	30	900	1.5	0.32	5	84	0.75	2	0.26	64	0.82	4	0.27	0.28	8	0.99
64	25	12	60	500	5.8	1.42	30	57	0.94	4	0.64	22	0.98	4	0.64	0.01	22	0.98

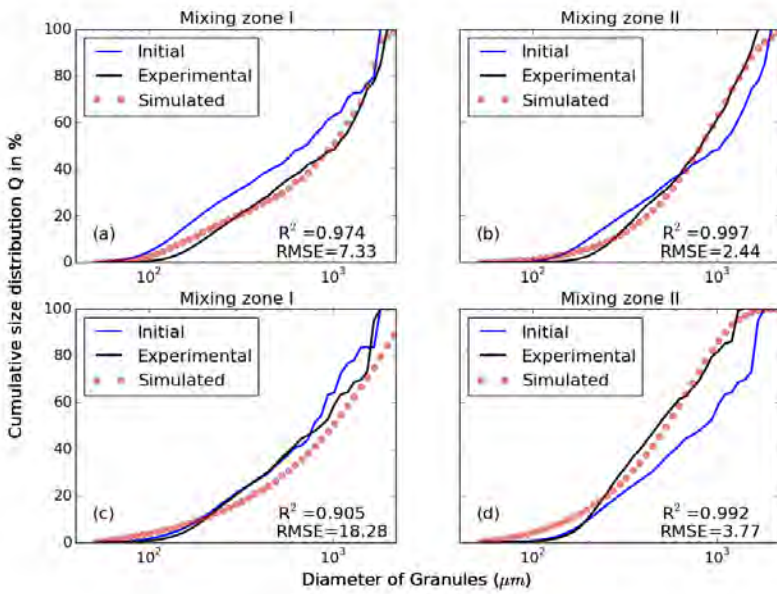
*Continued on next page*

Table C.1 – *Continued from previous page*

ID	MFR	NK	SA	RPM	$\bar{t}$	$t_{min}$	TIS			PFR+TIS				TIS+PFR+DFR				
							n	RSS	R <sup>2</sup>	n	PF	RSS	R <sup>2</sup>	n	PF	DF	RSS	R <sup>2</sup>
65	25	12	60	700	4	0.65	16	180	0.75	4	0.57	108	0.86	4	0.58	0.20	23	0.98
66	25	12	60	900	2.3	0.38	8	143	0.70	2	0.53	81	0.84	2	0.54	0.30	14	0.98



**Figure C.1:** Fit between the population balance model (PBM) simulated and experimentally measured granule size distribution (GSD) for twin-screw wet granulation with one mixing zone followed by the transport of the granulator at a low (top) and a high (bottom) screw speeds.



**Figure C.2:** Fit between the PBM simulated and experimentally measured GSD for twin-screw wet granulation with one mixing zones (I, II) of the granulator at a low (top) and a high (bottom) screw speeds.





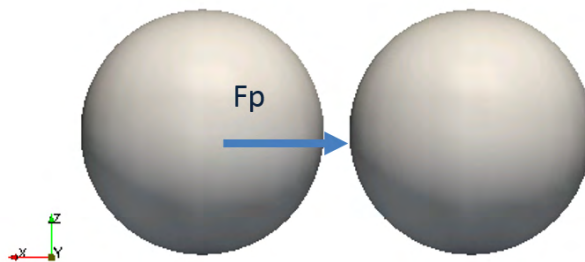
---

## Testing of the liquid transfer and bridge force models

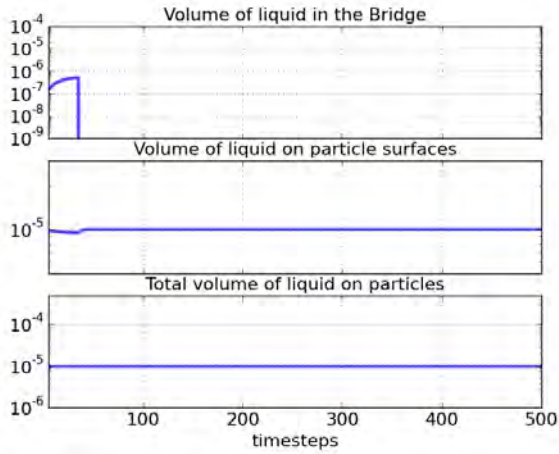
---

### Single particle-particle collision

A particle-particle collision set-up was used to demonstrate that the total liquid volume(mass) was conserved during the simulation and the force models were correctly implemented. To set-up this simulation a particle was set in motion towards a stationary particle, and the particle-particle collision was simulated using the parameters same as in the case of simple shear flow condition and the mixing zone of the twin-screw granulator (TSG) presented in Chapter 10 (Fig. D.1). Dynamics of the liquid present on the particles surfaces, liquid in the bridge by the collision event and the total liquid volume, i.e. sum of liquid present on particle surface and bridge was simulated by implementing the capillary force model by Mikami et al. (1998) and the liquid transfer during the event was tracked using the C model presented by Mohan et al. (2014).



**Figure D.1:** Simulation set-up for a single particle-particle collision.



**Figure D.2:** Dynamics of the liquid present on the particles surfaces, liquid in the bridge by the collision event and the total liquid volume associated to the particles.

The simulation data showed that the collision event resulted in transfer of the liquid present on the particle surface to the liquid bridge between the two particles (top and middle plots of Fig. D.2). While this transfer occurred, the total liquid volume/mass remained conserved (bottom plot of Fig. D.2). After collision, the bridge ruptured due to separation of the particles. In this process as well the total liquid remained conserved. This results of this test confirmed that the force models used for the multi-particle simulations presented in Chapter 10 were correctly implemented.

---

## Curriculum vitae

---

### Contact and personal information:

Name	Ashish Kumar
Address	Frans Spaestraat 17, Gent Belgium
Cell Phone	+32 483 51 29 21
E-mail	ashish.kumar@ugent.be
Date of Birth	June 22, 1983
Place of Birth	Varanasi
Nationality	Indian

### Education:

- 2010 - Currently: PhD Training, Ghent University, Belgium.
- 2009 - 2011: Professional Doctorate in Engineering (Bioprocess Technology), Technical University of Delft, The Netherlands.  
Thesis: Debottlenecking of manufacturing processes and utilities consumption in plasma products manufacturing.
- 2005 - 2007: Master in Technology (Biochemical Engineering), Harcourt Butler Technological Institute, India.  
Thesis: Process modelling of pretreatment of water hyacinth for pentose sugar extraction and utilization by *Pichia Stiptis* in ethanol fermentation
- 2001 - 2005: Bachelor in Technology (Biotechnology), AAI-Deemed University, India.  
Thesis: Biodiesel production from crude oil of *Jatropha Curcus* and *Pongamia Pinnata* by transesterification process

### Additional courses without examination:

- Kuopio workshop on continuous pharmaceutical manufacturing (Kuopio, Finland - August 20-22, 2014)

- NB Photonics Summer School (Ghent University, Belgium - June 17-21, 2014).
- 7<sup>th</sup> International Granulation Workshop Course (University of Sheffield, UK - June 24 -25, 2013).
- Getting started with High Performance Computing (Ghent University, Belgium - May 29 - June 5, 2013)
- Computational Fluid Dynamics (Ghent University, Belgium - September 17-21, 2012).

Research stay abroad:

February - April 2015, Institute for Process and Particle Engineering, Graz University of Technology, Austria

MSc. theses supervised:

- 2014: J. Dhondt, Development of regime map for continuous high shear wet granulation using twin screw granulator, in: Master of Drug Development, Ghent University
- 2015: M. Alakarjula, Investigation of process and equipment parameters affecting granule size distribution, torque, residence time distribution and mixing in a twins-screw wet granulation, in: Master of Pharmacy, University of Eastern Finland, Finland.

Professional Experience:

2011–2012: Process Engineer, Crucell Holland NV, The Netherlands

2007–2009: Assistant Manager, Dr. Reddy's Laboratories Ltd., India

Scientific Output:

Oral presentation:

1. A. Kumar, J. Dhondt, J. Vercruyssen, F. De Leersnyder, V. Vanhoorne, C. Vervaet, J. P. Remon, K. V. Gernaey, T. De Beer, I. Nopens, Development of regime map for steady-state High shear wet twin-screw granulation, in: 7th International Granulation Workshop, 2015
2. A. Kumar, M. Alakarjula, V. Vanhoorne, M. Toiviainen, M. Juuti, C. Vervaet, J. Ketolainen, K. V. Gernaey, I. Nopens, T. De Beer, Experimental investigation linking granulation performance with residence time, granulation liquid distributions in twin-screw granulation, in: 7th Pan-European QbD & PAT Science Conference (EuPAT 7), 2015

3. A. Kumar, K. V. Gernaey, I. Nopens, T. De Beer, Investigation of Twin Screw Granulation: Integrating Experimental and Computational Approaches, in: 29th International Forum and Exhibition Process Analytical Technology (Process Analysis & Control) - IFPAC, 2015
4. A. Kumar, J. Vercruyssen, M. Toiviainen, P.-E. Panouillot, M. Juuti, V. Vanhoorne, C. Vervaet, J. P. Remon, K. V. Gernaey, T. De Beer, I. Nopens, Model-based analysis and experimental validation of residence time distribution in twin-screw granulation, in: 29th International Forum and Exhibition Process Analytical Technology (Process Analysis & Control) - IFPAC, 2015
5. A. Kumar, K. V. Gernaey, T. De Beer, I. Nopens, Development of a population balance model for continuous twin-screw granulation in pharmaceutical manufacturing, in: AIChE Annual Meeting, 2014
6. A. Kumar, K. V. Gernaey, I. Nopens, T. De Beer, Experimental and model-based investigation of twin screw granulation: towards more profound process knowledge, in: 6th International Congress on Pharmaceutical Engineering, 2014
7. A. Kumar, J. Vercruyssen, M. Toiviainen, P.-E. Panouillot, M. Juuti, V. Vanhoorne, C. Vervaet, J. P. Remon, K. V. Gernaey, T. De Beer, I. Nopens, Experimental validation of residence time distribution in twin-screw granulation, in: 3rd European Conference on Process Analytics and Control Technology, 2014
8. A. Kumar, J. Vercruyssen, K. V. Gernaey, T. De Beer, I. Nopens, Experimental investigation of granule shape and size dynamics in twin-screw granulation, in: 28th International Forum and Exhibition Process Analytical Technology (Process Analysis & Control) - IFPAC, 2014
9. A. Kumar, J. Vercruyssen, M. Toiviainen, P.-E. Panouillot, M. Juuti, V. Vanhoorne, C. Vervaet, J. P. Remon, K. V. Gernaey, T. De Beer, I. Nopens, Experimental investigation of residence time distribution in twin-screw granulation, in: 28th International Forum and Exhibition Process Analytical Technology (Process Analysis & Control) - IFPAC, 2014

Poster:

1. A. Kumar, J. Vercruyssen, K. V. Gernaey, I. Nopens, T. De Beer, Analysis of a twin-screw granulation process using a combined experimental and computational approach, in: 7th International Granulation Workshop, 2015

2. A. Kumar, J. Vercruyssen, K. V. Gernaey, I. Nopens, T. De Beer, Analysis of a twin-screw granulation process using a combined experimental and computational approach, in: 7th Pan-European QbD & PAT Science Conference (EuPAT 7), 2015
3. A. Kumar, K. V. Gernaey, T. De Beer, I. Nopens, Model-based characterisation of twin-screw granulation system for continuous solid dosage manufacturing, in: 12th PSE and 25th ESCAPE Joint Event (PSE-ESCAPE), 2015
4. A. Kumar, M. Alakarjula, V. Vanhoorne, M. Ghijs, M. Toiviainen, M. Juuti, C. Vervaet, J. Ketolainen, K. V. Gernaey, I. Nopens, T. De Beer, Experimental Investigation of Residence Time, Granulation Liquid and Granule Size Distributions in Twin-Screw Granulation, in: 50th AAPS Arden House Conference, 2015
5. B. Van Snick, J. Holman, J. Vercruyssen, J. Van Renterghem, A. Kumar, T. De Beer, C. Vervaet, J.P. Remon, Process Development on a Continuous Direct Compression System, in: 29th International Forum and Exhibition Process Analytical Technology (Process Analysis & Control) - IFPAC
6. A. Kumar, K. V. Gernaey, T. De Beer, I. Nopens, One dimensional model of the prediction of residence time distribution granulation in a twin-screw granulator, in: 6th International Granulation Workshop, 2013
7. A. Kumar, J. Vercruyssen, K. V. Gernaey, I. Nopens, T. De Beer, An experimental study on effect of screw configuration in twin screw wet granulation, in: Knowledge for Growth, 2013
8. A. Kumar, J. Vercruyssen, K. V. Gernaey, T. De Beer, I. Nopens, Evaluation of particle shape and size evolution during high-shear wet granulation using twin-screw granulator, in: 6th Pan-European QbD & PAT Science Conference (EuPAT 6), 2013.

## Participant:

1. 5<sup>th</sup> Pan-European QbD & PAT Science Conference (EuPAT 5), May 8-10, 2012, Ghent, Belgium.
2. 5<sup>th</sup> International Conference on Population Balance Modelling, September 11-13, 2013, Bangalore, India.

## Peer-reviewed publications: A1:

1. A. Kumar, J. Dhondt, F. De Leersnyder, J. Vercruyssen, V. Vanhoorne, C. Vervaet, J. P. Remon, K. V. Gernaey, T. De Beer, I. Nopens, Evaluation of an in-line particle imaging tool for monitoring twin-screw granulation performance, Powder Technology (Accepted).

2. A. Kumar, J. Vercruyssen, V. Vanhoorne, M. Toiviainen, P.-E. Panouillot, M. Juuti, C. Vervaet, J. P. Remon, K. V. Gernaey, T. De Beer, I. Nopens, Conceptual framework for model-based analysis of residence time distribution in twin-screw granulation, *European Journal of Pharmaceutical Sciences* 71 (2015) 25–34.
3. A. Kumar, J. Vercruyssen, G. Bellandi, K. V. Gernaey, C. Vervaet, J. P. Remon, T. De Beer, I. Nopens, Experimental investigation of granule size and shape dynamics in twin-screw granulation, *International Journal of Pharmaceutics* 475 (1) (2014) 485–495.
4. A. Kumar, J. Vercruyssen, M. Toiviainen, P.-E. Panouillot, M. Juuti, V. Vanhoorne, C. Vervaet, J. P. Remon, K. V. Gernaey, T. De Beer, I. Nopens, Mixing and transport during pharmaceutical twin-screw wet granulation: Experimental analysis via chemical imaging, *European Journal of Pharmaceutics and Biopharmaceutics* 87 (2) (2014) 279–289.
5. A. Kumar, K. V. Gernaey, T. De Beer, I. Nopens, Model-based analysis of high shear wet granulation from batch to continuous processes in pharmaceutical production—a critical review, *European Journal of Pharmaceutics and Biopharmaceutics* 85 (3) (2013) 814–832.
6. A. Kumar, L. Singh, S. Ghosh, Bioconversion of lignocellulosic fraction of water-hyacinth (*Eichhornia crassipes*) hemicellulose acid hydrolysate to ethanol by *Pichia stipitis*, *Bioresource technology* 100 (13) (2009) 3293–3297.
7. M. H. Siddiqui, A. Kumar, K. K. Kesari, J. M. Arif, Biomining—a useful approach toward metal extraction, *Am Eurasian J Agron* 2 (2009) 84–88.
8. M. H. Siddiqui, A. Kumar, A. Farooqui, K. K. Kesari, Biodiesel production from crude oil of *Jatropha curcas* and *Pongamia pinnata* by transesterification process, *International Journal of Oil, Gas and Coal Technology* 4 (2) (2011) 192–206.

Peer-reviewed publication: A2:

A. Kumar, K. V. Gernaey, T. De Beer, I. Nopens, Model-based characterisation of twin-screw granulation system for continuous solid dosage manufacturing, *Computer Aided Chemical Engineering* 37 (2015) 2165–2170.

Web-article:

Understanding Continuous High Shear Wet Granulation in Pharmaceutical Production, in: Research Highlights, Pharmaceutical Solid State Research Cluster. <http://www.pssrc.org>



Invited speech:

Experimental and model-based investigation of twin screw granulation: towards more profound process knowledge, in: 2nd Continuous oral solid dosage forms production seminar, GEA Pharma Systems, Antwerp, Belgium, June 4th-5th, 2014.

Awards:

- 2015: Most Pharmaceutically Relevant Poster Award, 7th International Granulation Workshop
- 2013: Most Pharmaceutically Relevant Poster Award, 6th International Granulation Workshop
- 2009: Stellar Performer Award for the best performance of the Biologics unit at Dr. Reddy's Laboratories Ltd.





ISBN 978-9-0598983-6-3



9

789059

898363

